FACULTY OF SCIENCES

Sedimentary expression of internal waves on Quaternary contouritic processes along the Irish and Moroccan Atlantic margins

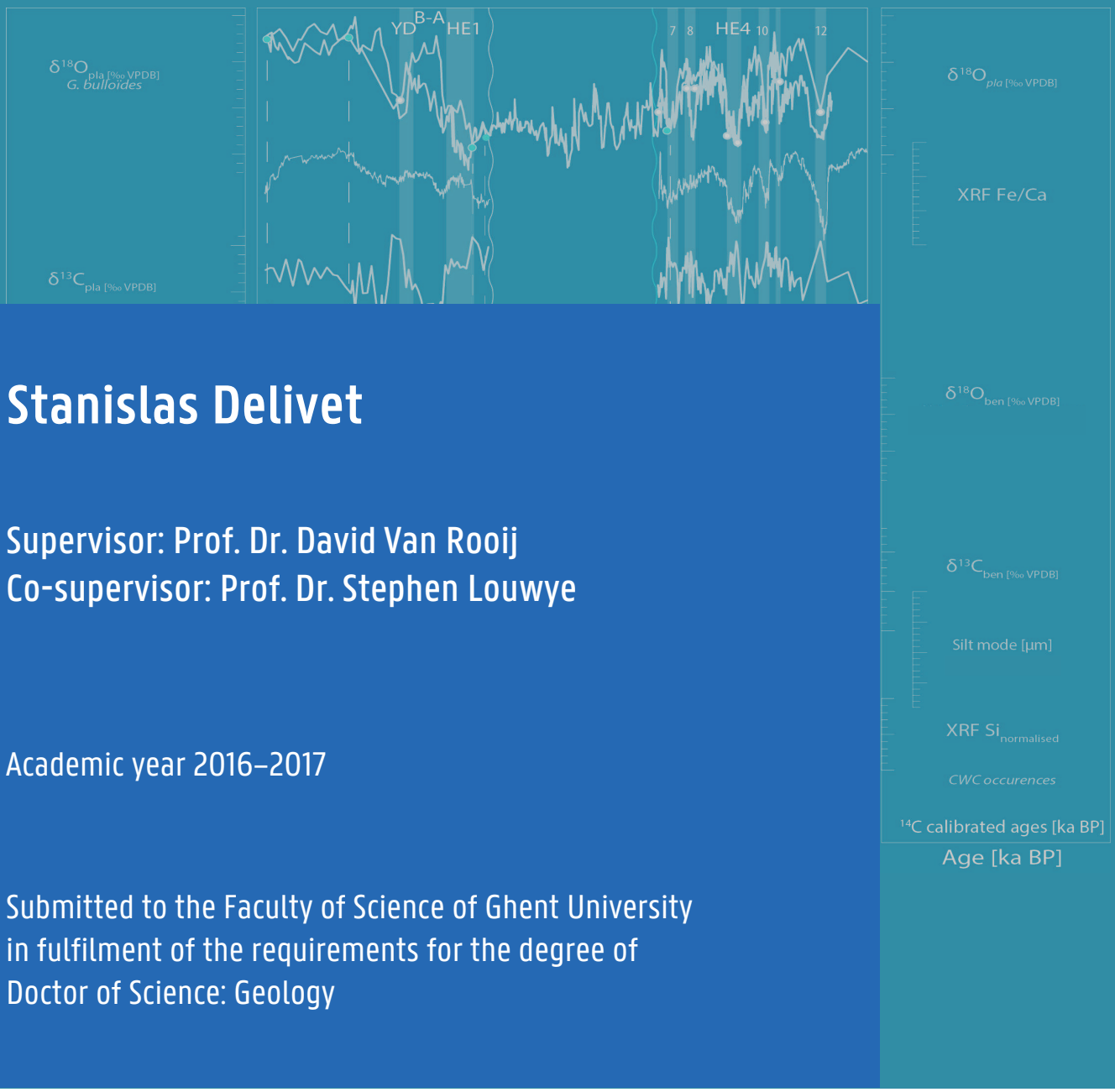

Stanislas Delivet

Supervisor: Prof. Dr. David Van Rooij
Co-supervisor: Prof. Dr. Stephen Louwye

Academic year 2016–2017

Submitted to the Faculty of Science of Ghent University
in fulfilment of the requirements for the degree of
Doctor of Science: Geology

GHENT UNIVERSITY

Members of the examination committee

Prof. Dr. David Van Rooij (supervisor, Ghent University, Belgium)

Prof. Dr. Stephen Louwye (co-supervisor, Ghent University, Belgium)

Prof. Dr. Marc De Batist (Ghent University, Belgium)

Prof. Dr. Thijs Vandenbroucke (Ghent University, Belgium)

Prof. Dr. Dominique Blamart (LSCE-IPSL & UVSQ, France)

Dr. Estefania Llave (IGME, Spain)

Prof. Dr. Nathalie Fagel (Université de Liège, Belgium)

Prof. Dr. Sébastien Bertrand (Ghent University, Belgium)

This study was carried out within the framework of a Ghent University BOF "Starting Grant".

This dissertation should be referred to as:

Delivet, S., 2016. Sedimentary expression of internal waves on Quaternary contouritic processes along the Irish and Moroccan Atlantic margins. Ph.D. Thesis, Ghent University, Belgium.

In an endless sea with you
Sailing under the rain
The only colour of my blues
Is made of dust and sand

Driftin'
It's every day the same
Clouds pass me by
And I'm bound to take my time
Until I find you

The wind may send me home to you
Before the harvest starts again
And if the light come shine on through
Will you still recall my name?

Driftin' [...]

I've been here and almost everywhere
I sailed the seven seas while you sat down on your chair
You've been good to me
And I've been good to you
Lost in the hands of gravity
Soon I'll get back to blue

Ulysses and the sea - PAPOOZ

Acknowledgements

My deepest acknowledgements are indeed directed towards for Prof. Dr. David Van Rooij, for his supervision/guidance (delete as appropriate) during those last years. I am very thankful for the trust you put in me throughout, for sharing science, correcting my awful manuscripts, solving problems quite efficiently as needed, and much more. Hope we got a bit closer to that ring we seek so badly..

The completion of this work wouldn't have been possible without the appropriate structure, which within the Department of Geology is still known as the Renard Centre of Marine Geology (RCMG). In particular I much appreciated moments spent with Prof. Dr. Marc De Batist in the Alps and in Switzerland. I also particularly want to thanks Prof. Dr. Sébastien Bertrand for his availability and advices, from which I greatly benefited from at some points. I wish to express my solidarity with him, pointing out that the keystroke sequence "e.r.t.r.a." is quite tough using an AZERTY keyboard.

This entire work also involved collaborations within the LSCE (France), the NIOZ (The Netherlands) and MARUM (Germany). I certainly received great insights and guidance from their respective team. In particular many thanks to Dominique Blamart, Franck, Claire, Natalia and Elisabeth from the LSCE. But also the technical staff such as Gulay Isguder, for her time and help with the foraminifera, and for her encouragements. Lucile, Fabien, Doris and the others I met there. From the Royal NIOZ, I wish especially to thanks Furu Mienis, Jan-Berend and Rineke which also took time to sit along, and have provided valuable scientific and technical inputs. Same regards towards Claudia Wienberg and Dierk from MARUM.

Indeed there is a bit of the soul of the entire staff of RCMG in this dissertation. I won't pretend being able to provide an exhaustive list. But as a matter of equity, those I forgot can claim for a hug. Marc Faure and Wim, Kurt, Koen, Tine. My regretted old office mates Michael and Maikel. Oscar, which I definitely need to cite here for not-hugging purpose. Agostina, Thomas TV, Thomas TM, Shan, Carmen, Philipp, Marteen, Inka, Elke, Nore, Evelien, Hui, An, Dawei, Eleonora, Katleen, Loïc, Mario… I much enjoyed company and work with of Tim Collart those last months. And I wish you best luck.

Finalement, j'aimerais remercier les personnes qui ont contribués à faire la vie à Gand si belle. A toutes celles et ceux qui l'ont faite d'amour et de bière fraiche, de vin rouge et blanc, d'art populaire, d'art culinaire, de vêtements équitables, de feux destructeurs, de parasites en tout genre, d'histoires de pigeon reproducteurs, de musique baroque, d'autre bruits plus expérimentaux, de 6b et de 7a, de promenades au parc… j'en passe et des meilleures…

Stanislas Delivet

Table of Content

Acknowledgements v

Scientific Highlights xi

Summary xii

Samenvatting xvi

List of Figures xxi

List of tables xxiv

List of Abbreviations xxv

1 Introduction 1–1

1.1 Large versus small-scaled contourite drifts 1–3

1.2 Internal tides versus seabed interactions 1–10

1.3 Evolution of the Mediterranean Outflow Water 1–15

1.4 Rationale of this study 1–20

References 1–23

2 Methodology 2–34

2.1 Seismic reflection 2–37

2.2 Borehole logging 2–39

2.2.1 Natural Gamma Ray 2–39

2.2.2 Dual induction resistivity 2–40

2.2.3 Compensated neutron density 2–41

2.2.4 P-wave velocity 2–41

2.3 Sediment core analysis 2–42

2.3.1 Multi-Sensor Core Logger 2–42

2.3.2 X-ray Fluorescence 2–43

2.3.3 Particle grain-size distribution 2–46

2.3.4 Foraminifera stratigraphy 2–48

2.3.5 Foraminifera stable Carbon and Oxygen isotope 2–50

2.3.6 Radiocarbon dating 2–53

2.3.7 Coccolith stratigraphy 2–54
References 2–55
3 Plio-Pleistocene bottom current variability at Goban Spur 3–62
Abstract 3–64
3.1 Introduction 3–65
3.2 Regional setting 3–67
3.2.1 Geological and geomorphological setting 3–67
3.2.2 Oceanographic setting 3–68
3.3 Material and methods 3–70
3.4 Results 3–72
3.4.1 Seabed morphology 3–72
3.4.2 Integrated stratigraphic framework 3–72
3.5 Discussion 3–78
3.5.1 Chronostratigraphic evolution 3–78
3.5.2 Sedimentary processes 3–80
3.5.3 Integrated regional margin evolution 3–88
3.6 Conclusions 3–93
Acknowledgements 3–93
References 3–94
4 Goban Spur bottom current variability across the four deglaciations 4–102
Abstract 4–103
Contributions 4–104
4.1 Introduction 4–105
4.2 Regional setting 4–107
4.2.1 Geological setting 4–107
4.2.2 Oceanographic setting 4–109
4.3 Material and methods 4–110
4.4 Results 4–112
4.5 Discussion 4–116

4.5.1 Framework and glacial termination pattern 4–116
4.5.2 Grain-size and local bottom current variability 4–119
4.5.3 MOW variability along the northeast Atlantic margin 4–121
4.6 Conclusions 4–125
Acknowledgments 4–125
References 4–126
5 Bottom current variability at the Pen Duick drift during the last 50 ky 5–138
Abstract 5–140
Contributions 5–140
5.1 Introduction 5–141
5.2 Regional setting 5–144
5.3 Material and methods 5–147
5.4 Results 5–150
5.4.1 Age model 5–150
5.4.2 Stable carbon isotopic record 5–152
5.4.3 XRF and grain-size distribution 5–152
5.5 Discussion 5–154
5.5.1 Stable isotopes, source and controls on sedimentation pattern 5–154
5.5.2 Bottom current variability 5–158
5.5.3 Hiatus, processes and implications 5–160
5.6 Conclusions 5–163
Acknowledgements 5–164
References 5–164
6 Early-middle Pleistocene Mediterranean Outflow Water controlled sedimentation along the Moroccan Atlantic Margin 6–176
Abstract 6–178
Contributions 6–179
6.1 Introduction 6–179
6.2 Regional setting 6–182

6.2.1 Geological setting 6–182
6.2.2 Oceanographic setting 6–183
6.3 Material and methods 6–185
6.3.1 Sediment analyses 6–185
6.3.2 Age model 6–186
6.3.3 Critical seabed slope calculation 6–186
6.4 Results 6–187
6.4.1 Coccolith assemblages 6–187
6.4.2 Age model and sedimentation rates 6–187
6.4.3 Sediment facies 6–188
6.4.4 Physical and geochemical data 6–190
6.4.5 Grain-size distribution 6–191
6.4.6 Seabed and internal tide reflection conditions 6–193
6.5 Discussion 6–193
6.5.1 General chronostratigraphic framework 6–193
6.5.2 Facies association 6–196
6.5.3 Sedimentary environment evolution 6–200
6.6 Conclusions 6–204
Acknowledgements 6–205
References 6–206
7 Discussion, conclusions and outlook 7–216
7.1 Characteristics and diagnostic criteria of internal tidal deposits 7–219
7.1.1 Deep-marine tidal bottom currents 7–219
7.1.2 Geomorphological characteristics 7–220
7.1.3 Sediment facies 7–224
7.2 Summary of conclusions 7–231
7.3 Outlook 7–234
References 7–238

Scientific Highlights

This dissertation focuses on the mechanisms in which bottom currents dominated by internal wave processes controlled the large-scale architecture and sedimentary facies of marine sediments. Along the southern Irish margin, the build-up of large-scale sediment waves occurred throughout the Pleistocene, mainly ranging water depths between 1200 and 1600 m. This wave field could be attributed to the presence of energetic bottom currents, driven by enhanced internal wave and tide processes. The onset of these bottom currents was controlled by the introduction of the Mediterranean Outflow Water. The sedimentological analysis of the wave field at DSDP site 548 evidenced that the bottom current regime was climatically modulated over the past 500 ky. Enhanced bottom currents prevailed during interglacials, while they were reduced during glacials, which could be attributed to shifts in the Mediterranean Outflow Water northward advection.

Energetic and variable internal tidal bottom currents have also influenced the sedimentation along the Atlantic Moroccan margin. At about 650 m water depth, the variable influence of the Antarctic Intermediate Water is thought to have driven the climatically modulated bottom current regime. Over the last 50 ky, enhanced bottom currents prevailed during Heinrich Events, Dansgaard-Oeschger stadials, and have caused erosional and/or non-depositional conditions with the onset and during most of the Last Glacial Maximum. At 1000 m water depth, energetic to erosive bottom currents gradually developed as the glacial stages became more pronounced over the past 1500 ky. Increased influence of Mediterranean eddies forced by sea-level decrease is thought to have driven the bottom current variability and internal wave processes over this period.

This study highlights how changes in the general oceanic circulation pattern control local internal waves processes. These have a dramatic influence on the local sedimentation pattern and constitute important erosional processes. Furthermore, the presence of energetic bottom currents seems to positively influence the benthic cold-water corals ecosystems present along the Irish and Atlantic Moroccan margins, playing a major role for food particles availability.

Summary

The study of sediments primarily deposited by the action of bottom currents, namely contourites, aims to decipher information associated with the past circulation pattern, current velocities and oceanographic history. Energetic contour currents typically form large-scale, elongated contourite drifts, which are widespread over the ocean basins, representing a substantial portion of the marine sediment log-book. Those deposits are considered as a valuable marine sediment archive, overall representing relatively continuous records and characterised by high sedimentation rates. At present, numerous small-scaled contourite drifts are being discovered in environments where overall contour currents are much smaller. They are controlled by a combination of factors which includes topographically controlled intensification of bottom currents and the participation of different oceanographic processes such as mesoscale eddies and/or internal waves and tides, among others. Internal tides are being increasingly recognized as an important process affecting particles dynamics and sedimentation, thus largely participating to contouritic processes. Internal tides are further thought to be an important process for the development of benthic cold-water coral ecosystems.

The presence of numerous small-scale contourite drifts associated with extensive past and present cold-water coral ecosystems are characteristic of both the Irish and Atlantic Moroccan margins. Both margins consist of environments dominated by internal tide processes, within regions characterised by alternatively thriving and decaying cold-water coral ecosystems. Sediment drifts and cold-water corals are mainly found at depths ranging from ~200 to 1200 m, and are currently influenced by different water masses. Along the Irish margin, the Mediterranean Outflow Water has an essential influence, and both the Antarctic Intermediate Water and Mediterranean Outflow Water are important along the Atlantic Moroccan margin. However, unlike the established paradigm, records so far obtained from the contourite drifts of the Irish margin revealed a very complex history and the presence stratigraphic hiatuses that can range from a few thousands to several million years. Such hiatuses may be primarily induced by the action of energetic bottom currents, most probably associated with very variable internal tide regime. This limited constrains of the past bottom current and Mediterranean Outflow Water variability, as well as in establishing the relationships possibly existing between variable bottom currents and the cold-water coral ecosystems. Along the Atlantic Moroccan margin, there exist yet no sediment-based bottom current variability reconstructions.

This thesis attempts to contribute to the knowledge of past bottom current variability along the Irish margin, presumably mainly associated to changes in the behaviour and circulation of the Mediterranean Outflow Water. Along the Atlantic Moroccan margin, the aim is to constrain the

sedimentological expression of bottom currents and their variability within two distinct sites, respectively influenced by the Antarctic Intermediate Water and Mediterranean Outflow Water.

DSDP Site 548 was recovered from the Goban Spur submarine plateau at 1256 m water depth, at the southern tip of the Irish margin. The geomorphological analysis of newly collected high resolution seismic data revealed the evolution of the local sedimentary environment over the Plio-Pleistocene. The correlation of the seismic and borehole geochronology improved the understanding of the DSDP Site 548 stratigraphic unit boundaries. The sedimentary architecture of this part of the margin was inferred to be the result of slope failure induced changes in the local slope gradient, and long term changes in the circulation of the Mediterranean Outflow Water, both impacting on tide-topographic interactions. The initial introduction of the Mediterranean Outflow Water is thought to have occurred between 4.5 and 4.2 Ma, and could have played a preconditioning role to subsequent slope failure inferred between 2.5 and 2.15 Ma. From 2.15 Ma onwards, large-scale sediment waves developed, in close relationship with the seabed irregularities caused by different slope failure events. Large-scale sediment waves indicate an energetic depositional environment. More pronounced northward incursion of the Mediterranean Outflow Water is thought to be the driving mechanism for the sediment waves formation, which characterised an enhanced internal tide regime within its lower boundary. The sediment wave field at Goban Spur constitutes one of the few wave fields which could be primarily related to internal tidal process and seabed interactions. The initial development of large scale sediment waves at Goban Spur is roughly contemporary with the development of large cold-water coral mounds along the eastern slope of the Porcupine Seabight and Irish margin. In contrast to sites located along the Iberian margin, which recorded an increasing influence of the Mediterranean Outflow Water throughout the Plio-Pleistocene, both the Goban Spur and Porcupine Seabight have recorded a relatively decreased influence from ~0.5 Ma onwards. This might have been induced by the presence of a strong climatic modulation in the Mediterranean Outflow Water behaviour, which is the reason why this interval was further investigated.

Bottom current variability at DSDP Site 548 was investigated across the four penultimate deglaciations, which constitute the most sudden and marked climatic transitions of the past 0.5 Ma. XRF-scanning, planktonic foraminifera relative abundances and terrigenous grain-size distributions indicated a tight link between bottom current regime and climate changes. Depletion of fine silt and clay particles (below 10 μm grain-size) and relative enrichment in silt particles between 20 and 40 μm consistently occur during warm sea-surface temperature conditions. Those variations are thought to be mainly driven by changes in the local vertical water column stratification (pycnal gradient), attributed to latitudinal shifts in the northward advection of the Mediterranean Outflow Water. Such pycnal gradient changes have in turn influenced internal tides and tide-topography interactions,

which are known to induce particle hydrodynamic sorting at present. Enhanced tide-topographic interactions, characterizing periods of northward advection of the Mediterranean Outflow Water, were evidenced during interglacials of Marine Isotopic Stages 11, 9, 7 and 5. Glacials prior these periods were characterised by more sluggish bottom currents. It seems the Mediterranean Outflow Water only has reached Goban Spur latitudes during periods of production of dense (modern-like) North Eastern Atlantic Deep Water via the Wyville-Thompson Ridge. The absence of Mediterranean Outflow Water along the Irish margin might have contributed to the glacial degradation of environmental conditions for the cold-water coral ecosystems of the Porcupine Seabight, since reduced bottom currents affect the food particles availability for the corals.

The Atlantic Moroccan margin has been distinctly influenced by the shallow (~600 m water depth) northward incursion of the Antarctic Intermediate Water, and the deeper (800 to 1200 m water depth) incursion of the Mediterranean Outflow Water. The Antarctic Intermediate Water has seemingly influenced the formation of a sediment drift, which sequence was studied by means of a long piston core recovered at 642 m water depth (MD08-3227; ~35.2°N). Planktonic and benthic stable isotope measurements, along with a series of AMS ^{14}C dates, revealed a complex chronostratigraphic evolution since ~50 ka BP. Millennial-scale variations of the bottom current regime were inferred from changes in the terrigenous silt grain-size distribution, mainly varying between 6 and 30 µm. Increased advection of Antarctic Intermediate Water might be responsible for enhanced bottom current conditions, in particular during cold Dansgaard-Oeschger stadials, Heinrich Event 1 and the Younger Dryas. Overall high sedimentation rates are thought to be caused by significant input of sediments reworked by bottom currents. Energetic bottom currents are also thought to be the driving mechanism for a stratigraphic hiatus which extends from 33 ka to 19 ka BP. This hiatus is associated with a 10 cm thick foraminifera rich silty sand layer interpreted as a calcareous sandy contourite sequence. At this site, such bottom current induced erosional and/or non-depositional conditions are most probably caused by enhanced internal tidal processes, established during the gradual onset of the Last Glacial Maximum. The presence of bottom current controlled sedimentation, alternating with periods of bottom current induced erosional and/or non-depositional conditions, is analogous to the situation along the Irish margin. Furthermore, bottom current induced erosional and/or non-depositional conditions at the coring site coincide with a period of increased regional cold-water coral development. Again this may suggest a beneficial effect of energetic bottom currents for cold-water coral ecosystems.

The influence of the Mediterranean Outflow Water along the Atlantic Moroccan margin is studied by the means of a long piston core recovered at 968 m water depth (MD13-3447; ~35.15°N). The bottom of the core has been inferred to an age of ~1650 ka BP. Sediment facies are examined

together with spectrophotometry and XRF data, as well as coccolith assemblages analysis and terrigenous grain-size distributions. Climatically modulated bottom current regime is identified on the basis of terrigenous clay and silt variations (ranging between 4 and 30 μm), variable occurrence of discontinuous silt lenses and foraminifera rich sandy pockets, rust coloured and moderately bioturbated horizons. Gradually more energetic bottom currents are inferred in association with the onset of more pronounced glacials, in particular during the Early-Middle Pleistocene Transition. Increased Mediterranean mesoscale eddies incursion is thought to be the driving mechanism for the observed bottom current variability. Sea-level fall and hydraulic condition changes at the Strait of Gibraltar are thought to have caused higher Mediterranean Outflow Water flow velocities, which would have in turn increased the potential vorticity and the mesoscale eddies formation rate. Overall low sedimentation rates, mainly comprised between 1 and 2 cm/ky may be related to a sediment starved environment (core located on top of a submarine ridge), and may additionally indicate that transport largely dominated over sedimentation at this site. A probably slope-failure triggered turbiditic event marked an abrupt sedimentation change, possibly associated to a margin-wide tectonic adjustment at ca. 460 ka BP. The subsequent settlement of dominantly erosional and/or non-depositional conditions most probably reflect the onset of more energetic bottom currents, possibly caused by changes in the circulation pattern and/or changes of the local slope gradient. This period also roughly coincides with the migration of the cold-water coral from depths above 800 m towards depths ranging between 800 and 1000 m. The onset of more energetic bottom currents at those depths might have favoured such migration.

Overall, the Atlantic Moroccan and Irish margins are characterised by climatically modulated and bottom current controlled sedimentation, with variations between periods of moderate and energetic to erosive and/or non-depositional conditions. The changes are site specific and mostly asynchronous, which emphasizes on how changes in the local pycnal gradient may control sedimentation. A better understanding of the mechanisms driving tide-topography interactions constitute an important future challenge, especially regarding their role in causing short and long term erosional and/or non-depositional conditions. This study has provided distinct contourite sediment facies descriptions which might be considered as possible analogues for future sediment-based studies in internal tide dominated environments.

Samenvatting

De studie van sedimenten die voornamelijk afgezet worden door de werking van bodemstromingen, contourieten genaamd, heeft als doel informatie omtrent voorbije circulatiepatronen, stroomsnelheden en de oceanografische geschiedenis te ontcijferen. De werking van energieke contourstromen leidt typisch tot de vorming van grootschalige, langwerpige contourietdriften, die veelvuldig voorkomen in oceanische bekkens en aldus een aanzienlijk deel van het beschikbare mariene sedimentarchief beslaan. Deze afzettingen worden beschouwd als waardevolle mariene sedimentarchieven, die over het algemeen betrekkelijk continue reeksen bevatten en gekenmerkt worden door hoge sedimentatiesnelheden. Vandaag de dag worden ook talrijke kleinschalige contourietdriften ontdekt in omgevingen waar contourstromen doorgaans veel zwakker zijn. Deze afzettingen zijn het resultaat van een combinatie van factoren, waaronder het intensifiëren van bodemstromingen nabij topografische obstakels en de werking van oceanografische processen zoals o.a. mesoschalige eddies en/of interne getijden. Interne getijden worden in toenemende mate erkend als een belangrijk proces bij de dynamiek en afzetting van sedimenten, waardoor ze in grote mate bijdragen tot de aan contourieten gerelateerde processen. Bovendien worden interne getijden ook een belangrijke rol toegedicht bij de ontwikkeling van benthische koudwaterkoraal ecosystemen.

Zowel op de Ierse als de Atlantische Marokkaanse rand komen talrijke kleinschalige contourietdriften voor samen met omvangrijke vroegere en hedendaagse koudwaterkoraal ecosystemen. Beide randen herbergen omgevingen die onder invloed staan van interne getijden, in gebieden waarbinnen koudwaterkoraal ecosystemen afwisselend gedijen en in verval raken. Sedimentdriften en koudwaterkoralen worden hoofdzakelijk teruggevonden op waterdieptes tussen ~200 en 1200 m, en worden momenteel door verschillende watermassa's beïnvloed. Langsheen de Ierse rand speelt het *Mediterranean Outflow Water* een essentiële rol, terwijl zowel het *Antarctic Intermediate Water* als het *Mediterranean Outflow Water* van belang zijn langs de Atlantische Marokkaanse rand. Niettemin vertonen de tot dusver bemonsterde contourietsequenties op de Ierse rand, in tegenspraak met het gevestigde paradigma, een zeer complexe geschiedenis door de aanwezigheid van stratigrafische hiaten gaande van enkele duizenden tot miljoenen jaren. Dergelijke hiaten zouden voornamelijk veroorzaakt worden door de werking van sterke bodemstromingen, die wellicht verbonden zijn aan een zeer variabel regime van interne getijden. Dit beperkt in grote mate de mogelijkheid om vroegere bodemstromingen en de variabiliteit van het *Mediterranean Outflow Water* na te gaan, en om de mogelijke verbanden tussen wisselende bodemstromingen en koudwaterkoraal ecosystemen vast te stellen. Voor de Atlantische Marokkaanse rand bestonden er

tot nog toe geen reconstructies van de variabiliteit van de bodemstromingen op basis van sedimentkernen.

Deze thesis probeert de kennis over de temporele variabiliteit van bodemstromingen langs de Ierse rand te vervolledigen, die vermoedelijk grotendeels gelinkt is aan veranderingen in het gedrag en de circulatie van het *Mediterranean Outflow Water*. Langsheen de Atlantische Marokkaanse rand is de doelstelling om de sedimentologische expressie en variabiliteit van de bodemstromingen te evalueren op twee locaties, die respectievelijk beïnvloed worden door het *Antarctic Intermediate Water* en het *Mediterranean Outflow Water*.

DSDP Site 548 werd bemonsterd op het Goban Spur submarien plateau op 1256 m waterdiepte, nabij de zuidelijke punt van de Ierse rand. De geomorfologische analyse van nieuw verzamelde, hoge resolutie seismische data toont de evolutie van de lokale Plio- Pleistocene sedimentaire omgeving. De correlatie van de seismische stratigrafie met de stratigrafie van het boorgat liet toe om de grenzen van de stratigrafische eenheden in DSDP Site 548 beter te begrijpen. De sedimentaire opbouw van dit deel van de rand is het resultaat van door afschuivingen veroorzaakte lokale veranderingen in de steiltegraad van de helling, en van variaties in de circulatie van het *Mediterranean Outflow Water* op lange termijn, wat allebei een impact heeft op de interacties tussen de getijden en de topografie. De initiële introductie van het *Mediterranean Outflow Water* vond wellicht plaats rond 4.5 Ma, en zou een voorbereidende rol kunnen gespeeld hebben bij de daaropvolgende afschuiving van de continentale helling rond 2.5 Ma. Vanaf 2.5 Ma ontwikkelden zich grootschalige sedimentgolven in nauwe verbondenheid met de onregelmatige zeebodem, die een gevolg was van verschillende fases van afschuivingen. Deze grootschalige sedimentgolven wijzen op een energieke depositionele omgeving. De drijvende kracht achter de vorming van de sedimentgolven is waarschijnlijk een meer uitgesproken noordwaartse instroom van het *Mediterranean Outflow Water*, wat aanleiding gaf tot een sterker interne getijden regime aan de ondergrens van deze watermassa. Het gebied met sedimentgolven op Goban Spur is een van de weinige die in hoofdzaak gelinkt kan worden aan interne getijden en hun interactie met de zeebodem. De initiële ontwikkeling van grootschalige sedimentgolven op Goban Spur valt ruwweg samen met de ontwikkeling van grote koudwaterkoraalmounds langs de oostelijke helling van de Porcupine Seabight en de Ierse rand. In tegenstelling tot sites langs de Iberische rand, die een graduele toename van de invloed van het *Mediterranean Outflow Water* doorheen het Plio-Pleistoceen aangeven, vertonen zowel Goban Spur als de Porcupine Seabight een relatief verzwakte invloed vanaf ~0.5 Ma. Dit zou een gevolg kunnen zijn van een sterke, klimaatgedreven wijziging in het gedrag van het *Mediterranean Outflow Water*, wat de aanleiding is voor het verder onderzoeken van dit interval.

De variabiliteit in bodemstromingen ter hoogte van DSDP Site 548 werd onderzocht voor de vier laatste deglaciaties, die de meest plotse en uitgesproken klimaatveranderingen van de voorbije 0.5 Ma omvatten. XRF-scans, relatieve abundantie van planktonische foraminiferen en terrigene korrelgrootteverdelingen geven een nauw verband aan tussen het stroomregime van bodemstromingen en klimaatveranderingen. Er is een consistente afname van fijne silt- en kleideeltjes (korrelgrootte kleiner dan 10 µm) en een relatieve toename in siltdeeltjes (tussen 20 en 40 µm) tijdens periodes met hoge temperaturen aan het zeeoppervlak. Deze variaties worden vermoedelijk vooral gedreven door wijzigingen in de lokale verticale stratificatie van de waterkolom (de zogenoemde pycnale gradiënt), die toegeschreven kunnen worden aan verschuivingen in de breedtegraad tot waar de noordwaartse advectie van het *Mediterranean Outflow Water* reikt. Dergelijke veranderingen in de pycnale gradiënt beïnvloeden op hun beurt de interne getijden en hun interacties met de topografie, die gekend zijn tegenwoordig de hydrodynamische sortering van sedimentpartikels te kunnen veroorzaken. Een toename in getijde-topografische interacties tijdens periodes van noordwaartse advectie van het *Mediterranean Outflow Water* werd vastgesteld tijdens interglacialen van *Marine Isotopic Stages* 11, 9, 7 en 5. Glacialen voorafgaand aan deze periodes werden gekenmerkt door meer langzame bodemstromingen. Het lijkt erop dat het *Mediterranean Outflow Water* enkel de breedtegraad van Goban Spur bereikte tijdens periodes met productie van dicht (i.e. vergelijkbaar met het huidige) *Iceland-Scotland Ridge Overflow Water*. De afwezigheid van het *Mediterranean Outflow Water* langs de Ierse rand zou kunnen bijgedragen hebben tot de glaciale achteruitgang in omgevingsomstandigheden voor de koudwaterkoraal ecosystemen van de Porcupine Seabight, omdat een afname in bodemstromingen de beschikbaarheid van voedselpartikels voor de koralen beïnvloedt.

De Atlantische Marokkaanse rand werd sterk beïnvloed door de ondiepe (~600 m waterdiepte) noordwaartse instroom van het *Antarctic Intermediate Water*, en de diepere (800 tot 1200 m waterdiepte) instroom van mesoschalige eddies afgeleid van het *Mediterranean Outflow Water*. Het *Antarctic Intermediate Water* was klaarblijkelijk betrokken bij de vorming van een sedimentdrift, waarvan de sequentie bestudeerd werd door middel van een lange sedimentkern genomen op 642 m waterdiepte (MD08-3227; ~35.2°N). Metingen van stabiele isotopen op planktonische en benthische foraminiferen, in combinatie met een reeks AMS ^{14}C dateringen brachten een complexe chronostratigrafische evolutie tijdens de laatste ~50 ka BP aan het licht. Schommelingen in het bodemstromingsregime op een schaal van duizenden jaren konden afgeleid worden uit veranderingen in de korrelgrootteverdeling van het terrigene silt, die voornamelijk varieert tussen 6 en 30 µm. Een toename in de advectie van het *Antarctic Intermediate Water* is vermoedelijk verantwoordelijk voor de meer uitgesproken bodemstromingen, in het bijzonder tijdens koude

Dansgaard-Oeschger stadialen, Heinrich Event 1 en het Jongere Dryas-stadiaal. De in het algemeen hoge sedimentatiesnelheden zijn wellicht te wijten aan de significante input van sediment dat door bodemstromingen herwerkt werd. Energieke bodemstromingen zijn waarschijnlijk ook de oorzaak voor een stratigrafisch hiaat dat de periode van 33 ka tot 19 ka BP omspant. Dit hiaat is gelinkt aan een 10 cm dikke, kalkhoudende (foraminiferen-rijke), zandige contourietsequentie. Op deze locatie resulteren dergelijke door bodemstromingen veroorzaakte erosieve en/of non-depositionele condities waarschijnlijk uit een toenemende werking van interne getijden, gevestigd tijdens het geleidelijk op gang komen van het circulatiepatroon van het Laatste Glaciale Maximum. De door bodemstromingen gecontroleerde sedimentatie, afgewisseld met periodes van erosieve en/of non-depositionele omstandigheden zijn analoog met de situatie langsheen de Ierse rand. Bovendien vallen de erosieve en non-depositionele omstandigheden op de bemonsteringslocatie samen met een periode van toegenomen ontwikkeling van koudwaterkoralen in de regio. Dit zou opnieuw kunnen wijzen op het voordelige effect van energieke bodemstromingen op koudwaterkoraal ecosystemen.

De invloed van het *Mediterranean Outflow Water* langs de Atlantische Marokkaanse rand werd bestudeerd door middel van een lange sedimentkern genomen op 968 m waterdiepte (MD13-3447; ~35.15°N). De basis van de kern heeft een ouderdom van ~1650 ka BP. De sediment facies werden onderzocht, samen met spectrofotometrische en XRF data, de analyse van coccolieten assemblages en terrigene korrelgrootteverdelingen. Klimaatgebonden bodemstromingsregimes werden bepaald op basis van terrigene klei- en siltvariaties (gaande van 4 tot 30 µm), en het variabele voorkomen van discontinue siltlenzen, foraminiferen-rijke, zandige opgevulde holtes, en roestkleurige en matig gebioturbeerde horizonten. Er werd vastgesteld dat gradueel sterker wordende bodemstromingen zich manifesteren tijdens de aanzet van de meer uitgesproken glacialen, in het bijzonder tijdens de Vroeg-Midden Pleistocene Transitie. De toenemende invloed van mesoschalige eddies afgeleid van het *Mediterranean Outflow Water* is de drijvende kracht achter de geobserveerde variabiliteit in de bodemstromingen. Een zeespiegeldaling en veranderingen in de hydraulische condities nabij de Straat van Gibraltar worden verondersteld hogere stroomsnelheden van het *Mediterranean Outflow Water* te hebben veroorzaakt, met een toename in potentiële vorticiteit en snellere vorming van mesoschalige eddies tot gevolg. De over het algemeen lage sedimentatiesnelheden, voornamelijk tussen 1 en 2 cm/ky, zouden verband kunnen houden met de sediment-arme omgeving (de kern werd genomen op de top van een submariene rug), en zouden er daarnaast ook kunnen op wijzen dat op deze locatie sedimenttransport ruimschoots de bovenhand heeft gehad op sedimentatie. Een turbidietafzetting, waarschijnlijk getriggerd door een afschuiving van de helling, geeft een abrupte verandering in sedimentatie aan, die mogelijks ook gelinkt is aan een tektonische aanpassing rond ca. 460 ka BP over de gehele rand. Het daaropvolgende aanbreken van overwegend erosieve en/of

non-depositionele condities weerspiegelt zeer waarschijnlijk het begin van meer intense bodemstromingen, die mogelijks een gevolg zijn van veranderingen in het circulatiepatroon en/of wijzigingen in de lokale hellingsgraad. Deze periode valt ook ruwweg samen met de migratie van koudwaterkoralen van dieptes boven 800 m tot dieptes tussen 800 en 1000 m. De aanzet van meer energieke bodemstromingen op deze dieptes zou een dergelijke migratie kunnen gestimuleerd hebben.

Over het algemeen worden de Atlantische Marokkaanse en Ierse rand gekenmerkt door klimaatgedreven en door bodemstromingen gecontroleerde sedimentatie, met variaties tussen periodes met matige en krachtige tot erosieve en/of non-depositionele omstandigheden. De veranderingen hangen af van locatie tot locatie en zijn meestal asynchroon, wat benadrukt hoe veranderingen in de lokale pycnale gradiënt een sterk effect gehad hebben op de sedimentatie. Het beter begrijpen van de drijvende krachten achter getijde-topografische interacties vormt een belangrijke toekomstige uitdaging, voornamelijk met betrekking tot hun rol in het veroorzaken van erosieve en/of non-depositionele condities op korte en lange termijn. Deze studie verschaft duidelijke beschrijvingen van de sediment facies van contourieten, die beschouwd kunnen worden als een mogelijk analoog voor toekomstige studies gebaseerd op sedimentkernen in omgevingen die door interne getijden overheerst worden.

List of Figures

Figure 1.1 Diagram showing the main factors controlling the formation of Contourite Depositional Systems (after Faugères et al., 1993; Rebesco et al., 2014). 1–3

Figure 1.2 Map of the main contourite drifts and Contourite Depositional Systems along with global oceanic circulation pattern (graphical abstract from Rebesco et al., 2014). 1–4

Figure 1.3 Map of the North Atlantic Ocean showing the main large-scale Contourite Depositional Systems versus small-scale drift systems (modified from Rebesco et al., 2014). 1–5

Figure 1.4 Examples of large versus small-scaled moats and drifts structures formed along the MOW pathway. 1–6

Figure 1.5 Standard contourite facies model linked to variations in bottom current velocity (Gonthier et al., 1984; Stow and Faugères, 2008; Rebesco et al., 2014). 1–8

Figure 1.6 Schematic views of possible tide-topography interactions. 1–11

Figure 1.7 Simulation depicting the internal tide generation in response to a barotropic M2 semi-diurnal tidal forcing in a two layer ocean model (Simmons et al., 2004). 1–13

Figure 1.8 Examples of morpho-sedimentary products identified as primarily originating from (internal) tidal/topography interactions. 1–15

Figure 1.9 Map showing the circulation pattern of intermediate water masses within the northeast Atlantic and western Mediterranean Sea (from Hernández-Molina et al., 2011). 1–17

Figure 1.10 Sketch illustrating the role of bottom currents for living benthic cold-water corals (Hebbeln et al., 2016). 1–19

Figure 2.1 Sketch illustrating the convolution of a seismic source (wavelet) through a theoretical reflective sub-surface (modified from Al-Sadi, 1982). 2–38

Figure 2.2 Photograph of a Multi-Sensor Core Logger (MSCL) 2–43

Figure 2.3 Diagram showing incident and reflected X-ray, and the principle of XRF logging on split sediment core (Richter et al., 2006). 2–45

Figure 2.4 Diagram showing the principles of a Micromeritics Sedigraph and Malvern Mastersizer. 2–47

Figure 2.5 Plot representing the *N. incompta* versus *N. pachyderma* sinistral as a function of winter, summer and mean sea-surface temperatures at 80 m water depths. 2–49

Figure 2.6 Map of measured seawater $\delta^{18}O$ within the upper 5 meter of the surface oceans relative to the Standard Mean Ocean Water (SMOW; Schmidt, 1999; LeGrande and Schmidt, 2006). 2–51

Figure 2.7 Atlantic latitudinal cross section showing seawater Dissolved Inorganic Carbon $\delta^{13}C_{DIC}$ [‰] of the modern ocean and values inferred for the Last Glacial Maximum (Duplessy et al., 1988; Labeyrie et al., 1992). 2–52

Figure 3.1 Map and circulation pattern of the northeast Atlantic 3–67

Figure 3.2 High-resolution bathymetric map (courtesy of the Irish National Seabed Survey, GSI) and salinity profile showing the water mass stratification (World Ocean Database, 2009). 3–70

Figure 3.3 Two-way-travel time [TWT] versus depth chart, including the seismic stratigraphy, lithostratigraphy and chronostratigraphic data at DSDP Site 548 (leg 80), correlated with the SW/NE oriented seismic profile P010502..... 3–73

Figure 3.4 SW/NE oriented seismic profile (GS120610) and NW/SE oriented seismic profile (P010501). 3–74

Figure 3.5 SW/NE oriented seismic profile (GS120608)..... 3–78

Figure 3.6 NW/SE oriented seismic profile (GS120602)..... 3–80

Figure 3.7 Seismic geomorphological map of respectively unit U2 (a) and unit U1 (b)..... 3–83

Figure 3.8 Sketch illustrating the Plio-Pleistocene evolution of Goban Spur..... 3–86

Figure 3.9 Critical slope angle computed with respect to semi-diurnal internal tide propagation within present-day water column at Goban Spur. 3–88

Figure 3.10 Comparison of DSDP Site 548 at Goban Spur with IODP site U1387 at Cadiz CDS, the Le Danois CDS seismic stratigraphy and IODP site U1316 and U1317 at the Porcupine CDS, from proximal to distal (*i.e.* left to right) respective to the MOW source..... 3–89

Figure 4.1 Overview map of the north Atlantic Ocean with location of DSDP Site 548 and the main modern hydrological structures. 4–108

Figure 4.2 DSDP Site 548 showing its respective core and section divisions. 4–113

Figure 4.3 DSDP Site 548 age model and palaeo-environmental data compilation over the past 500 ky. 4–118

Figure 4.4 Grain-size distribution and plot of the main grain-size mode versus the N.pachyderma sinistral relative abundance (NPS %). 4–120

Figure 4.5 Schematic cross section of the glacial versus interglacial northeast Atlantic basin. ... 4–122

Figure 5.1 Multibeam bathymetric map of the Gulf of Cádiz and main hydrological structures (Van Rensbergen et al., 2005a; Zitellini et al., 2009). 5–143

Figure 5.2 High-resolution bathymetric map of the study area indicating the main seabed features in the area (Van Rensbergen et al., 2005a). 5–145

Figure 5.3 Core MD08-3227 multi-proxy record versus depth. 5–153

Figure 5.4 MD08-3227 bulk and terrigenous (bulk) grain-size distributions associated with the XRF Fe/Ca peak at 551-540 cm bsf. 5–155

Figure 5.5 Chronostratigraphic record obtained from core MD08-3227. 5–157

Figure 5.6 Sketch illustrating the different bottom current regimes and associated sedimentation patterns at the foot of the Pen Duick Escarpment. 5–161

Figure 6.1 Bathymetric map showing the position of core MD13-3447 with respect to the El Arraiche mud volcano province. 6–180

Figure 6.2 Salinity profiles showing the water mass stratification during (a) march and (b) September 1986 (World Ocean Database 2013). 6–184

Figure 6.3 MD13-3447 multi-proxy record versus depth.....6–192

Figure 6.4 Interpreted age model for the interval comprised between 2410 and 455 cm bsf. 6–194

Figure 6.5 Sedimentological log of a typical interval characterised by variable terrigenous silt grain-size distributions. 6–196

Figure 6.6 Sedimentological log of some key intervals, interpreted to be associated with stratigraphic gaps of variable duration. 6–198

Figure 6.7 Diagram illustrating the process through which the climatic modulation of the physical parameters is being deteriorated by the action of enhanced bottom currents. 6–201

Figure 6.8 Critical slope angle computed with respect to semi-diurnal internal tide propagation within a Antarctic Intermediate Water and a Mediterranean Outflow Water dominated profile ...6–203

Figure 7.1 Plio-Pleistocene evolution of some major sites of the Mediterranean Outflow Water Contourite Drift Complex. 7–222

Figure 7.2 Examples of existing internal tide and wave driven deposits (modified from He et al. (2008); original figure in Gao et al., 1998). 7–225

Figure 7.3 Examples of sedimentary traction features formed under different bottom current regime.....7–229

List of tables

Table 2-1 Distribution of the natural radioactivity levels for some minerals and rock types (Modified after Russell, 1944). 2–40

Table 4-1 DSDP Site 548 age model and associated interval sedimentation rates. 4–115

Table 4-2 Averaged geophysical and geochemical properties for each interpreted Marine Isotopic Stage, along with NPS relative abundances, coarse lithic grain counts and first grain-size mode.4–119

Table 5-1 MD08-3227 AMS ^{14}C ages. 5–150

Table 5-2 MD08-3227 age model and associated interval sedimentation rates. 5–151

Table 6-1 MD13-3447 interpreted age model. 6–189

Table 7-1 Summary of the main characteristics and sedimentological observations for the investigated sediment cores. 7–228

List of Abbreviations

AAIW	Antarctic Intermediate Water
AABW	Antarctic Bottom Water
AC	Azores Current
B-A	Bølling-Allerød interstadial
BIIS	British-Irish Ice-Sheet
bsf	below sea floor
CDS	Contourite Depositional System
D-O	Dansgaard–Oeschger events
DSDP	Deep-Sea Drilling Program
DSOW	Denmark Strait Overflow Water
EMPT	Early-Middle Pleistocene Transition
ENACW	Eastern North Atlantic Central Water
EPD	Early Pliocene Discontinuity
GIS	Greenland Ice-Sheet
GNAIW	Glacial North Atlantic Water
GR	Gamma Ray
HE	Heinrich Event
IPC	Iberian Poleward Current
IRD	Ice-Rafted Debris
ISOW	Iceland-Scotland Overflow Water
IODP	Integrated Ocean Discovery Program
LIS	Laurentide Ice-Sheet
LQD	Late Quaternary Discontinuity
LPD	Lower Pliocene Discontinuity
LSW	Labrador Sea Water
MIS	Marine Isotopic Stage
MOW	Mediterranean Outflow Water
MPD	Middle Pleistocene Discontinuity
MS	Magnetic Susceptibility
NADW	North Atlantic Deep Water
NPS	*Neogloboquadrina pachyderma* sinistral
ODP	Ocean Drilling Program
RD1	Porcupine Seabight Regional Discontinuity 1

wd	water depth
XRF	X-Ray Fluorescence
YD	Younger Dryas

CHAPTER 1

Introduction

Contourite drifts are defined as sediments primarily deposited and/or substantially reworked by the action of bottom currents (Faugères et al., 1993; Rebesco et al., 2005; 2008). Bottom currents are deep-water currents capable of eroding, transporting and depositing sediments along the seafloor (Hernández-Molina et al., 2016a). Those may result from the interaction of various oceanographic processes such as hyperpycnal flows, geostrophic contour currents, mesoscale eddies, internal tides and waves, benthic storms and cascading processes of various origin (Fig. 1.1; Faugères et al., 1999; Rebesco et al., 2014; Hernández-Molina et al., 2016a). Contourite drifts typically form localized sediment depocenters, characterised by the intimate association of various depositional (*e.g.* contourite drifts) and erosive (*e.g.* moats/channels) features, of which morphology and lithology highly depend on the local circulation pattern and intensity (Fig. 1.1; Stow et al., 2002a; Hernandez-Molina et al., 2003; 2009; 2016b; Llave et al., 2007; García et al., 2009; 2016). Contouritic sediments constitute one of the three end-members within a continuum of deep-sea sedimentary facies that includes pelagic and turbiditic (density driven) sediments (Rebesco et al., 2014). They often represent fast accumulating sediment bodies and are known as one of the best marine sedimentary archive, providing information on past ocean composition, properties, circulation pattern and dynamics (Gonthier et al., 1984; Faugères et al., 1993; 1999; Wold, 1994; Dunbar, 2001; Richter et al., 2001; Hassold et al., 2006; Hunter et al., 2007; Knutz, 2008; Rebesco et al., 2014; Hernández-Molina et al., 2016c; Van Rooij et al., 2016).

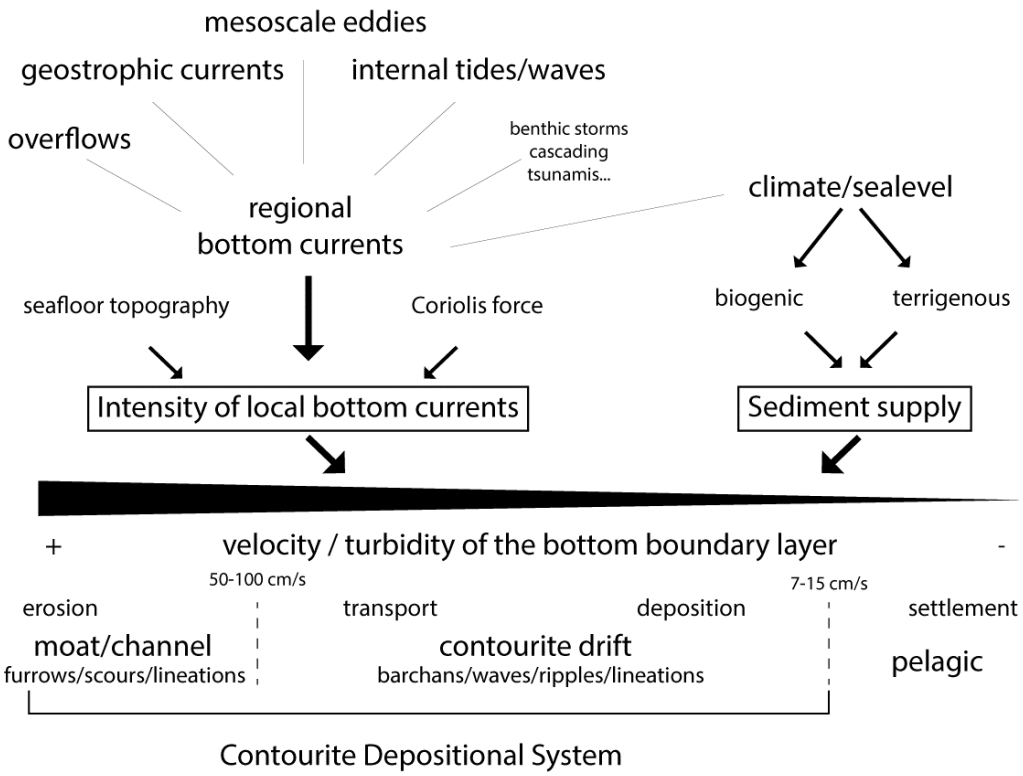

Figure 1.1 Diagram showing the main factors controlling the formation of Contourite Depositional Systems (after Faugères et al., 1993; Rebesco et al., 2014). Pre-existing seabed and bottom current interactions control particles transport and deposition, as well as the turbidity of the bottom boundary layer. The diagram indicates the pelagic versus contourite drift and erosional threshold velocity ranges (Beaulieu, 2002; Nichols, 2009; Stow et al., 2009). Note that Contourite Depositional Systems integrate erosional and depositional bottom current induced features, including bedforms.

1.1 Large versus small-scaled contourite drifts

As a matter of fact, contourite drifts were first described from the myriad of large-scale sediment bodies found over the seafloor (Fig. 1.2; Rebesco et al., 2014). Those are mainly found in association with sites of production of deep water and gateways, where well-identified (hyperpycnal) overflows and/or energetic (geostrophic) contour currents interact with the pre-existing seabed morphology (Fig. 1.2; Faugères et al., 1999; Rebesco et al., 2014). Contourites sensus-stricto are defined within deep and intermediate water depths below 300 m, since shallower bottom current sands might also have been influenced by surficial processes (Viana et al., 1998; Stow et al., 2002b). Contourite drift development is thus mainly controlled by the bottom current regime, the sediment supply and the physiographic context, and is most generally classified from their geomorphological characteristics (Faugères et al., 1993; Viana et al., 1998; 2002; Stow et al., 2002b; Hernández-Molina et al., 2008a; b; Rebesco et al., 2014). Giant elongated mounded or separated drifts are found when bottom currents interact with a sloping seabed, whereas sheeted drifts are rather

formed on broad low slope gradient areas and abyssal plains (see Rebesco et al., 2014 for a thorough classification). Giant elongated drifts are associated with contouritic moats or channels which are erosional and/or non-depositional structures along which the flow is focused (Faugères et al., 1999; Stow et al., 2002a).

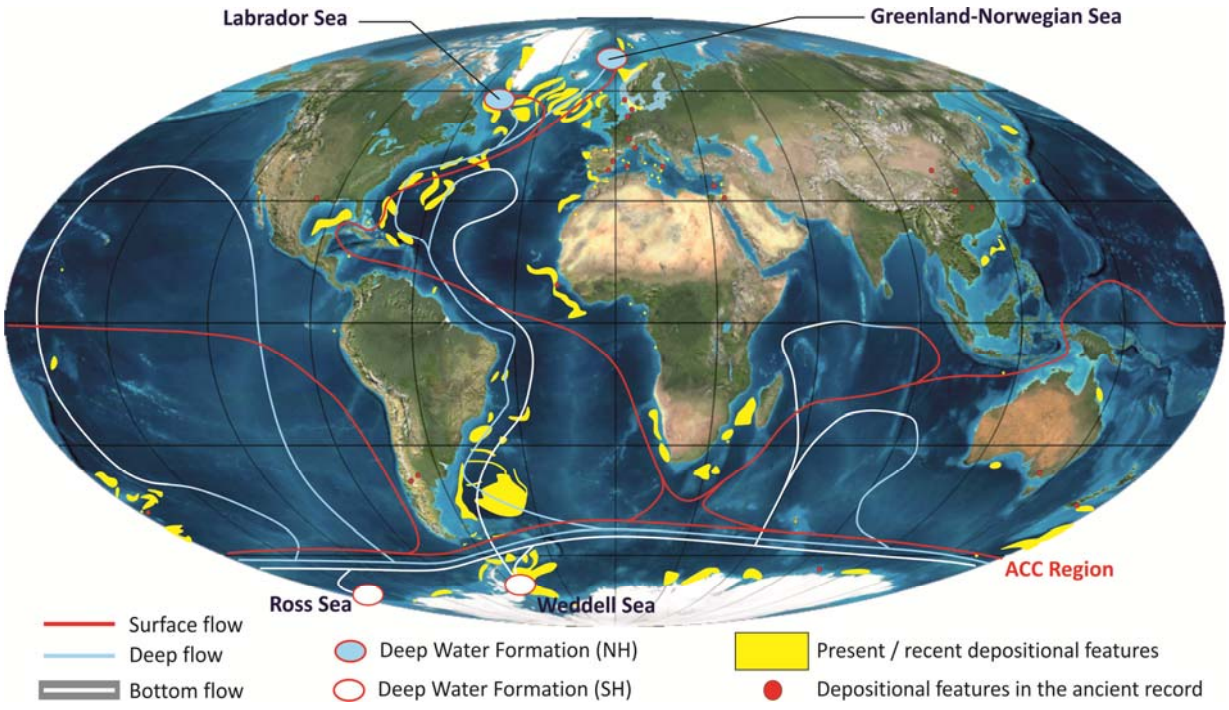

Figure 1.2 Map showing the location of the main contourite drifts and Contourite Depositional Systems along with global oceanic circulation pattern. Note contourite drifts are mainly found associated with sites of production and circulation of deep-water masses as well as gateways controlling exchanges between different basins (graphical abstract from Rebesco et al., 2014).

Within the North Atlantic Ocean, giant elongated drifts typically formed from the action of the Denmark Strait, Iceland Sea and Wyville-Thompson Ridge Overflows, the main contributors to the formation of the North Atlantic Deep Water (NADW; Wold, 1994; Faugères et al., 1993). Those cover large areas, have elongations that may reach up to several hundreds of kilometres and vertical accumulations ranging between 200 and 3000 m (Fig. 1.3; Dowling and McCave, 1993; Hassold et al., 2006; Hunter et al., 2007; MacLachlan et al., 2008; Sayago-Gil et al., 2010; Müller-Michaelis et al., 2013). Owing to the Coriolis force, the NADW forms a deep western boundary undercurrent which subsequently interacted with the western Atlantic basin to form large-scale contourite drifts, from the Gloria drift to the New Foundland drift (Fig. 1.3; McCave and Tucholke, 1986; Faugères et al., 1993; 1999; Piper, 2005; Rebesco et al., 2014).

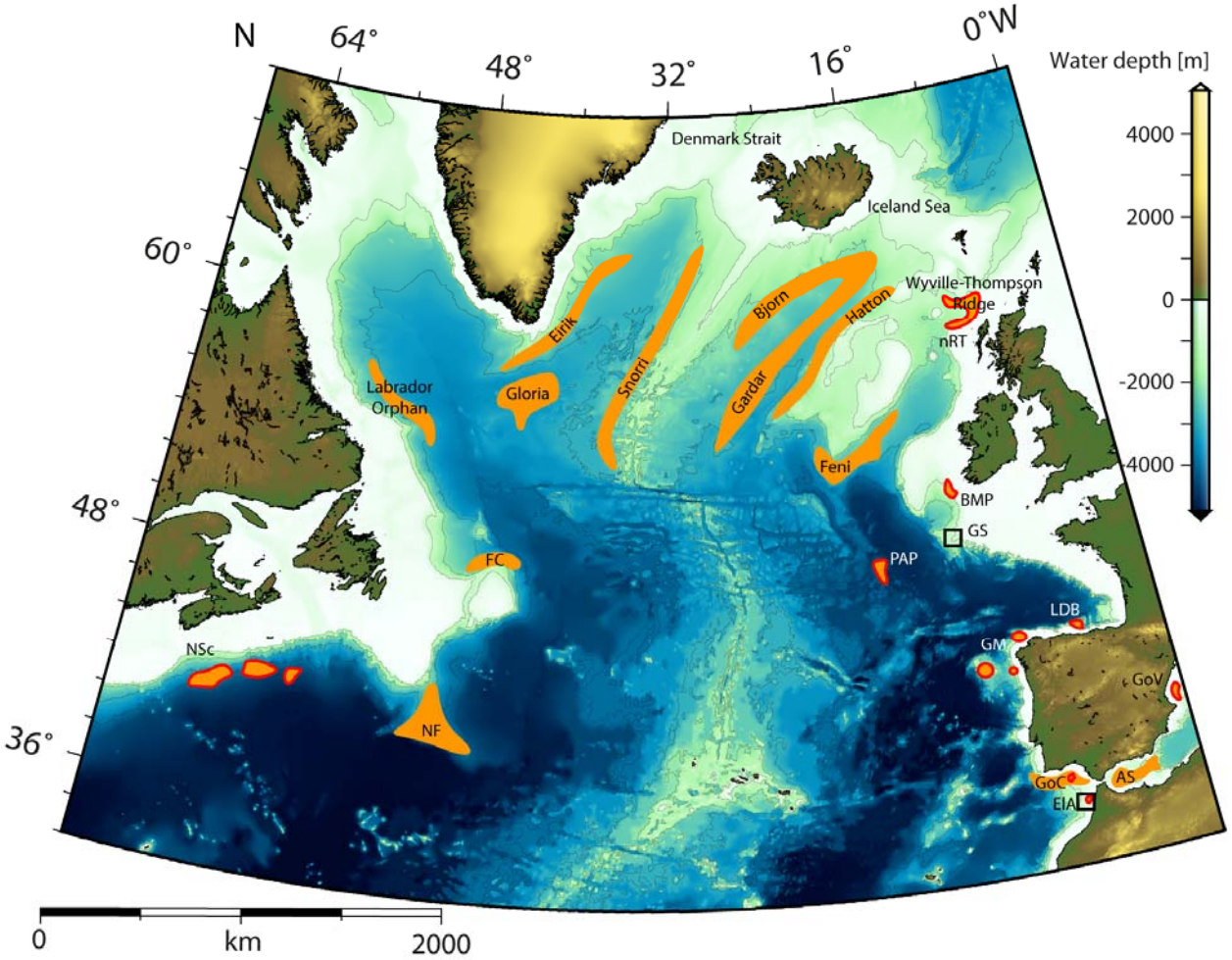

Figure 1.3 Map of the North Atlantic Ocean showing the main large-scale Contourite Depositional Systems (orange areas) versus small-scale drift systems (red outline; modified from Rebesco et al., 2014). The black squares indicate the location of the studied areas. **EIA**: El Arraiche mud volcano province; **GoC**: Gulf of Cádiz; **AS**: Alboran Sea; **GoV**: Gulf of Valencia; **GM**: Galician Margin; **LDB**: Le Danois Bank; **GS**: Goban Spur; **BMP**: Belgica Mound Province; **nRT**: northern Rockall Trough; **PAP**: Porcupine Abyssal Plain; **FC**: Flemish Cap; **NF**: New Foundland; **NSc**: Nova Scotia

The Contourite Depositional System of the northern Gulf of Cádiz and the Le Danois bank were analogically formed by energetic contour currents associated with the northward propagation of the Mediterranean Outflow Water (MOW; Van Rooij et al., 2010; Llave et al., 2011; Roque et al., 2012; Hernández-Molina et al., 2016c). Noticeably, the drifts morphology tends to be less elongated in outer-shelf and slope environments, which might be caused by the somewhat less continuous physiography for the structures to develop (Viana et al., 1998; Hernández-Molina et al., 2008a). Likewise, the Faro and the Le Danois drifts form an elongated contourite drift of few tens of kilometres long, rather representing intermediate scaled drifts (Fig. 1.4; Van Rooij et al., 2010; Hernández-Molina et al., 2016b). Those last examples largely contributed to establish the present day fundamental genetical processes driving the fossilization of past water masses circulation pattern and variability, into contourite drifts (Faugères et al., 1999; Rebesco and Camerlenghi, 2008), contouritic bedforms (Wynn and Stow, 2002; Stow et al., 2009; Kuijpers and Nielsen, 2015) and their respective sedimentary facies (Gonthier et al., 1984; Stow et al., 2002a; McCave and Hall, 2006b; Mulder et al., 2013; Alonso et al., 2016; Nishida, 2016).

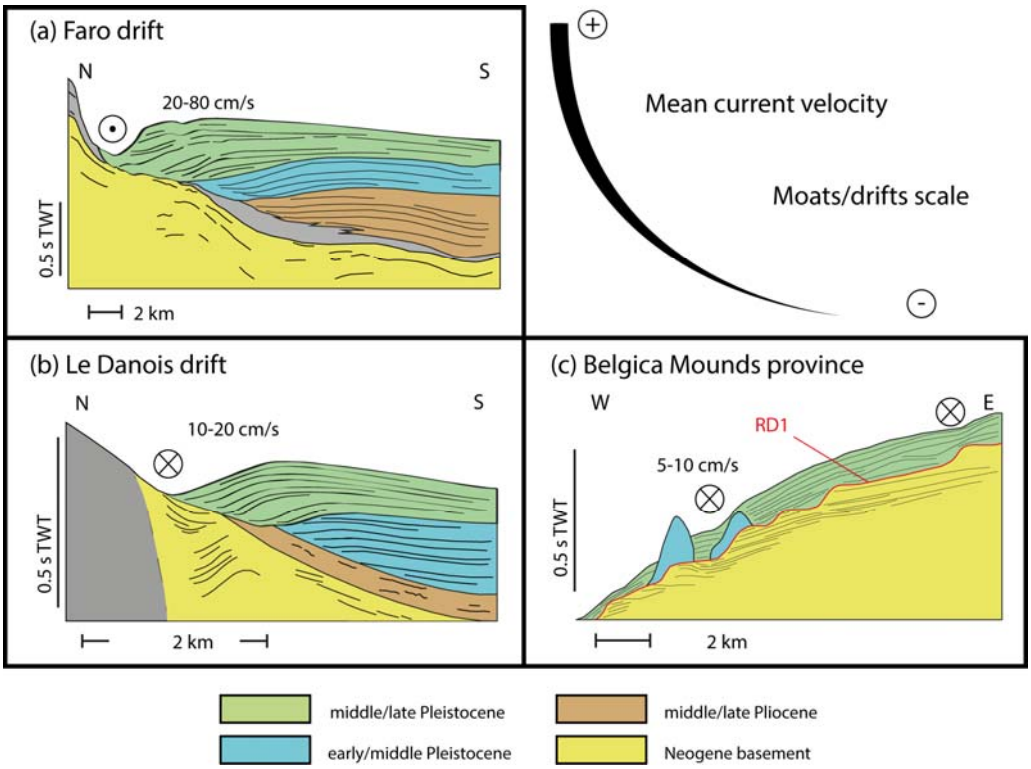

Figure 1.4 Examples of large versus small-scaled moats and drifts structures formed along the MOW pathway. (a) Interpreted seismic profile of the Faro drift from the northern Gulf of Cádiz (Hernández-Molina et al., 2014). Mean near bottom velocities associated with the hyperpycnal MOW flow are derived from Nelson et al. (1999) and Hernández-Molina et al. (2011). (b) Interpreted seismic profile of the Le Danois drift (Van Rooij et al., 2010). Mean near bottom velocities are derived from González-Pola et al. (2012). (c) Interpreted seismic profile from the Belgica Mounds province along the eastern slope of the Porcupine Seabight (Van Rooij et al., 2003; Kano et al., 2007). Mean near bottom velocities are derived from White (2007b). Note the presence of a complex and large regional discontinuity RD1.

In particular, the study of the northern Gulf of Cádiz Contourite Depositional System, to which the Faro drift belongs (Fig. 1.4a), allowed the definition of the current standard contourite facies model that links sediment facies variations as a function of bottom current intensity (Fig. 1.5; Faugères et al., 1984; Gonthier et al., 1984; Llave et al., 2006; Toucanne et al., 2007; Mulder et al., 2013; Hernández-Molina et al., 2016c). In this area, the MOW progressively evolves from a powerful overflow water, with velocities up to 200 cm/s near the Strait of Gibraltar, into an energetic contour current, flowing from ~20 to 40 cm/s south Cape St Vincent, depending on the branch and depth considered (Baringer and Price, 1999; Iorga and Lozier, 1999; Hernández-Molina et al., 2006; Carracedo Segade et al., 2015).

The standard contourite model is composed of three facies of indifferently clastic and calcareous dominated sediments, thus mainly distinguished from their respective grain-size and textural variations (Fig. 1.5). Muddy to silty and sandy facies may be organized into coarsening and finning upward sequences (Faugères et al., 1984; Gonthier et al., 1984), which can be linked to more or less energetic currents through winnowing of the fine particles in favour to the coarser ones (McCave et al., 1995; 2006a; Stow and Faugères, 2008; Rebesco et al., 2014). However, this model often suffers from the lack of unambiguous diagnostic criteria, since hydrodynamic sorting also is an important process in turbiditic environments, and similar variation might result from changes in terrigenous and/or biogenic supply in pelagic environments (Mulder et al., 2013; Alonso et al., 2016). The identification of sediment traction structures may provide important additional criteria, although those are not always observed, especially within mud dominated drifts (Shanmugam, 2008; Stow and Faugères, 2008). Therefore, an important effort is still being made in order to integrate and better characterize bedding and traction structures, degrees of bioturbation, mottled silt facies, irregular silt and/or sand pockets, gradational and/or sharp contacts, microstructures and ichnofacies into a less ambiguous model (Rodríguez-Tovar et al., 2015a; b; Alonso et al., 2016; Hernández-Molina et al., 2016c; Nishida, 2016; Takashimizu et al., 2016). Still nowadays, the application of this model requires a precise knowledge of the oceanographic and physiographic settings, which in particular may be difficult to obtain for ancient records (Rebesco et al., 2014).

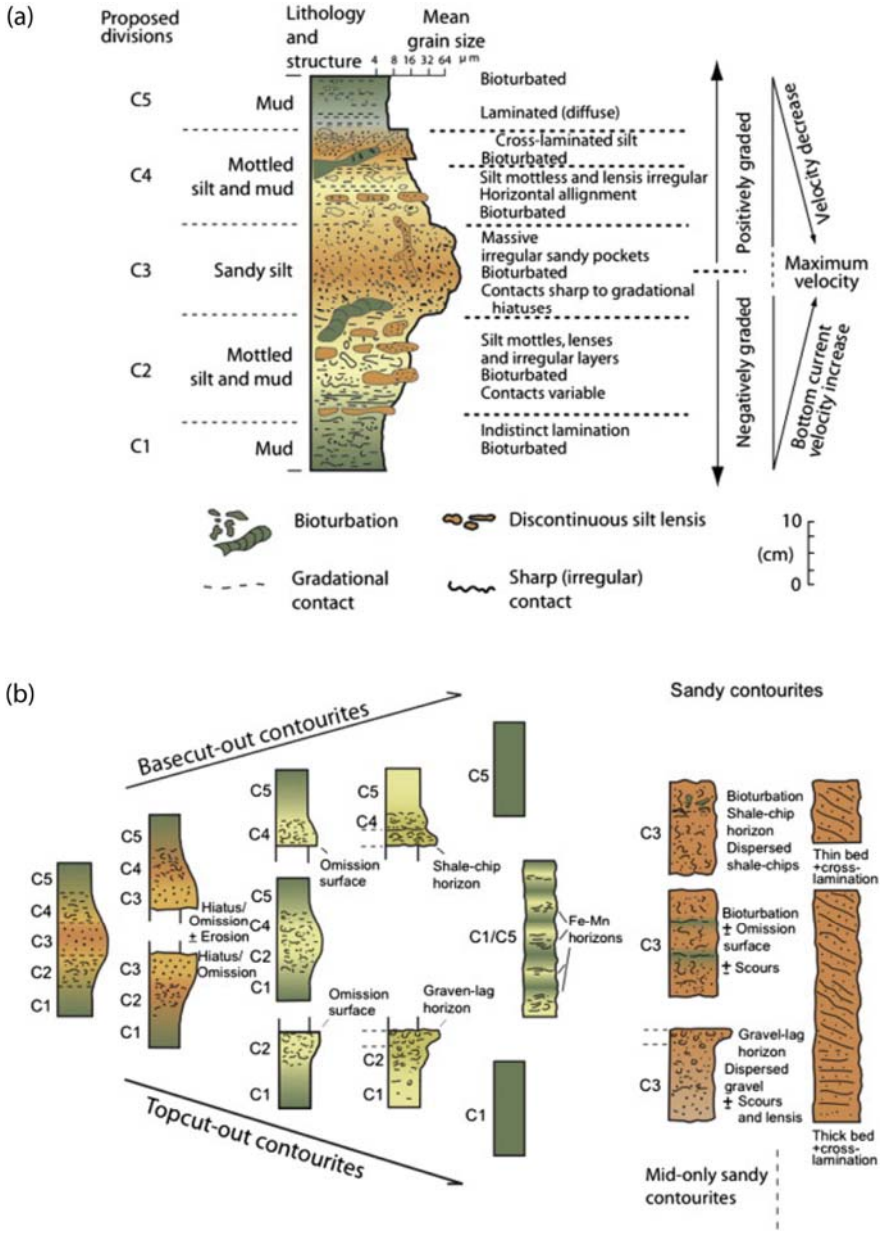

Figure 1.5 (a) Standard contourite facies model linked to variations in bottom current velocity (Gonthier et al., 1984; Stow and Faugères, 2008; Rebesco et al., 2014). (b) Variations of the standard contourite facies model, resulting from the existence of incomplete, basecut-out and topcut-out sequences, muddy and sandy contourites, commonly encountered within contouritic successions (Stow and Faugères, 2008; Rebesco et al., 2014).

The on-going discovery of a variety of small-scaled (laterally ranging a few km) contourite drifts highlights their ubiquitous occurrence, which now includes shallow seas and lakes (Fig. 1.3; Gilli et al., 2005; Van Daele et al., 2016). The Nova Scotia continental margin (Fig. 1.3) is one typical example where numerous small-scaled drifts are found in association with large-scale sediment waves and various current structures (Calvin Campbell and Mosher, 2016). The MOW formed a Contourite Depositional Complex along the northwest European margin that provides a unique example of the gradation existing between drifts scale and mean current velocities (Fig. 1.4). Small-scaled drifts often present striking geomorphological similarities with their large-scale counterparts, which largely contributed to enforce the contourite paradigm (Rebesco et al., 2008; 2014; Van Rooij et al., 2016). However, those are in contrast mainly associated with seabed irregularities, structural highs and topographic obstacles, and thus interpreted as topographically-driven drifts formed by local disturbance of the current lines (Zhang and Boyer, 1991; Rebesco et al., 2014; Falcini et al., 2016). This is because the mean contour currents, associated with thermohaline circulation, generally do not exceed 7 – 9 cm/s when considering a large portion of the ocean (Scott et al., 2010), which mostly does not exceed the sediment resuspension/transport thresholds (Figs. 1.1; Gao et al., 1998; Beaulieu, 2002; Nichols, 2009; Stow et al., 2009).

This applies to the contourite drift structures recognized along the Porcupine Seabight and Irish margin, as well as the Atlantic Moroccan Margin (Fig. 1.3c; Van Rooij et al., 2007a; 2009; Vandorpe et al., 2016). The elongation of those structures, if any exists, is conditioned by the organisation of the topographic obstacles against which they develop, and drifts tend to be isolated to each other (Van Rooij et al., 2007; Vandorpe et al., 2016). In such environments, the influence of internal waves is also often cited as an important process, modulating the contour currents towards erosional and transport threshold velocities and thus enabling contouritic processes (Ribbe and Holloway, 2001; Masson et al., 2002; Mosher and Thomson, 2002; Stow et al., 2002b; Van Rooij et al., 2003; Mienis et al., 2006; Zhang et al., 2015). When mean contour currents are slow, the bottom current regime is generally dominated by internal tides/waves motion (Gao et al., 1998; White, 2007a; He et al., 2008; White and Dorschel, 2010; Mienis et al., 2012). This raises the question about the respective importance of contour versus internal tide/wave currents. Those topographically controlled drifts traditionally have been identified as small scaled end-members within a continuum of features driven by contour current processes. However, those may as well be identified as the result of different bottom current processes such as internal tides/waves. Further than only aiding contouritic processes, internal waves processes are being increasingly recognized for playing an important mechanism driving the architecture of global margins (Gao et al., 1998; Cacchione et al., 2002; He et al., 2008; Pomar et al., 2012; Shanmugam, 2013a; Van Rooij et al., 2016).

1.2 Internal tides versus seabed interactions

Internal tides can be defined as internal waves of tidal frequency, propagating in a density stratified fluid driven by gravitational restoring forces (Lamb, 2014). Internal waves occur in a larger spectrum comprising diurnal, semi-diurnal frequencies and their harmonics, and cover a very large spectrum of higher frequencies (van Haren et al., 2002; van Haren, 2011). However, high-frequency internal waves mainly originate from the dispersion and non-linear interactions of semi-diurnal internal tides and seabed interactions, which further represent more than 60% of the total internal wave potential energy (van Haren et al., 2002; Garrett and Kunze, 2007). Thus, the moon forced semi-diurnal tidal motions (~2 cycles/day or $\sigma_{M2} = 1.405 \times 10^{-4}\, rad/s$) represent the most important forcing mechanism and often the dominant frequency when studying seabed and internal waves interactions (Shanmugam, 2013a). Tidal motions cause a vertical displacement of the density surfaces of the ocean interior, which may range from tens to several tens of meters, associated with a barotropic (along isopycnal or parallel to the pressure gradient) tidal current (Simmons et al., 2004; Garrett and Kunze, 2007). In some locations, the vertical tidal motions may reach up to 100 m, such as for example along the Atlantic Moroccan margin (Mienis et al., 2012). Those typically interact with the basin margins and a baroclinic (per definition internal) tide response occurs over the seabed, consisting in bi-directional motions having a certain angle compared to the isopycnals (Fig. 1.6). Intense boundary flow associated with bottom turbulence and mixing typically occurs when the slope gradient is equal to the natural internal wave angle of energy propagation (Ribbe and Holloway, 2001; Gayen and Sarkar, 2010, 2011). Such tide-topography interactions are said near-critical, and are the primary mechanism for the generation of internal (baroclinic) tides/waves, which further propagate within the water column (Simmons et al., 2004; Müller et al., 2012). As a consequence, energetic internal tide/wave beams radiate from areas where tide-topography interactions are near-critical (Fig. 1.7; Nycander, 2005; Klymak et al., 2011; Sánchez-Garrido et al., 2011; Shanmugam, 2013a).

The reflection conditions are predictable (Fig. 1.6b), and can be calculated as a dimensionless ratio (1) using equations of Southard and Cacchione (1972):

(1) $$l = \gamma/c$$

(2) $$c = \arctan\left(\sqrt{\left(\frac{\sigma^2 - f^2}{N^2 - \sigma^2}\right)}\right)$$

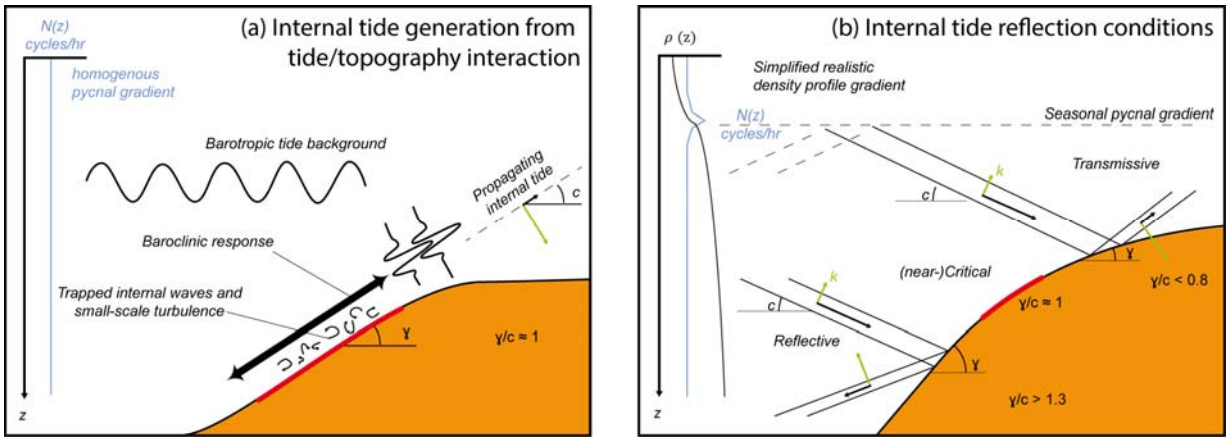

Figure 1.6 Schematic views of possible tide-topography interactions. (a) Barotropic tide-topography interactions producing an intense baroclinic (internal) tidal flow at the boundary layer. This specifically occurs when the seabed slope angle is equal to the natural internal tide angle of energy propagation (near-critical conditions; modified from Gayen and Sarkar, 2011). (b) Overview of the possible reflection conditions with respect to an internal tidal beam propagating at c[°] incidence (black arrows), interacting with a γ[°] sloping seabed (modified after Lamb, 2014). Transmissive and reflective conditions are indicated as function of the γ/c ratio. The reflected beams are narrower (shorter wave lengths), have slower group velocity and increased wave vector k. Depth $z[m]$ can be represented as the buoyancy frequency $N(z)$, which is expressed as the local variations in the vertical density gradient $\rho(z)$ (Garrett and Kunze, 2007).

Equation (1) is the ratio between the local slope gradient γ of the concerned region and c is the natural angle of energy propagation of the internal tidal beam relative to the horizontal (Fig. 1.6b). The angle c is given by equation (2) which depends on the frequency of the considered internal wave σ (here the M2 semi-diurnal tide as the main forcing frequency). The parameter f is the Coriolis frequency which depends on the latitude considered. The Coriolis frequency varies from 0 at the equator to $\pm 1.458 \times 10^{-4}\, rad/s$ at the poles, being defined as positive (negative) in the Northern (Southern) Hemisphere (Gao et al., 1998). N is the Brunt-Vaisala frequency or buoyancy frequency and is the angular frequency at which oscillate an infinitesimal portion of fluid after a small vertical displacement within a liquid at equilibrium. N is a measure of the local vertical density gradient in a stratified water column (*e.g.* Fig. 1.6b) and is given by (3):

(3) $$N = \sqrt{(\frac{g}{\rho_0})(\frac{\partial \rho}{\partial z})}$$

Where g is the gravitational constant, ρ_0 a constant reference pressure and $\frac{\partial \rho}{\partial z}$ the local density gradient as derivative of the depth z. Given equations (1) to (3), it is possible to calculate the reflection conditions at any site over the margin and compare it to bounding relation (4) from McPhee-Shaw (2006):

(4) $$0.8 < \gamma/c < 1.3$$

When the l ratio falls within limits defined by (4), reflection conditions are (near-)critical (Southard and Cacchione, 1972; Cacchione et al., 2002; McPhee-Shaw and Kunze, 2002; Lamb, 2014). Under such conditions (Fig. 1.6), near bottom velocities potentially exceed 40 cm/s and shear stresses are maximal, generally well above the threshold of sediment erosion and transport (Ribbe and Holloway, 2001; Cacchione et al., 2002; Turnewitsch et al., 2008). When ratio γ/c is largely above 1, a substantial portion of the incident internal tide beam is reflected backwards into the basin. The reflected beam is both composed of internal tides and internal waves of shorter wave lengths due to the dissipation of energy (Egbert and Ray, 2000; Klymak et al., 2011; Lamb, 2014). When ratio γ/c is largely below 1, the incident internal tide beam is mainly transmitted forwards. It might experience series of reflections between the continental shelf and the surface mixed surface layer until the energy fully dissipates (Fig. 1.6b; Klymak et al., 2011; Lamb, 2014).

Internal waves generated from such (barotropic) tide-topography interactions (Fig. 1.6a) may have frequencies ranging between the buoyancy frequency N and the local inertial frequency f (van Haren et al., 2002; White and Dorschel, 2010). As a result, near-inertial internal waves motions may dominate the bottom current regime in some locations such as for example within the Gulf of Valencia (Fig. 1.8; van Haren et al., 2013; Ribó et al., 2015) or within the central North Sea (van Haren et al., 1999). High frequency and large amplitude internal waves are typically formed when tidal currents interact with shallow sills, forming regular wave packets travelling within the intermediate ocean and permanent thermocline (Apel, 2000, 2002; Sánchez-Garrido et al., 2011; Shanmugam, 2013). However, in many locations the internal wave response mainly occurs at the forcing (tidal) frequency, such as for example along open continental margins of the northwest European margin (Shanmugam, 2003; Dorschel et al., 2007; Mienis et al., 2007; White and Dorschel, 2010; Mienis et al., 2012; Mulder et al., 2012). In such cases, the bottom current regime can be denominated as internal tidal bottom currents, or deep-sea marine tidal currents when located below the permanent pycnocline and sea surface processes (Shanmugam, 2013). Beyond the frequency spectrum of internal waves at a particular location, internal waves and tides and topography interactions respond to similar forces although they may take various forms (Lamb, 2014). The frequency of the internal waves, as well as the morphology of the bottom topography must be taken into account in order to predict and understand the nature of such interactions (Garrett and Kunze, 2007).

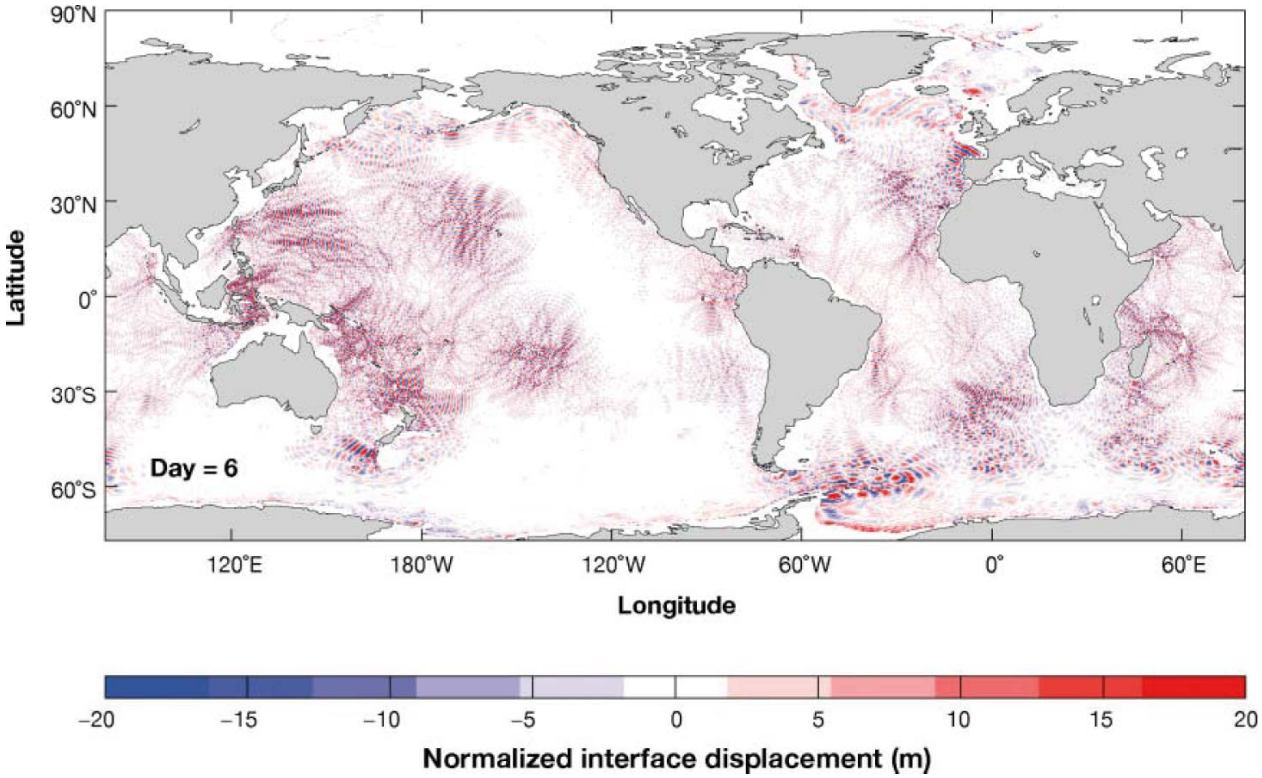

Figure 1.7 Simulation depicting the internal tide generation in response to a barotropic M2 semi-diurnal tidal forcing in a two layer ocean model (Simmons et al., 2004). The map shows the normalised interface displacement at 1100 m water depths after 6 days of forcing. Beam-like internal tides are generated from significant (near-critical) topographic features (Fig. 1.5a). Note the increasing wave length with latitude is here mainly apparent (map projection) although also occurs due to variations in the Coriolis frequency f.

Increased bottom boundary layer turbidity and hydrodynamic sorting of particles, driven by (internal) tide-topography interactions, were directly observed on Goban Spur and Irish margin (van Weering et al., 1998; 2001; Thomsen and Gust, 2000; McCave et al., 2001). Similarly, the internal tide ability to rework and enhance the basinwards transport of sediments was also directly observed along the Iberian margin (Schmidt et al., 2002; van Weering et al., 2002). Enhanced internal tide processes along marked pycnal gradients were also proposed to play a role for the generation and propagation of intermediate nepheloid layer within the open ocean, thus playing an important role on particles dispersal and sediment redistribution (Thomsen and Gust, 2000; McPhee-Shaw et al., 2002; 2006; Puig et al., 2004). Kilometre-scale topographic obstacles may also cause local critical reflection conditions (Garrett and Kunze, 2007), which were subsequently inferred to cause increased sediment particles fluxes as far deep as the Porcupine Abyssal Plain (Figs 1.1; Turnewitsch et al., 2008; Peine et al., 2009). Internal tides and waves seem thus capable of inducing erosional and/or non-depositional conditions over large time-scales (several millions of years), and were thus

proposed as a potential driving mechanism for explaining global aspects of continental margin morphologies (Cacchione et al., 2002).

However, the recognition of internal wave morpho-sedimentary features has been far more challenging (Fig. 1.8). Examples are the formation of contouritic terraces associated with marked pycnal gradients at water mass boundaries, presumably causing locally erosive and/or non-depositional conditions (Fig. 1.8a). This is because pycnal gradients have an important potential energy for baroclinic motions to develop (Shanmugam, 2013). Those were described in different environments as for example along the Argentinian margin (Preu et al., 2013), the Galician continental margin (Maestro et al., 2013; Hernández-Molina et al., 2016a) and the Alboran Sea (Ercilla et al., 2016; Juan et al., 2016). Up to now, only few small-scaled contourite drift structures (Fig. 1.8b; Vandorpe et al., 2016) and few large-scale sediment wave fields (Fig. 1.8c; He et al., 2008; Ribó et al., 2015) could be primarily related to deep-sea tidal and/or internal wave bottom currents.

The first internal tide sediment facies description was introduced by Gao and Eriksson (1991). Since then, only few similar studies, strictly based on outcrops, could be conducted and mainly rely on the clear identification of bi-directional sediment traction structures (He et al., 2008; Bádenas et al., 2012; Gao et al., 2013). However, tide-topography interactions and associated internal tides/waves processes are recognized as a largely under-explored mechanism in modern series (Gao et al., 1998; Mosher and Thomson, 2002; Howe et al., 2006; He et al., 2008). The reasons are partly explained by the fact that traction structures and lateral facies changes are broadly not observed when working from sediment cores. Sediments potentially re-suspended from internal tidal processes are easily redistributed by the background oceanic circulation, ultimately leading to very similar morphological and sedimentological characteristics (Pomar et al., 2012; Shanmugam, 2013a, b). There still exists no consensus on objective morpho-sedimentary diagnostic criteria to distinguish internal tide deposits from contour currents ones (Pomar et al., 2012; Shanmugam, 2013b). A large knowledge gap regarding the sedimentary facies of those deposits, a clear lack of core based sedimentary studies, and the absence of firmly established lithological analogue still persist (Shanmugam, 2008; Bádenas et al., 2012; Hanebuth et al., 2015). However, understanding those characteristics may be useful in order to trace changes in the past ocean circulation pattern, the water column stratification, and could solve many problems inherent to incomplete records since they seem to constitute an important erosional process.

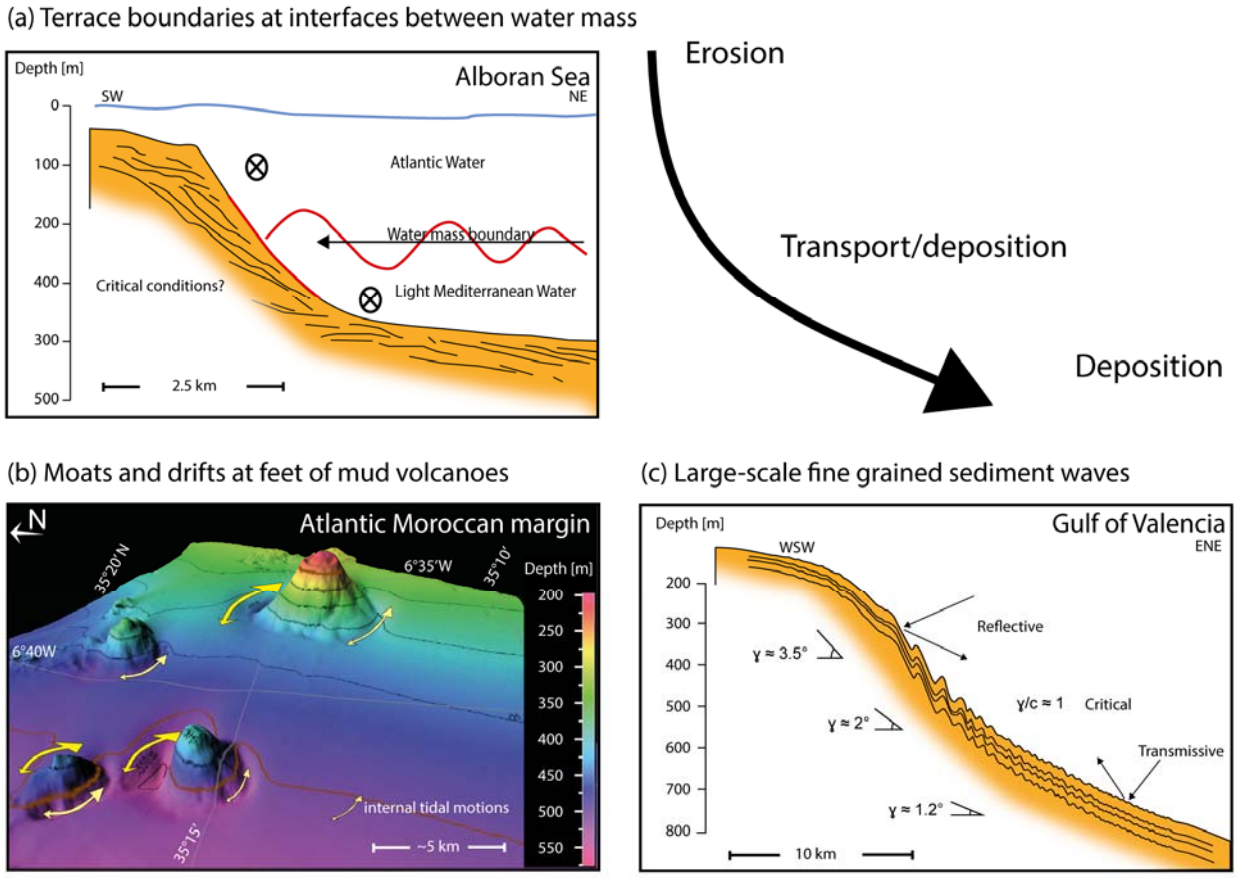

Figure 1.8 Examples of morpho-sedimentary products identified as primarily originating from (internal) tidal/topography interactions. (a) Contouritic terraces formed by an enhanced internal tidal regime at water mass boundaries causing local erosive/non depositional conditions in the Alboran Sea (Ercilla et al., 2016; Juan et al., 2016). (b) Asymmetric moats and drift structures interpreted to relate to internal tidal processes in the Atlantic Moroccan margin (Vandorpe et al., 2016). (c) Large-scale fine-grained sediment waves morphology as function of reflection conditions from the Gulf of Valencia (Ribó et al., 2016).

1.3 Evolution of the Mediterranean Outflow Water

The study of the MOW-induced contourite drifts along the northwest European margin (Fig. 1.4; 1.9) offers a unique opportunity to investigate large-scale versus small-scale contourite drifts, and the relative importance of different bottom current processes such as contour currents, mesoscale eddies and internal tidal currents (Hernández-Molina et al., 2011; 2016a; Zhang et al., 2015). The abrupt change in the margin orientation at Cape St Vincent strongly affects the MOW causing important flow instabilities and the formation of MOW-derived mesoscale eddies (Fig. 1.9; Cherubin et al., 2000; Barbosa Aguiar et al., 2013). The portion of the MOW which is not detached from the main flow evolves as a relatively less energetic contour current (< 40 cm/s) which propagates along the northwest European margin, while the rest forms an eddy-driven flow propagating southwestward within the intermediate open Atlantic Ocean (Fig. 1.9; Serra et al., 2005; 2010; Lozier and Nicole, 2008; Bozec et al., 2011). Along the Iberian margin, the northward flowing branch

is responsible for the formation of different contourite drifts systems and topographically controlled drifts, where energetic mesoscale eddies and internal tidal processes gain in importance with respect to contouritic processes (García Lafuente et al., 2008; Van Rooij et al., 2010; Hanebuth et al., 2015; Zhang et al., 2015; Hernández-Molina et al., 2016a). In a more distal domain, hereafter referred to as the Goban Spur and Porcupine Seabight, the MOW mostly equilibrated within the background thermohaline circulation, at water depths ranging from 800 to 1000 m (Iorga and Lozier, 1999; Bozec et al., 2011).

The initial inception of modern-like MOW is thought to occur briefly after the post-Messinian re-opening of the Strait of Gibraltar at about 5.33 Ma (Marchès et al., 2010; Llave et al., 2011; Roque et al., 2012). However, the first clear evidence of MOW controlled sedimentation was only recognized from ~4.5 Ma within the northern Gulf of Cádiz (Hernández-Molina et al., 2016b). Along distal areas, such as Goban Spur, clear evidences relate the influence of the MOW from about 3.6 Ma during the middle-late Pliocene (Khélifi et al., 2009; 2014). Subsequently, the northern Gulf of Cádiz Contourite Depositional System could be subdivided into three main contouritic phases, primarily driven by tectonic processes, sea-level and climatic oscillations (Hernández-Molina et al., 2014; 2016b). Those contouritic phases overall document successive relative intensifications of contouritic processes, respectively occurring from 4.5, 3.2 and ~2 Ma onwards, and separated by margin wide discontinuities (Hernández-Molina et al., 2016b). A very comparable morpho-sedimentary evolution has taken place along northern Iberian margin, with the development of the Le Danois Contourite Depositional System (Van Rooij et al., 2010).

Along the Porcupine Seabight, the MOW typically induced topographically controlled contourite drifts, associated with important provinces of cold-water coral mounds from about 2.5 Ma onwards (Van Rooij et al., 2003; 2007a; 2009; Rüggeberg et al., 2007; Thierens et al., 2010; Raddatz et al., 2014). The association of past living cold-water corals and cold-water coral mounds is also characteristic of the Atlantic Moroccan margin, which is influenced by the incursion of the MOW mesoscale eddies (Foubert et al., 2008; Wienberg et al., 2010; Van Rooij et al., 2011; Vandorpe et al., submitted). This suggested a certain analogy between those sites, potentially linked to the dynamic of the MOW (Van Rooij et al., 2011). However, the past and present connectivity between those proximal versus distal sites is only partly resolved (Rogerson et al., 2012). Both the MOW and cold-water coral occurrences undergo a strong climatic modulation (Wienberg et al., 2010; Frank et al., 2011; Rogerson et al., 2012; Raddatz et al., 2014). The MOW composition and behaviour are modulated by climatic conditions over the Mediterranean Sea, and more importantly by hydraulic forcing at the Strait of Gibraltar, and the Atlantic composition and circulation pattern (Rogerson et al., 2012; Rohling et al., 2014).

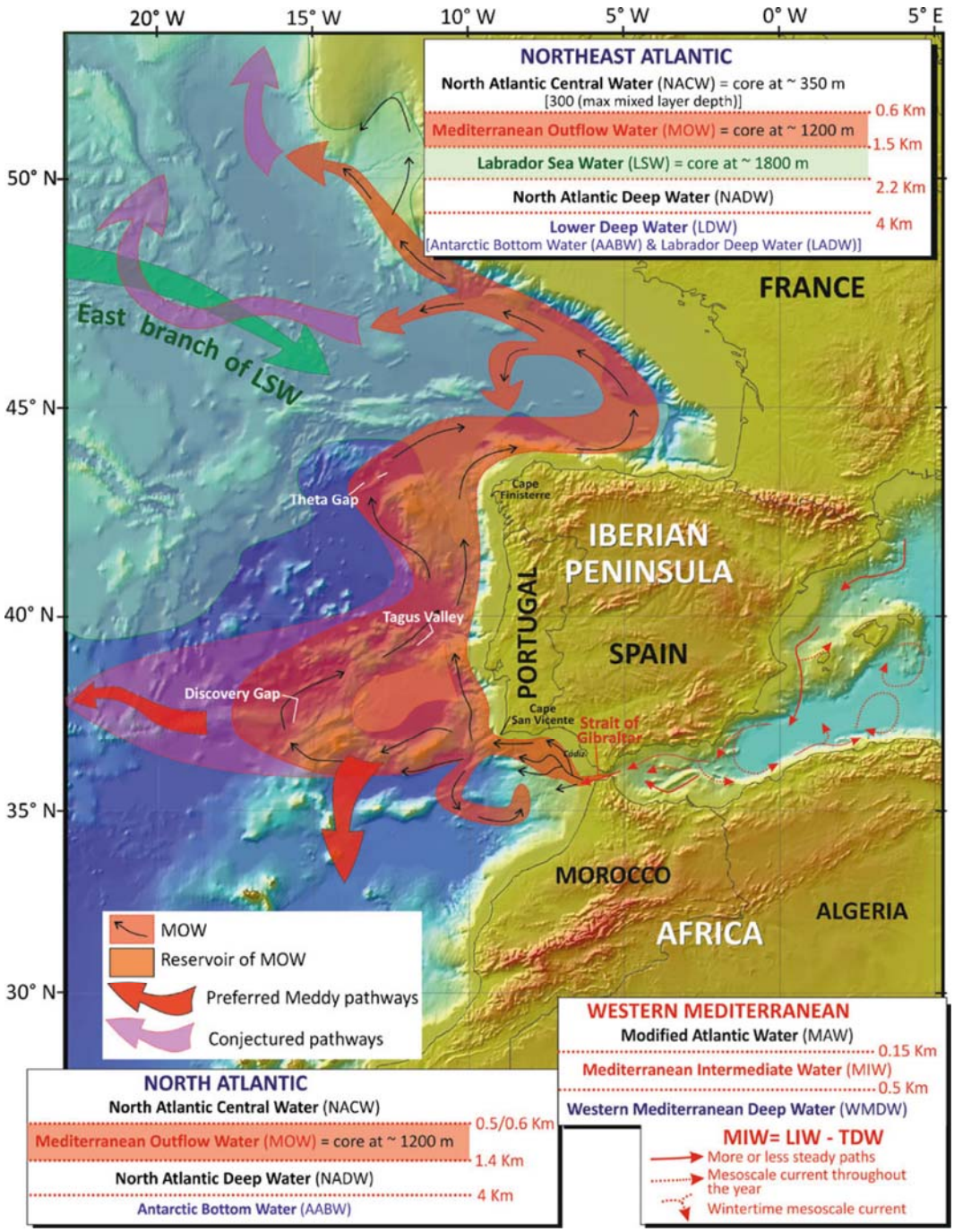

Figure 1.9 Map showing the circulation pattern of intermediate water masses within the northeast Atlantic and western Mediterranean Sea (from Hernández-Molina et al., 2011). The MOW main depth range is indicated with respect to the northeast Atlantic water column. Note the MOW propagation is conditioned by its northward advection, or geostrophic branch, as well as by the dynamic and pathways of the forming Mediterranean mesoscale eddies (meddies).

During glacial periods of the middle/late Pleistocene, low sea-level stands and associated climate aridification over the Mediterranean Sea caused the formation of a denser MOW plume (Rogerson et al., 2005; Bahr et al., 2015). This influenced the main flow pathways over sub-millennial to millennial time-scales, and ultimately influenced the settling depth range of the MOW salinity anomaly along the Iberian and Irish margin (Ercilla et al., 2008a; b; Li et al., 2011; Maestro et al., 2013; Raddatz et al., 2014; Hernández-Molina et al., 2016a). Those variations may in turn have caused changes in the deep-sea tidal bottom currents occurring along the pycnal gradients formed at the MOW lower and upper interface (Rice et al., 1990; Whitea, 2007; Maestro et al., 2013; Raddatz et al., 2014; Hernández-Molina et al., 2016a).

During recent glacial periods, cold-water corals are known to thrive along the Atlantic Moroccan margin while being absent from the Irish margin, and reciprocally during interglacials (Frank et al., 2011). Cold-water corals are known to be strongly dependent on primary productivity particulate organic matter export, as well as the presence of energetic bottom currents, which both play a role in terms of food particles availability and sediment delivery for the mounds formation (Fig. 1.10; Wienberg and Titschack, 2015; Hebbeln et al., 2016). During the past climate cycle, the migration of the sub-polar front has controlled the primary productivity pattern and might as well have controlled the distribution of cold water corals (Frank et al., 2011). Internal tides are also thought to have played an important role in driving the past and present cold-water coral mound distribution along the Porcupine Seabight and Rockall Trough (Fig. 1.10; Rice et al., 1990; White et al., 2001; 2005; 2007b; Mienis et al., 2007; 2009; Mohn et al., 2014). This point towards processes associated with the composition and propagation of the MOW, as well as secondary processes occurring along its upper and lower interfaces (Raddatz et al., 2014). During the last glacial maximum (23 to 18 ka BP), the MOW most probably remained confined along the Portuguese margin (Schönfeld and Zahn, 2000), which would have also contributed to the deterioration of environmental conditions for the cold-water corals of the Irish margin (Li et al., 2011; Raddatz et al., 2014).

Within the Porcupine Seabight, the complex seabed palaeo-topography and overall steep slopes regionally led to the presence of (sub-)critical slopes with respect to propagation of semi-diurnal internal tides (Rice et al., 1990; White et al., 2007a; Mohn et al., 2014). Records obtained from sediment drifts and coral mounds exhibit complex sequences bearing frequent stratigraphic hiatuses, ranging from thousands to hundreds of thousands years, substantially limiting palaeo-environmental reconstructions associated to the MOW and cold-water coral ecosystems (Dorschel et al., 2007; Rüggeberg et al., 2007; Van Rooij et al., 2007b; Raddatz et al., 2011; 2014). Thus, the knowledge of the past bottom current variability is largely incomplete and unresolved on millennial time-scales. Additionally, the cold-water coral mounds of the Porcupine Seabight are being rooted on a regional

discontinuity regional discontinuity RD1 spanning at least ~7 My and which could be, at least partly, attributed to the action of energetic bottom currents (Fig. 1.4c; Van Rooij et al., 2003; Kano et al., 2007; Huvenne et al., 2009; Raddatz et al., 2014). Consequently, the palaeo-environmental reconstruction for this part of the margin is also largely incomplete over the late Miocene to Pliocene period. From within the Atlantic Moroccan margin, there exists yet no sediment based bottom current variability reconstructions. This tends to emphasize on the importance to constrain the expression and variability of internal tidal dominated bottom currents over the sedimentary record. This also has implications for the understanding of the past distal MOW variability within the intermediate northeast Atlantic, as well as sedimentary environment changes and their effect on benthic cold-water coral ecosystems.

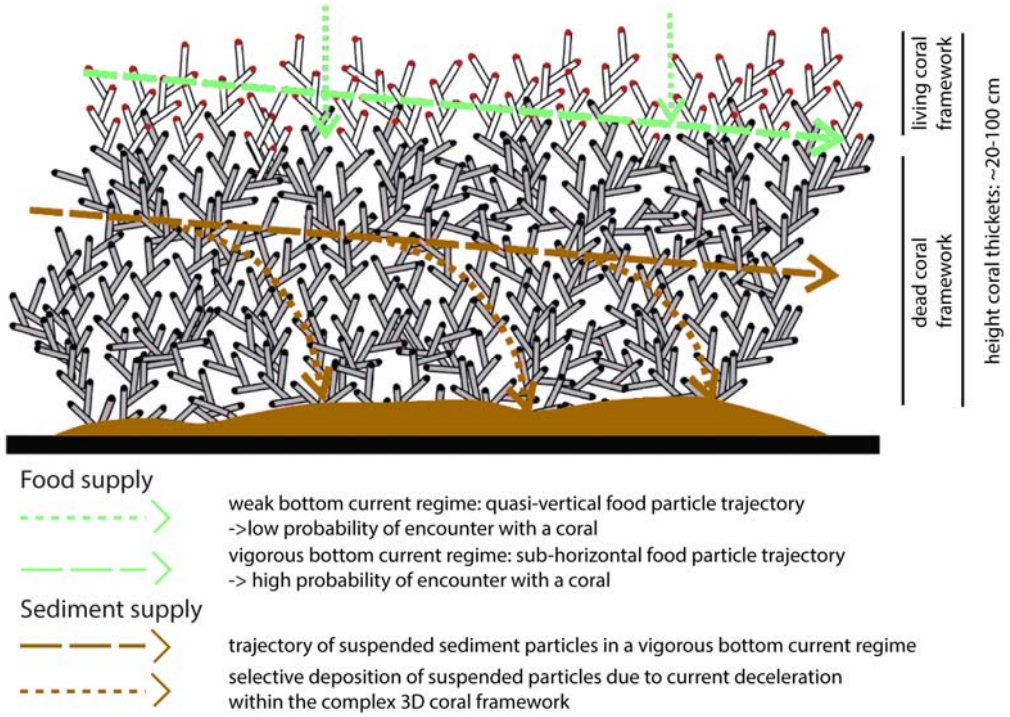

Figure 1.10 Sketch illustrating the role of bottom currents for living benthic cold-water corals (Hebbeln et al., 2016). Bottom currents play a major role in terms of food particles availability for the living coral. Increased sediment delivery contributes to framework stabilization, playing a role for cold-water coral mound formation.

1.4 Rationale of this study

This study aims to contribute to the comprehension, significance and variability of contouritic processes within sedimentary environments in which bottom currents are dominated by deep-sea tidal bottom currents, and to examine their potential to reconstruct the past circulation patterns and variability. Additionally, this work aims to contribute to the knowledge of the past variability of the MOW at a millennial time-scale resolution, both towards its distal northern and southern pathways. Millennial scale bottom current variability reconstructions are intended in order to better constrain the regional palaeo-environmental variations over periods of alternatively thriving and decaying cold-water coral ecosystems (Wienberg et al., 2010; Frank et al., 2011; Raddatz et al., 2014). This study is mainly based on sediment core analysis, which may provide substantial information on sediment facies presumably deposited in internal tide dominated bottom current environments. This Ph.D. dissertation is organized in 4 distinct research chapters focused on three different study areas, in which however some common research questions consistently apply:

- How is the bottom current intensity expressed in terms of large scale sediment geomorphological architecture and sediment facies variations?
- Are sediment facies variations of small-scaled contourite drifts comparable to variations existing in their large-scale counterparts?
- How is the recorded bottom current intensity related to water mass circulation and other oceanographic processes?
- How do the above mechanisms play a role in terms of erosional processes?
- How do the above mechanisms influence cold-water coral ecosystems and is there a coupling between the existence of those ecosystems and the bottom currents (palaeo-)intensity?

The first area of interest is the Goban Spur, located at the boundary between the Celtic and Irish margin, at the southern tip of the Porcupine Seabight (Fig. 1.3). Being located along the present day MOW lower boundary (Fig. 1.9), this site has successively been cored during the DSDP leg 80 (Site 548), and studied for the importance of oceanographic processes on sediment dynamics throughout the Ocean Margin Exchange (OMEX) program (Thomsen and van Weering, 1998; Huthnance et al., 2001). It is also known to form a smooth submarine plateau, and thus the impact of internal tides can be expected to be less marked than along the Porcupine slopes (Rice et al., 1990). Based on sub-surface geomorphological observations using high resolution seismic data, **chapter three** aims to assess the potential of Goban Spur in monitoring the past variability of the MOW. This may help to

constrain the Plio-Pleistocene stratigraphic framework and depositional environment variability which dominated DSDP Site 548, at an intermediate site between the Iberian margin and the Porcupine Seabight. Thus Goban Spur may represent a critical site in order to better understand the (suite of) processes that have led to the creation of the large RD1 unconformity, as well as the subsequent formation of CWC mounds and associated contourite drifts of the Porcupine Contourite Depositional System.

Chapter four is based on DSDP Site 548 sediment record spanning the middle-late Pleistocene. The objectives are to investigate glacial versus interglacial changes in the bottom current regime throughout the past 500 ky. Several studies from the Porcupine Seabight inferred that the MOW might have settled within deeper water depths during glacial periods, and thus may have no longer influenced the cold-water coral of this margin (Thierens et al., 2010; Raddatz et al., 2014). The objective is to determine whether the MOW still propagated towards those latitudes, or experienced latitudinal shifts between the Irish and Iberian margin, in a possibly similar pattern than during the past climate cycle (Schönfeld and Zahn, 2000). If such shifts are observed, the objective is to determine their precise timing, which remains poorly constrained along the complex Porcupine Seabight, specifically beyond the last climate cycle ~110 ka BP (Dorschel et al., 2005; Ovrebo et al., 2006; Rüggeberg et al., 2007; Van Rooij et al., 2007b). Likewise, this may help in constraining the bottom environment variability with respect to the cold-water coral ecosystems of the Porcupine Seabight.

Subsequently, two distinct studies are focused on the bottom current variability along the Moroccan Atlantic margin. The two sites were selected from their respective depth with respect to the currently known contourite drifts of this portion of the margin, as well as the present day position of the MOW mesoscale eddies in this sector (Mienis et al., 2012; Vandorpe et al., 2016). **Chapter five** is based on a sequence recovered from an important topographically controlled drift of this region (Vandorpe et al., 2014). It constitutes the only site which was recovered from a sediment drift sensus stricto, while the others were recovered in open slope settings. Even though it was recently shown to not have been influenced by the southward flow of the MOW, the bottom currents and sediment dynamics are seemingly dominated by internal tidal processes, of which past variability remain unconstrained at the millennial time-scale (Mienis et al., 2012; Vandorpe et al., 2016). Independently of the MOW, the extensive presence of cold-water coral mounds in the surrounding makes this site an interesting analogue for studying bottom currents in relation with cold-water coral ecosystems. Using multiproxy palaeo-environmental record, the objective is to constrain the bottom current variability which was responsible for the formation of the sediment drift at millennial time-scales, and to compare it with known regional occurrences of cold-water coral of this sector. This

constitutes a first step in establishing whether or not bottom currents have played a role for their development, in a possibly similar pattern than that observed along the Porcupine Seabight.

Chapter six is based on a sediment core which was recovered at 968 m water depths, currently clearly influenced by the regular incursion of Mediterranean mesoscale eddies (Mienis et al., 2012; Vandorpe et al., 2016). The sediment core was recovered in an open slope setting characterised by a low slope gradient. The objective is to assess the early-middle Pleistocene bottom current variability, possibly mainly associated to the Mediterranean mesoscale eddies dynamic and/or internal tide processes. This might constitute the first bottom current record driven by the MOW south of the Strait of Gibraltar. Variations in the past behaviour, formation rate and impact of the Mediterranean mesoscale eddies are fundamental in order to understand past changes in the behaviour and distribution of the MOW within the intermediate northeast Atlantic.

Finally, **chapter seven** aims to review some singular observations and main results obtained throughout, in order to provide a more general discussion with respect to the importance and impact of internal tidal contouritic processes in the northeast Atlantic. The main depositional and erosional features observed in this study are reviewed. The objective is to point out the existence or the absence of discriminating criteria between internal tide and contour current processes. The main conclusions of this thesis are drawn and outlooks for possible further studies are considered.

References

Apel, J.R., 2000. Solitons near Gibraltar: views from the European remote sensing satellites. Report GOA 1.

Apel, J.R., 2002. Oceanic internal waves and solitons. An atlas of oceanic internal solitary waves, 1-40.

Alonso, B., Ercilla, G., Casas, D., Stow, D.A.V., Rodriguez-Tovar, F.J., Dorador, J., Hernandez-Molina, F.J., 2016. Contourite vs gravity-flow deposits of the Pleistocene Faro Drift (Gulf of Cadiz): Sedimentological and mineralogical approaches. Marine Geology 377, 77-94.

Bádenas, B., Pomar, L., Aurell, M., Morsilli, M., 2012. A facies model for internalites (internal wave deposits) on a gently sloping carbonate ramp (Upper Jurassic, Ricla, NE Spain). Sedimentary Geology 271–272, 44-57.

Bahr, A., Kaboth, S., Jiménez-Espejo, F.J., Sierro, F.J., Voelker, A.H.L., Lourens, L., Röhl, U., Reichart, G.J., Escutia, C., Hernández-Molina, F.J., Pross, J., Friedrich, O., 2015. Persistent monsoonal forcing of Mediterranean Outflow Water dynamics during the late Pleistocene. Geology.

Barbosa Aguiar, A.C., Peliz, Á., Carton, X., 2013. A census of Meddies in a long-term high-resolution simulation. Progress In Oceanography 116, 80-94.

Baringer, M.O., Price, J.F., 1999. A review of the physical oceanography of the Mediterranean outflow. Marine Geology 155, 63-82.

Beaulieu, S.E., 2002. Accumulation and Fate of Phytodetritus on the Sea Floor, Oceanography and Marine Biology, An Annual Review, Volume 40. CRC Press, pp. 171-232.

Bozec, A., Lozier, M.S., Chassignet, E.P., Halliwell, G.R., 2011. On the variability of the Mediterranean Outflow Water in the North Atlantic from 1948 to 2006. Journal of Geophysical Research-Oceans 116.

Cacchione, D.A., Pratson, L.F., Ogston, A.S., 2002. The Shaping of Continental Slopes by Internal Tides. Science 296, 724-727.

Calvin Campbell, D., Mosher, D.C., 2016. Geophysical evidence for widespread Cenozoic bottom current activity from the continental margin of Nova Scotia, Canada. Marine Geology 378, 237-260.

Carracedo Segade, L.I., Gilcoto, M., Mercier, H., Pérez, F.F., 2015. Quasi-synoptic transport, budgets and water mass transformation in the Azores–Gibraltar Strait region during summer 2009. Progress In Oceanography 130, 47-64.

Cherubin, L., Carton, X., Paillet, J., Morel, Y., Serpette, A., 2000. Instability of the Mediterranean Water undercurrents southwest of Portugal: effects of baroclinicity and of topography. Oceanologica Acta 23, 551-573.

Dorschel, B., Hebbeln, D., Rüggeberg, A., Dullo, C., Freiwald, A., 2005. Growth and erosion of a cold-water coral covered carbonate mound in the Northeast Atlantic during the Late Pleistocene and Holocene. Earth and Planetary Science Letters 233, 33-44.

Dorschel, B., Hebbeln, D., Foubert, A., White, M., Wheeler, A.J., 2007. Hydrodynamics and cold-water coral facies distribution related to recent sedimentary processes at Galway Mound west of Ireland. Marine Geology 244, 184-195.

Dowling, L.M., McCave, I.N., 1993. Sedimentation on the Feni Drift and late Glacial bottom water production in the northern Rockall Trough. Sedimentary Geology 82, 79-87.

Dunbar, G.B., 2001. A Detailed Characterization of Dansgaard-Oeschger Cycles at Site 1063 (Bermuda Rise), in: Keigwin, L.D., Rio, D., Acton, G.D., Arnold, E. (Eds.), Proc. ODP, Sci. Results, pp. 1-24.

Egbert, G.D., Ray, R.D., 2000. Significant dissipation of tidal energy in the deep ocean inferred from satellite altimeter data. Nature 405, 775-778.

Ercilla, G., Casas, D., Estrada, F., Vázquez, J.T., Iglesias, J., García, M., Gómez, M., Acosta, J., Gallart, J., Maestro-González, A., 2008a. Morphosedimentary features and recent depositional architectural model of the Cantabrian continental margin. Marine Geology 247, 61-83.

Ercilla, G., García-Gil, S., Estrada, F., Gràcia, E., Vizcaino, A., Váquez, J.T., Díaz, S., Vilas, F., Casas, D., Alonso, B., Dañobeitia, J., Farran, M., 2008b. High-resolution seismic stratigraphy of the Galicia Bank Region and neighbouring abyssal plains (NW Iberian continental margin). Marine Geology 249, 108-127.

Ercilla, G., Juan, C., Hernández-Molina, F.J., Bruno, M., Estrada, F., Alonso, B., Casas, D., Farran, M.l., Llave, E., García, M., Vázquez, J.T., D'Acremont, E., Gorini, C., Palomino, D., Valencia, J., El Moumni, B., Ammar, A., 2016. Significance of bottom currents in deep-sea morphodynamics: An example from the Alboran Sea. Marine Geology 378, 157-170.

Falcini, F., Martorelli, E., Chiocci, F.L., Salusti, E., 2016. A general theory for the effect of local topographic unevenness on contourite deposition around marine capes: An inverse problem applied to the Italian continental margin (Cape Suvero). Marine Geology.

Faugères, J.-C., Gonthier, E., Stow, D.A.V., 1984. Contourite drift molded by deep Mediterranean outflow. Geology 12, 296-300.

Faugères, J.-C., Mézerais, M.L., Stow, D.A.V., 1993. Contourite drift types and their distribution in the North and South Atlantic Ocean basins. Sedimentary Geology 82, 189-203.

Faugères, J.-C., Stow, D.A.V., Imbert, P., Viana, A.R., 1999. Seismic features diagnostic of contourite drifts. Marine Geology 162, 1-38.

Foubert, A., Depreiter, D., Beck, T., Maignien, L., Pannemans, B., Frank, N., Blamart, D., Henriet, J.-P., 2008. Carbonate mounds in a mud volcano province off north-west Morocco: Key to processes and controls. Marine Geology 248, 74-96.

Frank, N., Freiwald, A., Lopez-Correa, M., Wienberg, C., Eisele, M., Hebbeln, D., Van Rooij, D., Henriet, J.-P., Colin, C., Van Weering, T., de Haas, H., Buhl-Mortensen, P., Roberts, J.M., De Mol, B., Douville, E., Blamart, D., Hatte, C., 2011. Northeastern Atlantic cold-water coral reefs and climate. Geology 39, 743-746.

Gao, Z., He, Y., Li, X., Duan, T., Wang, Y., Liu, M., 2013. Review of research in internal-wave and internal-tide deposits of China. Journal of Palaeogeography 2, 56-65.

Gao, Z.Z., Eriksson, K.A., 1991. Internal-tide deposits in an Ordovician submarine channel: Previously unrecognized facies? Geology 19, 734-737.

Gao, Z.Z., Eriksson, K.A., He, Y.B., Luo, S.S., Guo, J.H., 1998. Deep-Water Traction Current Deposits - A Study of Internal Tides, Internal Waves, Contour Currents and Their Deposits. Science Press, Beijing.

García Lafuente, J., Garrido, J.C.S., Díaz del Río, G., Aldeanueva, F.C., Marcote, D., Sánchez Román, A., 2008. Low-frequency variability of the Mediterranean undercurrent off Galicia, northwestern Iberian Peninsula. Journal of Marine Systems 74, 351-363.

García, M., Hernández-Molina, F.J., Llave, E., Stow, D.A.V., León, R., Fernández-Puga, M.C., Diaz del Río, V., Somoza, L., 2009. Contourite erosive features caused by the Mediterranean Outflow Water in the Gulf of Cadiz: Quaternary tectonic and oceanographic implications. Marine Geology 257, 24-40.

García, M., Hernández-Molina, F.J., Alonso, B., Vázquez, J.T., Ercilla, G., Llave, E., Casas, D., 2016. Erosive sub-circular depressions on the Guadalquivir Bank (Gulf of Cadiz): Interaction between bottom current, mass-wasting and tectonic processes. Marine Geology 378, 5-19.

Garrett, C., Kunze, E., 2007. Internal Tide Generation in the Deep Ocean. Annual Review of Fluid Mechanics 39, 57-87.

Gayen, B., Sarkar, S., 2010. Turbulence During the Generation of Internal Tide on a Critical Slope. Physical Review Letters 104, 218502.

Gayen, B., Sarkar, S., 2011. Direct and large-eddy simulations of internal tide generation at a near-critical slope. Journal of Fluid Mechanics 681, 48-79.

Gilli, A., Anselmetti, F.S., Ariztegui, D., Beres, M., McKenzie, J.A., Markgraf, V., 2005. Seismic stratigraphy, buried beach ridges and contourite drifts: the Late Quaternary history of the closed Lago Cardiel basin, Argentina (49°S). Sedimentology 52, 1-23.

Gonthier, E., Faugères, J.-C., Stow, D.A.V., 1984. Contourite facies of the Faro Drift, Gulf of Cadiz, in: Stow, D.A.V., Piper, D.J.W. (Eds.), Fine Grained Sediments, Deep-Water Processes and Facies. Geological Society, London, pp. 275-291.

González-Pola, C., Díaz del Río, G., Ruiz-Villarreal, M., Sánchez, R.F., Mohn, C., 2012. Circulation patterns at Le Danois Bank, an elongated shelf-adjacent seamount in the Bay of Biscay. Deep Sea Research Part I: Oceanographic Research Papers 60, 7-21.

Hanebuth, T.J.J., Zhang, W., Hofmann, A.L., Löwemark, L.A., Schwenk, T., 2015. Oceanic density fronts steering bottom-current induced sedimentation deduced from a 50 ka contourite-drift record and numerical modeling (off NW Spain). Quaternary Science Reviews 112, 207-225.

Hassold, N.J.C., Rea, D.K., van der Pluijm, B.A., Parés, J.M., Gleason, J.D., Ravelo, A.C., 2006. Late Miocene to Pleistocene paleoceanographic records from the Feni and Gardar Drifts: Pliocene reduction in abyssal flow. Palaeogeography, Palaeoclimatology, Palaeoecology 236, 290-301.

He, Y., Gao, Z., Luo, J., Luo, S., Liu, X., 2008. Characteristics of internal-wave and internal-tide deposits and their hydrocarbon potential. Petroleum Science 5, 37-44.

Hebbeln, D., Van Rooij, D., Wienberg, C., 2016. Good neighbours shaped by vigorous currents: Cold-water coral mounds and contourites in the North Atlantic. Marine Geology 378, 171-185.

Hernández-Molina, F.J., Llave, E., Stow, D.A.V., 2008a. Continental Slopes Contourites, in: Rebesco, M., Camerlenghi, A. (Eds.), Contourites. Elsevier.

Hernández-Molina, F.J., Maldonado, A., Stow, D.A.V., 2008b. Sediment drift of Abyssal plains and oceanic basins, in: Rebesco, M., Camerlenghi, A. (Eds.), Contourites. Elsevier.

Hernandez-Molina, F.J., Paterlini, M., Violante, R., Marshall, P., de Isasi, M., Somoza, L., Rebesco, M., 2009. Contourite depositional system on the Argentine Slope: An exceptional record of the influence of Antarctic water masses. Geology 37, 507-510.

Hernández-Molina, F.J., Llave, E., Stow, D.A.V., Garcia, M., Somoza, L., Vazquez, J.T., Lobo, F.J., Maestro, A., del Rio, V.D., Leon, R., Medialdea, T., Gardner, J., 2006. The contourite depositional system of the Gulf of Cadiz: A sedimentary model related to the bottom current activity of the Mediterranean outflow water and its interaction with the continental margin. Deep-Sea Research Part Ii-Topical Studies in Oceanography 53, 1420-1463.

Hernández-Molina, F.J., Serra, N., Stow, D., Llave, E., Ercilla, G., Van Rooij, D., 2011. Along-slope oceanographic processes and sedimentary products around the Iberian margin. Geo-Marine Letters, 1-27.

Hernández-Molina, F.J., Stow, D.A.V., Alvarez-Zarikian, C.A., Acton, G., Bahr, A., Balestra, B., Ducassou, E., Flood, R., Flores, J.-A., Furota, S., Grunert, P., Hodell, D., Jimenez-Espejo, F., Kim, J.K., Krissek, L., Kuroda, J., Li, B., Llave, E., Lofi, J., Lourens, L., Miller, M., Nanayama, F., Nishida, N., Richter, C., Roque, C., Pereira, H., Sanchez Goñi, M.F., Sierro, F.J., Singh, A.D., Sloss, C., Takashimizu, Y., Tzanova, A., Voelker, A., Williams, T., Xuan, C., 2014. Onset of Mediterranean outflow into the North Atlantic. Science 344, 1244-1250.

Hernández-Molina, F.J., Hodell, D.A., Stow, D.A.V., Alvarez-Zarikian, C., 2016c. Virtual special issue on IODP Expedition 339: The Mediterranean outflow. Marine Geology 377, 1-6.

Hernández-Molina, F.J., Sierro, F.J., Llave, E., Roque, C., Stow, D.A.V., Williams, T., Lofi, J., Van der Schee, M., Arnáiz, A., Ledesma, S., Rosales, C., Rodríguez-Tovar, F.J., Pardo-Igúzquiza, E., Brackenridge, R.E., 2016b. Evolution of the gulf of Cadiz margin and southwest Portugal contourite depositional system: Tectonic, sedimentary and paleoceanographic implications from IODP expedition 339. Marine Geology 377, 7-39.

Hernández-Molina, F.J., Wåhlin, A., Bruno, M., Ercilla, G., Llave, E., Serra, N., Rosón, G., Puig, P., Rebesco, M., Van Rooij, D., Roque, D., González-Pola, C., Sánchez, F., Gómez, M., Preu, B., Schwenk, T., Hanebuth, T.J.J., Sánchez Leal, R.F., García-Lafuente, J., Brackenridge, R.E., Juan, C., Stow, D.A.V., Sánchez-González, J.M., 2016a. Oceanographic processes and morphosedimentary products along the Iberian margins: A new multidisciplinary approach. Marine Geology 378, 127-156.

Hernandez-Molina, J., Llave, E., Somoza, L., Fernandez-Puga, M.C., Maestro, A., Leon, R., Medialdea, T., Barnolas, A., Garcia, M., del Rio, V.D., Fernandez-Salas, L.M., Vazquez, J.T., Lobo, F., Dias, J.M.A., Rodero,

J., Gardner, J., 2003. Looking for clues to paleoceanographic imprints: A diagnosis of the Gulf of Cadiz contourite depositional systems. Geology 31, 19-22.

Howe, J.A., Stoker, M.S., Masson, D.G., Pudsey, C.J., Morris, P., Larter, R.D., Bulat, J., 2006. Seabed morphology and the bottom-current pathways around Rosemary Bank seamount, northern Rockall Trough, North Atlantic. Marine and Petroleum Geology 23, 165-181.

Hunter, S.E., Wilkinson, D., Stanford, J., Stow, D.A.V., Bacon, S., Akhmetzhanov, A.M., Kenyon, N.H., 2007. The Eirik Drift: a long-term barometer of North Atlantic deepwater flux south of Cape Farewell, Greenland, in: Viana, A.R., Rebesco, M. (Eds.), Economic and Palaeoceanographic Importance of Contourite Deposits. Geological Society, London, pp. 245-263.

Huthnance, J.M., Coelho, H., Griffiths, C.R., Knight, P.J., Rees, A.P., Sinha, B., Vangriesheim, A., White, M., Chatwin, P.G., 2001. Physical structures, advection and mixing in the region of Goban spur. Deep-Sea Research II 48, 2979-3021.

Huvenne, V.A.I., Van Rooij, D., De Mol, B., Thierens, M., O'Donnell, R., Foubert, A., 2009. Sediment dynamics and palaeo-environmental context at key stages in the Challenger cold-water coral mound formation: Clues from sediment deposits at the mound base. Deep Sea Research Part I: Oceanographic Research Papers 56, 2263-2280.

Iorga, M.C., Lozier, M.S., 1999. Signatures of the Mediterranean outflow from a North Atlantic climatology 2. Diagnostic velocity fields. Journal of Geophysical Research-Oceans 104, 26011-26029.

Juan, C., Ercilla, G., Javier Hernández-Molina, F., Estrada, F., Alonso, B., Casas, D., García, M., Farran, M.l., Llave, E., Palomino, D., Vázquez, J.-T., Medialdea, T., Gorini, C., D'Acremont, E., El Moumni, B., Ammar, A., 2016. Seismic evidence of current-controlled sedimentation in the Alboran Sea during the Pliocene and Quaternary: Palaeoceanographic implications. Marine Geology.

Kano, A., Ferdelman, T.G., Williams, T., Henriet, J.P., Ishikawa, T., Kawagoe, N., Takashima, C., Kakizaki, Y., Abe, K., Sakai, S., Browning, E., Li, X., the IODP Expedition 307 Scientists, 2007. Age constraints on the origin and growth history of a deep-water coral mound in northeast Atlantic drilled during Integrated Ocean Drilling Program Expedition 307. Geology 35, 1051-1054.

Khélifi, N., Sarnthein, M., Andersen, N., Blanz, T., Frank, M., Garbe-Schonberg, D., Haley, B.A., Stumpf, R., Weinelt, M., 2009. A major and long-term Pliocene intensification of the Mediterranean outflow, 3.5-3.3 Ma ago. Geology 37, 811-814.

Khélifi, N., Sarnthein, M., Frank, M., Andersen, N., Garbe-Schönberg, D., 2014. Late Pliocene variations of the Mediterranean outflow. Marine Geology 357, 182-194.

Klymak, J.M., Alford, M.H., Pinkel, R., Lien, R.-C., Yang, Y.J., Tang, T.-Y., 2011. The Breaking and Scattering of the Internal Tide on a Continental Slope. Journal of Physical Oceanography 41, 926-945.

Knutz, P.C., 2008. Chapter 24 Palaeoceanographic Significance of Contourite Drifts, in: Rebesco, M., Camerlenghi, A. (Eds.), Developments in Sedimentology. Elsevier, pp. 511-535.

Kuijpers, A., Nielsen, T., 2015. Near-bottom current speed maxima in North Atlantic contourite environments inferred from current-induced bedforms and other seabed evidence. Marine Geology.

Lamb, K.G., 2014. Internal Wave Breaking and Dissipation Mechanisms on the Continental Slope/Shelf. Annual Review of Fluid Mechanics 46, 231-254.

Li, X., Takashima, C., Kano, A., Sakai, S., Chen, Y., Xu, B., Iodp Expedition, S., 2011. Pleistocene geochemical stratigraphy of the borehole 1317E (IODP Expedition 307) in Porcupine Seabight, SW of Ireland: applications to palaeoceanography and palaeoclimate of the coral mound development. Journal of Quaternary Science 26, 178-189.

Llave, E., Schönfeld, J., Hernandez-Molina, F.J., Mulder, T., Somoza, L., Diaz-del Rio, V., Sanchez-Almazo, I., 2006. High-resolution stratigraphy of the Mediterranean outflow contourite system in the Gulf of Cadiz during the late Pleistocene: The impact of Heinrich events. Marine Geology 277, 241-262.

Llave, E., Hernandez-Molina, F.J., Somoza, L., Stow, D.A.V., Diaz del Rio, G., 2007. Quaternary evolution of the contourite depositional system in the Gulf of Cadiz, in: Viana, A.R., Rebesco, M. (Eds.), Economic and Palaeoceanographic Significance of Contourite Deposits. Geological Society, London, pp. 49-79.

Llave, E., Matias, H., Hernández-Molina, F., Ercilla, G., Stow, D., Medialdea, T., 2011. Pliocene–Quaternary contourites along the northern Gulf of Cadiz margin: sedimentary stacking pattern and regional distribution. Geo-Marine Letters, 1-14.

Lozier, M.S., Nicole, M.S., 2008. On the Temporally Varying Northward Penetration of Mediterranean Overflow Water and Eastward Penetration of Labrador Sea Water. Journal of Physical Oceanography 38, 2097-2103.

MacLachlan, S.E., Elliott, G.M., Parson, L.M., 2008. Investigations of the bottom current sculpted margin of Hatton Bank, NE Atlantic. Marine Geology 253, 170-184.

Maestro, A., López-Martínez, J., Llave, E., Bohoyo, F., Acosta, J., Hernández-Molina, F.J., Muñoz, A., Jané, G., 2013. Geomorphology of the Iberian Continental Margin. Geomorphology 196, 13-35.

Marchès, E., Mulder, T., Gonthier, E., Cremer, M., Hanquiez, V., Garlan, T., Lecroart, P., 2010. Perched lobe formation in the Gulf of Cadiz: Interactions between gravity processes and contour currents (Algarve Margin, Southern Portugal). Sedimentary Geology 229, 81-94.

Masson, D.G., Howe, J.A., Stoker, M.S., 2002. Bottom-current sediment waves, sediment drifts and contourites in the northern Rockall Trough. Marine Geology 192, 215-237.

McCave, I.N., Tucholke, B.E., 1986. Deep current-controlled sedimentation in the western North Atlantic, in: Vogt, P.R., Tucholke, B.E. (Eds.), The Geology of North America, Volume M, The Western North Atlantic Region. Geological Society of America, pp. 451-468.

McCave, I.N., Manighetti, B., Robinson, S.G., 1995. Sortable silt and fine sediment size/composition slicing: Parameters for palaeocurrent speed and palaeoceanography. Paleoceanography 10, 593-610.

McCave, I.N., Hall, I.R., Antia, A.N., Chou, L., Dehairs, F., Lampitt, R.S., Thomsen, L., van Weering, T.C.E., Wollast, R., 2001. Distribution, composition and flux of particulate material over the European margin at 47°-50°N. Deep-Sea Research II 48, 3107-3139.

McCave, I.N., Hall, I.R., 2006a. Size sorting in marine muds: Processes, pitfalls, and prospects for paleoflow-speed proxies. Geochemistry, Geophysics, Geosystems 7.

McCave, I.N., Hall, I.R., 2006b. Size sorting in marine muds: Processes, pitfalls, and prospects for paleoflow-speed proxies, Geochemistry Geophysics Geosystems.

McPhee-Shaw, E., 2006. Boundary–interior exchange: Reviewing the idea that internal-wave mixing enhances lateral dispersal near continental margins. Deep Sea Research Part II: Topical Studies in Oceanography 53, 42-59.

McPhee-Shaw, E.E., Kunze, E., 2002. Boundary layer intrusions from a sloping bottom: A mechanism for generating intermediate nepheloid layers. Journal of Geophysical Research: Oceans 107, 3-1-3-16.

Mienis, F., van Weering, T., de Haas, H., de Stigter, H., Huvenne, V., Wheeler, A., 2006. Carbonate mound development at the SW Rockall Trough margin based on high resolution TOBI and seismic recording. Marine Geology 233, 1-19.

Mienis, F., de Stigter, H., White, M., Duineveld, G.C.A., de Haas, H., van Weering, T., 2007. Hydrodynamic controls on cold-water coral growth and carbonate-mound development at the SW and SE Rockall Trough Margin, NE Atlantic Ocean. Deep-Sea Research I 54, 1655-1674.

Mienis, F., de Stigter, H.C., de Haas, H., van Weering, T.C.E., 2009. Near-bed particle deposition and resuspension in a cold-water coral mound area at the Southwest Rockall Trough margin, NE Atlantic. Deep Sea Research Part I: Oceanographic Research Papers 56, 1026-1038.

Mienis, F., De Stigter, H.C., De Haas, H., Van der Land, C., Van Weering, T.C.E., 2012. Hydrodynamic conditions in a cold-water coral mound area on the Renard Ridge, southern Gulf of Cadiz. Journal of Marine Systems 96–97, 61-71.

Mohn, C., Rengstorf, A., White, M., Duineveld, G., Mienis, F., Soetaert, K., Grehan, A., 2014. Linking benthic hydrodynamics and cold-water coral occurrences: A high-resolution model study at three cold-water coral provinces in the NE Atlantic. Progress In Oceanography 122, 92-104.

Mosher, D.C., Thomson, R.E., 2002. The Foreslope Hills: large-scale, fine-grained sediment waves in the Strait of Georgia, British Columbia. Marine Geology 192, 275-295.

Mulder, T., Zaragosi, S., Garlan, T., Mavel, J., Cremer, M., Sottolichio, A., Sénéchal, N., Schmidt, S., 2012. Present deep-submarine canyons activity in the Bay of Biscay (NE Atlantic). Marine Geology 295–298, 113-127.

Mulder, T., Hassan, R., Ducassou, E., Zaragosi, S., Gonthier, E., Hanquiez, V., Marchès, E., Toucanne, S., 2013. Contourites in the Gulf of Cadiz: a cautionary note on potentially ambiguous indicators of bottom current velocity. Geo-Marine Letters 33, 357-367.

Müller-Michaelis, A., Uenzelmann-Neben, G., Stein, R., 2013. A revised Early Miocene age for the instigation of the Eirik Drift, offshore southern Greenland: Evidence from high-resolution seismic reflection data. Marine Geology 340, 1-15.

Müller, M., Cherniawsky, J.Y., Foreman, M.G.G., von Storch, J.S., 2012. Global M2 internal tide and its seasonal variability from high resolution ocean circulation and tide modeling. Geophysical Research Letters 39.

Nelson, C.H., Baraza, J., Maldonado, A., Rodero, J., Escutia, C., Barber, J.H., 1999. Influence of the Atlantic inflow and Mediterranean outflow currents on Late Quaternary sedimentary facies of the Gulf of Cadiz continental margin. Marine Geology 155, 99-129.

Nichols, G.A., 2009. Sedimentology and Stratigraphy, second ed. Wiley-Blackwell, Chichester (419 pp.).

Nishida, N., 2016. Microstructure of muddy contourites from the Gulf of Cádiz. Marine Geology 377, 110-117.

Nycander, J., 2005. Generation of internal waves in the deep ocean by tides. Journal of Geophysical Research: Oceans 110, C10028.

Ovrebo, L.K., Haughton, P.D.W., Shannon, P.M., 2006. A record of fluctuating bottom currents on the slopes west of the Porcupine Bank, offshore Ireland - implications for Late Quaternary climate forcing. Marine Geology 225, 279-309.

Peine, F., Turnewitsch, R., Mohn, C., Reichelt, T., Springer, B., Kaufmann, M., 2009. The importance of tides for sediment dynamics in the deep sea—Evidence from the particulate-matter tracer 234Th in deep-sea environments with different tidal forcing. Deep Sea Research Part I: Oceanographic Research Papers 56, 1182-1202.

Piper, D.J.W., 2005. Late Cenozoic evolution of the continental margin of eastern Canada. Norwegian Journal of Geology 85, 231-244.

Pomar, L., Morsilli, M., Hallock, P., Bádenas, B., 2012. Internal waves, an under-explored source of turbulence events in the sedimentary record. Earth-Science Reviews 111, 56-81.

Preu, B., Hernández-Molina, F.J., Violante, R., Piola, A.R., Paterlini, C.M., Schwenk, T., Voigt, I., Krastel, S., Spiess, V., 2013. Morphosedimentary and hydrographic features of the northern Argentine margin: The interplay between erosive, depositional and gravitational processes and its conceptual implications. Deep Sea Research Part I: Oceanographic Research Papers 75, 157-174.

Puig, P., Palanques, A., Guillén, J., El Khatab, M., 2004. Role of internal waves in the generation of nepheloid layers on the northwestern Alboran slope: Implications for continental margin shaping. Journal of Geophysical Research: Oceans 109, C09011.

Raddatz, J., Rüggeberg, A., Margreth, S., Dullo, W.-C., 2011. Paleoenvironmental reconstruction of Challenger Mound initiation in the Porcupine Seabight, NE Atlantic. Marine Geology 282, 79-90.

Raddatz, J., Rüggeberg, A., Liebetrau, V., Foubert, A., Hathorne, E.C., Fietzke, J., Eisenhauer, A., Dullo, W.-C., 2014. Environmental boundary conditions of cold-water coral mound growth over the last 3 million years in the Porcupine Seabight, Northeast Atlantic. Deep Sea Research Part II: Topical Studies in Oceanography 99, 227-236.

Rebesco, M., 2005. SEDIMENTARY ENVIRONMENTS | Contourites, in: Selley, R.C., Cocks, L.R.M., Plimer, I., R. (Eds.), Encyclopedia of Geology. Elsevier, Oxford, pp. 513-528.

Rebesco, M., Camerlenghi, A., 2008. Contourites, Developments in Sedimentology. Elsevier.

Rebesco, M., Hernández-Molina, F.J., Van Rooij, D., Wåhlin, A., 2014. Contourites and associated sediments controlled by deep-water circulation processes: State-of-the-art and future considerations. Marine Geology 352, 111-154.

Ribbe, J., Holloway, P.E., 2001. A model of suspended sediment transport by internal tides. Continental Shelf Research 21, 395-422.

Ribó, M., Puig, P., Urgeles, R., Van Rooij, D., Muñoz, A., 2015. Spatio-temporal evolution of sediment waves developed on the Gulf of Valencia margin (NW Mediterranean) during the Plio-Quaternary. Marine Geology.

Ribó, M., Puig, P., van Haren, H., 2015. Hydrodynamics over the Gulf of Valencia continental slope and their role in sediment transport. Deep Sea Research Part I: Oceanographic Research Papers 95, 54-66.

Ribó, M., Puig, P., Muñoz, A., Lo Iacono, C., Masqué, P., Palanques, A., Acosta, J., Guillén, J., Gómez Ballesteros, M., 2016. Morphobathymetric analysis of the large fine-grained sediment waves over the Gulf of Valencia continental slope (NW Mediterranean). Geomorphology 253, 22-37.

Rice, A.L., Thurston, M.H., New, A.L., 1990. Dense aggregations of a hexactinellid sponge, *Pheromena carpenteri*, in the Porcupine Seabight (northeast Atlantic Ocean), and possible causes. Progress In Oceanography 24, 179-196.

Richter, T.O., Lassen, S., van Weering, T.C.E., de Haas, H., 2001. Magnetic susceptibility patterns and provenance of ice-rafted material at Feni Drift, Rockall Trough: implications for the history of the British-Irish ice sheet. Marine Geology 173, 37-54.

Rodríguez-Tovar, F.J., Dorador, J., Grunert, P., Hodell, D., 2015a. Deep-sea trace fossil and benthic foraminiferal assemblages across glacial Terminations 1, 2 and 4 at the “Shackleton Site” (IODP Expedition 339, Site U1385). Global and Planetary Change 133, 359-370.

Rodríguez-Tovar, F.J., Dorador, J., Martin-Garcia, G.M., Sierro, F.J., Flores, J.A., Hodell, D.A., 2015b. Response of macrobenthic and foraminifer communities to changes in deep-sea environmental conditions from Marine Isotope Stage (MIS) 12 to 11 at the “Shackleton Site”. Global and Planetary Change 133, 176-187.

Rogerson, M., Rohling, E.J., Weaver, P.P.E., Murray, J.W., 2005. Glacial to interglacial changes in the settling depth of the Mediterranean Outflow plume. Paleoceanography 20.

Rogerson, M., Rohling, E.J., Bigg, G.R., Ramirez, J., 2012. Paleoceanography of the Atlantic-Mediterranean exchange: Overview and first quantitative assessment of climatic forcing. Reviews of Geophysics 50, RG2003.

Rohling, E.J., Foster, G.L., Grant, K.M., Marino, G., Roberts, A.P., Tamisiea, M.E., Williams, F., 2014. Sea-level and deep-sea-temperature variability over the past 5.3 million years. Nature 508, 477-482.

Roque, C., Duarte, H., Terrinha, P., Valadares, V., Noiva, J., Cachão, M., Ferreira, J., Legoinha, P., Zitellini, N., 2012. Pliocene and Quaternary depositional model of the Algarve margin contourite drifts (Gulf of Cadiz, SW Iberia): Seismic architecture, tectonic control and paleoceanographic insights. Marine Geology 303–306, 42-62.

Rüggeberg, A., Dullo, C., Dorschel, B., Hebbeln, D., 2007. Environmental changes and growth history of a cold-water carbonate mound (Propeller Mound, Porcupine Seabight). International Journal of Earth Sciences 96, 57-72.

Sánchez-Garrido, J.C., Sannino, G., Liberti, L., García Lafuente, J., Pratt, L., 2011. Numerical modeling of three-dimensional stratified tidal flow over Camarinal Sill, Strait of Gibraltar. Journal of Geophysical Research: Oceans 116.

Sayago-Gil, M., Long, D., Hitchen, K., Díaz-del-Río, V., Fernández-Salas, L.M., Durán-Muñoz, P., 2010. Evidence for current-controlled morphology along the western slope of Hatton Bank (Rockall Plateau, NE Atlantic Ocean). Geo-Marine Letters 30, 99-111.

Schmidt, S., van Weering, T.C.E., Reyss, J.L., van Beek, P., 2002. Seasonal deposition and reworking at the sediment-water interface on the northwestern Iberian margin. Progress In Oceanography 52, 331-348.

Schönfeld, J., Zahn, R., 2000. Late Glacial to Holocene history of the Mediteranean Outflow. Evidence from benthic foraminiferal assemblages and stable isotopes at the Portuguese margin. Palaeogeography, Palaeoclimatology, Palaeoecology 159, 85-111.

Scott, R.B., Arbic, B.K., Chassignet, E.P., Coward, A.C., Maltrud, M., Merryfield, W.J., Srinivasan, A., Varghese, A., 2010. Total kinetic energy in four global eddying ocean circulation models and over 5000 current meter records. Ocean Modelling 32, 157-169.

Serra, N., Ambar, I., Käse, R.H., 2005. Observations and numerical modelling of the Mediterranean outflow splitting and eddy generation. Deep Sea Research Part II: Topical Studies in Oceanography 52, 383-408.

Serra, N., Ambar, I., Boutov, D., 2010. Surface expression of Mediterranean Water dipoles and their contribution to the shelf/slope – open ocean exchange. Ocean Sci. 6, 191-209.

Shanmugam, G., 2003. Deep-marine tidal bottom currents and their reworked sands in modern and ancient submarine canyons. Marine and Petroleum Geology 20, 471-491.

Shanmugam, G., 2008. Chapter 5 Deep-water Bottom Currents and their Deposits, in: Rebesco, M., Camerlenghi, A. (Eds.), Developments in Sedimentology. Elsevier, pp. 59-81.

Shanmugam, G., 2013b. Comment on “Internal waves, an under-explored source of turbulence events in the sedimentary record” by L. Pomar, M. Morsilli, P. Hallock, and B. Bádenas [Earth-Science Reviews, 111 (2012), 56–81]. Earth-Science Reviews 116, 195-205.

Shanmugam, G., 2013a. Modern internal waves and internal tides along oceanic pycnoclines: Challenges and implications for ancient deep-marine baroclinic sands. AAPG Bulletin 97, 799-843.

Simmons, H.L., Hallberg, R.W., Arbic, B.K., 2004. Internal wave generation in a global baroclinic tide model. Deep Sea Research Part II: Topical Studies in Oceanography 51, 3043-3068.

Southard, J.B., Cacchione, D.A., 1972. Experiments on Bottom Sediment Movement by Breaking InternalWaves. In: Swift, D.J., Duane, D.B., Pilkey, O.H. (Eds.), Shelf Sediment Transport: Process and Pattern. Hutchinson & Ross, Stroudsburg, Pa., Dowden, pp. 83–97.

Stow, D.A.V., Faugères, J.-C., Howe, J.A., Pudsey, C.J., Viana, A.R., 2002b. Bottom currents, contourites and deep-sea sediment drifts: current state-of-the-art, in: Stow, D.A.V., Pudsey, C.J., Howe, J.A., Faugères, J.-C., Viana, A.R. (Eds.), Deep-Water Contourite Systems: Modern Drifts and Ancient Series, Seismic and Sedimentary Characteristics. Geological Society, London, pp. 7-20.

Stow, D.A.V., Pudsey, C.J., Howe, J.A., Faugères, J.-C., Viana, A.R., 2002a. Deep-Water Contourite Systems: Modern Drifts and Ancient Series, Seismic and Sedimentary characteristics. Geological Society, London.

Stow, D.A.V., Faugères, J.C., 2008. Chapter 13 Contourite Facies and the Facies Model, in: Rebesco, M., Camerlenghi, A. (Eds.), Developments in Sedimentology. Elsevier, pp. 223-256.

Stow, D.A.V., Hernandez-Molina, F.J., Llave, E., Sayago-Gil, M., del Rio, V.D., Branson, A., 2009. Bedform-velocity matrix: The estimation of bottom current velocity from bedform observations. Geology 37, 327-330.

Takashimizu, Y., Kawamura, R., Rodríguez-Tovar, F.J., Dorador, J., Ducassou, E., Hernández-Molina, F.J., Stow, D.A.V., Alvarez-Zarikian, C.A., 2016. Reworked tsunami deposits by bottom currents: Circumstantial evidences from Late Pleistocene to Early Holocene in the Gulf of Cádiz. Marine Geology 377, 95-109.

Thierens, M., Titschack, J., Dorschel, B., Huvenne, V.A.I., Wheeler, A.J., Stuut, J.B., O'Donnell, R., 2010. The 2.6 Ma depositional sequence from the Challenger cold-water coral carbonate mound (IODP Exp. 307): Sediment contributors and hydrodynamic palaeo-environments. Marine Geology 271, 260-277.

Thomsen, L., van Weering, T.C.E., 1998. Spatial and temporal variability of particulate matter in the benthic boundary layer at the N.W. European Continental Margin (Goban Spur). Progress In Oceanography 42, 61-76.

Thomsen, L., Gust, G., 2000. Sediment erosion thresholds and characteristics of resuspended aggregates on the western European continental margin. Deep Sea Research Part I: Oceanographic Research Papers 47, 1881-1897.

Toucanne, S., Mulder, T., Schönfeld, J., Hanquiez, V., Gonthier, E., Duprat, J., Cremer, M., Zaragosi, S., 2007. Contourites of the Gulf of Cadiz: A high-resolution record of the paleocirculation of the Mediterranean outflow water during the last 50,000 years. Palaeogeography, Palaeoclimatology, Palaeoecology 246, 354-366.

Turnewitsch, R., Reyss, J.-L., Nycander, J., Waniek, J.J., Lampitt, R.S., 2008. Internal tides and sediment dynamics in the deep sea—Evidence from radioactive 234Th/238U disequilibria. Deep Sea Research Part I: Oceanographic Research Papers 55, 1727-1747.

Van Daele, M., Bertrand, S., Meyer, I., Moernaut, J., Vandoorne, W., Siani, G., Tanghe, N., Ghazoui, Z., Pino, M., Urrutia, R., De Batist, M., 2016. Late Quaternary evolution of Lago Castor (Chile, 45.6°S): Timing of the deglaciation in northern Patagonia and evolution of the southern westerlies during the last 17 kyr. Quaternary Science Reviews 133, 130-146.

van Haren, H., Maas, L., Zimmerman, J.T.F., Ridderinkhof, H., Malschaert, H., 1999. Strong inertial currents and marginal internal wave stability in the central North Sea. Geophysical Research Letters 26, 2993-2996.

van Haren, H., Maas, L., van Aken, H., 2002. On the nature of internal wave spectra near a continental slope. Geophysical Research Letters 29, 57-51-57-53.

van Haren, H., Ribó, M., Puig, P., 2013. (Sub-)inertial wave boundary turbulence in the Gulf of Valencia. Journal of Geophysical Research: Oceans 118, 2067-2073.

van Haren, H., 2011. Internal wave–turbulence pressure above sloping sea bottoms. Journal of Geophysical Research: Oceans 116.

Van Rooij, D., De Mol, B., Huvenne, V., Ivanov, M.K., Henriet, J.-P., 2003. Seismic evidence of current-controlled sedimentation in the Belgica mound province, upper Porcupine slope, southwest of Ireland. Marine Geology 195, 31-53.

Van Rooij, D., Blamart, D., Kozachenko, M., Henriet, J.-P., 2007a. Small mounded contourite drifts associated with deep-water coral banks, Porcupine Seabight, NE Atlantic Ocean, in: Viana, A.R., Rebesco, M. (Eds.), Economic and Palaeoceanographic Importance of Contourite Deposits. Geological Society, London, pp. 225-244.

Van Rooij, D., Blamart, D., Richter, T.O., Wheeler, A.J., Kozachenko, M., Henriet, J.-P., 2007b. Quaternary sediment dynamics in the Belgica mounds province, Porcupine Seabight: Ice rafting events and contour current processes. International Journal of Earth Sciences 96, 121-140.

Van Rooij, D., Huvenne, V.A.I., Blamart, D., Henriet, J.P., Wheeler, A., de Haas, H., 2009. The Enya mounds: a lost mound-drift competition. International Journal of Earth Sciences 98, 849-863.

Van Rooij, D., Iglesias, J., Hernández-Molina, F.J., Ercilla, G., Gomez-Ballesteros, M., Casas, D., Llave, E., De Hauwere, A., Gil, S.G., Acosta, J., Henriet, J.P., 2010. The Le Danois Contourite Depositional System: interactions between the Mediterranean Outflow Water and the upper Cantabrian slope (North Iberian margin). Marine Geology 274, 1-20.

Van Rooij, D., Blamart, D., De Mol, L., Mienis, F., Pirlet, H., Wehrmann, L.M., Barbieri, R., Maignien, L., Templer, S.P., de Haas, H., Hebbeln, D., Frank, N., Larmagnat, S., Stadnitskaia, A., Stivaletta, N., van Weering, T., Zhang, Y., Hamoumi, N., Cnudde, V., Duyck, P., Henriet, J.P., 2011. Cold-water coral mounds on the Pen Duick Escarpment, Gulf of Cadiz: The MiCROSYSTEMS project approach. Marine Geology 282, 102-117.

Van Rooij, D., Campbell, C., Rueggeberg, A., Wahlin, A., 2016. The contourite log-book: significance for palaeoceanography, ecosystems and slope instability. Marine Geology 378, 1-4.

van Weering, T.C.E., Hall, I.R., de Stigter, H.C., McCave, I.N., Thomsen, L., 1998. Recent sediments, sediment accumulation and carbon burial at Goban Spur, N.W. European Continental Margin (47-50°N). Progress In Oceanography 42, 5-35.

van Weering, T.C.E., De Stigter, H.C., Balzer, W., Epping, E.H.G., Graf, G., Hall, I.R., Helder, W., Khripounoff, A., Lohse, L., McCave, I.N., Thomsen, L., Vangriesheim, A., 2001. Benthic dynamics and carbon fluxes on the NW European continental margin. Deep-Sea Research II 48, 3191-3221.

van Weering, T.C.E., de Stigter, H.C., Boer, W., de Haas, H., 2002. Recent sediment transport and accumulation on the NW Iberian margin. Progress In Oceanography 52, 349-371.

Vandorpe, T., Van Rooij, D., de Haas, H., 2014. Stratigraphy and paleoceanography of a topography-controlled contourite drift in the Pen Duick area, southern Gulf of Cádiz. Marine Geology 349, 136-151.

Vandorpe, T., Martins, I., Vitorino, J., Hebbeln, D., García, M., Van Rooij, D., 2016. Bottom currents and their influence on the sedimentation pattern in the El Arraiche mud volcano province, southern Gulf of Cadiz. Marine Geology 378, 114-126.

Vandorpe, T., Wienberg, C., Hebbeln, D., Van den Berghe, M., Gaide, S., Wintersteller, P., Van Rooij, D., submitted. Initiation and aggradation of buried cold-water corals mounds in the Atlantic Moroccan Coral Province, southern Gulf of Cádiz. Palaeogeography, Palaeoclimatology, Palaeoecology.

Viana, A.R., Faugères, J.-C., Stow, D.A.V., 1998. Bottom-current-controlled sand deposits - a review of modern shallow- to deep-water environments. Sedimentary Geology 115, 53-80.

Viana, A.R., 2002. Seismic expression of shallow- to deep-water contourites along the south-eastern Brazilian margin. Marine Geophysical Researches 22, 509-521.

White, M., 2001. Hydrography and physical dynamics at the NE Atlantic margin that influence the deep water cold reef ecosystem. Dept. of Oceanography, NUI, Galway, Ireland, Galway.

White, M., Mohn, C., de Stigter, H., Mottram, G., 2005. Deep-water coral development as a function of hydrodynamics and surface productivity around the submarine banks of the Rockall Trough, NE Atlantic, in: Freiwald, A., Roberts, J.M. (Eds.), Cold-Water Corals and Ecosystems. Springer Berlin Heidelberg, pp. 503-514.

White, M., 2007a. Benthic dynamics at the carbonate mound regions of the Porcupine Sea Bight continental margin. International Journal of Earth Sciences 96, 1-9.

White, M., Roberts, J.M., van Weering, T., 2007b. Do bottom-intensified diurnal tidal currents shape the alignment of carbonate mounds in the NE Atlantic? Geo-Marine Letters 27, 391-397.

White, M., Dorschel, B., 2010. The importance of the permanent thermocline to the cold water coral carbonate mound distribution in the NE Atlantic. Earth and Planetary Science Letters 296, 395-402.

Wienberg, C., Frank, N., Mertens, K.N., Stuut, J.-B., Marchant, M., Fietzke, J., Mienis, F., Hebbeln, D., 2010. Glacial cold-water coral growth in the Gulf of Cádiz: Implications of increased palaeo-productivity. Earth and Planetary Science Letters 298, 405-416.

Wienberg, C., Titschack, J., 2015. Framework-Forming Scleractinian Cold-Water Corals Through Space and Time: A Late Quaternary North Atlantic Perspective, in: Rossi, S., Bramanti, L., Gori, A., Orejas Saco del Valle, C. (Eds.), Marine Animal Forests: The Ecology of Benthic Biodiversity Hotspots. Springer International Publishing, Cham, pp. 1-34.

Wold, C.N., 1994. Cenozoic sediment accumulation on drifts in the northern North Atlantic. Paleoceanography 9, 917-941.

Wynn, R.B., Stow, D.A.V., 2002. Classification and characterisation of deep-water sediment waves. Marine Geology 192, 7-22.

Zhang, W., Hanebuth, T.J.J., Stöber, U., 2015. Short-term sediment dynamics on a meso-scale contourite drift (off NW Iberia): Impacts of multi-scale oceanographic processes deduced from the analysis of mooring data and numerical modelling. Marine Geology.

Zhang, X.H., Boyer, D.L., 1991. Current Deflections in the Vicinity of Multiple Seamounts. Journal of Physical Oceanography 21, 1122-1138.

CHAPTER 2

Methodology

This Ph.D. dissertation is organized as research article compilation. Most of them are intended for publication, and thus provide a specific material and methods section. However, this chapter provides some additional details and principles on methods used throughout. High resolution seismic reflection methods were used for geomorphological analysis, with the objective to link the sediment architecture to the (palaeo-)circulation pattern on large timescales (>10 ky). In this study, seismic reflection was used along with borehole logging. This allows combining borehole chronostratigraphy with seismic geomorphological information, mainly using concepts similar to sequence stratigraphy (Catuneanu et al., 2009; 2015). The last section relate to measurements performed on sediment cores, which can be used to determine sediment facies and depositional environment changes on sub-millennial to millennial time-scales.

2.1 Seismic reflection

Seismic reflection is an exploration technique that allows the imaging of the subsurface using acoustic waves. The method aims to trace the subsurface geophysical heterogeneities, which are defined as boundaries between two mediums of different acoustic impedance, characterizing the underground reflectivity (Fig. 2.1; Veeken and Moerkerken, 2013; Onajite, 2014a). In marine environment, it uses a seismic source which emits an acoustic pulse of known frequency and length (wavelet), along with a streamer composed of hydrophones, which can be mounted in a single channel (this dissertation), or in a series of channels of known relative offset (multichannel). In a single channel system, each emitted a wavelet in a certain geographic location (shot point), is recorded during an appropriate time into a single trace (Fig. 2.1), of which geo-referencing is ensured by the use of a GPS. The seismic trace is the convolution of the wavelet throughout the sub-surface reflectivity (Fig. 2.1), and is expressed in second Two-Way travel Time [TWT]. The sub-surface reflectivity, or impedance, can be defined as a function of the variation of subsurface geophysical parameters such as the density (ρ), the Poisson coefficient (E) and the Young module (v) (Onajite, 2014b). Laterally continuous and persistent seismic reflections form reflectors. Those may be seen as surfaces of similar acoustic impedance. In the sedimentary record, such surfaces might correspond to facies changes and thus can be interpreted as time-lines (Vail et al., 1977). Boundaries formed by the terminations of seismic reflectors, or abrupt changes in their organization are defined as seismic discontinuities, and may relate to geological unconformities, faults or variety of other geological features (Catuneanu et al., 2009). Thus, seismic reflection profiles fairly well represent the lateral and vertical structure of the sub-surface, which however remain expressed in TWT. This leads to the appearance of complex vertical distortions, inherent to the sub-surface velocity profile (Stewart, 2011).

This study has made use of a dataset acquired with a system composed of an SIG sparker seismic source and a single channel streamer, having an offset of a few meters, and which were towed behind the R/V Belgica. The SIG sparker is made of a multi-tip spark-array which converts an electric pulse (up to 600 J) into an acoustic one. The acoustic source, or wavelet, ranges from ~200 to ~3000 Hz and is centred around 800 Hz, allowing a theoretical vertical resolution of several tens of centimetres. The recording was performed during the 3 seconds following the source emission, using a sampling rate of 10 kHz. The horizontal resolution is defined by the shot point frequency and the vessel velocity. Here, the vessel velocity was limited to approximately 3 knots, thus allowing a horizontal resolution of a few meters. Series of traces acquired along the same heading are compiled into a 2D seismic profile, and series of seismic profiles acquired within a certain region are compiled into a survey. The seismic profiles were processed using RadEx Pro Software (DECO Geophysical).

Processing consisted in applying a bandpass filtering; cutting frequencies beyond ~200 and 1200 Hz, in order focus on the main frequency signal around 800 Hz. A swell-filtering was applied in order to correct vertical offsets of neighbouring traces caused by the swell. An exponential amplitude correction, increasing gain through time using 3 dB/ms constant was applied. Amplitude corrections are used in order to compensate the loss of energy of the seismic wavelet which occurs through time.

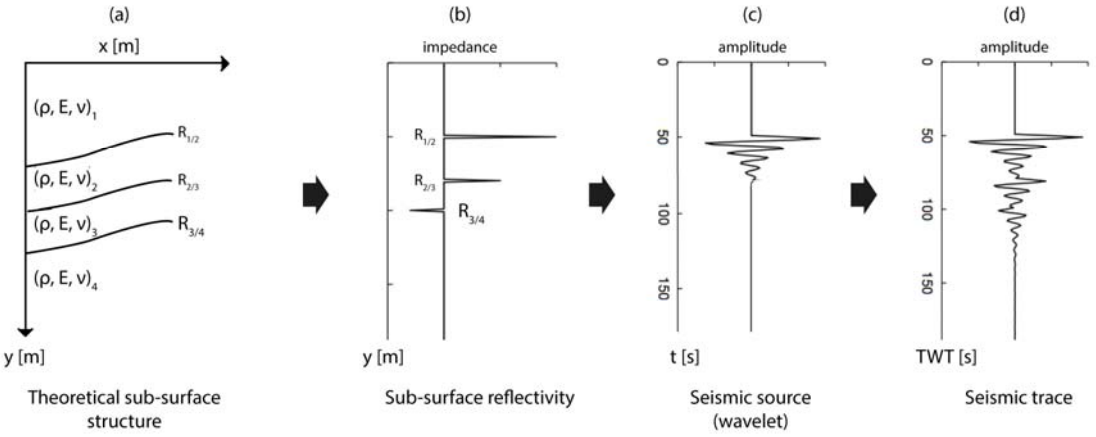

Figure 2.1 Sketch illustrating the convolution of a seismic source (wavelet) through a theoretical reflective sub-surface (modified from Al-Sadi, 1982). (a) The sub-surface reflectivity is defined through physical parameters (ρ: density; E: Young modulus; v: Poisson's ratio). (b) Representation of the theoretical sub-surface reflectivity coefficient. (c) Shape and length of the seismic source (wavelet) used. (d) Recorded seismic trace, corresponding to the convolution of (c) through (b).

2.2 Borehole logging

Borehole logging is a technique that uses specifically designed tools in order to measure series of in-situ bedrock properties throughout a drilled hole. It allows the acquisition of some parameters that might dramatically be altered when measured in de-confined environments (*e.g.* p-waves velocity, porosity and permeability). It constitutes a cheap and fast alternative to coring for exploration drilling and when sediment core analysis is not a primary objective. Borehole logging has been routinely performed since the initiation of the Deep Sea Drilling Project (DSDP) in 1969, which was followed by the Ocean Drilling Program (ODP) and the Integrated Ocean Discovery Program (IODP), respectively in 1985 and 2004. Today, the IODP and the U.S. Implementing Organization (USIO) provide an online database integrating core and borehole data acquired during its program, as well as detailed technical information and guidelines intended to promote a harmonized scientific interpretation (http://iodp.ldeo.columbia.edu/DATA/). There has been sustained industrial development of these tools, in particular related to the oil and gas industry, which resulted in the present day existence of various methods related to the acquisition of various geophysical parameters, which includes borehole imagery and borehole sampling (Lewis and McConchie, 1994; Darling, 2005). Here we review few of some logs which were performed at the DSDP Site 548, and further presented in this dissertation (de Graciansky et al., 1985a).

2.2.1 Natural Gamma Ray

The natural Gamma Ray (GR) is a passive technique which uses an appropriate Geiger counter in order to measure the local GR emissions (Russell, 1944). Gamma rays mainly originate from the radioactive disintegration of the Uranium, Thorium and Potassium elements (Serra et al., 1980; Quirein et al., 1982). In clastic environments, those elements are widely representative for the presence of clays and silts minerals, and certain minerals such as potash rich salts (Table 2.1). Mature sands (quartzite) and non-clastic, carbonated and biogenic sediments are largely depleted in such minerals (Quirein et al., 1982; Vasconcelos et al., 2012). Likewise, the measure of the GR may be more indicative for some lithologies and mineralogies than others, and is particularly indicative for the presence of clay and silts minerals (Russell, 1944). There exists no straightforward relation between the measured GR intensity and the bedrock lithology; although it is tied-up with variations in composition associated to terrigenous fraction changes (Table 2.1). Such changes are potentially related to sea-level fluctuations, terrigenous supply and/or sedimentary environment adjustments (Sierro et al., 2000; Lofi et al., 2016). Results are obtained in number of counts per second [cps/s] and are often subsequently express using the American Petroleum Institute [API] standard (Fig. 2.1),

in which the GR response of a concrete block at University of Houston was defined to have a radioactivity of 200 API.

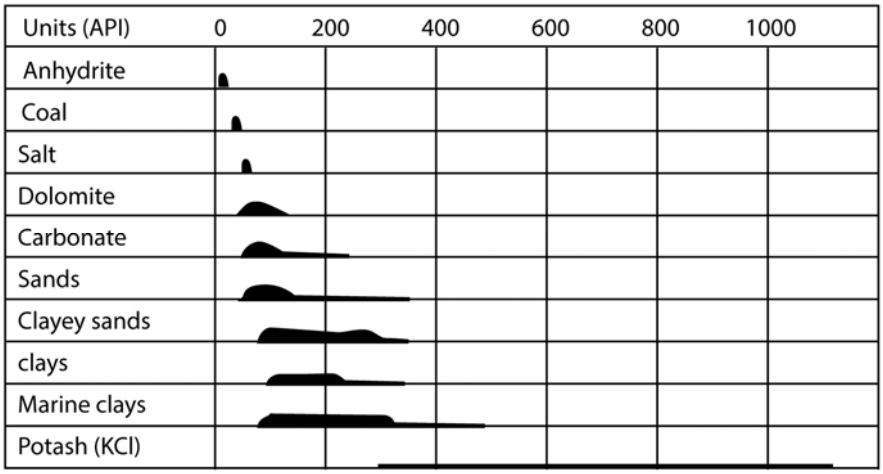

Table 2-1 Distribution of the natural radioactivity levels for some minerals and rock types (Modified after Russell, 1944).

2.2.2 Dual induction resistivity

The dual induction tool is an active method which provides a measure of the formation resistivity (Doll, 1949). Induction tools have the advantage of being operational in air-drilled boreholes and oil based drill muds. They are more reliable than resistivity tools using electrodes, which is why they are widely used in marine boreholes. The tool is made of an emitting coil array which induce an electromagnetic (primary) field from an alternating currents (generally of few tenth of kHz), which propagates within the formation. Another coil array measures the secondary magnetic field which is emitted in response to the primary magnetic field excitation. The secondary magnetic field is proportional to the formation conductivity. The distance between the arrays controls the distance of investigation around the borehole. The larger the spacing the larger the investigation range. Three distinct measures of the resistivity are generally performed in order to provide information on mud-invasion process which might occur in permeable formations (Kennedy, 2015). The spacing generally varies from a few centimetres to a few metres (generally 5 and 8 feet) in order to provide a measure on the flushed, transition and uninvaded zone, respectively (Kennedy, 2015). At DSDP Site 548, measurements used both a 5 and 8 feet arrays spacing (de Graciansky et al., 1985a). However, no significant differences were recorded throughout, thus only the long spaced array (deep induction) was presented. The common unit system is the ohm per metre [Ω.m], and results are typically displayed using logarithmic scale. The ability of the bed rock to conduct an electrical current, or

equivalent resistivity, is a complex function of the sediment mineralogy (existence of some conductive minerals), the porosity, permeability and porosity fluid conductivity (*e.g.* brine, fresh water, oil; Darling, 2005; Mwenifumbo et al., 2009).

2.2.3 Compensated neutron density

The density was measured using the compensated neutron density tool which makes use of a neutron source (generally Americium/Beryllium) to bombard the sediment and measures the returning neutrons via two neutron detectors. The neutrons are primarily influenced by the presence of hydrogen, which causes significant energy loss for the neutrons that subsequently propagate at low, thermal velocities. The attenuation in the neutron response between the two detectors provides a measure of this attenuation process. Attenuation will typically be proportional to the amount of Hydrogen in the formation (Hydrogen index). Assuming the hydrogen index is primarily represented by the porosity fluid, the returning signal is greatly dependent on the porosity, as well as the nature of the fluid (*e.g.* water versus hydrocarbon; Tittle, 1961). Calibration to obtain the density can be simply obtained measuring the hydrogen index between two chosen references, and applying corrections for salinity, bound water and lithology. The presence of hydrocarbon and free gas will dramatically under-evaluate the porosity measurement because of their reduced density (Tittle, 1961; Lewis and McConchie, 1994; Darling, 2005). At DSDP Site 548, the neutron density (%) was calculated applying no specific correction (de Graciansky et al., 1985b).

2.2.4 P-wave velocity

The in-situ compressional p-wave velocity was measured using a long spaced sonic tool. It is composed of two transmitters (2 feet apart) and 4 receivers each spaced from ~2.5 to 3.5 m (8, 10, 10 and 12 feet respectively). This setup allows a measure of p-wave velocities with a vertical resolution of 0.6 m (de Graciansky et al., 1985b). This technique importantly relies on the picking of arrival times of the log recorded from each receiver, also called microseismogram. The velocities measured depend on the same geophysical parameters (ρ, E, v) defining the sub-surface reflectivity in seismic reflection (Fig. 1.1), and thus may be of critical importance when comparing the seismic and borehole stratigraphy.

2.3 Sediment core analysis

2.3.1 Multi-Sensor Core Logger

The GeoTek Multi-Sensor Core Logger (MSCL) allows non-destructive measurements of a series of geophysical parameters on full and split cores (Weaver and Schultheiss, 1990). The system is constituted of a core track equipped of a pusher for semi-automated and depth referenced measurements (Fig. 2.2). The devices mounted on the track can be customized. The core length and thickness are measured using laser sensors, by appropriately calibrating the core pusher to the zero position (for lengths) and measuring a reference thickness close to that of the actual measured core. The sediment (gamma) density is measured through statistical attenuation of a gamma ray beam that travels throughout the core. It is composed of a gamma ray source (generally Cesium 137), set in front of a gamma ray counter. The attenuation of the gamma beam mainly occurs through Compton Effect, and is highly dependent on the thickness and the density of the material it has travelled through. This method allows the measurement of the bulk sediment density and fractional porosity after application of a calibration routine (Weber et al., 1997). Calibration is made by measuring the gamma attenuation through a material of known density (generally aluminium) at different known thicknesses. The relation between the gamma attenuation and the corresponding density is then interpolated using a second order equation. Note that to infer the sediment density, precise measurement of the core thickness is necessary. For sediments, results are generally expressed in gram per cubic centimetres [g/cm^3].

The magnetic susceptibility is a measure of the degree of magnetization of a material when excited by a known magnetic field (Auffret et al., 1981; Chi and Mienert, 1996; Weber et al., 1997). The magnetic susceptibility is expressed in international unit system (SI) and is typically influenced by the presence of ferric and ferromagnetic grains, and in a lesser extent to some clay minerals, providing sometimes a useful proxy for sediment provenance (Richter et al., 2001; Voelker et al., 2006; Larrasoana et al., 2008).

The colour spectrophotometry provides detailed sediment reflectance properties within the visible light spectrum. Within marine sediments, the lightness may be greatly sensitive to the relative proportion of white grains (*e.g.* biogenic carbonates) and darker materials (*e.g.* mud), which thus can be used as a sediment composition proxy (Giosan et al., 2002a; Giosan et al., 2002b; Hodell et al., 2013; Bahr et al., 2014; Hodell et al., 2015). The calibration involves the use black and white reference reflectance, and results are generally presented in the international CIELab colour space parameters as: lightness (L*), red/green ratio (a*), and the green/blue ratio (b*). The core is imaged using a colour line scan camera mounted with a LED lighting box, allowing scanning at a

resolution comprised between ~200 and 300 dpi depending on the setting. The entire system is controlled through a measurement unit which allows real-time collection and calibration of the data (Fig. 2.2).

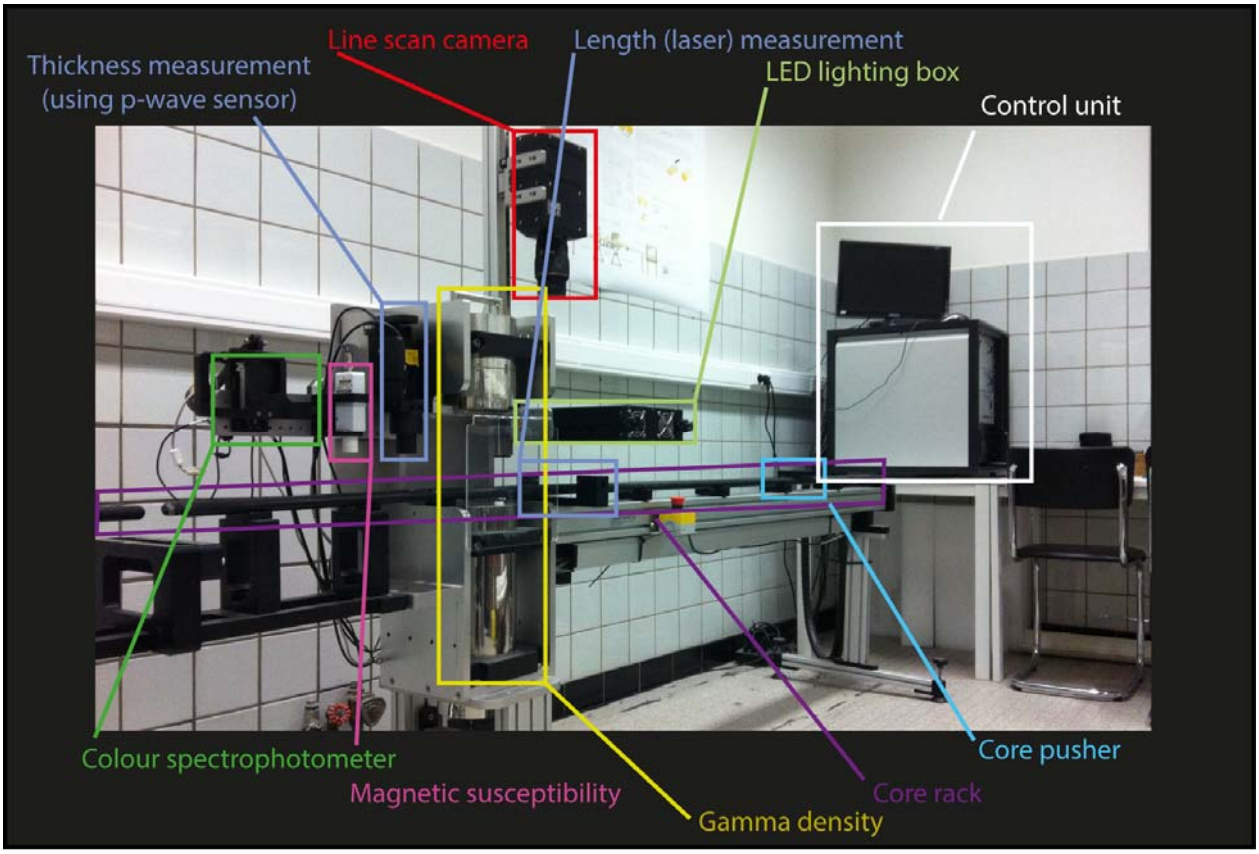

Figure 2.2 Photograph of a Multi-Sensor Core Logger (MSCL) showing the different measurements units in the system.

2.3.2 X-ray Fluorescence

X-ray Fluorescence (XRF) core scanning is a non-destructive method that allows analysis of surface split sediment cores to obtain a semi-quantitative elemental concentration (Richter et al., 2006). The Avaatech system is made of an X-ray source and a detector for the emitted response, set at 90° in a prism configuration (Fig. 2.3). The prism cell, that allows contact with the sediment core, is flushed in a helium atmosphere in order to avoid the complete absorption of the emitted sample soft radiations that would occur in regular atmosphere. The core surface is carefully cleaned, flattened and covered with a 4 µm thin SPEXCertiPrep Ultralene foil to avoid the prism cell contamination, reduce core surface desiccation, and reduce as much as possible sediment surface

and texture effects (Richter et al., 2006). The surface analysed is generally 1.2 cm wide for 1 cm long downcore, and is kept large enough in order to obtain statistically reproducible measurements. For the same statistical considerations, the sediment surface is excited during a certain integration time, and the reflected radiation is counted during the same integration time. When excited by X-ray radiations, different elements return to ground state by emitting photons of lower energy (or lower wavelength) that is dependent on one particular atom and its external electrons configuration (Weltje and Tjallingii, 2008). The analysis of the reflected spectrum allows the identification of certain peaks of energy [keV] which depends on each element and their relative concentrations. Measurements using a 10 kV and 30 kV of X-ray energy typically allows recognition of elements which mass is comprised between the Aluminium and Zirconium, respectively ranging from 26.98 and 91.22 atomic mass unit. However, high uncertainties must be expected for light elements due to small reflected energy spectrum, and for heavy elements due to limitations in the detectors. Results are processed using appropriate software and reported to as number of counts per elements [cps]. However, when studying sediment cores, the effect of the porosity (typically ranging from 30 to 70%), as well as roughness changes of the sediments are important. Additional inhomogeneity along the sediment surface also will affect the energy of the reflected beam. Therefore, the method is rarely calibrated to an absolute composition and the relative abundances in element composition are expressed as elemental ratios following recommendations from Richter et al. (2006) and Weltje and Tjallingii (2008). Alternatively, the normalization of one element is expressed by the element counts divided by the total counts; all elements included Weltje and Tjallingii (2008). This might be useful when trying to isolate variations of one single element, since ratios represent relative variations of two elements.

This study makes particular use of the XRF normalised Ti ratio ($Ti_{norm\ =}Ti_{counts/}total_{counts}$) and XRF Fe/Ca ratio, which often provide suitable terrigenous and terrigenous versus biogenic proxies (Jimenez-Espejo et al., 2008; Toucanne et al., 2009). Within marine sediments, Calcium element are primarily represented by the biogenic production of carbonates, while Iron and Ti are indicative for terrigenous clay and silt particles, and/or heavy minerals, which might originate from the erosion of continental igneous, volcanic and metamorphic rocks (Mojtahid et al., 2005; Hodell et al., 2013). Thus XRF Fe/Ca ratio typically represent overall variations in terrigenous versus biogenic content of sediments (Toucanne et al., 2009; Bahr et al., 2014). Here, it is preferred the use of XRF Ti_{norm} instead of Ti/Ca ratio in order to obtain a signal of the terrigenous content which would not be heavily imprinted by variations in the (biogenic) carbonate content. Moreover, The Titanium element is less sensitive to bottom water and sediment redox conditions than Iron (Bahr et al., 2014; Rodrigo-Gámiz et al., 2014). This is because titanium oxides are stable and weathering resistant

minerals, generally not altered within continental and marine sediments (Salminen, 2005). Iron is known to be often associated with post depositional changes in its red-ox state and solubility properties, in particular due to the presence and decomposition of organic matter (Berner, 1984; Croudace et al., 2015). Ti is also generally contained in heavy minerals, and can be used in some cases as proxy for aeolian dust input, along with zirconium and silica (Rodrigo-Gámiz et al., 2014; Bahr et al., 2015).

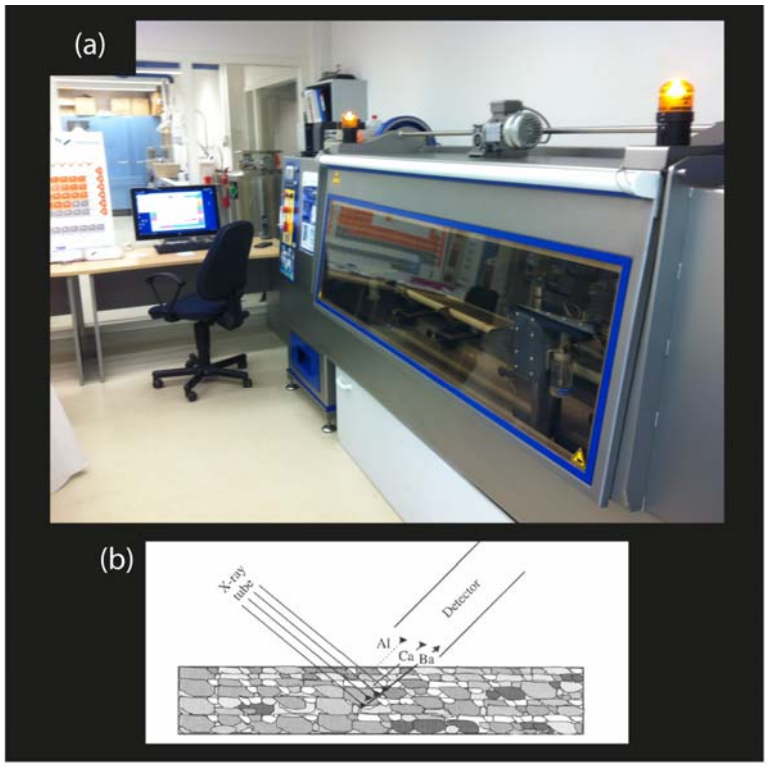

Figure 2.3 (a) Photograph of the Avaatech XRF core scanner. (b) Diagram showing incident and reflected X-ray, and the principle of XRF logging on split sediment core (Richter et al., 2006).

In this study, silica variations (XRF Si_{norm}) were used along the Atlantic Moroccan margin. This ratio may primarily reflect variations in the sediment quartz grains content, which might be controlled by variations of aeolian dust inputs along the western African margin (Tjallingii et al., 2008). Within the northern Gulf of Cádiz, the XRF Zr/Al ratio was successfully used as a proxy for bottom current intensity. Zircon is a weathering resistant and heavy mineral whereas aluminium is widely represented within clay and silts particles (Croudace et al., 2015). Thus XRF Zr/Al ratio may in some cases represent the relative enrichment in heavy minerals, possibly driven by bottom current controlled hydrodynamic sorting of particles (Bahr et al., 2014; Bahr et al., 2015). However Zircon is

a rare mineral which might explain why no conclusive variations in the XRF Zr/Al ratio could be observed in this study.

2.3.3 Particle grain-size distribution

Terrigenous and bulk sediment grain-sizes were performed using two methods. The first method used a Micromeritics Sedigraph III, which allows the measurement of the relative grain-size mass distribution of a sample in the clay/silt range, below 63 µm. It is made of a vertical sedimentation column and an X-ray detector which allows measuring the absorption of a known X-ray source, in particular in relation to the turbidity within the sedimentation column (Fig. 2.4; Bianchi et al., 1999). It is thus based on two principles (i) difference in particles sedimentation velocity within a water column defined through Stokes law and (ii) the absorption of an X-ray beam, depending on the concentration of particle present at a certain level within the sedimentation column, using Beer-Lambert law (Allen, 2003). The Sedigraph is particularly interesting when studying the dynamical properties since it is based on sedimentation velocities of the particles (McCave and Hall, 2006). Measurements are performed on samples pre-sieved with a 63 µm mesh, and result in the relative grain-size distribution fraction comprised between 2 and 63 µm. The samples were dried overnight at 60°C and about 0.02 to 0.04 g was taken for the analysis. The removal of carbonated (biogenic) fraction was performed using a two-fold acetic acid wash. This is generally performed prior measurement in order to focus on the terrigenous fractions, which may be linked to hydrodynamic conditions during sedimentation (McCave and Hall, 2006). Samples were then stirred using a rotating wheel in a 0.2% Sodium Hexametaphosphate solution for at least 24 h before measurement, and homogenously dispersed within the sedimentation column. The X-ray absorption is measured in a high portion of the water column at regular time interval (Fig. 2.4). The observed increase in the X-ray beam through time (decrease of absorption) is then converted into relative grain-size distribution (Bianchi et al., 1999).

The second method is based on visible light beam diffraction through a homogenously dispersed sediment sample, and was performed using a Malvern Mastersizer 3000. The scatter of the beam directly depends on the size and shape of the particles, which are generally assumed to be spherical. This method allows the measurement of the relative grain-size distribution comprised between 0.01 and 1500 µm, which range is substantially larger than with the Sedigraph. Required sample size is also smaller and may range from 20 to 80 mg of sediment depending on its bulk density and pre-treatment applied. For terrigenous measurements, the samples are treated by a two-fold acetic acid wash and 0.2% Sodium Hexametaphosphate in order to prevent particles flocculation (McCave and Hall, 2006). For bulk sediment analyses, samples were formerly boiled in a hydrogen peroxide

solution (35%), in order to remove possible organic matter content and ensure the dispersion of the sample. The sample is then dispersed into the Malvern unit using Hydro-MV module, and the angular variation and intensity of different diffracted light beam (using wavelengths within the red and blue) is measured, and expressed as a function of particles grain-size distribution (Bianchi et al., 1999; McCave and Hall, 2006).

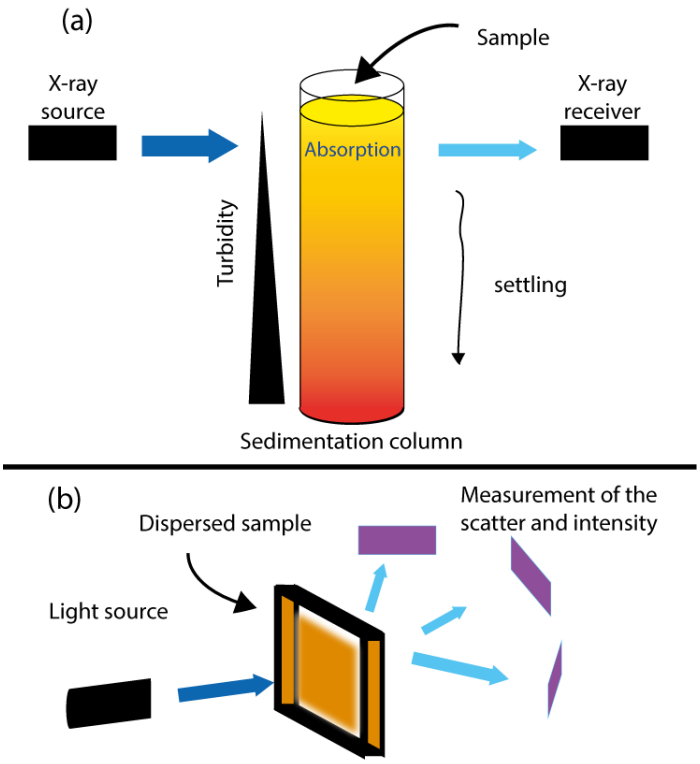

Figure 2.4 (a) Diagram showing the principle of a Micromeritics Sedigraph. X-ray absorption can be seen as a function of particles settlement. (b) Diagram showing the principle of a Malvern Mastersizer. Particle sizes control light scatter angle.

All grain-size measurements are generally expressed as relative weight or volume fraction of particles of equivalent sphere diameter, and grain-size fractions expressed and displayed using the Krumbein phi scale (Blott and Pye, 2001):

$$\Phi = -log_2 (D/D_0)$$

Where D is the equivalent sphere diameter of the particles, D_0 a reference particle size of 1 mm.

Bottom current (palaeo-)intensities were studied using variations in the main (first) mode which was generally comprised between ~6 and 55 μm. Different studies have focused on calculation of different statistical parameters associated to the grain-size distribution within the sortable silt grain-

size, ranging between 10 and 63 µm. Within this grain-size range, it is assumed that selective deposition of particles is primarily driven by bottom current induced selective deposition and winnowing of fine fraction (McCave, 1984). This is because silt particles below 10 µm are more subject to variable cohesive/non-cohesive behaviour during cycles of suspension deposition and resuspension (McCave and Hall, 2006). However, calculation of statistical parameters, such as the sortable silt index, as well as grain-size distribution sorting, skewness and kurtosis (Blott and Pye, 2001), may be problematic when different sediments sources are present, in particular related to ice rafter debris and aeolian sources (McCave et al., 1995; Bianchi et al., 1999; McCave and Hall, 2006). The presence of different mode must be carefully considered in order to avoid any misleading interpretation. This is particularly the case when large ice rafter debris input occurs (McCave and Hall, 2006). In this study, presence of variable amount of IRD and or bimodal grain-size distributions in the silt range occurred, and it was thus decided to study the main modes relative variations. Along it is systematically provided full range grain-size distribution plots representative for the whole samples, in order to avoid the introduction of potentially misleading parameters for the reader.

2.3.4 Foraminifera stratigraphy

Planktonic foraminifera are protists known to have distinct environmental preferences, of which varying temperatures might represent one of the most selective parameters (Kucera, 2007; Khare et al., 2012; Pados and Spielhagen, 2014). Such property allowed the early use of foraminifera assemblages for past sea-surface temperatures reconstructions (Imbrie and Kipp, 1971). It is based on the assumption that the preferred present-day living environment of one or more given species did not significantly vary through time (Bauch et al., 2003; Darling et al., 2006). Thus, the identification of similar past assemblages to present day ones, at one given geographic place, might reflect similar temperatures, salinities, and potentially seasonality amplitude in the sea-surface oceanic conditions (Waelbroeck et al., 1998; de Vernal et al., 2006). However this tool requires homogenized databases (Kipp, 1976), which were provided through different programs such as CLIMAP project (McIntyre and Cline, 1981), the EPILOG project (Mix et al., 2001) and the MARGO (Kucera et al., 2005). Open access and referenced databases are accessible via the World Data Center PANGAEA (https://www.pangaea.de). In parallel, different analytical methods were developed in order assign specific assemblages to their environment parameters, and reconstruct palaeo-oceanographic changes via transfer functions methods (Kipp, 1976), Modern Analogue Technique (Prell and United, 1985; Pflaumann et al., 1996; Pflaumann et al., 2003), subsequently revised by Waelbroeck et al. (1998).

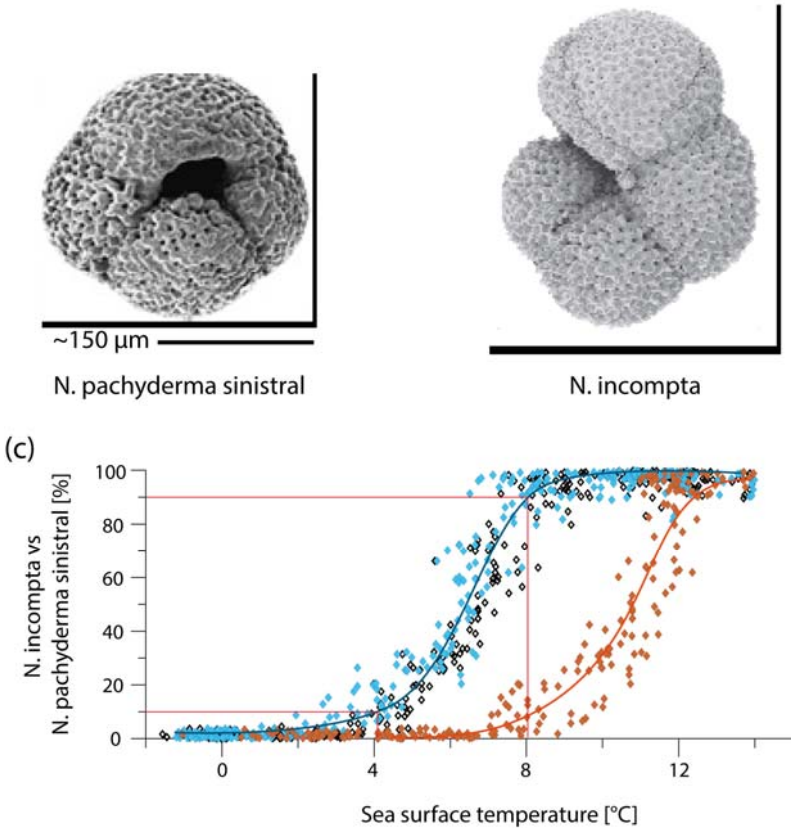

Figure 2.5 (a) Photograph of *N. pachyderma* sinistral specimens and (b) of *N. incompta* (*N.* pachyderma dextral) specimens (from Darling et al., 2006). (c) Plot representing the *N. incompta* versus *N. pachyderma* sinistral as a function of winter, summer and mean sea-surface temperatures at 80 m water depths (blue, orange and black diamond, respectively). Historical mean and seasonal decadal averages of 80 m water depth sea temperatures were obtained from (Locarnini et al., 2013). Core top foraminifera counts and relative abundances were obtained from the MARGO database (Kucera et al., 2005). Note, only Atlantic counts between 30 and 82°N are displayed. The red lines indicate temperatures corresponding to 4 and 8°C respectively, beyond which one or the other species largely dominates the assemblages.

This study made use of the relative abundance between the *Neogloboquadrina pachyderma* sinistral (left coiling) compared to relative abundance *N. incompta*, also referred to as *N. pachyderma* dextral. Those two species are known to exhibit distinct environmental preference which provides an excellent proxy for tracing past shifts of the northeast Atlantic sub-polar fronts (Mojtahid et al., 2005; Eynaud et al., 2009a; Vázquez Riveiros et al., 2013). *N. pachyderma* sinistral is dwelling within water depths associated with the chlorophyll maximum, generally around 20 to 80 m water depths (Kohfeld et al., 1996; Pados and Spielhagen, 2014), and has a strong affinity with cold polar to sub-polar environments (Fig. 2.5). In contrast, the *N. incompta* dwells within the upper thermocline, generally ranging around 100 m water depths (Darling et al., 2006), and is characteristic for warmer, sub-polar to sub-tropical sea-surface temperatures (Fig. 2.5). The relative abundance ratio between the two species is shown to be highly indicative for changes in winter sea-surface temperature ranging from 4 to 8°C (Fig. 2.5c). Note there exists a morphological gradation

from *N. pachyderma* dextral sensus stricto to *N. dutertrei* (Kipp, 1976) to which this study refer to as *N. incompta* sensus Darling et al. (2006). In this study, foraminifer counts were performed on the sieved sediment fraction above 150 µm, and about 200 specimens of cumulated *N. incompta* and *N. pachyderma* were counted for each sample in order to ensure statistically reproducible results.

2.3.5 Foraminifera stable Carbon and Oxygen isotope

Palaeo-oceanographic and palaeo-climatological variations were also studied by the means of stable Oxygen and Carbon isotope compositions of planktonic and benthic foraminifer carbonated shells. Those two elements may represent the two most common elements in the ocean, and are a major constituent of Foraminifera micro-organisms which form $CaCO_3$ shells (Rohling and Cooke, 1999; Rohling, 2013). These techniques are based on understanding and tracing isotope fractionation processes between ^{18}O versus ^{16}O (and ^{13}C versus ^{12}C) which represent respectively 99.63 and 0.1995% (98.89 and 1.11%) of the total Oxygen (Carbon) on earth (Ravelo and Hillaire-Marcel, 2007). Ratios between those respective isotopes can be measured from seawater and/or planktonic shells using Isotope Ratio Mass Spectrometry (IRMS), and are most commonly expressed as a delta (δ) of the sample ratio compared to a standard using following notation:

$$\delta^{18}O = \frac{(\frac{^{18}O}{^{16}O})_{sample} - (\frac{^{18}O}{^{16}O})_{standard}}{(\frac{^{18}O}{^{16}O})_{standard}} \times 1000$$

$$\delta^{13}C = \frac{(\frac{^{13}C}{^{12}C})_{sample} - (\frac{^{13}C}{^{12}C})_{standard}}{(\frac{^{13}C}{^{12}C})_{standard}} \times 1000$$

Both $\delta^{18}O$ and $\delta^{13}C$ are thus expressed as per mil [‰] ratio deviation from the appropriate standard (Ravelo and Hillaire-Marcel, 2007). Fractionation processes in nature may be driven by complex interplays between oceanographic, climatological, geological and biological processes, from which only the major ones are mentioned here (Rohling and Cooke, 1999).

In the ocean, changes in $\delta^{18}O$ seawater signature are primarily driven by fractionation through evaporation/precipitation processes, since evaporation is observed to cause $\delta^{18}O$ seawater increase (Fig. 2.6). As consequence, the $\delta^{18}O$ signature of the global ocean may vary significantly when depleted $\delta^{18}O$ precipitations are stored in the form of ice-sheets at high latitudes (Schmidt, 1999;

Rohling, 2013). During the Last Glacial Maximum (ca. 23 ka BP), such process has been responsible of a global seawater $\delta^{18}O$ enrichment, which could be estimated to a global mean of 0.95 ‰ (Waelbroeck et al., 2002). Measuring $\delta^{18}O$ from carbonated foraminifera, other effects must be taken into account, such as the temperature of calcification, salinity and biological vital effects which might vary from one species to the other (Kim and O'Neil, 1997). In particular, decreasing temperatures of calcification is responsible for increased foraminifer $\delta^{18}O$, evaluated to ~0.23 ‰/°C by Kim and O'Neil (1997).

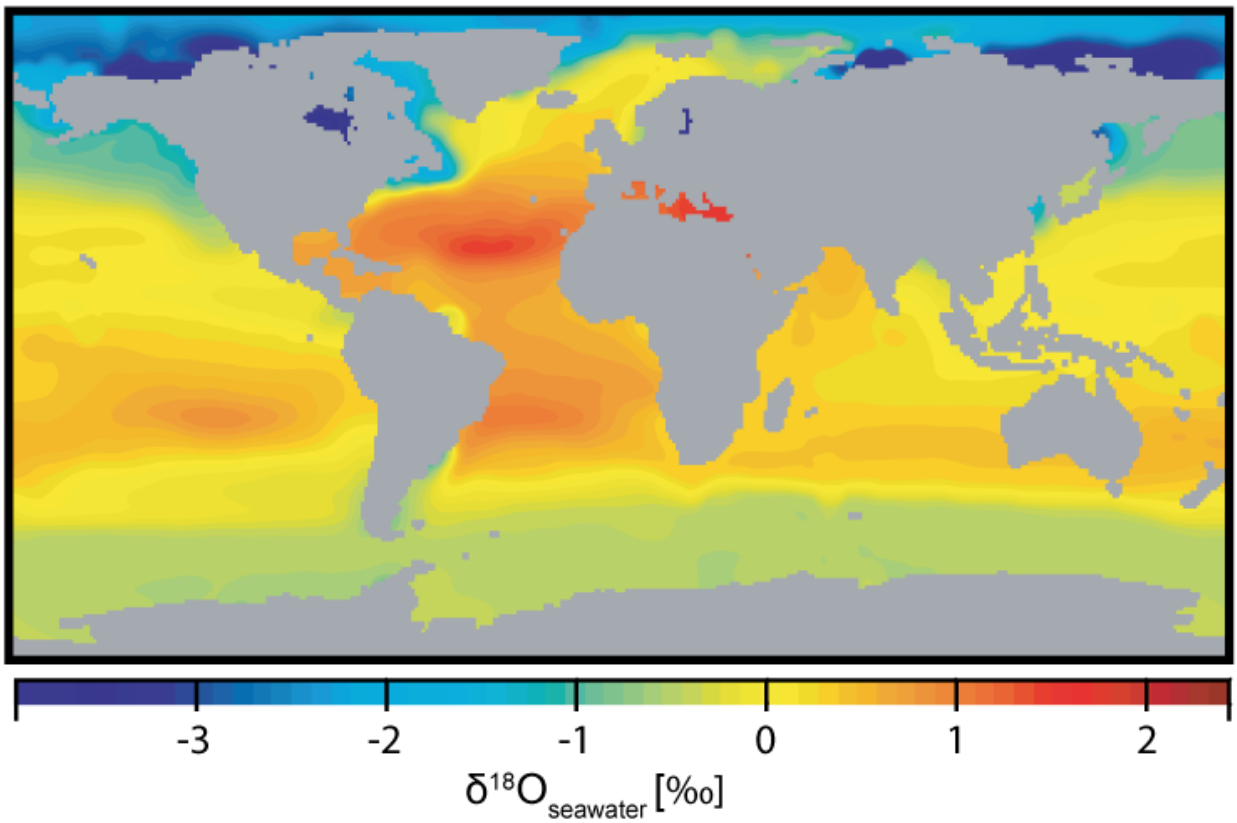

Figure 2.6 (a) Map of measured seawater $\delta^{18}O$ within the upper 5 meter of the surface oceans relative to the Standard Mean Ocean Water (SMOW; Schmidt, 1999; LeGrande and Schmidt, 2006). The ^{16}O depletion in tropical and sub-tropical latitudes is associated to a relative enrichment at high latitudes, evidencing evaporation-precipitation driven isotopic fractionation (Rohling and Cooke, 1999; Rohling, 2013). Note significant ^{16}O uptake from the global ocean occurs through ice-sheet expansion.

The fractionation of carbon isotopes is mainly controlled through exchanges between the ocean, atmosphere and terrestrial biosphere reservoirs, which are integrant parts of the global carbon cycle. Oceanic variations of dissolved inorganic $\delta^{13}C$ are commonly influenced by biogenic processes such as respiration, photosynthesis and carbonate precipitation (Ravelo and Hillaire-Marcel, 2007). At sub-tropical latitudes and regions characterised by high planktonic foraminifera productivity, sea-surface ^{12}C depletion occurs through biogenic export (Fig. 2.7; Eberwein and Mackensen, 2006). The

subsequent sedimentation of dead biogenic material might further cause ^{12}C enrichment of bottom water through enhanced particulate organic matter fluxes (Hoogakker et al., 2006). Likewise, specific processes associated to the fossilisation of the seawater $\delta^{13}C$ signature into precipitated biogenic carbonate are not straightforward and might be influenced by species-specific vital kinetic fractionation, and equilibrium between dissolved inorganic carbon, particulate organic carbon and CO_2 partial pressure changes (Rohling and Cooke, 1999; Eberwein and Mackensen, 2006; Ravelo and Hillaire-Marcel, 2007). Isotopic $\delta^{13}C$ variations in biogenic carbonates are traditionally used as palaeo-productivity proxies and in certain cases might be indicative of oceanic circulation and deep sea convection (Fig. 2.7). $\delta^{18}O$ and $\delta^{13}C$ have proven useful for palaeo-climatic and palaeo-oceanographic reconstructions (Duplessy, 1999; Waelbroeck et al., 2001), as well as reconstructions of past sea-level changes (Waelbroeck et al., 2002; Rohling et al., 2014).

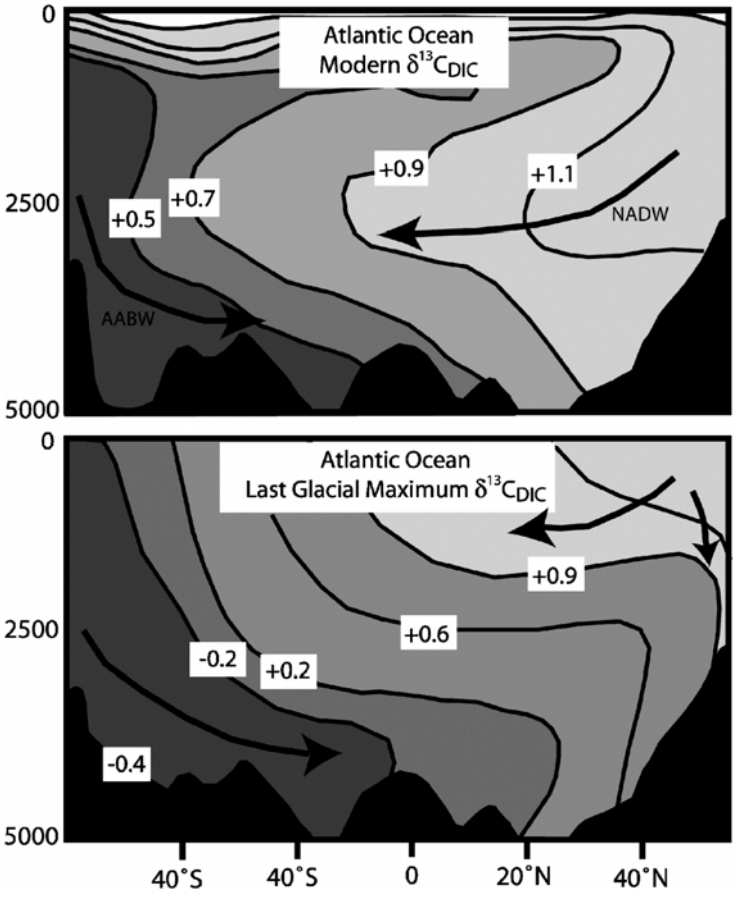

Figure 2.7 South to North Atlantic latitudinal cross section showing seawater Dissolved Inorganic Carbon $\delta^{13}C_{DIC}$ [‰] of the modern ocean and values inferred for the Last Glacial Maximum (Duplessy et al., 1988; Labeyrie et al., 1992). Note the deep sea convection associated to the North Atlantic meridional circulation is responsible for the formation of a deep high $\delta^{13}C_{DIC}$ anomaly.

In this study, $\delta^{18}O$ and $\delta^{13}C$ were obtained from carbonated tests of planktonic and benthic foraminifera using Isotope Ratio Mass Spectrometry. Planktonic *Globigerinoides bulloides* were selected from sieved fractions between 250 and 315 µm, and measurements were performed on 15 to 30 individuals in order to provide enough carbonate for measurements. Benthic *Cibicides pachyderma* specimens were selected from the same fraction and ranged from 2 to 4 individuals. All measurements were expressed using the Pee Dee Belemnite international standard reference [V-PDB]. The mean external reproducibility (1σ) of carbonate standard is of 0.05 ‰ for $\delta^{18}O$ and 0.04 ‰ for $\delta^{13}C$. Benthic and planktonic foraminifera broken specimen as well as specimen showing signs of dissolution where discarded for measurement. Well reserved specimens were considered pristine and selected for measurement. However, sediment drifts are subject to bottom current reworked sediment input which might corrupt the signal. Moreover, early diagenetic effects and dissolution are still susceptible to occur and simple microscopic diagnostic may not be sufficient (Ravelo and Hillaire-Marcel, 2007). Here the presence of bottom current reworked sediment input most probably explains the 0.4 to 1 ‰ deviation from available nearby records. However it seems the millennial-scale Dansgaard-Oeschger variability was still captured and provided sufficient record quality in order to establish the $\delta^{18}O$ chronostratigraphic tuning.

2.3.6 Radiocarbon dating

Radiocarbon dating is a technique using radioactive decaying of ^{14}C atoms relative concentration in order to determine one sample age. ^{14}C can be used for dating as old as 50 ka BP, most recently using Accelerated Mass Spectrometer. ^{14}C is a short-lived radioactive element of half-time constant of 5730 ± 40yr, and thus primary ^{14}C is virtually inexistent (Libby et al., 1949; Anderson and Libby, 1951; Bronk Ramsey, 2008). Radiocarbon is mainly produced in the high atmosphere by the reaction of nitrogen atoms and neutrons under cosmic ray excitation (Bronk Ramsey, 2008). Before the newly produced radiocarbon disintegrates into nitrogen, it may be exchanged between the different compartments involved in the carbon cycle, among which the biosphere is important (Hua, 2009). Living organisms are considered in equilibrium with the relative presence of ^{14}C in their environment. When those die, this equilibrium no longer exists and ^{14}C begins to decay with respect to the stable ^{12}C, providing a radioactive clock. However, equilibriums existing between the production rate, and fluxes between the different biologic, atmospheric, oceanic and geologic compartments are very complex (Hua, 2009; Reimer et al., 2013). In general, the initial $^{14}C/^{12}C$ ratio of a sample is unknown, and thus, time-dependent calibrations for ^{14}C ages are required and differ for each compartment of the carbon cycle (Bronk Ramsey, 2008; Wood, 2015). Thus, there has been important effort to constrain these variations/exchanges in the ocean, in order to provide suitable

and precise reservoir age corrections for foraminifera based radiocarbon dating (Stuiver and Reimer, 1998; Reimer et al., 2013). Both marine and terrestrial radiocarbon dating requires the assessment of the dated organism environment and place in its environment (Bronk Ramsey, 2008).

In this study, radiocarbon dates were obtained from samples selected along the Atlantic Moroccan margin. Mono-specific planktonic *G. bulloides* and *G. ruber* were picked, depending on the dominant foraminifer species. Approximately 3 mg of specimen were picked from the fraction above 150 µm. In absence of specific reservoir corrections along the Atlantic Moroccan margin, the calibration was done using a standard marine reservoir correction of 0.4 ky, using the Marine 13 calibration curve from Reimer et al. (2013).

2.3.7 Coccolith stratigraphy

The coccoliths (fossil coccolithophores) are nannofossil marine phytoplanktons which represent one of the most important biogenic carbonate sources in marine sediments (Beaufort and Heussner, 1999). Various Coccoliths sub-species are known to appear and disappear through time, providing distinct stratigraphic markers throughout the Quaternary (Pujos, 1988), and up to the Miocene (Raffi et al., 2006). Calibrated periods of coccolith species most common occurrence or highest and lowest consistent occurrences provide distinct stratigraphic ranges, which may vary as function of time and geographic location (Raffi, 2002). One common example is the last apearance of *Pseudoemiliana lacunosa* which exctints at ~420 ka BP after the end of the Early-Middle Pleisocene revolution (de Graciansky et al., 1985a). However, coccolith stratigraphic markers are various within the past 2.7 Ma (Raffi et al., 2006).

References

Al-Sadi, H.N., 1982. Seismic Exploration: Technique and processing. Birkhauser Verlag, Basel.

Allen, T., 2003. 7 - Gravitational sedimentation methods of particle size determination, Powder Sampling and Particle Size Determination. Elsevier, Amsterdam, pp. 359-391.

Anderson, E.C., Libby, W.F., 1951. World-Wide Distribution of Natural Radiocarbon. Physical Review 81, 64-69.

Auffret, G.A., Sichler, B., Coléno, B., 1981. Deep-sea sediments texture and magnetic fabric, indicators of bottom currents regime. Oceanologica Acta 4, 475-488.

Bahr, A., Jiménez-Espejo, F.J., Kolasinac, N., Grunert, P., Hernández-Molina, F.J., Röhl, U., Voelker, A.H.L., Escutia, C., Stow, D.A.V., Hodell, D., Alvarez-Zarikian, C.A., 2014. Deciphering bottom current velocity and paleoclimate signals from contourite deposits in the Gulf of Cádiz during the last 140 kyr: An inorganic geochemical approach. Geochemistry, Geophysics, Geosystems 15, 3145-3160.

Bahr, A., Kaboth, S., Jiménez-Espejo, F.J., Sierro, F.J., Voelker, A.H.L., Lourens, L., Röhl, U., Reichart, G.J., Escutia, C., Hernández-Molina, F.J., Pross, J., Friedrich, O., 2015. Persistent monsoonal forcing of Mediterranean Outflow Water dynamics during the late Pleistocene. Geology.Bauch, D., Darling, K., Simstich, J., Bauch, H.A., Erlenkeuser, H., Kroon, D., 2003. Palaeoceanographic implications of genetic variation in living North Atlantic Neogloboquadrina pachyderma. Nature 424, 299-302.

Beaufort, L., Heussner, S., 1999. Coccolithophorids on the continental slope of the Bay of Biscay – production, transport and contribution to mass fluxes. Deep Sea Research Part II: Topical Studies in Oceanography 46, 2147-2174.

Berner, R.A., 1984. Sedimentary pyrite formation: An update. Geochimica et Cosmochimica Acta 48, 605-615.

Bianchi, G.G., Hall, I.R., McCave, I.N., Joseph, L., 1999. Measurement of the sortable silt current speed proxy using the Sedigraph 5100 and Coulter Multisizer IIe: precision and accuracy. Sedimentology 46, 1001-1014.

Blott, S.J., Pye, K., 2001. GRADISTAT: a grain size distribution and statistics package for the analysis of unconsolidated sediments. Earth Surface Processes and Landforms 26, 1237-1248.

Bronk Ramsey, C., 2008. Radiocarbon dating: revolution in understanding. Archaeometry 50, 249-275.

Catuneanu, O., 2015. Sequence Stratigraphy, Reference Module in Earth Systems and Environmental Sciences. Elsevier.

Catuneanu, O., Abreu, V., Bhattacharya, J.P., Blum, M.D., Dalrymple, R.W., Eriksson, P.G., Fielding, C.R., Fisher, W.L., Galloway, W.E., Gibling, M.R., Giles, K.A., Holbrook, J.M., Jordan, R., Kendall, C.G.S.C., Macurda, B., Martinsen, O.J., Miall, A.D., Neal, J.E., Nummedal, D., Pomar, L., Posamentier, H.W., Pratt, B.R., Sarg, J.F., Shanley, K.W., Steel, R.J., Strasser, A., Tucker, M.E., Winker, C., 2009. Towards the standardization of sequence stratigraphy. Earth-Science Reviews 92, 1-33.

Chi, J., Mienert, J., 1996. Linking physical property records of Quaternary sediments to Heinrich events. Marine Geology 131, 57-73.

Croudace, I.W., Rothwell, G., (eds.), 2015. Micro-XRF Studies of Sediment Cores: Applications of a non-destructive tool for the environmental sciences. Springer Netherlands.Darling, K.F., Kucera, M., Kroon, D., Wade, C.M., 2006. A resolution for the coiling direction paradox in Neogloboquadrina pachyderma. Paleoceanography 21.

Darling, T., 2005. Chapter 5 - Advanced log interpretation techniques, Well Logging and Formation Evaluation. Gulf Professional Publishing, Burlington, pp. 67-102.

de Graciansky, P.C., Poag, C.W., Cunningham, R., Loubere, P., Masson, D.G., Mazzullo, J.M., Montadert, L., Müller, C., Otsuka, K., Reynolds, L.A., Sigal, J., Snyder, S.W., Townsend, H.A., Vaos, S.P., Waples, D., 1985b. Initial Reports of the Deep Sea Drilling Project. U.S. Government Printing Office, Washington.

de Graciansky, P.C., Poag, C.W., Cunningham, R., Loubere, P., Masson, D.G., Mazzullo, J.M., Montadert, L., Müller, C., Otsuka, K., Reynolds, L.A., Sigal, J., Snyder, S.W., Vaos, S.P., Waples, D., 1985a. Site 548, in: de Graciansky, P.C., Poag, C.W., Cunningham, R., Loubere, P., Masson, D.G., Mazzullo, J.M., Montadert, L.,

Müller, C., Otsuka, K., Reynolds, L.A., Sigal, J., Snyder, S.W., Vaos, S.P., Waples, D. (Eds.), Initial Reports of the Deep Sea Drilling Project. U.S. Government Printing Office, Washington, pp. 33-122.

de Vernal, A., Rosell-Melé, A., Kucera, M., Hillaire-Marcel, C., Eynaud, F., Weinelt, M., Dokken, T., Kageyama, M., 2006. Comparing proxies for the reconstruction of LGM sea-surface conditions in the northern North Atlantic. Quaternary Science Reviews 25, 2820-2834.

Doll, H.G., 1949. Introduction to Induction Logging and Application to Logging of Wells Drilled With Oil Base Mud.

Duplessy, J.-C., 1999. Oceanography: Climate and the Gulf Stream. Nature 402, 593-595.

Duplessy, J.C., Shackleton, N.J., Fairbanks, R.G., Labeyrie, L., Oppo, D., Kallel, N., 1988. Deepwater source variations during the last climatic cycle and their impact on the global deepwater circulation. Paleoceanography 3, 343-360.

Eberwein, A., Mackensen, A., 2006. Regional primary productivity differences off Morocco (NW-Africa) recorded by modern benthic foraminifera and their stable carbon isotopic composition. Deep Sea Research Part I: Oceanographic Research Papers 53, 1379-1405.

Eynaud, F., de Abreu, L., Voelker, A., Schönfeld, J., Salgueiro, E., Turon, J.-L., Penaud, A., Toucanne, S., Naughton, F., Sánchez Goñi, M.F., Malaizé, B., Cacho, I., 2009a. Position of the Polar Front along the western Iberian margin during key cold episodes of the last 45 ka. Geochemistry, Geophysics, Geosystems 10.

Eynaud, F., Cronin, T.M., Smith, S.A., Zaragosi, S., Mavel, J., Mary, Y., Mas, V., Pujol, C., 2009b. Morphological variability of the planktonic foraminifer Neogloboquadrina pachyderma from ACEX cores: Implications for Late Pleistocene circulation in the Arctic Ocean. Micropaleontology 55, 101-116.

Giosan, L., Flood, R.D., Aller, C.A., 2002a. Paleoceanographic significance of sediment color on western North Atlantic drifts: I. Origin of color. Marine Geology 189, 25-41.

Giosan, L., Flood, R.D., Grützner, J., Mudie, P., 2002b. Paleoceanographic significance of sediment color on western North Atlantic Drifts: II. Late Pliocene-Pleistocene sedimentation. Marine Geology 189, 43-61.

Hodell, D., Crowhurst, S., Skinner, L., Tzedakis, P.C., Margari, V., Channell, J.E.T., Kamenov, G., Maclachlan, S., Rothwell, G., 2013. Response of Iberian Margin sediments to orbital and suborbital forcing over the past 420 ka. Paleoceanography 28, 185-199.

Hodell, D., Lourens, L., Crowhurst, S., Konijnendijk, T., Tjallingii, R., Jimenez-Espejo, F., Skinner, L., Tzedakis, P.C., Members, S.S.P., 2015. A reference time scale for Site U1385 (Shackleton Site) on the SW Iberian Margin. Global and Planetary Change 133, 49-64.

Hoogakker, B.A.A., Rohling, E.J., Palmer, M.R., Tyrrell, T., Rothwell, R.G., 2006. Underlying causes for long-term global ocean [delta]13C fluctuations over the last 1.20[no-break space]Myr. Earth and Planetary Science Letters 248, 15-29.

Hua, Q., 2009. Radiocarbon: A chronological tool for the recent past. Quaternary Geochronology 4, 378-390.

Imbrie, J., Kipp, N.G., 1971. A new micropaleontological method for quantitative paleaclimatology: Application to a late Pleistocene Caribbean core. The Late Cenozoic Glacial Ages, edited by K. K. Turekian. Yale Univ. Press, New Haven, Conn, 71-181.

Jimenez-Espejo, F.J., Martinez-Ruiz, F., Rogerson, M., González-Donoso, J.M., Romero, O.E., Linares, D., Sakamoto, T., Gallego-Torres, D., Rueda Ruiz, J.L., Ortega-Huertas, M., Perez Claros, J.A., 2008. Detrital input, productivity fluctuations, and water mass circulation in the westernmost Mediterranean Sea since the Last Glacial Maximum. Geochemistry, Geophysics, Geosystems 9.

Kennedy, M., 2015. Chapter 5 - Logs Part II: Porosity, Resistivity and Other Tools, in: Martin, K. (Ed.), Developments in Petroleum Science. Elsevier, pp. 107-149.

Khare, N., Mazumder, A., Govil, P., 2012. Do changes in coiling directions in planktonic foraminifera correspond to dimorphic reproduction? Oceanology 52, 364-371.

Kim, S.-T., O'Neil, J.R., 1997. Equilibrium and nonequilibrium oxygen isotope effects in synthetic carbonates. Geochimica et Cosmochimica Acta 61, 3461-3475.

Kipp, N.G., 1976. New Transfer Function for Estimating Past Sea-Surface Conditions from Sea-Bed Distribution of Planktonic Foraminiferal Assemblages in the North Atlantic. Geological Society of America Memoirs 145, 3-42.

Kohfeld, K.E., Fairbanks, R.G., Smith, S.L., Walsh, I.D., 1996. Neogloboquadrina pachyderma (sinistral coiling) as paleoceanographic tracers in polar oceans: Evidence from northeast water polynya plankton tows, sediment traps, and surface sediments. Paleoceanography 11, 679-699.

Kucera, M., Rosell-Melé, A., Schneider, R., Waelbroeck, C., Weinelt, M., 2005. Multiproxy approach for the reconstruction of the glacial ocean surface (MARGO). Quaternary Science Reviews 24, 813-819.

Kucera, M., 2007. Chapter Six Planktonic Foraminifera as Tracers of Past Oceanic Environments, in: Claude, H.M., Anne De, V. (Eds.), Developments in Marine Geology. Elsevier, pp. 213-262.

Labeyrie, L.D., Duplessy, J.-C., Duprat, J., Juillet-Leclerc, A., Moyes, J., Michel, E., Kallel, N., Shackleton, N.J., 1992. Changes in the vertical structure of the North Atlantic Ocean between glacial and modern times. Quaternary Science Reviews 11, 401-413.

Larrasoana, J.C., Roberts, A.P., Rohling, E.J., 2008. Magnetic susceptibility of eastern Mediterranean marine sediments as a proxy for Saharan dust supply? Marine Geology 254, 224-229.

LeGrande, A.N., Schmidt, G.A., 2006. Global gridded data set of the oxygen isotopic composition in seawater. Geophysical Research Letters 33.

Lewis, D.W., McConchie, D., 1994. Borehole Sedimentology, Analytical Sedimentology. Springer US, Boston, MA, pp. 182-197.

Libby, W.F., Anderson, E.C., Arnold, J.R., 1949. Age Determination by Radiocarbon Content: World-Wide Assay of Natural Radiocarbon. Science 109, 227-228.

Locarnini, R.A., Mishonov, A.V., Antonov, J.I., Boyer, T.P., Garcia, H.E., Baranova, O.K., Zweng, M.M., Paver, C.R., Reagan, J.R., Johnson, D.R., Hamilton, M., Seidov, D., 2013. World Ocean Atlas 2013, Volume 1: Temperature. S. Levitus, Ed., A. Mishonov Technical Ed.; NOAA Atlas NESDIS 73, 40.

Lofi, J., Voelker, A.H.L., Ducassou, E., Hernández-Molina, F.J., Sierro, F.J., Bahr, A., Galvani, A., Lourens, L.J., Pardo-Igúzquiza, E., Pezard, P., Rodríguez-Tovar, F.J., Williams, T., 2016. Quaternary chronostratigraphic framework and sedimentary processes for the Gulf of Cadiz and Portuguese Contourite Depositional Systems derived from Natural Gamma Ray records. Marine Geology 377, 40-57.

McCave, I.N., 1984. Erosion, transport and deposition of fine-grained marine sediments, in: Stow, D.A.V., Piper, D.J.W. (Eds.), Fine Grained Sediments, Deep-Water Processes and Facies. Geological Society, London, pp. 35-69.

McCave, I.N., Manighetti, B., Robinson, S.G., 1995. Sortable silt and fine sediment size/composition slicing: Parameters for palaeocurrent speed and palaeoceanography. Paleoceanography 10, 593-610.

McCave, I.N., Hall, I.R., 2006. Size sorting in marine muds: Processes, pitfalls, and prospects for paleoflow-speed proxies. Geochemistry, Geophysics, Geosystems 7.

McIntyre, A., Cline, R., 1981. CLIMAP. Seasonal reconstruction of the Earth's surface at the last glacial maximum. Geol. Soc. Am. Map Chart Ser. MC-36, 1-18.

Mix, A.C., Bard, E., Schneider, R., 2001. Environmental processes of the ice age: land, oceans, glaciers (EPILOG). Quaternary Science Reviews 20, 627-657.

Mojtahid, M., Eynaud, F., Zaragosi, S., Scourse, J.D., Bourillet, J.F., Garlan, T., 2005. Palaeoclimatology and palaeohydrography of the glacial stages on Celtic and Armorican margins over the last 360000 yrs. Marine Geology 224, 57-82.

Mwenifumbo, C.J., Barrash, W., Knoll, M.D., 2009. Capacitive conductivity logging and electrical stratigraphy in a high-resistivity aquifer, Boise Hydrogeophysical Research Site. Geophysics 74, E125-E133.

Onajite, E., 2014a. Chapter 2 - Understanding Seismic Wave Propagation, Seismic Data Analysis Techniques in Hydrocarbon Exploration. Elsevier, Oxford, pp. 17-32.

Onajite, E., 2014b. Chapter 14 - Understanding Reflection Coefficient, Seismic Data Analysis Techniques in Hydrocarbon Exploration. Elsevier, Oxford, pp. 213-228.

Pados, T., Spielhagen, R.F., 2014. Species distribution and depth habitat of recent planktic foraminifera in Fram Strait, Arctic Ocean. 2014.

Pflaumann, U., Duprat, J., Pujol, C., Labeyrie, L.D., 1996. SIMMAX: A modern analog technique to deduce Atlantic sea surface temperatures from planktonic foraminifera in deep-sea sediments. Paleoceanography 11, 15-35.

Pflaumann, U., Sarnthein, M., Chapman, M., d'Abreu, L., Funnell, B., Huels, M., Kiefer, T., Maslin, M., Schulz, H., Swallow, J., van Kreveld, S., Vautravers, M., Vogelsang, E., Weinelt, M., 2003. Glacial North Atlantic: Sea-surface conditions reconstructed by GLAMAP 2000. Paleoceanography 18.

Prell, W.L., United, S., 1985. The stability of low-latitude sea-surface temperatures: an evaluation of CLIMAP reconstruction with emphasis on the positive SST anomalies. U.S. Dept. of Energy, Office of Energy Research, Office of Basic Energy Sciences, Carbon Dioxide Research Division, Washington, D.C.

Pujos, A., 1988. Spatio-temporal distribution of some quaternary coccoliths. Oceanologica Acta 11, 65 - 77.

Quirein, J.A., Gardner, J.S., Watson, J.T., 1982. Combined Natural Gamma Ray Spectral/Litho-Density Measurements Applied to Complex Lithologies.

Raffi, I., 2002. Revision of the early-middle pleistocene calcareous nannofossil biochronology (1.75–0.85 Ma). Marine Micropaleontology 45, 25-55.

Raffi, I., Backman, J., Fornaciari, E., Pälike, H., Rio, D., Lourens, L., Hilgen, F., 2006. A review of calcareous nannofossil astrobiochronology encompassing the past 25 million years. Quaternary Science Reviews 25, 3113-3137.

Ravelo, A.C., Hillaire-Marcel, C., 2007. Chapter Eighteen The Use of Oxygen and Carbon Isotopes of Foraminifera in Paleoceanography, in: Claude, H.M., Anne De, V. (Eds.), Developments in Marine Geology. Elsevier, pp. 735-764.

Reimer, P.J., Bard, E., Bayliss, A., Beck, J.W., Blackwell, P.G., Bronk Ramsey, C., Buck, C.E., Cheng, H., Edwards, R.L., Friedrich, M., Grootes, P.M., Guilderson, T.P., Haflidason, H., Hajdas, I., Hatté, C., Heaton, T.J., Hoffmann, D.L., Hogg, A.G., Hughen, K.A., Kaiser, K.F., Kromer, B., Manning, S.W., Niu, M., Reimer, R.W., Richards, D.A., Scott, E.M., Southon, J.R., Staff, R.A., Turney, C.S.M., van der Plicht, J., 2013. IntCal13 and Marine13 Radiocarbon Age Calibration Curves 0–50,000 Years cal BP.

Richter, T.O., Lassen, S., van Weering, T.C.E., de Haas, H., 2001. Magnetic susceptibility patterns and provenance of ice-rafted material at Feni Drift, Rockall Trough: implications for the history of the British-Irish ice sheet. Marine Geology 173, 37-54.

Richter, T.O., van der Gaast, S., Koster, B., Vaars, A., Gieles, R., de Stigter, H.C., De Haas, H., van Weering, T.C.E., 2006. The Avaatech XRF Core Scanner: technical description and applications to NE Atlantic sediments, in: Rothwell, R.G. (Ed.), New techniques in Sediment Core Analysis. Geological Society, London, pp. 39-50.

Rodrigo-Gámiz, M., Martínez-Ruiz, F., Rodríguez-Tovar, F.J., Jiménez-Espejo, F.J., Pardo-Igúzquiza, E., 2014. Millennial- to centennial-scale climate periodicities and forcing mechanisms in the westernmost Mediterranean for the past 20,000 yr. Quaternary Research 81, 78-93.

Rohling, E.J., Cooke, S., 1999. Stable oxygen and carbon isotope ratios in foraminiferal carbonate shells. Sen Gupta, B.K. (eds.) Modern Foraminifera. Dordrecht, The Netherlands, Kluwer Academic, 239-258.

Rohling, E.J., 2013. PALEOCEANOGRAPHY, PHYSICAL AND CHEMICAL PROXIES | Oxygen Isotope Composition of Seawater A2 - Elias, Scott A, in: Mock, C.J. (Ed.), Encyclopedia of Quaternary Science (Second Edition). Elsevier, Amsterdam, pp. 915-922.

Rohling, E.J., Foster, G.L., Grant, K.M., Marino, G., Roberts, A.P., Tamisiea, M.E., Williams, F., 2014. Sea-level and deep-sea-temperature variability over the past 5.3 million years. Nature 508, 477-482.

Russell, W.L., 1944. The total gamma ray activity of sedimentary rocks as indicated by Geiger counter determinations. Geophysics 9, 180-216.

Salminen, R., (ed.), 2005. Geochemical Atlas of Europe. Part 1: Background Information, Methodology and Maps. Espoo: Geological Survey of Finland' for details.

Schmidt, G.A., 1999. Forward modeling of carbonate proxy data from planktonic foraminifera using oxygen isotope tracers in a global ocean model. Paleoceanography 14, 482-497.

Serra, O., Baldwin, J., Quirein, J., 1980. Theory, Interpretation, And Practical Applicatons Of Natural Gamma Ray Spectroscopy.

Sierro, F.J., Ledesma, S., Flores, J.-A., Torrescusa, S., del Olmo, W.M., 2000. Sonic and gamma-ray astrochronology: Cycle to cycle calibration of Atlantic climatic records to Mediterranean sapropels and astronomical oscillations. Geology 28, 695-698.

Stewart, S.A., 2011. Vertical exaggeration of reflection seismic data in geoscience publications 2006-2010. Marine and Petroleum Geology 28, 959-965.

Stuiver, M., Reimer, P.B., T., 1998. High-precision radiocarbon age calibration for terrestrial and marine samples. Radiocarbon 40, 1127-1151.

Tittle, C.W., 1961. Theory of neutron logging I. Geophysics 26, 27.

Tjallingii, R., Claussen, M., Stuut, J.B.W., Fohlmeister, J., Jahn, A., Bickert, T., Lamy, F., Rohl, U., 2008. Coherent high- and low-latitude control of the northwest African hydrological balance. Nature Geoscience 1, 670-675.

Toucanne, S., Zaragosi, S., Bourillet, J.F., Cremer, M., Eynaud, F., Van Vliet-Lanoë, B., Penaud, A., Fontanier, C., Turon, J.L., Cortijo, E., Gibbard, P.L., 2009. Timing of massive 'Fleuve Manche' discharges over the last 350 kyr: insights into the European ice-sheet oscillations and the European drainage network from MIS 10 to 2. Quaternary Science Reviews 28, 1238-1256.

Vail, P.R., Mitchum, J.R.M., Todd, R.G., Widmier, J.M., S., Thompson III, J.B., Sangree, J.B., Bubb, J.N., Hatlelid, W.G., 1977. Seismic stratigraphy and global changes of sea-level. in C.E. Payton (ed.), Seismic stratigraphy - Applications to hydrocarbon exploration. American Association Petroleum Geologists Memoir 26, 49-212.

Vasconcelos, M.A.R., Leite, E.P., Crósta, A.P., 2012. Contributions of gamma-ray spectrometry to terrestrial impact crater studies: The example of Serra da Cangalha, northeastern Brazil. Geophysical Research Letters 39.

Vázquez Riveiros, N., Waelbroeck, C., Skinner, L., Duplessy, J.-C., McManus, J.F., Kandiano, E.S., Bauch, H.A., 2013. The “MIS 11 paradox” and ocean circulation: Role of millennial scale events. Earth and Planetary Science Letters 371–372, 258-268.

Veeken, P.C.H., Moerkerken, B.v., 2013. 2 - The seismic reflection method and its constraints, Seismic Stratigraphy and Depositional Facies Models. Academic Press, pp. 15-104.

Voelker, A.H.L., Lebreiro, S.M., Schonfeld, J., Cacho, I., Erlenkeuser, H., Abrantes, F., 2006. Mediterranean outflow strengthening during northern hemisphere coolings: A salt source for the glacial Atlantic? Earth and Planetary Science Letters 245, 39-55.

Waelbroeck, C., Labeyrie, L., Duplessy, J.C., Guiot, J., Labracherie, M., Leclaire, H., Duprat, J., 1998. Improving past sea surface temperature estimates based on planktonic fossil faunas. Paleoceanography 13, 272-283.

Waelbroeck, C., Duplessy, J.-C., Michel, E., Labeyrie, L., Paillard, D., Duprat, J., 2001. The timing of the last deglaciation in North Atlantic climate records. Nature 412, 724-727.

Waelbroeck, C., Labeyrie, L., Michel, E., Duplessy, J.C., McManus, J.F., Lambeck, K., Balbon, E., Labracherie, M., 2002. Sea-level and deep water temperature changes derived from benthic foraminifera isotopic records. Quaternary Science Reviews 21, 295-305.

Weaver, P.P.E., Schultheiss, P.J., 1990. Current methods for obtaining, logging and splitting marine sediment cores. Marine Geophysical Researches 12, 85-100.

Weber, M.E., Niessen, F., Kuhn, G., Wiedicke, M., 1997. Calibration and application of marine sedimentary physical properties using a multi-sensor core logger. Marine Geology 136, 151-172.

Weltje, G.J., Tjallingii, R., 2008. Calibration of XRF core scanners for quantitative geochemical logging of sediment cores: Theory and application. Earth and Planetary Science Letters 274, 423-438.

Wood, R., 2015. From revolution to convention: the past, present and future of radiocarbon dating. Journal of Archaeological Science 56, 61-72.

CHAPTER 3

Plio-Pleistocene bottom current variability at Goban Spur

The content of this chapter has been published as:

Delivet, S., Van Eetvelt, B., Monteys, X., Ribó, M., Van Rooij, D., 2016. Seismic geomorphological reconstructions of Plio-Pleistocene bottom current variability at Goban Spur. Marine Geology 378, 261-275.

Abstract

High-resolution single channel sparker reflection seismic data revealed the presence of large-scale sediment waves nearby DSDP Site 548, located on Goban Spur. They developed in a gentle terraced environment which contrasts with the canyon-incised Celtic margin, and the relatively smooth Porcupine Seabight to the north. Based upon the morphological characteristics of the observed seabed and buried sediment waves, energetic alongslope bottom currents are thought to be the driving mechanism for the sediment wave development. These currents are driven on their turn by an enhanced internal tide regime that could be attributed to the introduction of the Mediterranean Outflow Water. The DSDP Site 548 downhole geophysical data and the seismic stratigraphic analysis allowed the differentiation of three sequences that relate to evolutionary stages since the lower Pliocene. The sequences are bounded by local erosional events, associated with mass wasting events, which seem to occur roughly synchronously to major northern hemisphere glaciations, respectively during the Lower Pleistocene (~2.5 to 2.15 Ma), and the Middle Pleistocene (~0.45 Ma). The lower sequence (from ~4.5 to ~2.15 Ma) shows no morphological evidence of bottom-current driven sedimentation. It is however settled over a smooth erosional surface which could indicate the introduction of the Mediterranean Outflow Water. The intermediate sequence is characterised by large-scale sediment waves that have gradually developed in close association with palaeo-seafloor irregularities. It is inferred that the sedimentation resumed with a relative bottom current energy increase. The youngest sequence recorded active sediment wave formation, similar to the previous sequence. Although the Goban Spur sediment waves cannot be regarded as contourite drifts as such, their stratigraphic evolution corresponds to other well-documented contourite depositional systems, influenced by the Mediterranean Outflow Water.

3.1 Introduction

Goban Spur is a marginal submarine plateau at a latitude of 49°N in the northeast Atlantic Ocean (Fig. 3.1), located at the boundary of the northwest trending Celtic margin and the roughly northward trending Porcupine Seabight and Irish margin. Since the drilling of DSDP Site 548 (1256 m water depth) in 1984, it has been of great interest in terms of palaeoceanographic and climatic studies, allowing a certain focus with respect to the investigation of the dynamics of the northeast Atlantic intermediate water masses, especially regarding the Mediterranean Outflow Water (MOW; Caralp et al., 1985; Poag et al., 1985; Loubere, 1987; Khélifi et al., 2009, 2014; Rogerson et al., 2012). Nowadays, the MOW forms a geostrophic poleward boundary undercurrent after having exited the Gibraltar Strait (Fig. 3.1). It reaches its most distal extension north of the Porcupine Bank (Iorga and Lozier, 1999a, b; Van Aken, 2000; McCartney and Mauritzen, 2001). Since the lower Pliocene, it has been involved in the formation of large Contourite Depositional Systems (CDS) all along the NE Atlantic margin. From its most proximal to most distal location, this concerns the Gulf of Cádiz CDS (Hernández-Molina et al., 2006, 2011, 2014; Llave et al., 2006, 2011; Toucanne et al., 2007; García et al., 2009; Hanquiez et al., 2010; Roque et al., 2012), the Ortegal CDS (Hernández-Molina et al., 2011), the Le Danois CDS (Ercilla et al., 2008; Van Rooij et al., 2010) and the Porcupine CDS (Van Rooij et al., 2007, 2009; Huvenne et al., 2009).

At its most distal occurrence within the Porcupine Seabight, IODP expedition 307 has evidenced that the MOW introduction locally established favourable hydrodynamic conditions for the development of cold-water coral mounds from the late Pliocene (Huvenne et al., 2009; Raddatz et al., 2011), as an important part of the Porcupine CDS. During the present-day, it has been shown that the strong bottom currents in the eastern Porcupine Seabight are due to internal waves of tidal period (*i.e.* internal tides) at the upper interface between the MOW and the Eastern North Atlantic Water (White, 2007; Van Rooij et al., 2009). The complex palaeotopography of the Porcupine Seabight slope (Van Rooij et al., 2007) may have contributed to enhance the tidally modulated bottom currents, driving the formation of a complex CDS in close association with the cold-water coral mounds. However, the existence of a large erosional unconformity RD1, acting as the base of the Belgica cold-water coral mounds, regionally represents large hiatuses (from 6.6 to 8.2 My) and was possibly created by several incision phases (Kano et al., 2007; Louwye et al., 2008; Van Rooij et al., 2009). The sedimentation first resumed in the form of cold-water coral mound accretion at ~2.7 Ma and lagged in off-mound setting, from about 1.24 Ma at site U1318 to about 0.5 Ma depending on the local morphology (Kano et al., 2007; Huvenne et al., 2009). Therefore, the events leading to this Miocene/Pliocene RD1 unconformity are difficult to investigate and a precise timing of the MOW introduction within the Porcupine Seabight is difficult to assess. Hence, also information regarding

the past MOW dynamics along its most distal part, from the southern Bay of Biscay (Le Danois CDS) onwards, is missing.

DSDP Site 548 on Goban Spur is relatively isolated from active sedimentary systems and represents a morphologically relatively gentle environment (Figs. 3.2a, b). It recorded a more complete sequence, especially regarding the Miocene to Pliocene transition (Loubere, 1987), which is mostly missing in the Porcupine CDS. It is currently situated within the MOW lower interface (Figs. 3.2c, d), which differs with the Belgica cold-water coral mound province within the Porcupine CDS. Only limited amplitude effects of internal tides can be expected due to the local morphology (Rice et al., 1990; Iorga and Lozier, 1999b; New et al., 2001; White and Dorschel, 2010).

Based upon a new dataset of very high resolution single channel reflection seismic data, centred on DSDP Site 548, this study aims to improve the local Plio-Pleistocene stratigraphic framework and to provide an overview of the local and contemporary sediment dynamics, influenced by an already rather distal MOW. As such, this will assist to improve our knowledge of the MOW palaeoceanography in the northern Bay of Biscay, at an intermediate site between the Porcupine CDS and the Le Danois CDS. Goban Spur may be considered as a key site to better understand the (suite of) processes that have led to the creation of the large RD1 unconformity, as well as the subsequent formation of cold-water coral mounds and associated contourite drifts within the Porcupine CDS.

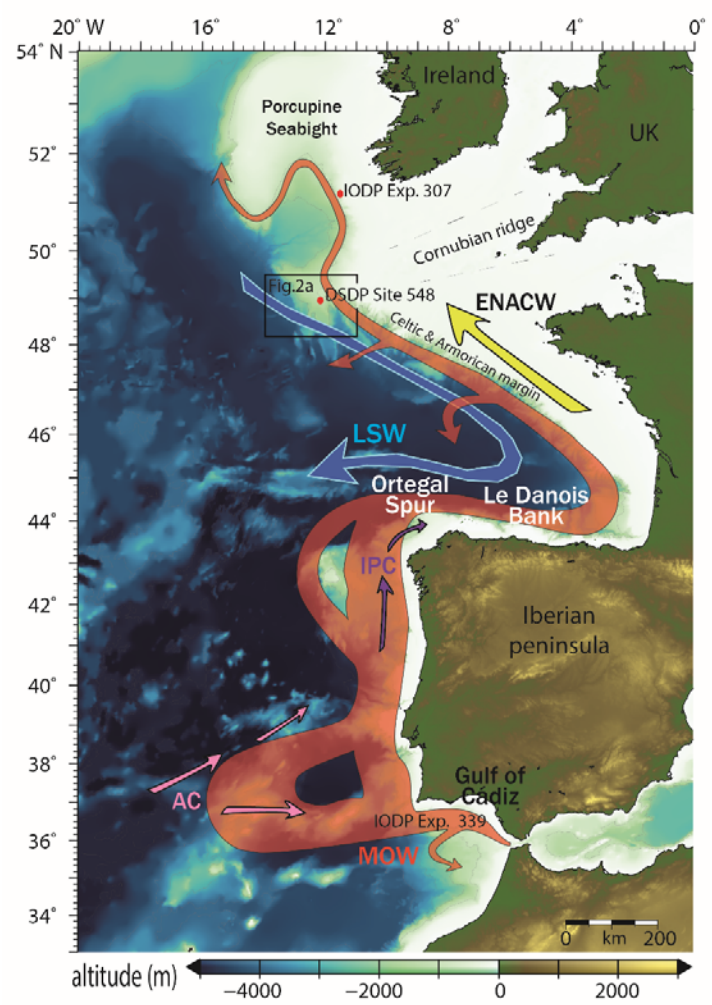

Figure 3.1 Location of the study area and other areas referred to in the text. The arrows indicate the main circulation pattern. **AC**: Azores Current; **IPC**: Iberian Poleward Current; **ENACW**: Eastern North Atlantic Central Water; **MOW**: Mediterranean Outflow Water; **LSW**: Labrador Sea Water.

3.2 Regional setting

3.2.1 Geological and geomorphological setting

The study area is located on the upper slope along the southwestern limb of the Goban Spur submarine plateau, with water depths ranging between 900 and 1600 m. The Goban Spur continental slope consists of NW-SE elongated terraces, formed by different sub-parallel escarpments, such as the Pendragon Escarpment (Fig. 3.2a). These terraces correspond to half-graben structures inherited from the early Cretaceous north Atlantic rift, which gradually steps down towards the Porcupine abyssal plain (Naylor and Shannon, 1982; Louvel et al., 1997). The buoyant Hercynian basement is believed to constitute the southwestern prolongation of the Cornubian Ridge (Dingle and Scrutton, 1979; Fig. 3.1). Canyon systems are poorly developed along the adjacent

slopes, which strongly contrasts with the typically canyon incised Celtic and Armorican margins of the northern Bay of Biscay (Bourillet et al., 2006; Zaragosi et al., 2006). The northern boundary forms a gentle northward dipping slope leading to the Porcupine Seabight. The western terraced slope is slightly crosscut by two sinuous canyon valleys, of which the head walls are located at about 20 km west/southwest of DSDP Site 548, separated by a structural high (Figs. 3.2a, b).

The sediment cover at Goban Spur is relatively thin (*e.g.* 530 m at DSDP Site 548), and is thus considered as sediment starved margin (Dingle and Scrutton, 1979). This is both due to the buoyant basement and to its distal emplacement with respect to its drainage basin; the Great Sole drainage basin, located more to the east (Zaragosi et al., 2006). The sediments retrieved within DSDP Site 548 have an early Cretaceous to Holocene age and mostly consist of sub-littoral to pelagic sediments, mainly composed of foraminifer and nannofossil ooze. A more distinct terrigenous input consisting of very coarse ice-rafted debris occurs from the late Pliocene and becomes marked within the middle to late Pleistocene section, providing an excellent glacial to interglacial alternating record (de Graciansky et al., 1985). The settlement of the poleward oceanic circulation on the shelves from the Neogene to the present-day is often cited as an important sediment lateral advection process (van Weering et al., 1998; Shannon et al., 2005). It may have substantially contributed to the sediment input, transported from the Armorican shelf (Auffret et al., 2002; Cunningham et al., 2005).

3.2.2 Oceanographic setting

The present-day hydrography at Goban Spur is closely linked to the residual circulation pattern of shelf water masses within the Bay of Biscay. Below the approximately 200 m deep surface mixed layer, the Eastern North Atlantic Central Water (ENACW) is found, centred at about 500 m water depth (Figs. 3.2c, d). This relatively saline and warm water mass (~35.5 and 10.5 to 11°C) is formed by winter cooling of the Iberian poleward current, the northernmost branch of the Azores Current which enters the Bay of Biscay and propagates poleward along the continental shelf (Pingree and Le Cann, 1990; Van Aken, 2000). In summer, the strong influence of the Saharan northeastern trade winds drives the formation of a seasonal upwelling within the Gulf of Cádiz. This causes the vanishing of the Iberian poleward current, resulting in a strong seasonal modulation of the ENACW (Pingree and Le Cann, 1992). With depth, the salinity increases to a maximum of about 35.6 (and 9 to 10°C), signing the residual signal of the MOW (Figs. 3.2c, d; Van Aken, 2000; Huthnance et al., 2001). Centred at about 800 m water depth, the MOW poleward advection (Fig. 3.1) occurs as a thermohaline geostrophic current (Iorga and Lozier, 1999a). It propagates within the Porcupine Seabight with a mean flow ranging from 2 to 10 cm/s (White, 2007). Below the MOW, at

approximately 1800 m depth, the salinity decreases to a minimum (~34.9 and ~5°C), characterizing the young eastern branch of the Labrador Sea Water (LSW; Figs. 3.2c, d). The LSW is formed by open-sea winter surface cooling, leading to deep water convection within the Labrador Sea (Sy et al., 1997). It spreads towards the southeast within the Bay of Biscay (Paillet et al., 1998).

The study area ranges from 1000 to 1600 m water depth which corresponds to the interface between MOW and LSW (Fig. 3.2c). Direct near seabed current data, consisting of the long term Royal NIOZ BOBO Lander measurements, were obtained from the "OMEX station II" (Fig. 3.2a), respectively at 1296 and 1453 m water depths (Thomsen and van Weering, 1998). The previous authors indicated a strong seasonal NNW/SSE current modulation, and basin-ward directed peak velocities, perpendicular to the local contours. The highest flow velocities are observed in winter (35 – 37 cm/s) and were not exceeding 10 cm/s in summer (Huthnance et al., 2001). The cyclic semi-diurnal flow reversal was attributed to an internal tide regime. Internal tides are defined as barotropic currents of tidal frequency flowing over the seabed (Lamb, 2014). Their interaction with the seabed between 1000 and 1470 m water depth is known to be associated with seasonal major re-suspension events and nepheloid layer generation causing lateral sediment advection from the shelf towards the basin (Thomsen and van Weering, 1998; van Weering et al., 1998).

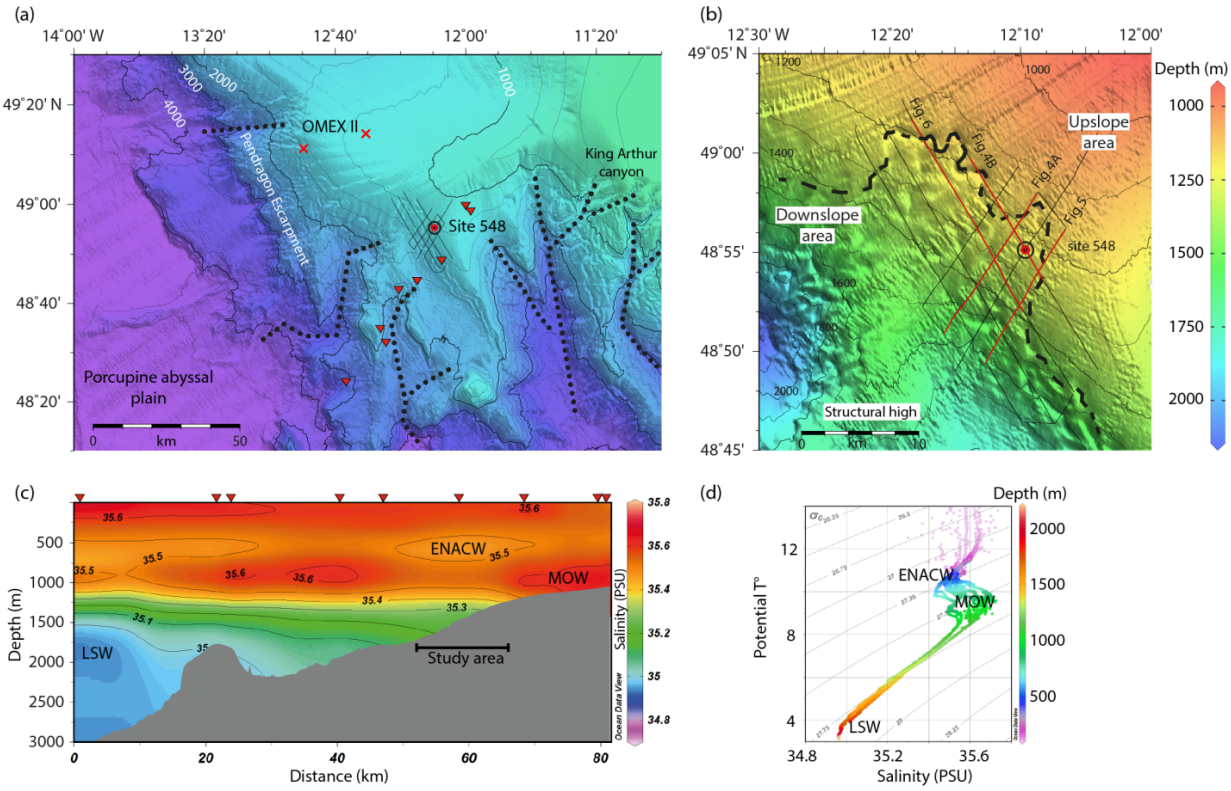

Figure 3.2 (a) High-resolution bathymetric map (courtesy of the Irish National Seabed Survey, GSI). The location of the DSDP Site 548, the CTD stations (red triangles) and the OMEX II stations (crosses) Thomsen and van Weering, (1998) are indicated. The dotted lines indicate the location of the main canyon structures in the area. (b) High-resolution bathymetric map of the study area indicating the seismic data coverage and figures location. The dashed line marks the edge of the escarpment delimiting the "upslope" versus "downslope" areas referred in the text. Note the presence of a structural high separating two different canyon structures. (c) Salinity profile showing the water mass stratification. CTD stations (red triangles) and their respective location are indicated in the general map - Fig. 2a- (World Ocean Database, 2009). (d) Potential temperature versus salinity diagram showing density and water mass properties.

3.3 Material and methods

Two sets of high-resolution single channel reflection seismic data, both using an SIG sparker source, have been used. The first set consists of two lines, acquired during the R/V Belgica cruise ST0112 in May 2001, oriented 31° and 149°, and centred on DSDP Site 548. These profiles were acquired using a 500 J energy source, resulting in a 200 to 3000 Hz signal, with a 3 s record length and a sampling rate of 10 kHz. The second dataset has been acquired during the R/V Belgica cruise ST1217 in June 2012. It constitutes an extension of the two previous lines, forming a network of roughly 3 km spaced parallel lines (Fig. 3.2b). The sparker source was fired every 3 s at 600 J with a record length of 2.7 s using a 10 kHz sampling rate. The processing of the seismic data was performed using the RadEx Pro Software (DECO Geophysical) and consisted of a swell filter, an

Ormsby bandpass filter with a low-cut ramp of 150 to 190 Hz and a high cut ramp ranging from 1200 to 1300 Hz and an amplitude correction of 3 dB/ms.

The DSDP Site 548 geophysical downhole logging data (Fig. 3.3) were obtained from the IODP-USIO log database (de Graciansky et al., 1985). They consist of the natural Gamma-Ray (GR), the compensated neutron and formation density compensated tools, a long spaced sonic tool (P-wave velocity) and a dual induction tool (Resistivity). The correlation between the identified seismic and downhole geophysical units has been performed using the Kingdom Software Suite (Fig. 3.3).

In addition, this study has made use of the high resolution bathymetric data acquired within the Irish National Seabed Survey (INSS) conducted by the Geological Survey of Ireland (Figs. 3.2a, b). The multibeam data have been acquired during the course of 2000 using the Kongsberg EM120 echosounder system. The data processing was carried out using appropriate hydrographic software applying horizontal and vertical corrections following the international hydrographic organization (IHO) standards order 2 (Dorschel et al., 2010).

Vertical CTD salinity profiles (Figs. 3.2c, d) were extracted from the World Ocean Database 2009, and were downloaded from the National Oceanographic Data Centre (NODC) platform. The salinity cross section and the temperature versus salinity diagram were made using Ocean Data View (ODV) software (Schlitzer, 2012). The potential temperature was computed from ODV software, using a standard reference pressure of 1 bar. Additionally, the southernmost CTD station was used to compute the internal tide reflection conditions as well as the critical slope angle at Goban Spur (Fig. 3.9), using the equations from Southard and Cacchione (1972):

$$c = \arctan\left(\sqrt{\left(\frac{\sigma^2 - f^2}{N^2 - \sigma^2}\right)}\right)$$

The c parameter is the angle of the internal wave energy propagation relative to the horizontal direction. N is the Brunt-Vaisala frequency [cycl/h], and was computed using the ODV software. Outliers due to noise in the record (Schlitzer, 2012) were deleted, whereas the noise was reduced applying an 11 point average filtering. The used Coriolis parameter f at 49°N was $1.16858 \times 10^{-4}\, rad/s$. In absence of precise record, comprehensively imaging the local internal wave frequency (σ) at Goban Spur, the computation used a theoretical semi-diurnal internal tide train frequency of 29°/h ($1.442 \times 10^{-4}\, rad/s$). Three reflection conditions for internal tides normally incident onto a slope are possible. Critical reflection conditions are reached when the bottom slope (γ) roughly equals the angle of the internal wave energy propagation relative to the horizontal direction (c): γ ≈

c. Reflective conditions are reached when the ration γ/c > 1, and transmissive conditions when γ/c < 1 (Cacchione et al., 2002).

3.4 Results

3.4.1 Seabed morphology

The current seabed morphology of the study area forms a smooth, gently southwest dipping surface (~1.5°). The slope only significantly increases towards the southern and western limits of the study area where a series of shallow incised canyon valleys are recognized (Figs. 3.2a, dotted lines). The dip locally exceeds 3° towards the south, leading to an extended terrace with depths ranging from 1800 to 2000 m (Fig. 3.2a). Towards the west of the study area, the slope abruptly increases to generally more than 5° (Fig. 3.2b). This structure is recognized as the head of a sinuous slope canyon crosscutting the terraced slope. It is separated from the southern part by the presence of a structural high (Fig. 3.2b). The bathymetric data evidences the presence of an approximately 20 km wide, sinuous-edged escarpment, which is open towards the south west (Fig. 3.2b, dashed line). This escarpment's opening can be linked up to the western canyon heads (Fig. 3.2a). It delimits the hereafter called "upslope" and "downslope" areas. The upslope area refers to the north, northeast and eastern parts of the study area where bathymetry does generally not exceeds 1200 m and where the seabed is smooth and uniform. In contrast, the downslope area represents the deeper (> 1200 m) central, southern and western part of the study area (Fig. 3.2b), where a complex seabed is present. Here, the rough seafloor corresponds to the presence of a sediment wave field, clearly imaged from the seismic data (next section). However, a comprehensive description of the sediment wave field imaged from the bathymetric data is not possible since the wave amplitudes are relatively limited in the uppermost seismic unit, and the crests do not form a clear relief within the overall 1.5° slope gradient.

3.4.2 Integrated stratigraphic framework

The seismic stratigraphy is based on well-constrained regional unconformities, and their correlation to the identified seismic facies (Fig. 3.3). The units and unconformities have been numbered from recent to old following the DSDP Site 548 stratigraphic subdivisions proposed by de Graciansky et al. (1985), and is described here from old to young.

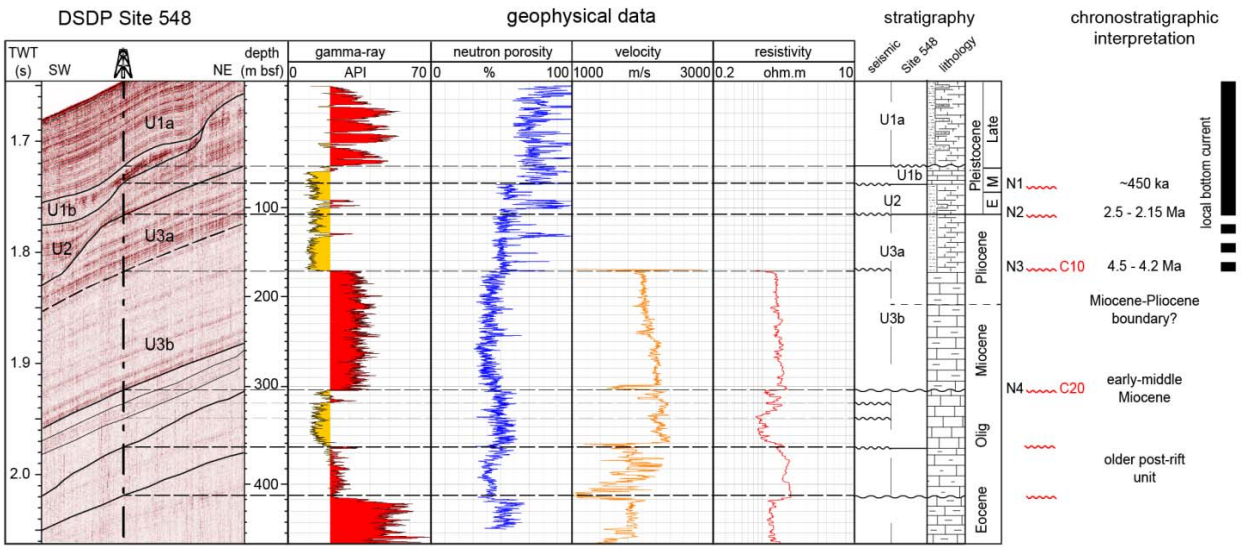

Figure 3.3 Two-way-travel time [TWT] versus depth chart, including the seismic stratigraphy, lithostratigraphy and chronostratigraphic data at DSDP Site 548 (leg 80), correlated with the SW/NE oriented seismic profile P010502. The displayed downhole logging data consist of natural Gamma Ray, neutron porosity log, velocity log and deep induction resistivity (de Graciansky et al., 1985). Note that the TWT domain is kept linear, whereas the depth scale is stretched or squeezed between the different tie points (dashed lines).

3.4.2.1 Palaeogene to early Miocene post rift unit

The initial DSDP Site 548 hole reached the Hercynian basement at a total depth of 551.5 m below seafloor (bsf). The Hercynian basement is not recognized in this study since it is located beyond the seismic investigation depth. The deepest feature recognized on the seismic profiles corresponds to a stratigraphic unconformity at 412 m bsf (either 2.025 s TWT on Fig. 3.3), corresponding to the top of DSDP Site 548 stratigraphic unit 5 (de Graciansky et al., 1985). The seismic interval extending from 1.92 to 2.025 s TWT (Fig. 3.3) is characterised by variable amplitudes and southwest dipping reflectors. From bottom to top, the sub-parallel, low to medium amplitude continuous reflectors (Fig. 3.4a) evolve to gently undulating sub-parallel, medium to low amplitude continuous reflectors. There are several seismic unconformities that are marked by series of toplap and onlap configurations (Figs. 3.3, 3.4a). The top of the sequence is formed by an unconformity, respectively referred to as the local N4 unconformity, and evidenced by the presence of a series toplap towards the north (Figs. 3.4a, 3.5, 3.6).

This seismic unit was correlated to the stratigraphic interval extending from 412 to 304.75 m bsf, and corresponding to Palaeogene post rift deposits. It mainly consists of greenish light grey foraminifer and nannofossil ooze chalks with variable physical properties (Fig. 3.3) associated to changes in terrigenous content (de Graciansky et al., 1985). Its top is identified as early-middle Miocene unconformity representing a 4 My hiatus (de Graciansky et al., 1985). A step-like decrease

in the GR record occurs respectively at 412 and 376 m bsf, and correlates with different seismic

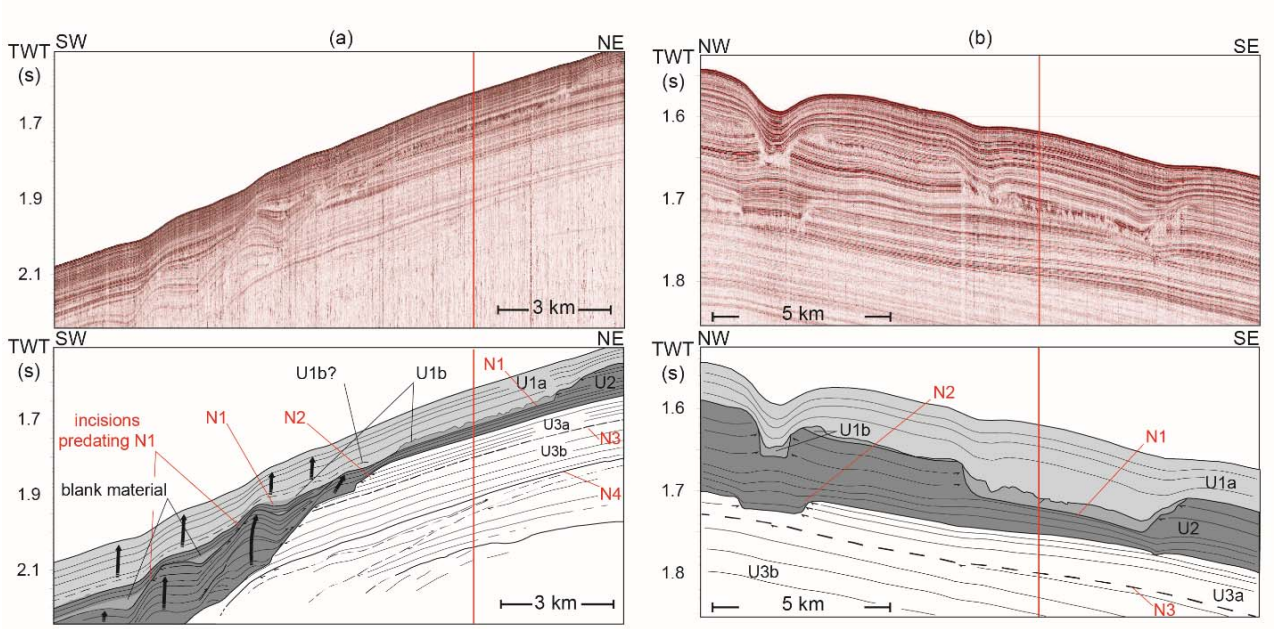

Figure 3.4 (a) SW/NE oriented seismic profile (GS120610) and interpreted seismic stratigraphy (location Fig. 3.2b). The black arrows indicate the sediment wave crests within units U2 and U1. Note the presence of different scarps formed prior the N1 unconformity, and associated with acoustically transparent bodies, associated with the sediment wave troughs in unit U2. (b) NW/SE oriented seismic profile (P010501) showing the typical U-shaped morphology of recent N2 and N1 unconformities. Unit U1b is interpreted as a partial infilling of N1. The vertical red lines indicate where the profiles cross each other (Fig. 2b).

unconformities (Fig. 3.3).

3.4.2.2 Unit U3

The seismic unit 3 (U3) is fairly homogenous in thickness within the entire study area. It is a thick package (0.16 to 0.19 s TWT) of parallel to sub-parallel continuous reflectors with variable amplitudes, gently draping the N4 unconformity (Figs. 3.4a, 3.5, 3.6). This seismic unit has been subdivided into two subunits, U3a and U3b, due to the presence of a subtle unconformable contact N3 formed by local top-lap, associated with a significant change in seismic facies and geometry (Figs. 3.3, 3.5). The U3b seismic facies consists of a typical couple of medium to high-amplitude continuous reflectors at the base, followed by a thicker interval (~0.1 s TWT) of low to medium amplitude sub-parallel continuous reflectors (Fig. 3.6). The upper U3a is represented by an approximately 0.06 s TWT thick package of very high to medium/high amplitude continuous parallel reflectors (Fig. 3.5).

Unit U3 has been affected by the erosive N2 discontinuity towards the south and southwest (Figs. 3.4a, 3.5). Its morphology is complex and consists of various small escarpments (*e.g.* Fig. 3.6). These scarps are formed by a series of toplap terminations, corresponding to relatively steep

truncations (vertically more than 0.16 s TWT over approximately 1 km in length) into U3 (Figs. 3.4, 3.6). They are separated by "flat", stratigraphically coherent surfaces forming a general U-shaped morphology (Fig. 3.4b). The cross-correlation with the northeasternmost scarp results in the inference an approximately 15 km wide, southwest opened amphitheatre-like structure (fig. 3.7a). In the upslope area, as well as in the vicinity of DSDP Site 548, unit U3 has presumably not been affected by the N2 discontinuity (Fig. 3.3).

The lithostratigraphic U3 is described by de Graciansky et al.(1985) as a single unit. It has a late Miocene to late Pliocene age, and ranges from 108.5 to 304.75 m bsf (Fig. 3.3). It consists of nannofossil ooze which alternates with marly nannofossil oozes, lithologically expressed by a very variable (pluri-decimetric, up to 4 m) bedding (Fig. 3.3). Within this study, the stratigraphic unit U3 also has been subdivided in two seismic subunits U3a and U3b on the basis of downhole log data. U3b extends from 304 to 171 m bsf and has a relatively homogenous GR (~35 API), associated with a homogenous velocity and resistivity (Fig. 3.3). Subunit U3a extends from 171 to 108.5 m bsf and is characterised by a general decrease in GR (from about 35 to 10 API), associated with an increase in neutron porosity (Fig. 3.3). A peak in GR (*i.e.* 30 API), associated with an increase in neutron porosity, is present at about 130 m depth, and may reflect variations in terrigenous content (de Graciansky et al., 1985). The Miocene/Pliocene boundary was documented at ~210 m bsf (de Graciansky et al. 1985) and correlated to a local maximum in GR (up to 50 API), as well as in neutron density, associated with a slight decrease P-wave velocity.

3.4.2.3 Unit U2

In the upslope area, U2 consists of high amplitude continuous parallel reflectors with a gentle southwest dip (Figs. 3.4, 3.5). Its thickness increases towards the southwest, where the reflectors adopt a wavy structure forming a series of sediment waves (Figs. 3.4a, 3.5, 3.6).

This inferred sediment wave field covers an area of approximately 160 km². The sediment waves have an individual wavelength of about 1.5 km along the NE/SW seismic lines (Figs. 3.4, 3.5). The waves are asymmetric with an elongated downslope facing flank that can reach up to ~1 km in length against generally a couple of hundred metres for the upslope facing flank (Figs. 3.4a, 3.5). A clear gradual and differential thickening of the upslope facing flank compared to the downslope facing flank is observed. These waves are systematically found in association with the scarp formed by the N2 unconformity (Figs. 3.4, 3.5). The wave troughs develop lateral to the steep flank of unconformity N2 (Figs. 3.4a, 3.5). The lower reflectors of U2 onlap upon the N2 surface as they tend to become parallel to the palaeo-seabed. The wave troughs vary from well-rounded to relatively flat as the palaeo-depth increases (Fig. 3.4a). This wave field distinctly migrates towards the northwest

along NW/SE oriented profiles (Fig. 3.6), and towards the northeast along NE/SW oriented profiles. Due to the steep and irregular base of the unit, the wave amplitudes were measured along continuous reflectors from the bottom to the top of the unit. The obtained amplitudes were subtracted from the crests to the adjacent troughs. The obtained wave amplitudes gradually increase up to 0.03 s TWT from the base to the top of the unit (Fig. 3.5).

Towards the top, seismic unit U2 is crosscut by the N1 unconformity consisting of sharp-edged scarps separated by flat-bottomed, stratigraphically coherent surfaces (Fig. 4b). Again, truncations are nearly vertical along NW/SE oriented seismic lines and relatively steep along NE/SW lines (0.065 s TWT over ~700 m). Different scarps that truncate deeper into U2 are found towards the southwest, as previously described for the N2 discontinuity (Fig. 3.5). As with unconformity N2, N1 draws an approximately 15 km wide southwest opened amphitheatre-like structure (Fig. 3.7b). The unconformity N1 also corresponds to the vertical prolongation of the seabed escarpment delineated from the bathymetric data (Fig. 3.2b). As N1 cross-cuts the wavy morphology of U2 in the downslope area, it tends to erode the wave crests, forming a series of toplap (Fig. 3.4a). Unit U2 is not affected by N1 in the upslope area (Figs. 3.4a, 3.5). In the downslope area, one discontinuity, predating and morphologically similar to N1, can be observed (Fig. 3.4a).

Unit U2 is early Pleistocene to late Pliocene in age and consists of a complex alternation of silt, clay, nannofossil and foraminiferal oozes. It has a relatively coarse silty lithology, and generally consists of fining upward sequences (de Graciansky et al., 1985; Fig. 3.3). Its GR response is relatively low (around 15 API), even considering the presence of GR peaks (~30 API) at the base of the unit (respectively at 92 and 98 m depth). Those are associated with large peaks in neutron porosity which may denote coarse, terrigenous rich intervals (Fig. 3.3). The Pliocene/Pleistocene boundary, located at 108.5 m bsf, was described as conformable by de Graciansky et al. (1985). However, the seismic profiles have revealed its nature as an erosional unconformity, separating units U2 and U3 (Figs. 3.3, 3.4, 3.5).

3.4.2.4 Unit U1

Unit U1 is composed of the youngest deposits, and can also be subdivided in two subunits. Subunit U1b is only found as a partial infilling of the N1 discontinuity (Figs. 3.4a, 3.b, 3.6) and is a relatively thin unit (~0.02 s TWT at DSDP Site 548). It consists of discontinuous and variable amplitude reflectors to acoustically transparent zones. Figure 4 evidences that the wave troughs within unit U2 are in some places filled with an acoustically transparent facies, systematically observed in association with the erosional truncation within N1 and similar unconformities of the downslope area.

Subunit U1a is made of erosion free, cyclic alternations of low to high amplitude, continuous sub-parallel reflectors, observed as variable 0.005 to 0.01 s TWT thick intervals. The thickness of U1a averages 0.06 s TWT in the upslope area, increasing to an excess of 0.18 s TWT downslope. The development of wavy structures comparable to the sediment waves observed in unit U2 is also identified. Sediment waves are asymmetric with a ~1 km long downslope facing flank against 100 to 200 m long upslope facing flank. However, the wave troughs seem to be less properly developed in some places (*e.g.* Fig 4a) which resulted to an apparent decrease in wave length. The waves are found lateral to the steep flanks in the N1 palaeotopography and show a gradual increase in wave amplitude from the bottom to the top of the unit. The total amplitude may reach up to 0.02 s TWT, but generally points out values lower than 0.015 s TWT. These sediment waves do not show any clear migration direction, and most simply form aggrading wavy reflectors.

The stratigraphic U1b (59.9 to 72 m bsf) can be differentiated from U1a by a marked decrease in terrigenous fraction in favour to the carbonate fraction which is expressed by a low GR, below 20 API. Very few interbedded layers are recognized in the core descriptions. The contact between U1a and U1b is described as very sharp and erosive (de Graciansky et al., 1985).

Unit U1a (0-59.9 m bsf) has a middle Pleistocene to present age and is characterised by an intensively bioturbated alternation of marly nannofossil oozes and calcareous mud. The beds are generally formed by fining upward sequences (de Graciansky et al., 1985). The thickness of the beds may vary from 1 to 80 cm, and occasionally contain ice rafted debris. This unit is characterised by a cyclic alternation of relatively thick (up to 10 m) intervals of rather high GR (up to 50 API), and thin intervals (< 2 m) of low GR response 20 API (Fig. 3.3).

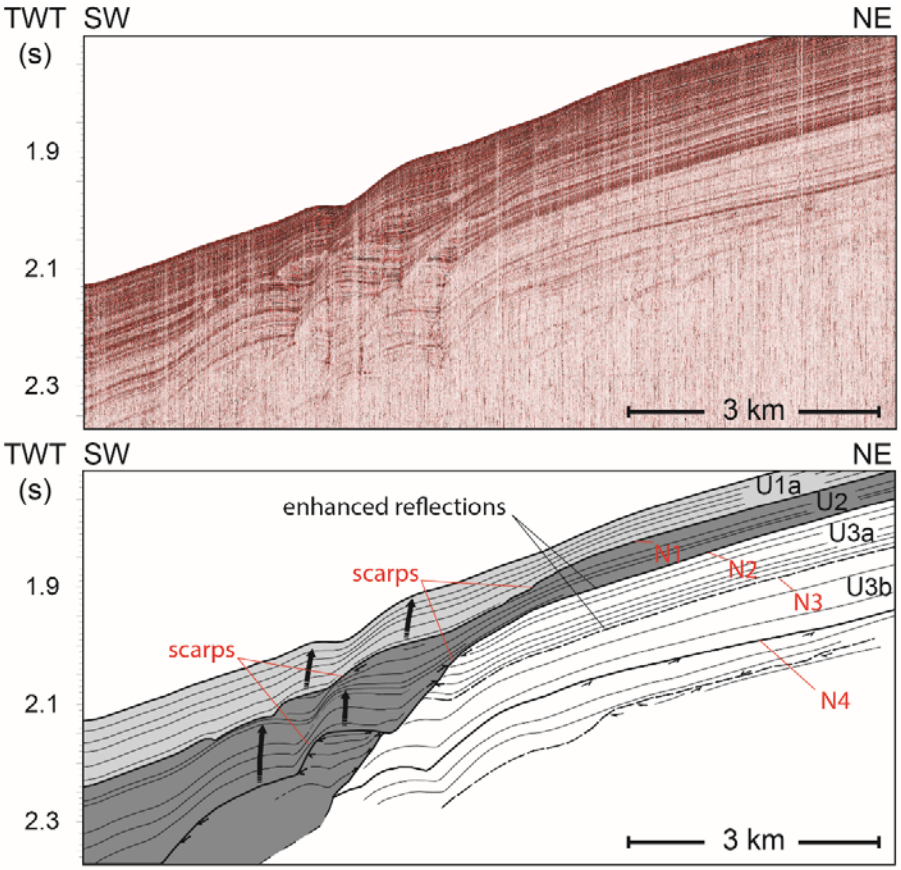

Figure 3.5 SW/NE oriented seismic profile (GS120608) and interpreted seismic stratigraphy (see location Fig. 3.2b) showing localised sediment waves (black arrows) associated with the N2 and N1 discontinuities scarps. Note the clear change in seismic facies within unit U3, and the high amplitude reflectors of U3a.

3.5 Discussion

3.5.1 Chronostratigraphic evolution

The base of unit U3 marks a clear change in the general sedimentation pattern within the vicinity of DSDP site 548. The U3 seismic facies is relatively homogenous compared to the set of morphologically variable unconformities observed below the discontinuity N4, which was attributed an early-middle Miocene age (de Graciansky et al., 1985). Such an early-middle Miocene has been identified as well within the Porcupine Seabight and within the Rockall Trough margin, and referred to as the regional C20 unconformity (McDonnell and Shannon, 2001; Shannon et al., 2005; Stoker et al., 2005b). This erosional event was attributed to strong changes in oceanic circulation during a global seasea-levellevel low stand. The N4 discontinuity is thus proposed to correspond to the local expression of the regional C20 event.

Unit U3 was attributed a lower/middle Miocene to upper Pliocene age and described as a continuous, erosion-free interval. The seismic data however evidenced the presence of a subtle N3 unconformity, and a sharp change in seismic facies, from the U3b medium/low amplitude reflectors to the high amplitude, continuous reflectors of U3a. This boundary, located at 171 m bsf, is characterised by a decrease of the clay/silt fraction as suggested by the distinct decrease in GR and the neutron porosity increase (Fig. 3.3). Given that the Pliocene/Miocene boundary is documented at 211 m bsf (de Graciansky et al., 1985), N3 is correlated to the intra early Pliocene (Fig. 3.3) which is consistent with the Pliocene chronostratigraphy established by Khélifi et al. (2009). Such early intra-Pliocene unconformity, namely C10, has widely been recognised along the Rockall Trough and Porcupine Seabight (McDonnell and Shannon, 2001). Margin-wide analysis inferred that C10 (~4.2 Ma) was the combined result of tectonic margin tilting and submarine deep-water erosion, related to an increased NADW circulation (Stoker et al., 2005a, b; Elliott et al., 2006). Khélifi et al. (2009) demonstrated that the section correlated to U3a experienced different intensification of the MOW during the middle Pliocene. The observed enhanced reflection amplitudes, associated to a combined GR decrease and porosity increase, indicate a coarser, clay depleted lithology. Such change may be interpreted as the consequence of an increased bottom current regime and winnowing of the fine terrigenous fraction, presumably in association with the Pliocene MOW intensifications.

After the deposition of the Pliocene U3a, a set of complex unconformities was recognized (respectively N2 and N1), which marks the onset of the deposition of large scale sediment waves. Khélifi et al. (2009) correlated the interval from 127.5 to 134 m bsf, to an age spanning between 2.5 to 2.7 My. In this study, the N2 discontinuity was correlated to be shallower to 108.5 m bsf. Hence, N2 should be significantly younger than 2.5 Ma. Consequently, the sediment wave development lagged the onset of the MOW, and strong bottom currents may have preceded the development of the local erosional events N2 and N1.

The base of unit U1a has been correlated to the MIS 12 (~450 ka), which coincides with the disappearance of *Pseudoemiliana Lacunosa* (Vergnaud-Grazzini and Saliège, 1985). Despite the presence of the complex N1 unconformity and the lack of precise geochronology, the units U1b and U2 have been given an early to middle Pleistocene age, potentially spanning within the 2.5 to 0.45 My interval (de Graciansky et al., 1985; Vergnaud-Grazzini and Saliège, 1985).

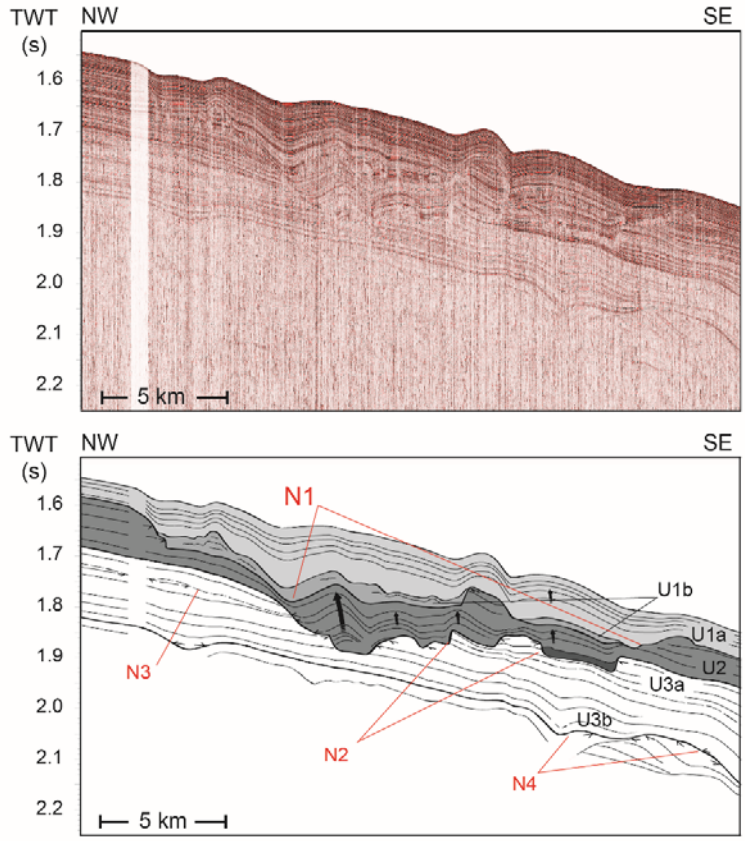

Figure 3.6 NW/SE oriented seismic profile (GS120602) and interpreted seismic stratigraphy (see location Fig. 3.2b). Unconformities N2 and N1 show a complex, stepped morphology. Note the relationship of the sediment waves (black arrows) with the palaeo-scarps formed by N2 and N1.

3.5.2 Sedimentary processes

3.5.2.1 Development of the N1 and N2 escarpments

The N2 and N1 unconformities show striking morphological similarities and are made of a series of palaeo-scarps. The scarps correspond to the incision of the gently southwest dipping (~1.5°) underlying deposits, typically forming steep toplap surfaces (Fig. 3.4). The observed successive submarine palaeo-escarpments are rooted in specific stratigraphic levels forming a simple U-shaped, to a more complex erosional surface (Figs. 3.4b, 3.6). Figure 3.7 shows the interpretative mapping of the northernmost limb of the N2 and N1 surfaces. The N2 and N1 limb respectively reach a total length of approximately 30 and 45 km, in a southwest opened amphitheatre-like structure (Fig. 3.7). The scarps are relatively steep as observed along NE/SW seismic lines (Figs. 3.4a, 3.5), and may represent a vertical incision of more than 0.16 s TWT (~150 m using a constant 1900 m/s subsurface velocity) over less than a kilometre in length. However, along the NW/SE oriented profiles, some scarps even appear to be steeper (*i.e.* to near vertical; Figs. 3.4b, 3.6). These

structures strongly suggest a system of headwall scars and slide walls belonging to mass wasting events. Such structures are typically observed within well-documented slides as the Storegga Slide (Jansen et al., 1987; Bryn et al., 2005b); or within the canyon head systems (Cunningham et al., 2005). Accordingly, stratigraphically coherent surfaces associated with N2 and N1 escarpments (Fig. 3.4b) constitute sliding planes (Bryn et al., 2005b).

At Goban Spur, these slope failures are associated with a relatively small slope gradient (~1.5°), and relatively low sedimentation rates (~3 to 19 cm/ky, Auffret et al., 2002). Such settings are not prone to induce oversteepening and unconsolidated sediment slope failure (Sultan et al., 2004; Leynaud et al., 2009). The applicable preconditioning factors here may include destabilisation via erosion at the foot of the sediment and bottom current controlled sedimentation (Bryn et al., 2005b; MacLachlan et al., 2008). The presence of bottom currents at Goban Spur was previously inferred from deposition of U3a, thus predating the N2 slope failure. Bottom currents form thin bedded sediments of varying grain-size, porosity and permeability. Permeability boundaries are horizons where pore pressure may accumulate, leading to the appearance of weak layers and sliding planes (Laberg et al., 2002; Bryn et al., 2005b). Consequently, bottom currents constitute a suitable and important precondition factor for the local slope failures. Additionally, the destabilized material most likely fed the two canyon heads southwest of the study area (Figs. 3.2a, 3.8). Those canyon valleys may have undergone some incision phases throughout the Plio-Pleistocene, particularly through regressive erosion of the canyon walls (Cunningham et al., 2005). Here, the slope failure scars are proposed to express an early stage of canyon initiation, associated with those pre-existing canyons (Figs. 3.2a, b, 3.8).

Unit U1b, which is present as a partial infill of the N1 unconformity, is characterised by a decrease in terrigenous clay (de Graciansky et al., 1985). Its irregular seismic facies suggests that it is alternatively constituted of more or less deformed material which may be interpreted as remnant debris near the failure scarp (Trincardi and Field, 1992; Canals et al., 2004). Such debris may be interpreted to correspond to the initial sliding stage such as described in Bryn et al. (2005a). The slope gradient is an important preconditioning factor for mass-wasting occurrence (Zaragosi et al., 2006). In the present case, limited slopes imply a relatively low gravitational energy gradient available for material destabilisation and mobilisation. Thus, the local low slope gradient may explain the presence of "left-over" near the failure, as hypothesized for unit U1b. Additionally, as previously stated, the N1 event was preceded by other discontinuity, also associated with acoustically transparent material (Fig. 3.4a). The conspicuous morphological similarity of this pre-existing discontinuity with N1 is here interpreted as expressing a multiphased event.

Unconformity N2 has a late Pliocene / Early Pleistocene age, and thus, the slope failure was likely triggered during the onset of widespread northern hemisphere glaciation, from about 2.7 to 2.1 My (Flesche Kleiven et al., 2002; Rohling et al., 2014). Additionally, the base of U1a may pin point the N1 slope failure to an age of ~450 ka (Vergnaud-Grazzini and Saliège, 1985) which roughly corresponds to the end of the Early-Middle Pleistocene transition, marked by the intensification of the north Atlantic glaciations (Raymo et al., 2004; Rohling et al., 2014; Bell et al., 2015). Such timing suggests N2 and N1 could be climatically triggered, through pore fluid excess caused by sea-level changes and sediment rate increase (Maslin et al., 2004; Leynaud et al., 2009). Likewise, the increase in Ice-rafted Debris (IRD) fluxes, in association with bottom current controlled sedimentation, was proposed to have driven the Plio-Pleistocene slope failures along the Irish margin (O'Reilly et al., 2007).

However the Goban Spur slope failures occurred in a deep water environment, relatively remote from sea-level variations and storm surges (Baltzer et al., 1998). Over the past climate cycle, the local sedimentation rates were observed to be variable and reached up to 20 cm/ky, which was mainly attributed to IRD input (Hall and McCave, 1998; Auffret et al., 2002). Such sedimentation rates may not be significant enough to induce pore fluid excess fast sediment loading (Maslin et al., 2004; Leynaud et al., 2009). The N2 and N1 slope failure surfaces cover an area in excess than 160 km², which corresponds to middle or small scaled mass-wasting events (Evans et al., 2005). The context and morphology of the slope failure are relatively similar to the slides of the Rockall Trough margin, such as the Afen slide (Wilson et al., 2004) and failures observed along the Hebrides slope (Strachan and Evans, 1991; Baltzer et al., 1998). Those examples, remote from sea-level variations and high sedimentation rates, are generally suggested to be seismically triggered, for which no Plio-Pleistocene evidence can be found for Goban Spur. One other trigger applicable in the area involves the internal tidal breaking (Cacchione et al., 2002). The action of internal tides over the sea bed induces a periodic loading that may lead to sediment liquefaction (Evans et al., 2005). Such process may have been continuously active throughout the entire Plio-Pleistocene time.

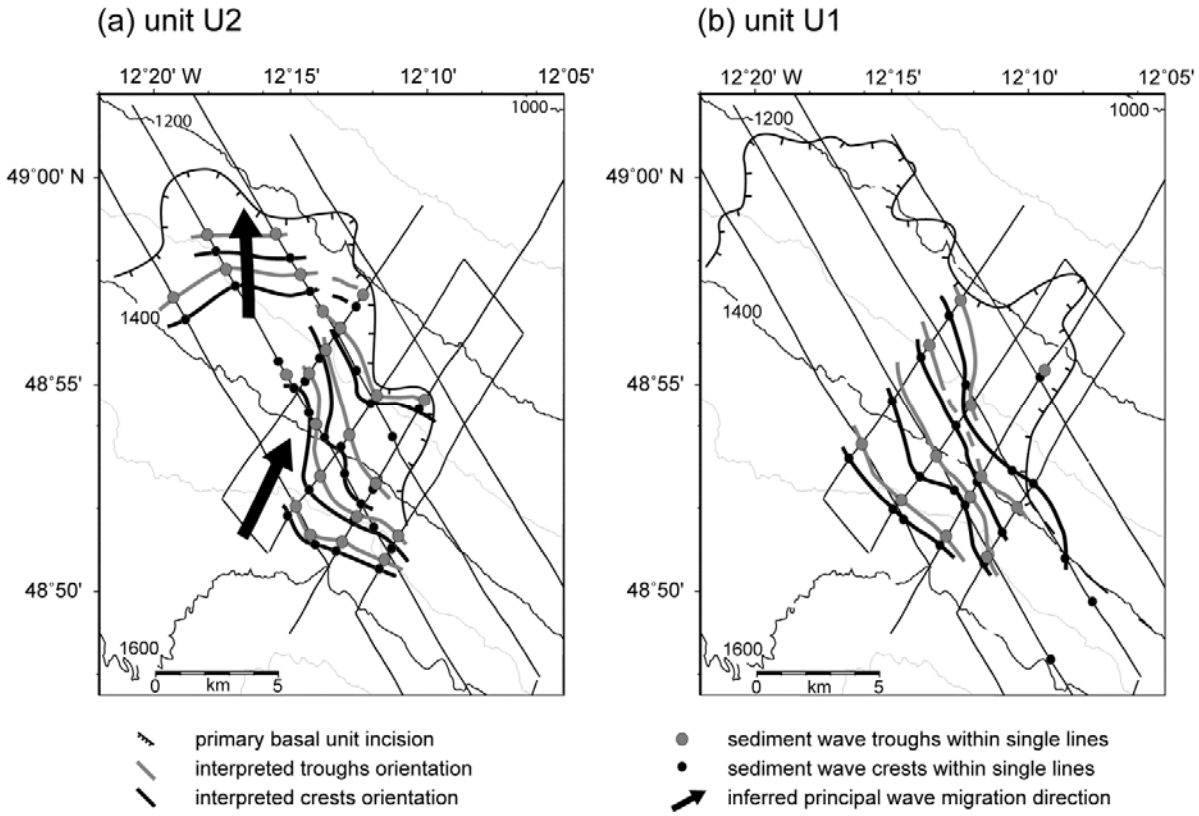

Figure 3.7 Seismic geomorphological map of respectively unit U2 (a) and unit U1 (b); the northernmost scarps of the N2 and N1 unconformities are mapped. The sediment waves are mapped along the single seismic profiles and a through correlation is proposed.

3.5.2.2 Sediment wave development

Figure 3.7 presents an overview map of the inferred sediment waves and their proposed correlation within units U2 and U1. The waves amplitude may exceed 28.5 m within unit U2, and are generally smaller than 14 m within unit U1 (using a constant arbitrary subsurface velocity of 1900 m/s). Such dimensions typically fall within the range of well-documented large-scale fine-grained (mud/silt dominated) sediment waves (Howe, 1996; Normark et al., 2002; Wynn and Stow, 2002).

The generally considered processes for building such sediment waves include (1) turbiditic currents, (2) alongslope bottom currents and (3) Multi-process formation, including gravity deformation process controlling the sediment deposition. Although sediment waves originating from soft sediment deformation are proven to exist (Kenyon et al., 1978; Faugères et al., 2002) many wave fields previously interpreted as such were later reinterpreted as depositional features. Typical examples are the "Humboldt slide" (Gardner et al., 1999; Lee et al., 2002) or the "Foreslope Hills" in the Strait of Georgia (Mosher and Thomson, 2002). Such reinterpretation, among other reasons, was motivated by the paradoxical absence of shear and/or detachment level observed at the base of the

waves. At Goban Spur, the waves are deposited over the N2 and N1 seismic unconformities which would constitute the surface along which sediment deformation occurred. The relationship between the sediment waves and those unconformities is clearly imaged here, and no shear or fold structures are recognized. The distinct reflectors at the base of the unit U2 gently onlap and tend to drape the N2 discontinuity (Fig. 3.5). Despite the presence of unit U1b, the same is observed for the base of U1a, where fewer onlap were recognized (Figs. 3.4a, 3.5). The reflectors continuity, differential thickening and the well-developed wave troughs support that these waves are depositional features, ruling out a sediment creeping origin (Lee et al., 2002).

The observed structures here are morphologically similar to other wave fields observed within the northern Rockall Trough (Masson et al., 2002) and to the "Foreslope Hills" (Mosher and Thomson, 2002), which were interpreted as bottom current induced sediment wave fields. However, they remain also similar to turbiditic formed sediment waves (Wynn et al., 2000; Normark et al., 2002; Migeon et al., 2010). Turbiditic induced sediment waves are generally observed on the continental rise/slope, mainly associated with turbiditic channel from which overspill may regularly occur, within the distal part of canyon systems. The Goban Spur environment is not favourable for the formation of energetic turbidity currents because of the lack of appropriate sediment source for the generation of hyperpycnal flow (Piper and Normark, 2009). Additionally, the lack of appropriate slope gradient does not allow acquisition of momentum in the density flow. Therefore, the Goban Spur sediment wave field is most likely bottom current induced.

The waves migrate upslope, in an overall NNE direction, except for the northern part of unit U2 (Fig. 3.7a) where the crest orientation changed to an E/W orientation. Still, the waves are recognized to migrate upslope in a northward direction. Such orientation is in fact consistent with the local contour orientation, and more particularly to the N2 unconformity, which drew an "embayment"-like morphology in the subsurface (Figs. 3.7, 3.8). This observation emphasises the existing relationship between the sediment wave development and palaeo-seabed morphologies as proposed in the evolution sketch Figure 3.8.

Such relationship resembles various infill drifts typically observed along the Irish and Norwegian margin where moat and drift systems are found in association with headwall scarps (Bryn et al., 2005b; Evans et al., 2005; Laberg et al., 2005). In other words, the hitherto called sediment waves could be regarded as a series of amalgamated and aggradational moats and drifts, developed by focusing of bottom currents against the sea-floor irregularities (N2 and N1 scarps). As such, the observed deposit would represent an infill drift in the sense of Rebesco et al. (2014). However, distinctive moats against the unconformity wall, formed by a series of onlap over the N1 and N2 escarpments, are not observed (Rebesco et al., 2001; 2005; Stow and Faugères, 2008). Infill drifts

are formed by a topographically enhanced flow, which transports the sediments from the moat to the drift. Here, the reflectors tend to become parallel to the escarpments with onlap formation, and they evolve to be connected to the adjacent structure in an aggradational pattern. It means that deposition still occurred where current lines are expected to reach their maximum intensity and prevent sedimentation.

The "infill drift" as well as "amalgamated moats and drifts", formed from different small filaments of current, require a clear, identified flow pattern. The sediment waves have been observed between 1200 and 1600 m water depths, within the current MOW lower boundary. The winter maximum flow at ~1450 m water depth (Fig. 3.1a) amounts up to 37 cm/s (Thomsen and van Weering, 1998), which is significant enough to mobilise sediment and generate large-scale mud waves and bedforms (Stow et al., 2009). However, mean alongslope flow velocities are observed to be reduced at Goban Spur (~5 cm/s), whereas bottom currents are dominated by a reversed flow, and changes in orientation from NNW/SSE to NNE/SSW (van Weering et al., 1998). The morphological forcing exerted by the Celtic margin, which topographically constrains the poleward shelf currents, does no longer exist at Goban Spur, and the current lines are observed to overshoot the contours (Huthnance et al., 2001). Therefore, an infill drift, driven by topographically enhanced flow is difficult to explain within the present-day settings.

In most cases, the formation mechanism for mud waves invoking bottom currents is the lee-wave model (Flood, 1988; Howe, 1996). This is because in those environments, bottom current flow velocities are relatively limited; generally reaching mean maximums of about 40 cm/s along open slopes, free of morphological constraints (Migeon et al., 2001). However, previous authors (*e.g.* Mosher and Thomson, 2002) often pointed out the over-simplification of that model with respect to the actual bottom current regime. Indeed the lee-wave model is based on unidirectional flow whereas many sediment wave fields are found in highly variable current directions (Masson et al., 2002; Mienis et al., 2006). When such a consistent unidirectional flow is lacking, multi-process formed waves (*i.e.* hybrid turbiditic and bottom current origin) may be invoked, as well as an internal tidal influence (Howe, 1996). Internal tides were already considered as an end-member that could drive the generation and migration of large scale sediment waves (Faugères et al., 2002; Van Rooij et al., 2010). Some well-known sediment wave fields were reinterpreted as internal tidal deposits because of the aforementioned reasons. This concerns in particular the Rockall Trough sediments waves (He et al., 2008), the Gulf of Valencia sediment waves (Ribó et al., 2016), as well as within ancient onshore outcrops, with the introduction of the "internalite" term (*e.g.* Bádenas et al., 2012).

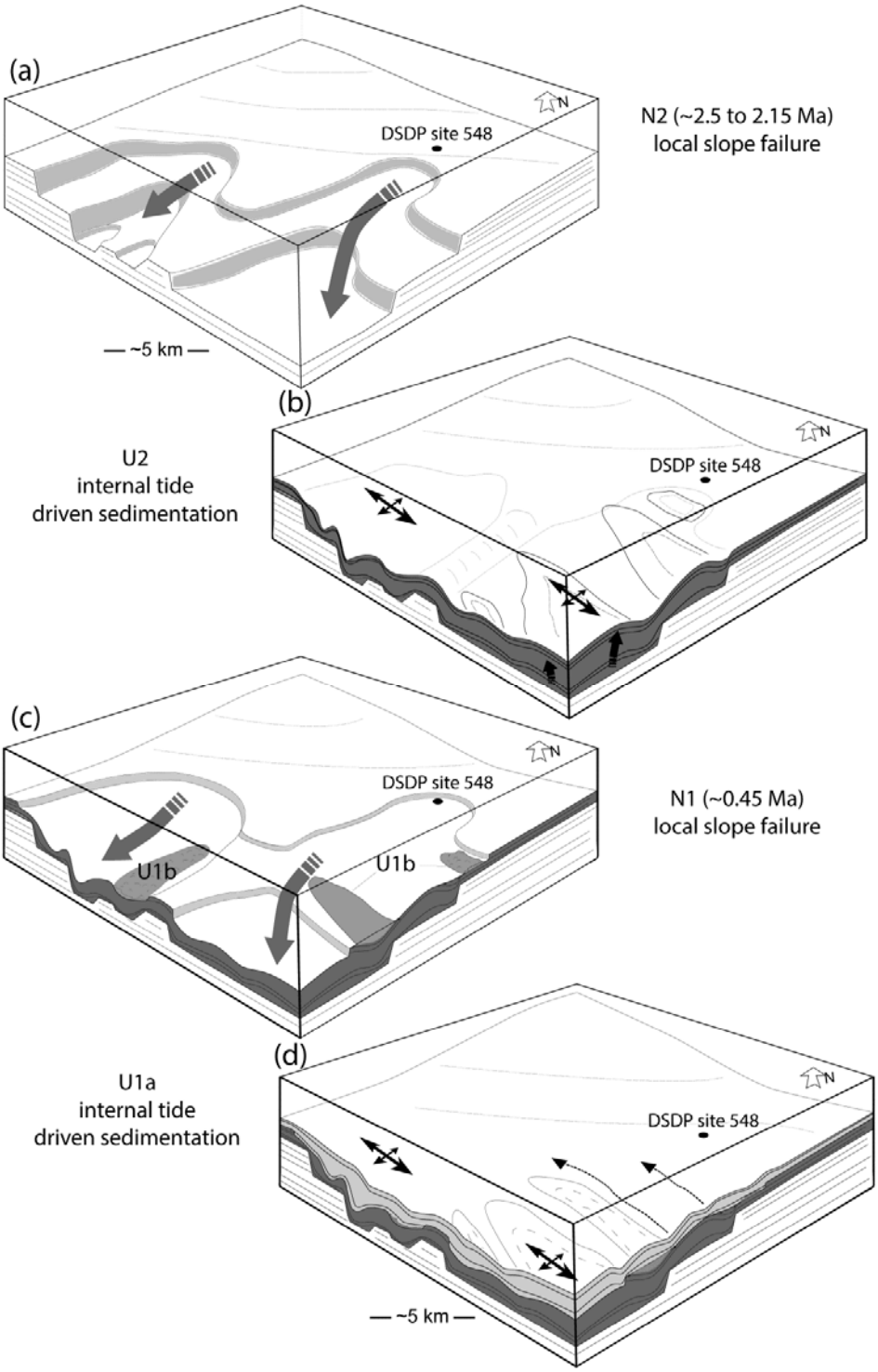

Figure 3.8 Sketch illustrating the Plio-Pleistocene evolution of the study area. (a) The N2 slope failure, presumably triggered between 2.5 to 2.15 Ma, creates steep seabed irregularities. The arrows indicate the probable sediment transport direction (b) U2 sediment waves development against previously formed seabed irregularities through the action of internal tides. The arrows indicate the present-day dominant bottom current flow directions (c) N1 slope failure presumably triggered ~0.45 Ma ago, with reduced slope gradient and remnant debris (i.e. U1b) near the failure scarp. The arrows indicate the probable sediment transport direction (d) development of the aggradational and low amplitude sediment waves of U1a.

Internal tides ability to induce sediment resuspension generating near seabed nepheloid layers, evidenced in various regions (Schmidt et al., 2002; Puig et al., 2004; Mienis et al., 2009), was also directly observed at Goban Spur (Huthnance et al., 2001). Internal tide and seabed interaction models predict a seaward-directed net bottom current flow (Gao et al., 1998), which is also corroborated at Goban Spur (van Weering et al., 1998). Those energetic, though intermittent, seaward bottom currents are consistent with lee-wave generated fine-grained sediment waves (Flood, 1988). This accordance between the maximum near seabed recorded bottom current and the wave crest orientation and upstream migration was also proposed to explain the formation of the "Foreslope Hills" wave field in Mosher and Thomson (2002).

However, it seems that the internal tidal process does not require the lee-wave model generation and simple oscillation models can be considered (Bádenas et al., 2012; Pomar et al., 2012). In the deep ocean, the simple reflection characteristic conditions of internal tide over a bottom slope may be sufficient to characterise the nature and energy of their interaction. The reflection conditions depend on the propagation of the internal tide energy (c) and the slope angle (γ) of approach relative to the seabed (Southard and Cacchione, 1972; White, 2003; Puig et al., 2004; Bonnin et al., 2006). When the ratio γ/c is lower, equal or higher than 1, the reflection conditions may evolve from "transmissive", "critical" to "reflective". Near seabed velocities and bottom shear stress are higher when near critical conditions are reached (Rice et al., 1990). The expected critical slope angle with respect to the present-day upper water mass stratification varies from 2.5 to 5° (Fig. 3.9), which is well in agreement with previous studies (Cacchione et al., 2002). Therefore, present-day reflection conditions at Goban Spur (1.5° slope) are transmissive. Those transmissive reflection conditions may have prevailed during the entire deposition of unit U1a, leading to the development of aggradational waves. Such similar aggradational (stationary) waves developed under transmissive reflection conditions are also described on the lower part of the gulf of Valencia continental slope (Ribó et al., 2016). In contrast, the palaeo-scarps formed by the N2 discontinuity, through direct change of the local dip, may have led to reach near-critical conditions at Goban Spur, leading to the formation of high amplitude, upslope migrating waves of unit U2.

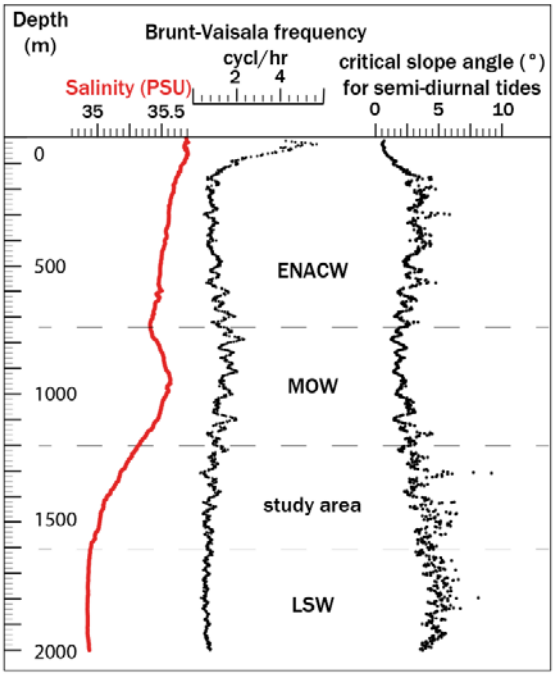

Figure 3.9 Critical slope angle computed with respect to semi-diurnal internal tide propagation within present-day water column at Goban Spur. The typical values, ranging from 2.5 to 4° are obtained within the study area. Nowadays, the slope gradient is lower than the critical slope angle which denotes "transmissive" reflection conditions, that has driven the formation of the sediment waves of U1a. Near "critical" reflection conditions may have prevailed during the U2 deposition.

3.5.3 Integrated regional margin evolution

Figure 3.10 shows a chronostratigraphic comparison between DSDP Site 548 and three other key sites for the study of MOW palaeoceanography along the NE Atlantic margin (Fig. 3.1); (1) IODP Exp. 339, within the northern Gulf of Cádiz (2) IODP Exp. 307, within the Porcupine Basin, and (3) The Le Danois CDS. The Le Danois CDS is also included in the table due to its remarkably similar morphological evolution with respect to the Cádiz CDS. It represents a topographically constrained MOW-induced drift, and the only CDS within the Bay of Biscay. The correlation is based upon morpho-sedimentary arguments because of the boreholes absence at this site (Van Rooij et al., 2010). The presented Cádiz CDS geochronology was extracted from site U1387 because it represents the most complete and comprehensive record within the Cádiz CDS (Hernández-Molina et al., 2014; 2016). Moreover, this site is located within the Faro drift, and is controlled by the interaction of the MOW upper core with the northern slope of the Gulf of Cádiz (Roque et al., 2012).

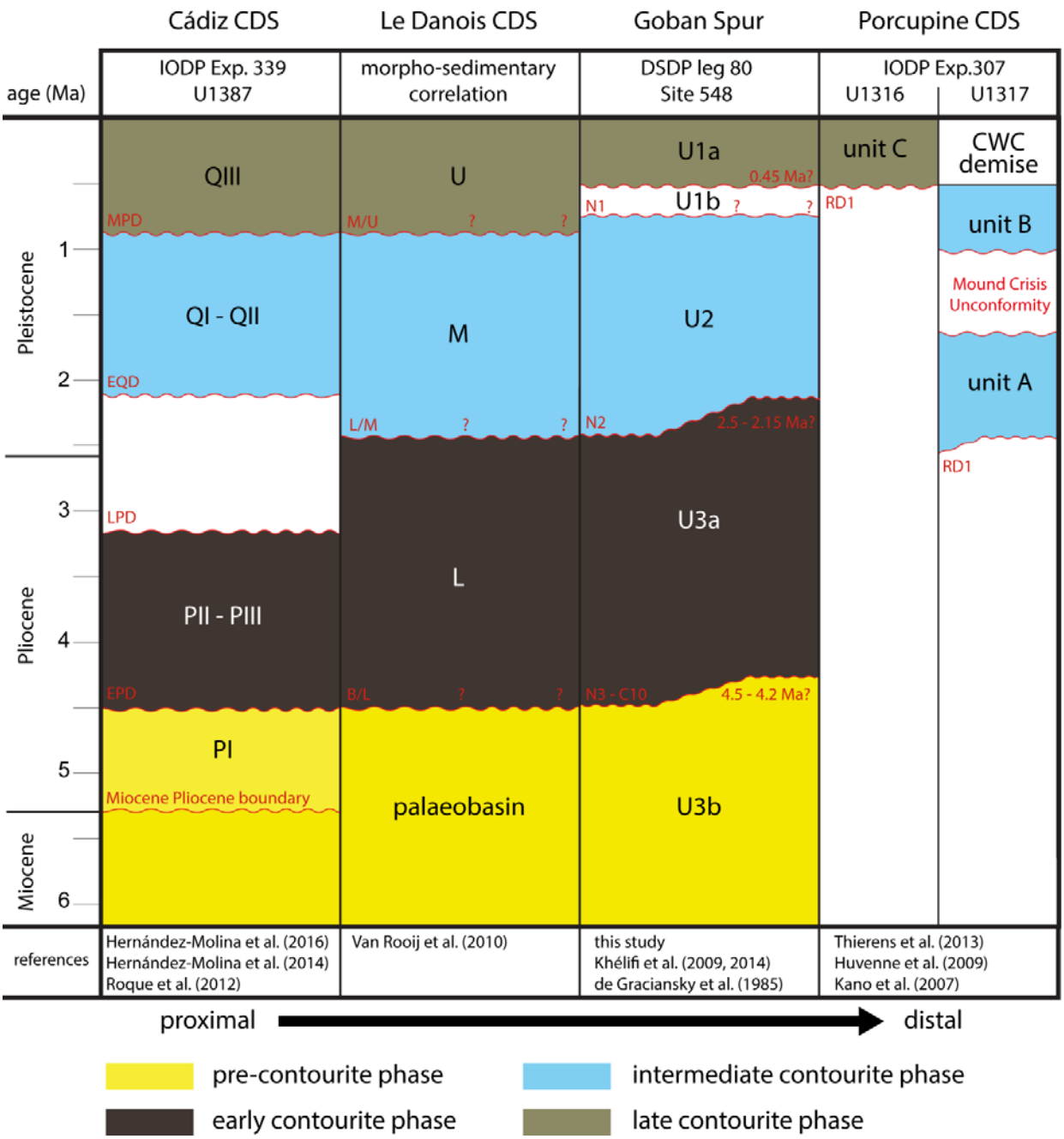

Figure 3.10 Comparison of DSDP Site 548 at Goban Spur with IODP site U1387 at Cadiz CDS, the Le Danois CDS seismic stratigraphy and IODP site U1316 and U1317 at the Porcupine CDS, from proximal to distal (*i.e.* left to right) respective to the MOW source. The names and timings of the major local unconformities are indicative for each site (see specific references). Each phase is assigned with respective local seismic unit name, and is separated by unconformities indicated in red. The regional C10 and RD1 events, respectively from the Rockall Trough and Porcupine Seabight are indicated.

The position and the dynamic behaviour of the MOW at Goban Spur also depend on the northeast Atlantic intermediate water mass stratification and its circulation pattern. The latter depends on the respective density and dynamics of the underlying LSW or the density of the past Atlantic intermediate water masses, strongly associated with the state of the Atlantic Meridional Overturning Circulation throughout the Pliocene and Pleistocene (Raymo et al., 2004). Significant changes can be expected in terms of deep-water production within the Nordic seas, however, little evidence was found for changes in the contribution of the LSW over most of the Pleistocene (Raymo et al., 2004; Stein et al., 2006; Bell et al., 2015). In spite of the increasing number of studies that evidence strong changes in the north Atlantic water column stratification, specifically during the last climatic cycle and the past 600 ky (Thornalley et al., 2015), it is postulated here that the MOW variability is a primary driver in the Goban Spur margin evolution.

Khélifi et al. (2009, 2014) documented intermittent incursions of the warm and salty MOW within the early to late Pliocene (interval ranging ~130 to 165 m bsf at DSDP Site 548). More particularly, Khélifi et al. (2014) recorded potentially "stronger-than-today" MOW admixture at Rockall Plateau ODP Site 982 from about 3.6 Ma. Those still constitute the earliest clear indications about the influence of the MOW at Goban Spur and Rockall trough latitudes. It was inferred from benthic foraminifera $\delta^{18}O$ and $\delta^{13}C$ anomalies, Neodymium isotopes and benthic foraminifera Magnesium/Calcium ratios Khélifi et al. (2014). Data obtained from IODP expedition 307 within the Porcupine Seabight did not provide information on the initial inception of the MOW because of the presence of the RD1 unconformity (Fig. 3.10; Kano et al., 2007). It is generally acknowledged that the MOW probably existed from the Gibraltar opening at 5.33 Ma (Llave et al., 2011; Roque et al., 2012). However, the first clear and regional MOW "early contourite phase" within the Cádiz CDS is generally accepted to begin after the Early Pliocene Discontinuity (EPD) at about 4.5 Ma (Llave et al., 2011; Hernández-Molina et al., 2016). Prior to 4.5 Ma, the inception of the MOW is still unclear because of the severe influence of turbiditic and mass wasting processes, which occurred during the deposition of the northern Gulf of Cádiz PI seismic unit (Fig. 3.10; Hernández-Molina et al., 2014; 2016). Further north, Van Rooij et al. (2010) described the presence of a regional unconformity marking the onset of the "early contourite phase" at Le Danois CDS, which was correlated with the Cádiz EPD at about 4.5 Ma (Fig. 3.10). The aforementioned authors state noticeable, but probably moderate MOW bottom current in its juvenile stage. Within this study, an increased bottom current regime was evidenced from enhanced seismic reflections within unit U3a, and was proposed to have possibly led to the formation of the smooth N3 unconformity. The N3 unconformity (171 m bsf) would, in that sense, be indicative for the early MOW introduction that potentially occurred between 5.33 and 3.6 Ma. Further north, within the Porcupine CDS and the associated Belgica cold-water

coral mounds, Fig. 3.10 shows the C10 event is enclosed within the very large and complex RD1 discontinuity which represents a hiatus of more than 6 Ma (Kano et al., 2007). Among other processes, enhanced bottom currents possibly prevented sedimentation until approximately 2.7 Ma (Van Rooij et al., 2007; Huvenne et al., 2009; Thierens et al., 2013). Thus it seems that DSDP Site 548 still has an important potential in determining the MOW initial introduction at those latitudes. The absence of continuous composite sediment cores section is an important limiting factor in extending the record from Khélifi et al. (2009) beyond 3.7 Ma.

The proximal MOW signal encompasses at least two major enhanced phases, also associated to regional discontinuities: the Lower Pliocene Discontinuity (LPD) from 3.3 to 3.0 Ma and the Early Quaternary Discontinuity (EQD) from 2.4 to 2.1 Ma (Hernández-Molina et al., 2016). A phase of MOW intensification at 3.3 - 3.0 Ma was also recorded at DSDP Site 548 (Khélifi et al., 2009). The second major intensification was accompanied by an enhanced cold-water coral accretion period within the Belgica mound province (Huvenne et al., 2009). The establishment of present-day circulation at ~2.1 Ma (Bell et al., 2015; Hernández-Molina et al., 2016), was previously suggested to be roughly contemporary with the local N2 slope failure event at Goban Spur. Within Le Danois CDS, a regional discontinuity was correlated to the base of the Quaternary (~2.58 Ma) with respect to the general evolution of the Cádiz CDS (Llave et al., 2011). From about 2.1 Ma onwards, all sites clearly entered in the stable "intermediate contourite phase" (Fig. 3.10). Elongated mounded drifts, developed within the Faro drift, are probably contemporary with the sheeted drift development within the Le Danois CDS. This intermediate phase is known as a flourishing cold-water coral period within the Porcupine Seabight (Fig. 3.10, Site U1317). Such cold-water coral development was attributed to contour currents, and enhanced by internal tides processes within the MOW upper interface (Rice et al., 1990; White, 2003, 2007; White and Dorschel, 2010; Raddatz et al., 2011). Meanwhile, enhanced internal tidal processes along the MOW lower interface were also inferred within the Porcupine Seabight (Van Rooij et al., 2007). The concomitant change of the Goban Spur seabed morphology (*i.e.* slope failure), and the onset of a "stable MOW" regime is proposed to have driven the wave development of unit U2 (Fig. 3.8).

Important changes in the MOW regime occurred during the Early Middle Pleistocene Transition (*i.e.* 0.9 to 0.6 Ma), resulting in the modern, climatically modulated MOW (Voelker et al., 2006; Rogerson et al., 2012). Within the Gulf of Cádiz, the MOW strengthening led to the onset of the "late contourite phase", with the formation of mounded and separated drifts over the Middle Pleistocene Discontinuity (MPD) (Hernández-Molina et al., 2016). The Le Danois CDS recorded a similar discontinuity associated with subsequent mounded and separated drifts development (Van Rooij et al., 2010). However, the growth of the cold-water coral mounds of the Belgica mound province

gradually decayed, to finally demise from about 0.5 Ma (Thierens et al., 2013). This suggests a (intermittent?) reduction of bottom currents within distal sites, further enabling sediment drift deposition (Fig. 3.10, Site U1316). Although sediment waves developed at Goban Spur during this period, they seem somehow less dynamic, with reduced differential thickening and migration pattern. However, as previously stated, differences observed in the wave development might be associated to significant reduction of the slope gradient associated with the local N1 slope failure. The "late contourite phase" seems to correspond to a decreased influence of the MOW with respect to the Goban Spur and the Belgica mound province. This could be in accordance with more variable (*i.e.* of intermittent occurrence) MOW regime in those distal areas, as suggested from Schönfeld and Zahn (2000).

3.6 Conclusions

This study provides a unique refreshing view and insight with respect to the record and processes that dominated the Goban Spur open slope during the Plio-Pleistocene. Despite its smooth topography and its rather isolated emplacement, it was characterised as relatively energetic sedimentary environment, associated with the development of large-scale sediment waves and punctuated by a series of slope failures. Morphological and stratigraphic evidence suggests that the Goban Spur evolution is primarily driven by the introduction and influence of the MOW. Significant bottom currents, associated with the poleward advection of the MOW, probably occurred from about 4.5 to 4.2 Ma, and may have played a preconditioning role to slope failure. Local slope failure episodes, probably triggered between 2.5 and 2.15 Ma and ~0.45 Ma, formed the seabed irregularities over which the sediment waves developed, marking a relative bottom current energy increase. The sediment waves were likely formed by the onset of energetic contour currents, which were in turn driven by an enhanced internal tide regime within the MOW lower interface. From 0.45 Ma onwards, a relative decrease in the MOW influence is observed with respect to Goban Spur and the Porcupine CDS. This strongly contrasts in comparison to the gradual MOW influence increase within the Cádiz and the Le Danois CDS throughout the Plio-Pleistocene.

Despite the importance the internal tides hold with respect to contourite drifts, as well as their inclusion in the term bottom current itself, the presented sediment wave system does not yet integrate within the contourites classification and diagnostic criteria. This suggests that more work needs to be done regarding the integration of internal tidal bottom current deposits, within or alongside, the contourite paradigm.

Acknowledgements

This study was carried out within the framework of a Ghent University BOF "Starting Grant". The authors wish to acknowledge the captains, crews and scientific participants of R/V Belgica cruises 2001/12 and 2012/17. Shiptime on board R/V Belgica was provided by BELSPO and RBINS–OD Nature. These research cruises were carried out within the framework of the EC FP6 IP HERMES and EC FP7 IP HERMIONE projects. We also wish to express our gratitude to the Geological Survey of Ireland for providing the high resolution multibeam data. The authors wish to express their gratitude to Thomas Vandorpe for his input and constructive discussions. We also personally acknowledge Dierk Hebbeln (MARUM, Germany), Michel Lopez (UM2, France) and Michael Sarnthein (University of Kiel, Germany), for their encouragements and input.

References

Auffret, G.A., Zaragosi, S., Dennielou, B., Cortijo, E., Van Rooij, D., Grousset, F.E., Pujol, C., Eynaud, F., Siegert, M., 2002. Terrigenous fluxes at the Celtic margin during the last glacial cycle. Marine Geology 188, 79-108.

Bádenas, B., Pomar, L., Aurell, M., Morsilli, M., 2012. A facies model for internalites (internal wave deposits) on a gently sloping carbonate ramp (Upper Jurassic, Ricla, NE Spain). Sedimentary Geology 271–272, 44-57.

Baltzer, A., Holmes, R.W., Evans, D., 1998. Debris flows on the Sula Sgeir Fan, NW of Scotland, in: Stoker, M.S., Evans, D., Cramp, A. (Eds.), Geological Processes on Continental Margins: Sedimentation, Mass-Wasting and Stability. Geological Society, London, pp. 105-115.

Bell, D.B., Jung, S.J.A., Kroon, D., 2015. The Plio-Pleistocene development of Atlantic deep-water circulation and its influence on climate trends. Quaternary Science Reviews 123, 265-282.

Bonnin, J., Van Haren, H., Hosegood, P., Brummer, G.-J.A., 2006. Burst resuspension of seabed material at the foot of the continental slope in the Rockall Channel. Marine Geology 226, 167-184.

Bourillet, J.F., Zaragosi, S., Mulder, T., 2006. The French Atlantic margin and deep-sea submarine systems. Geo-Marine Letters 26, 311-315.

Bryn, P., Berg, K., Forsberg, C.F., Solheim, A., Kvalstad, T.J., 2005a. Explaining the Storegga Slide. Marine and Petroleum Geology 22, 11-19.

Bryn, P., Berg, K., Stoker, M.S., Haflidason, H., Solheim, A., 2005b. Contourites and their relevance for mass wasting along the Mid-Norwegian Margin. Marine and Petroleum Geology 22, 85-96.

Cacchione, D.A., Pratson, L.F., Ogston, A.S., 2002. The Shaping of Continental Slopes by Internal Tides. Science 296, 724-727.

Canals, M., Lastras, G., Urgeles, R., Casamor, J.L., Mienert, J., Cattaneo, A., De Batist, M., Haflidason, H., Imbo, Y., Laberg, J.S., Locat, J., Long, D., Longva, O., Masson, D.G., Sultan, N., Trincardi, F., Bryn, P., 2004. Slope failure dynamics and impacts from seafloor and shallow sub-seafloor geophysical data: case studies from the COSTA project. Marine Geology 213, 9-72.

Caralp, M.H., Pujol, C., Duprat, J., Labracherie, M., 1985. Quaternaty paleoceanography of the northeastern Atlantic: microfaunal and stable isotope evidence at sites 548 and 549. Initial Reports of the Deep Sea Drilling Project. U.S. Government Printing Office, Washington, pp. 817-820.

Cunningham, M.J., Hodgson, S., Masson, D.G., Parson, L.M., 2005. An evaluation of along- and down-slope sediment transport processes between Goban Spur and Brenot Spur on the Celtic Margin of the Bay of Biscay. Sedimentary Geology 179, 99-116.

de Graciansky, P.C., Poag, C.W., Cunningham, R., Loubere, P., Masson, D.G., Mazzullo, J.M., Montadert, L., Müller, C., Otsuka, K., Reynolds, L.A., Sigal, J., Snyder, S.W., Vaos, S.P., Waples, D., 1985. Site 548. Initial Reports of the Deep Sea Drilling Project. U.S. Government Printing Office, Washington, pp. 33-122.

Dingle, R.V., Scrutton, R.A., 1979. Sedimentary succession and tectonic history of a marginal plateau (Goban Spur, Southwest of Ireland). Marine Geology 33, 45-69.

Dorschel, B., Wheeler, A.J., Monteys, X., Verbruggen, K., 2010. Atlas of the Deep-Water Seabed: Ireland. Springer Netherlands.

Elliott, G.M., Shannon, P.M., Haughton, P.D.W., Praeg, D., O'Reilly, B., 2006. Mid- to Late Cenozoic canyon development on the eastern margin of the Rockall Trough, offshore Ireland. Marine Geology 229, 113-132.

Ercilla, G., Casas, D., Estrada, F., Vázquez, J.T., Iglesias, J., García, M., Gómez, M., Acosta, J., Gallart, J., Maestro-González, A., 2008. Morphosedimentary features and recent depositional architectural model of the Cantabrian continental margin. Marine Geology 247, 61-83.

Evans, D., Harrison, Z., Shannon, P.M., Laberg, J.S., Nielsen, T., Ayers, S., Holmes, R.W., Hoult, R., Lindberg, B., Haflidason, H., Long, D., Kuijpers, A., Andersen, E.S., Bryn, P., 2005. Palaeoslides and other mass failures of Pliocene to Pleistocene age along the Atlantic continental margin of NW Europe. Marine and Petroleum Geology 22, 1131-1148.

Faugères, J.-C., Gonthier, E., Mulder, T., Kenyon, N.H., Cirac, P., Griboulard, R., Berné, S., Lesuavé, R., 2002. Multi-process generated sediment waves on the Landes Plateau (Bay of Biscay, North Atlantic). Marine Geology 182, 279-302.

Flesche Kleiven, H., Jansen, E., Fronval, T., Smith, T.M., 2002. Intensification of Northern Hemisphere glaciations in the circum Atlantic region (3.5–2.4 Ma) – ice-rafted detritus evidence. Palaeogeography, Palaeoclimatology, Palaeoecology 184, 213-223.

Flood, R.D., 1988. A lee wave model for deep-sea mudwave activity. Deep-Sea Research 35, 973-983.

Gao, Z.Z., Eriksson, K.A., He, Y.B., Luo, S.S., Guo, J.H., 1998. Deep-Water Traction Current Deposits - A Study of Internal Tides, Internal Waves, Contour Currents and Their Deposits. Science Press, Beijing.

García, M., Hernández-Molina, F.J., Llave, E., Stow, D.A.V., León, R., Fernández-Puga, M.C., Diaz del Río, V., Somoza, L., 2009. Contourite erosive features caused by the Mediterranean Outflow Water in the Gulf of Cadiz: Quaternary tectonic and oceanographic implications. Marine Geology 257, 24-40.

Gardner, J.V., Prior, D.B., Field, M.E., 1999. Humboldt Slide - a large shear-dominated retrogressive slope failure. Marine Geology 154, 323-338.

Hall, I.R., McCave, I.N., 1998. Late Glacial to Recent accumulation fluxes of sediments at the shelf edge and slope of NW Europe, 48-50°N, in: Stoker, M.S., Evans, C.D.R., Cramp, A. (Eds.), Geological Processes on Continental Margins: Sedimentation, Mass-Wasting and Stability. Geological Society, London, pp. 339-350.

Hanquiez, V., Mulder, T., Toucanne, S., Lecroart, P., Bonnel, C., Marchès, E., Gonthier, E., 2010. The sandy channel-lobe depositional systems in the Gulf of Cadiz: Gravity processes forced by contour current processes. Sedimentary Geology 229, 110-123.

He, Y., Gao, Z., Luo, J., Luo, S., Liu, X., 2008. Characteristics of internal-wave and internal-tide deposits and their hydrocarbon potential. Petroleum Science 5, 37-44.

Hernández-Molina, F.J., Llave, E., Stow, D.A.V., Garcia, M., Somoza, L., Vazquez, J.T., Lobo, F.J., Maestro, A., del Rio, V.D., Leon, R., Medialdea, T., Gardner, J., 2006. The contourite depositional system of the Gulf of Cadiz: A sedimentary model related to the bottom current activity of the Mediterranean outflow water and its interaction with the continental margin. Deep-Sea Research Part Ii-Topical Studies in Oceanography 53, 1420-1463.

Hernández-Molina, F.J., Serra, N., Stow, D., Llave, E., Ercilla, G., Van Rooij, D., 2011. Along-slope oceanographic processes and sedimentary products around the Iberian margin. Geo-Marine Letters, 1-27.

Hernández-Molina, F.J., Stow, D.A.V., Alvarez-Zarikian, C.A., Acton, G., Bahr, A., Balestra, B., Ducassou, E., Flood, R., Flores, J.-A., Furota, S., Grunert, P., Hodell, D., Jimenez-Espejo, F., Kim, J.K., Krissek, L., Kuroda, J., Li, B., Llave, E., Lofi, J., Lourens, L., Miller, M., Nanayama, F., Nishida, N., Richter, C., Roque, C., Pereira, H., Sanchez Goñi, M.F., Sierro, F.J., Singh, A.D., Sloss, C., Takashimizu, Y., Tzanova, A., Voelker, A., Williams, T., Xuan, C., 2014. Onset of Mediterranean outflow into the North Atlantic. Science 344, 1244-1250.

Hernández-Molina, F.J., Sierro, F.J., Llave, E., Roque, C., Stow, D.A.V., Williams, T., Lofi, J., Van der Schee, M., Arnáiz, A., Ledesma, S., Rosales, C., Rodríguez-Tovar, F.J., Pardo-Igúzquiza, E., Brackenridge, R.E., 2016. Evolution of the gulf of Cadiz margin and southwest Portugal contourite depositional system: Tectonic, sedimentary and paleoceanographic implications from IODP expedition 339. Marine Geology.

Howe, J.A., 1996. Turbidite and contourite sediment waves in the northern Rockall Trough, North Atlantic Ocean. Sedimentology 43, 219-234.

Huthnance, J.M., Coelho, H., Griffiths, C.R., Knight, P.J., Rees, A.P., Sinha, B., Vangriesheim, A., White, M., Chatwin, P.G., 2001. Physical structures, advection and mixing in the region of Goban spur. Deep-Sea Research II 48, 2979-3021.

Huvenne, V.A.I., Van Rooij, D., De Mol, B., Thierens, M., O'Donnell, R., Foubert, A., 2009. Sediment dynamics and palaeo-environmental context at key stages in the Challenger cold-water coral mound formation: Clues from sediment deposits at the mound base. Deep Sea Research Part I: Oceanographic Research Papers 56, 2263-2280.

Iorga, M.C., Lozier, M.S., 1999a. Signatures of the Mediterranean outflow from a North Atlantic climatology 1. Salinity and density fields. Journal of Geophysical Research-Oceans 104, 25985-26009.

Iorga, M.C., Lozier, M.S., 1999b. Signatures of the Mediterranean outflow from a North Atlantic climatology 2. Diagnostic velocity fields. Journal of Geophysical Research-Oceans 104, 26011-26029.

Jansen, E., Befring, S., Bugge, T., Eidvin, T., Holtedahl, H., Sejrup, H.P., 1987. Large submarine slides on the Norwegian continental margin: Sediments, transport and timing. Marine Geology 78, 77-107.

Kano, A., Ferdelman, T.G., Williams, T., Henriet, J.P., Ishikawa, T., Kawagoe, N., Takashima, C., Kakizaki, Y., Abe, K., Sakai, S., Browning, E., Li, X., the IODP Expedition 307 Scientists, 2007. Age constraints on the origin and growth history of a deep-water coral mound in northeast Atlantic drilled during Integrated Ocean Drilling Program Expedition 307. Geology 35, 1051-1054.

Kenyon, N.H., Belderson, R.H., Stride, A.H., 1978. Channels, canyons and slump folds between South-West Ireland and Spain. Oceanologica Acta 1, 369-380.

Khélifi, N., Sarnthein, M., Andersen, N., Blanz, T., Frank, M., Garbe-Schonberg, D., Haley, B.A., Stumpf, R., Weinelt, M., 2009. A major and long-term Pliocene intensification of the Mediterranean outflow, 3.5-3.3 Ma ago. Geology 37, 811-814.

Khélifi, N., Sarnthein, M., Frank, M., Andersen, N., Garbe-Schönberg, D., 2014. Late Pliocene variations of the Mediterranean outflow. Marine Geology 357, 182-194.

Laberg, J.S., Vorren, T.O., Mienert, J., Evans, C.D.R., Lindberg, B., Ottesen, D., Kenyon, N.H., Henriksen, S., 2002. Late Quaternary palaeoenvironment and chronology in the Traenadjupet Slide area offshore Norway. Marine Geology 188, 35-60.

Laberg, J.S., Stoker, M.S., Dahlgren, K.I.T., de Haas, H., Haflidason, H., Hjelstuen, B.O., Nielsen, T., Shannon, P.M., Vorren, T.O., van Weering, T.C.E., Ceramicola, S., 2005. Cenozoic alongslope processes and sedimentation on the NW European Atlantic margin. Marine and Petroleum Geology 22, 1069-1088.

Lamb, K.G., 2014. Internal Wave Breaking and Dissipation Mechanisms on the Continental Slope/Shelf. Annual Review of Fluid Mechanics 46, 231-254.

Lee, H.J., Syvitski, J.P.M., Parker, G., Orange, D., Locat, J., Hutton, E.W.H., Imran, J., 2002. Distinguishing sediment waves from slope failure deposits: field examples, including the 'Humboldt slide', and modelling results. Marine Geology 192, 79-104.

Leynaud, D., Mienert, J., Vanneste, M., 2009. Submarine mass movements on glaciated and non-glaciated European continental margins: A review of triggering mechanisms and preconditions to failure. Marine and Petroleum Geology 26, 618-632.

Llave, E., Schönfeld, J., Hernández-Molina, F.J., Mulder, T., Somoza, L., Diaz-del Rio, V., Sanchez-Almazo, I., 2006. High-resolution stratigraphy of the Mediterranean outflow contourite system in the Gulf of Cadiz during the late Pleistocene: The impact of Heinrich events. Marine Geology 277, 241-262.

Llave, E., Matias, H., Hernández-Molina, F., Ercilla, G., Stow, D., Medialdea, T., 2011. Pliocene–Quaternary contourites along the northern Gulf of Cadiz margin: sedimentary stacking pattern and regional distribution. Geo-Marine Letters, 1-14.

Loubere, P., 1987. Changes in mid-depth north-Atlantic and mediterranean circulation during the late Pliocene - isotopic and sedimentological evidence. Marine Geology 77, 15-38.

Louvel, V., Dyment, J., Sibuet, J.-C., 1997. Thinning of the Goban Spur continental margin and formation of early oceanic crust: constraints from forward modelling and inversion of marine magnetic anomalies. Geophysical Journal International 128, 188-196.

Louwye, S., Foubert, A., Mertens, K., Van Rooij, D., the IODP Exp. 307 Scientific Party, 2008. Integrated stratigraphy and palaeoecology of the Lower and Middle Miocene of Porcupine Basin. Geological Magazine 145, 321-344.

MacLachlan, S.E., Elliott, G.M., Parson, L.M., 2008. Investigations of the bottom current sculpted margin of Hatton Bank, NE Atlantic. Marine Geology 253, 170-184.

Maslin, M., Owen, M., Day, S., Long, D., 2004. Linking continental-slope failures and climate change: Testing the clathrate gun hypothesis. Geology 32, 53-56.

Masson, D.G., Howe, J.A., Stoker, M.S., 2002. Bottom-current sediment waves, sediment drifts and contourites in the northern Rockall Trough. Marine Geology 192, 215-237.

McCartney, M.S., Mauritzen, C., 2001. On the origin of the warm inflow to the Nordic Seas. Progress In Oceanography 51, 125-214.

McDonnell, A., Shannon, P.M., 2001. Comparative Tertiary stratigraphic evolution of the Porcupine and Rockall basins, in: Shannon, P.M., Haughton, P., Corcoran, D. (Eds.), The Petroleum Exploration of Ireland's Offshore Basins. Geological Society, London, pp. 323-344.

Mienis, F., van Weering, T., de Haas, H., de Stigter, H., Huvenne, V., Wheeler, A., 2006. Carbonate mound development at the SW Rockall Trough margin based on high resolution TOBI and seismic recording. Marine Geology 233, 1-19.

Mienis, F., de Stigter, H.C., de Haas, H., van Weering, T.C.E., 2009. Near-bed particle deposition and resuspension in a cold-water coral mound area at the Southwest Rockall Trough margin, NE Atlantic. Deep Sea Research Part I: Oceanographic Research Papers 56, 1026-1038.

Migeon, S., Savoye, B., Zanella, E., Mulder, T., Faugères, J.-C., Weber, O., 2001. Detailed seismic-reflection and sedimentary study of turbidite sediment waves on the Var Sedimentary Ridge (SE France): significance for sediment transport and deposition and for the mechanisms of sediment-wave construction. Marine and Petroleum Geology 18, 179-208.

Migeon, S., Ducassou, E., Le Gonidec, Y., Rouillard, P., Mascle, J., Revel-Rolland, M., 2010. Lobe construction and sand/mud segregation by turbidity currents and debris flows on the western Nile deep-sea fan (Eastern Mediterranean). Sedimentary Geology 229, 124-143.

Mosher, D.C., Thomson, R.E., 2002. The Foreslope Hills: large-scale, fine-grained sediment waves in the Strait of Georgia, British Columbia. Marine Geology 192, 275-295.

Naylor, D., Shannon, P.M., 1982. The Geology of Offshore Ireland and West Britain. Graham & Trotman ltd., London.

New, A.L., Barnard, S., Herrmann, P., Molines, J.-M., 2001. On the origin and pathway of the saline inflow to the Nordic Seas: insights from models. Progress In Oceanography 48, 255-287.

Normark, W.R., Piper, D.J.W., Posamentier, H., Pirmez, C., Migeon, S., 2002. Variability in form and growth of sediment waves on turbidite channel levees. Marine Geology 192, 23-58.

O'Reilly, B.M., Shannon, P.M., Readman, P.W., 2007. Shelf to slope sedimentation processes and the impact of Plio–Pleistocene glaciations in the northeast Atlantic, west of Ireland. Marine Geology 238, 21-44.

Paillet, J., Arhan, M., McCartney, M.S., 1998. Spreading of Labrador Sea Water in the eastern North Atlantic. Journal of Geophysical Research-Oceans 103, 10223-10239.

Pingree, R.D., Le Cann, B., 1990. Structure, strength and seasonality of the slope currents in the Bay of Biscay region. Journal of the Marine Biological Association of the United Kingdom 70, 857-885.

Pingree, R.D., Le Cann, B., 1992. Three anticyclonic Slope Water Oceanic eDDIES (SWODDIES) in the southern Bay of Biscay in 1990. Deep-Sea Research 39, 1147-1176.

Piper, D.J.W., Normark, W.R., 2009. Processes That Initiate Turbidity Currents and Their Influence on Turbidites: A Marine Geology Perspective. Journal of Sedimentary Research 79, 347-362.

Poag, C.W., Reynolds, L.A., Mazzullo, J.M., Keigwin, L.D., 1985. Foraminiferal, lithic, and isotopic changes across four major unconformities at Deep Sea Drilling Project Site 548, Goban Spur. Initial Reports of the Deep Sea Drilling Project. U.S. Government Printing Office, Washington, pp. 539-555.

Pomar, L., Morsilli, M., Hallock, P., Bádenas, B., 2012. Internal waves, an under-explored source of turbulence events in the sedimentary record. Earth-Science Reviews 111, 56-81.

Puig, P., Palanques, A., Guillén, J., El Khatab, M., 2004. Role of internal waves in the generation of nepheloid layers on the northwestern Alboran slope: Implications for continental margin shaping. Journal of Geophysical Research: Oceans 109, C09011.

Raddatz, J., Rüggeberg, A., Margreth, S., Dullo, W.-C., 2011. Paleoenvironmental reconstruction of Challenger Mound initiation in the Porcupine Seabight, NE Atlantic. Marine Geology 282, 79-90.

Raymo, M.E., Oppo, D.W., Flower, B.P., Hodell, D.A., McManus, J.F., Venz, K.A., Kleiven, K.F., McIntyre, K., 2004. Stability of North Atlantic water masses in face of pronounced climate variability during the Pleistocene. Paleoceanography 19, PA2008.

Rebesco, M., Stow, D.A.V., 2001. Seismic expression of contourites and related deposits: A preface. Marine Geophysical Researches 22, 303-308.

Rebesco, M., 2005. SEDIMENTARY ENVIRONMENTS | Contourites, in: Selley, R.C., Cocks, L.R.M., Plimer, I., R. (Eds.), Encyclopedia of Geology. Elsevier, Oxford, pp. 513-528.

Rebesco, M., Hernández-Molina, F.J., Van Rooij, D., Wåhlin, A., 2014. Contourites and associated sediments controlled by deep-water circulation processes: State-of-the-art and future considerations. Marine Geology 352, 111-154.

Ribó, M., Puig, P., Muñoz, A., Lo Iacono, C., Masqué, P., Palanques, A., Acosta, J., Guillén, J., Gómez Ballesteros, M., 2016. Morphobathymetric analysis of the large fine-grained sediment waves over the Gulf of Valencia continental slope (NW Mediterranean). Geomorphology 253, 22-37.

Rice, A.L., Thurston, M.H., New, A.L., 1990. Dense aggregations of a hexactinellid sponge, *Pheromena carpenteri*, in the Porcupine Seabight (northeast Atlantic Ocean), and possible causes. Progress In Oceanography 24, 179-196.

Rogerson, M., Rohling, E.J., Bigg, G.R., Ramirez, J., 2012. Paleoceanography of the Atlantic-Mediterranean exchange: Overview and first quantitative assessment of climatic forcing. Reviews of Geophysics 50, RG2003.

Rohling, E.J., Foster, G.L., Grant, K.M., Marino, G., Roberts, A.P., Tamisiea, M.E., Williams, F., 2014. Sea-level and deep-sea-temperature variability over the past 5.3 million years. Nature 508, 477-482.

Roque, C., Duarte, H., Terrinha, P., Valadares, V., Noiva, J., Cachão, M., Ferreira, J., Legoinha, P., Zitellini, N., 2012. Pliocene and Quaternary depositional model of the Algarve margin contourite drifts (Gulf of Cadiz, SW Iberia): Seismic architecture, tectonic control and paleoceanographic insights. Marine Geology 303–306, 42-62.

Schlitzer, R., 2012. Ocean Data View, http://odv.awi.de.

Schmidt, S., van Weering, T.C.E., Reyss, J.L., van Beek, P., 2002. Seasonal deposition and reworking at the sediment-water interface on the northwestern Iberian margin. Progress In Oceanography 52, 331-348.

Schönfeld, J., Zahn, R., 2000. Late Glacial to Holocene history of the Mediteranean Outflow. Evidence from benthic foraminiferal assemblages and stable isotopes at the Portuguese margin. Palaeogeography, Palaeoclimatology, Palaeoecology 159, 85-111.

Shannon, P.M., Stoker, M.S., Praeg, D., Van Weering, T.C.E., De Haas, H., Nielsen, T., Dahlgren, K.I.T., Hjelstuen, B.O., 2005. Sequence stratigraphic analysis in deep-water, underfilled NW European passive margin basins. Marine and Petroleum Geology 22, 1185-1200.

Southard, J.B., Cacchione, D.A., 1972. Experiments on bottom sediment movement by breaking internal waves. In: Swift, D.J., Duane, D.B., Pilkey, O.H. (Eds.), Shelf Sediment Transport: Process and Pattern. Hutchinson & Ross, Stroudsburg, Pa., Dowden, pp. 83–97.

Stein, R., Kanamatsu, T., Alvarez-Zarikian, C., Higgins, S., Channell, J.E.T., Aboud, E., Ohno, M., Acton, G.D., Akimoto, K., Bailey, I., Bjorklund, K.R., Evans, H., Nielsen, S.H.H., Fang, N., Ferretti, P., Gruetzner, J., Guyodo, Y.J.B., Hagino, K., Harris, R., Hatakeda, K., Hefter, J., Judge, S.A., Kulhanek, D.K., Nanayama, F., Rashid, H., Sierro, F.J., Voelker, A., Zhai, Q., 2006. North Atlantic Paleoceanography: The Last Five Million Years. EOS Transactions 87, 129-133.

Stoker, M.S., Hoult, R., Nielsen, T., Hjelstuen, B.O., Laberg, J.S., Shannon, P.M., Praeg, D., Mathiesen, A., van Weering, T.C.E., McDonnell, A., 2005a. Sedimentary and oceanographic responses to early Neogene compression on the NW European margin. Marine and Petroleum Geology 22, 1031-1044.

Stoker, M.S., Praeg, D., Hjelstuen, B.O., Laberg, J.S., Nielsen, T., Shannon, P.M., 2005b. Neogene stratigraphy and the sedimentary and oceanographic development of the NW European Atlantic margin. Marine and Petroleum Geology 22, 977-1005.

Stow, D.A.V., Faugères, J.C., 2008. Chapter 13 Contourite Facies and the Facies Model, in: Rebesco, M., Camerlenghi, A. (Eds.), Developments in Sedimentology. Elsevier, pp. 223-256.

Stow, D.A.V., Hernández-Molina, F.J., Llave, E., Sayago-Gil, M., del Rio, V.D., Branson, A., 2009. Bedform-velocity matrix: The estimation of bottom current velocity from bedform observations. Geology 37, 327-330.

Strachan, P., Evans, D., 1991. A local deep-water sediment failure on the NW slope of the UK. Scottish Journal of Geology 27, 107-111.

Sultan, N., Cochonat, P., Canals, M., Cattaneo, A., Dennielou, B., Haflidason, H., Laberg, J.S., Long, D., Mienert, J., Trincardi, F., Urgeles, R., Vorren, T.O., Wilson, C.K., 2004. Triggering mechanisms of slope instability processes and sediment failures on continental margins: a geotechnical approach. Marine Geology 213, 291-321.

Sy, A., Rhein, M., Lazier, J.R.N., Koltermann, K.P., Meincke, J., Putzka, A., Bersch, M., 1997. Surprisingly rapid spreading of newly formed intermediate waters across the North Atlantic Ocean. Nature 386, 675-679.

Thierens, M., Browning, E., Pirlet, H., Loutre, M.F., Dorschel, B., Huvenne, V.A.I., Titschack, J., Colin, C., Foubert, A., Wheeler, A.J., 2013. Cold-water coral carbonate mounds as unique palaeo-archives: the Plio-Pleistocene Challenger Mound record (NE Atlantic). Quaternary Science Reviews 73, 14-30.

Thomsen, L., van Weering, T.C.E., 1998. Spatial and temporal variability of particulate matter in the benthic boundary layer at the N.W. European Continental Margin (Goban Spur). Progress In Oceanography 42, 61-76.

Thornalley, D.J.R., Bauch, H.A., Gebbie, G., Guo, W., Ziegler, M., Bernasconi, S.M., Barker, S., Skinner, L.C., Yu, J., 2015. A warm and poorly ventilated deep Arctic Mediterranean during the last glacial period. Science 349, 706-710.

Toucanne, S., Mulder, T., Schönfeld, J., Hanquiez, V., Gonthier, E., Duprat, J., Cremer, M., Zaragosi, S., 2007. Contourites of the Gulf of Cadiz: A high-resolution record of the paleocirculation of the Mediterranean outflow water during the last 50,000 years. Palaeogeography, Palaeoclimatology, Palaeoecology 246, 354-366.

Trincardi, F., Field, M.E., 1992. Collapse and flow of lowstand shelf-margin deposits: An example from the eastern Tyrrhenian Sea, Italy. Marine Geology 105, 77-94.

Van Aken, H.M., 2000. The hydrography of the mid-latitude Northeast Atlantic Ocean II: The intermediate water masses. Deep-Sea Research I 47, 789-824.

Van Rooij, D., Blamart, D., Kozachenko, M., Henriet, J.-P., 2007. Small mounded contourite drifts associated with deep-water coral banks, Porcupine Seabight, NE Atlantic Ocean, in: Viana, A.R., Rebesco, M. (Eds.), Economic and Palaeoceanographic Importance of Contourite Deposits. Geological Society, London, pp. 225-244.

Van Rooij, D., Huvenne, V.A.I., Blamart, D., Henriet, J.P., Wheeler, A., de Haas, H., 2009. The Enya mounds: a lost mound-drift competition. International Journal of Earth Sciences 98, 849-863.

Van Rooij, D., Iglesias, J., Hernández-Molina, F.J., Ercilla, G., Gomez-Ballesteros, M., Casas, D., Llave, E., De Hauwere, A., Gil, S.G., Acosta, J., Henriet, J.P., 2010. The Le Danois Contourite Depositional System: interactions between the Mediterranean Outflow Water and the upper Cantabrian slope (North Iberian margin). Marine Geology 274, 1-20.

van Weering, T.C.E., Hall, I.R., de Stigter, H.C., McCave, I.N., Thomsen, L., 1998. Recent sediments, sediment accumulation and carbon burial at Goban Spur, N.W. European Continental Margin (47-50°N). Progress In Oceanography 42, 5-35.

Vergnaud-Grazzini, C., Saliège, J.F., 1985. Pleistocene climatic changes in surface waters of the Northeastern Atlantic: Oxygen and Carbon isotopic compositions of planktonic foraminifers at Deep Sea Drilling Project sites 548 and 549. Initial Reports of the Deep Sea Drilling Project. U.S. Government Printing Office, Washington, pp. 793-803.

Voelker, A.H.L., Lebreiro, S.M., Schonfeld, J., Cacho, I., Erlenkeuser, H., Abrantes, F., 2006. Mediterranean outflow strengthening during northern hemisphere coolings: A salt source for the glacial Atlantic? Earth and Planetary Science Letters 245, 39-55.

White, M., 2003. Comparison of near seabed currents at two locations in the Porcupine Sea Bight - implications for benthic fauna. Journal of the Marine Biological Association of the United Kingdom 83, 683-686.

White, M., 2007. Benthic dynamics at the carbonate mound regions of the Porcupine Sea Bight continental margin. International Journal of Earth Sciences 96, 1-9.

White, M., Dorschel, B., 2010. The importance of the permanent thermocline to the cold water coral carbonate mound distribution in the NE Atlantic. Earth and Planetary Science Letters 296, 395-402.

Wilson, C.K., Long, D., Bulat, J., 2004. The morphology, setting and processes of the Afen Slide. Marine Geology 213, 149-167.

World Ocean Database, 2009. http://www.nodc.noaa.gov/OC5/WOD09/pr_wod09.html.

Wynn, R.B., Weaver, P.P.E., Ercilla, G., Stow, D.A.V., Masson, D.G., 2000. Sedimentary processes in the Selvage sediment-wave field, NE Atlantic: new insights into the formation of sediment waves by turbidity currents. Sedimentology 47, 1181-1197.

Wynn, R.B., Stow, D.A.V., 2002. Classification and characterisation of deep-water sediment waves. Marine Geology 192, 7-22.

Zaragosi, S., Bourillet, J.F., Eynaud, F., Toucanne, S., Denhard, B., Van Toer, A., Lanfumey, V., 2006. The impact of the last European deglaciation on the deep-sea turbidite systems of the Celtic-Armorican margin (Bay of Biscay). Geo-Marine Letters 26, 317-329.

CHAPTER 4

Goban Spur bottom current variability across the four deglaciations

Part of the content of this chapter is intended for publication as:

Stanislas DELIVET, Dominique BLAMART, Frank BASSINOT, Claire WAELBROECK, Natalia VASQUEZ-RIVEIROS, Sebastien BERTRAND, Furu MIENIS, Jan-Berend STUUT, David VAN ROOIJ. Sedimentological expression and bottom current variability across four deglacial transitions of the past 500 ky (DSDP Site 548). Quaternary Science Reviews.

Abstract

Newly collected core data from DSDP Site 548 provides insight into the behaviour and northward extent of the Mediterranean Outflow Water across the four penultimate glacial terminations within the intermediate northeast Atlantic. Magnetic susceptibility, XRF data, *Neogloboquadrina pachyderma* sinistral relative abundance, as well as terrigenous grain-size analysis revealed local bottom current regime changes during distinct climate stages. Prior to each glacial termination, Marine Isotopic Stages 12, 10, 8 and 6 were characterised by large terrigenous grain-size distribution profile, dominated by fine silts particles (below 20 µm in grain-size) and a variable amount of ice rafted debris. In contrast, interglacial Marine Isotopic Stages 11, 9, 7 and 5 terrigenous grain-size distributions were dominated by coarser silt particles, ranging from 20 to 60 µm. Such variations are thought to be primarily driven by changes in the local bottom current regime and associated hydrodynamic sorting of particles. The local bottom current regime is driven by water column stratification changes associated with the presence of the Mediterranean Outflow Water which characterizes enhanced internal tides and tide-topographic interactions. The studied interglacials are associated with the presence of vigorous enhanced internal tidal regime, interpreted to reflect the presence of a stratified water column. Such internal tidal regime is thought to be relatively analogue to the present-day configuration, characterised by peak velocities up to 30 cm/s. Alternatively, the deposition of fine silt particles prior to each terminations suggests reduced effect of internal tides associated with well-mixed and relatively homogenous water column at these depths. Such conditions seemingly indicate the absence of the Mediterranean Outflow Water at those latitudes, possibly caused by changes in its flow regime and volume, or alternatively, by changes in the Atlantic meridional circulation pattern. It is observed that the Mediterranean Outflow Water only reached the Goban Spur and Porcupine Seabight latitudes during periods of production of a dense and ventilated, modern-like, North Atlantic Deep Water at ODP Site 980.

Contributions

This manuscript was written by S. Delivet. Core data sub-sampling were conducted by S. Delivet, in consultation with D. Van Rooij, D. Blamart, F. Bassinot, C. Waelbroeck, N. Vasquez-Riveiros. Analyses were carried out by S. Delivet in consultation with D. Van Rooij, S. Bertrand, D. Blamart and N. Vasquez-Riveiros. Interpretation and discussion of results were done by S. Delivet and D. Van Rooij in consultation with F. Mienis and J-B. Stuut.

4.1 Introduction

From the course of the Pliocene onwards, the Mediterranean Outflow Water (MOW) greatly influenced and governed the sedimentation and architecture of a substantial portion of the northwest European margin (Van Rooij et al., 2007a; Hernández-Molina et al., 2011; 2016a). The MOW is also known to significantly influence the north Atlantic density budget, emphasizing the importance of the structure and circulation pattern of intermediate water masses, as part of the global climate system (Bigg et al., 2003; Rogerson et al., 2012; Khélifi et al., 2014; van Ommen, 2015). The MOW is formed by the overflow of deep and saline (salinity > 38 at its source) Mediterranean waters exiting the Strait of Gibraltar (Baringer and Price, 1999; Iorga and Lozier, 1999; Mauritzen et al., 2001). It reaches its density equilibrium southwest of the Iberian margin and partly evolves as a poleward geostrophic undercurrent which can be traced as far north as the Porcupine Bank (Iorga and Lozier, 1999; Lozier and Nicole, 2008; Bozec et al., 2011). Witnesses of the existence of this flow pattern throughout the Plio-Pleistocene are mainly found in the form of topographically controlled sediment drifts, respectively along: the northern Gulf of Cádiz (Hernandez-Molina et al., 2003; 2016b), the Galician margin (Maestro et al., 2013; Hanebuth et al., 2015; Zhang et al., 2015), the Le Danois Bank (Ercilla et al., 2008; Van Rooij et al., 2010; González-Pola et al., 2012) and the Porcupine Seabight (De Mol et al., 2002; Van Rooij et al., 2003; 2007a). Nevertheless, the MOW variability and connectivity existing between those sites is only partly resolved, particularly regarding the past 500 ky (Rogerson et al., 2012; Raddatz et al., 2014). The last 500 ky is a characteristic period with respect to the modern climate regime, that is marked by a non-linear climate response to the astronomical forcing and high amplitude contrasts between glacial versus interglacial conditions (Martinson et al., 1987; Stocker and Johnsen, 2003; Lisiecki and Raymo, 2007). During this period, global climate changes and associated sea-level variations caused pronounced hydraulic forcing at the Strait of Gibraltar, both impacting the density, depth of settlement, and behaviour of the MOW plume within the Atlantic Ocean (Rogerson et al., 2012; Bahr et al., 2014; Rohling et al., 2014; Hernández-Molina et al., 2016b).

Within the Porcupine Seabight, the development of coral mounds, consisting in a cold-water coral framework embedded within a sediment matrix, commonly occurred at depths ranging from 500 to 1000 m (De Mol et al., 2002; Foubert et al., 2007; Huvenne et al., 2007; Van Rooij et al., 2009; Wienberg and Titschack, 2015). From ~500 ka BP onwards, the cold-water coral growth was mainly restricted to interglacial periods, indicating a strong environmental control (Dorschel et al., 2005; Kano et al., 2007; Rüggeberg et al., 2007; Frank et al., 2011). Cold-water coral growth depends on specific oceanographic conditions in which primary productivity export, temperature gradient and internal tide-topographic interactions are of primary importance (Dorschel et al., 2007; White et al.,

2007; Mohn et al., 2014; Wienberg and Titschack, 2015; Hebbeln et al., 2016). Nowadays, favourable conditions are met at the boundary between the MOW and the overlying Eastern North Atlantic Central Water (ENACW) which is associated with vigorous bottom currents attributed to an enhanced internal tide regime (Rice et al., 1990; White et al., 2007; 2010; Mohn et al., 2014). During glacial periods of the past 500 ky, the upper boundary of the MOW is thought to have shifted below the depth range of the cold-water coral mounds, affecting (among other factors) the bottom current-assisted food supply (Sakai et al., 2009; Raddatz et al., 2014). Different studies along the Iberian margin largely corroborated the glacial deepening of the MOW by about 300 to 600 m relative to the present day (Schönfeld and Zahn, 2000; Rogerson et al., 2005; Maestro et al., 2013; Bahr et al., 2015; Hernández-Molina et al., 2016a). Within the Porcupine Seabight, results obtained from the IODP Exp. 307 (Fig. 4.1) suggest this pattern might have been characteristic since ~500 ka BP (Huvenne et al., 2009; Thierens et al., 2013; Raddatz et al., 2014). However, it is unclear if the MOW shifted towards increased water depths during each respective glacial interval, or was simply absent from these latitudes. Schönfeld and Zahn (2000) found evidences that the MOW might have been confined along the western Iberian margin during the last glacial maximum, and hence, must have been absent at the latitudes of Porcupine Seabight. The absence of evidence about the glacial position of the MOW within the Porcupine Seabight might also be interpreted to reflect its confinement towards lower latitudes. Nowadays, the majority of the available records from the Porcupine Seabight were retrieved from cold-water coral mounds which often consist in discontinuous periods of aggradation, inducing limitations when establishing the timing of the bottom current regime changes (Dorschel et al., 2005; Rüggeberg et al., 2007; Thierens et al., 2010; 2013; Raddatz et al., 2011; 2014). The background sedimentation of this part of the margin has also been severely impacted by the presence of energetic bottom currents, inducing the presence of hiatuses commonly ranging from thousands to hundreds of thousands of years (Dorschel et al., 2005; Foubert et al., 2007; Rüggeberg et al., 2007; Van Rooij et al., 2007b). Yet, no precise palaeo-oceanographic record extending beyond the last glacial has been made available.

DSDP Site 548 is located on the Goban Spur sub-marine plateau at about 49°N, at the southern boundary of the Porcupine Seabight, and currently is influenced by the lower boundary of the MOW at 1256 m water depth (Caralp et al., 1985; Vergnaud-Grazzini and Saliège, 1985a; Khélifi et al., 2009; 2014). It is located in an open slope environment, broadly free of any geomorphological constrain that may lead to local anomalies in the velocity field (Huthnance et al., 2001), and might thus have recorded a more continuous sequence than the Porcupine Seabight slopes. Nowadays, the transition zone between the MOW and the underlying Labrador Sea Water (LSW) is also associated with enhanced internal tides which dominate the bottom current regime (van Weering et al., 1998;

2001). Large-scale sediment waves in this sector were proposed to reflect the long term enhanced internal tidal regime associated with the introduction of the MOW from the course of the Pliocene onwards (Delivet et al., 2016). Therefore, DSDP Site 548 is ideally situated in order to study recent shifts in the MOW along the southern Irish margin, and can be expected to be influenced by the deep glacial MOW plume, if present at these latitudes.

The aim of this study is to investigate glacial versus interglacial changes in the bottom current regime at DSDP Site 548 throughout distinct glacial terminations of the past 500 ky. The bottom current variability is characteristic for the northeast Atlantic intermediate water column stratification and associated internal tide regime, and most probably influenced by changes in the behaviour and circulation pattern of the MOW. The objective is to determine whether the MOW experienced depth and/or latitudinal shifts with respect to the Porcupine Seabight and Irish margin, and to establish the precise timing of those shifts. As such, this might help constraining the timing of the reintroduction of the MOW within the Porcupine Seabight, as an important food supply mechanism for the cold-water coral ecosystems of this part of the margin. This may ultimately contribute to characterise the past MOW northward advection proceeding, during and following different glacial terminations, as a pre-requisite to understand the mechanism in which the MOW influenced the intermediate North Atlantic Ocean density budget.

4.2 Regional setting

4.2.1 Geological setting

The Goban Spur submarine plateau formed during the early Cretaceous through the emplacement of a series of half-graben structures, and has developed as a passive margin since the late Cretaceous (Dingle and Scrutton, 1979; Naylor and Shannon, 1982; Louvel et al., 1997). This plateau forms the northwest prolongation of the Celtic continental margin, which has been effectively disconnected from the adjacent sedimentary systems: the Great Sole Basin to the east and the Gollum Channel System to the north (Hall and McCave, 1998; Wheeler et al., 2003; Bourillet et al., 2006). Goban Spur received a hemipelagic sedimentation over the entire Pleistocene, with sedimentation rates ranging from ~12 cm/ky during the Holocene, up to 20 cm/ky during the Last Glacial Maximum (Hall and McCave, 1998; Auffret et al., 2002). This region is located at the eastern edge of the Ruddiman Belt, characterised by the presence of IRD-rich (Heinrich event-like) layers, potentially originating from the calving of the Laurentide (LIS), the Greenland (GIS), Iceland (IIS), and the British Irish ice-sheets (BIIS) collapse (Fig. 4.1; Ruddiman, 1977; Heinrich, 1988; Auffret et al., 1999; Mojtahid et al., 2005; Jullien et al., 2006; Eynaud et al., 2007; Toucanne et al., 2009a;

Naafs et al., 2013). Thus, sediments mainly consist of nannofossil and foraminifer oozes alternating with coarse IRD deposits (de Graciansky et al., 1985; Auffret et al., 2002). Additionally, this region is highly sensitive to variations in the sub-polar front, which characterised the incursion of sub-polar sea-surface water masses towards the southeast north Atlantic Ocean (Fig. 4.1; McManus et al., 2004; Mojtahid et al., 2005; de Vernal et al., 2006; Eynaud et al., 2007; 2009; Voelker et al., 2010). From about 650 ka BP onwards, the glacial position of the sub-polar front set at ~37.5°N, and thus has repeatedly shifted from south to north of Goban Spur over the studied period of time (Maiorano et al., 2015). DSDP Site 548 last ~500 ky deposits (Vergnaud-Grazzini and Saliège, 1985b) were retrieved from the downslope flank of a large scale deep sea sediment wave (Delivet et al., 2016).

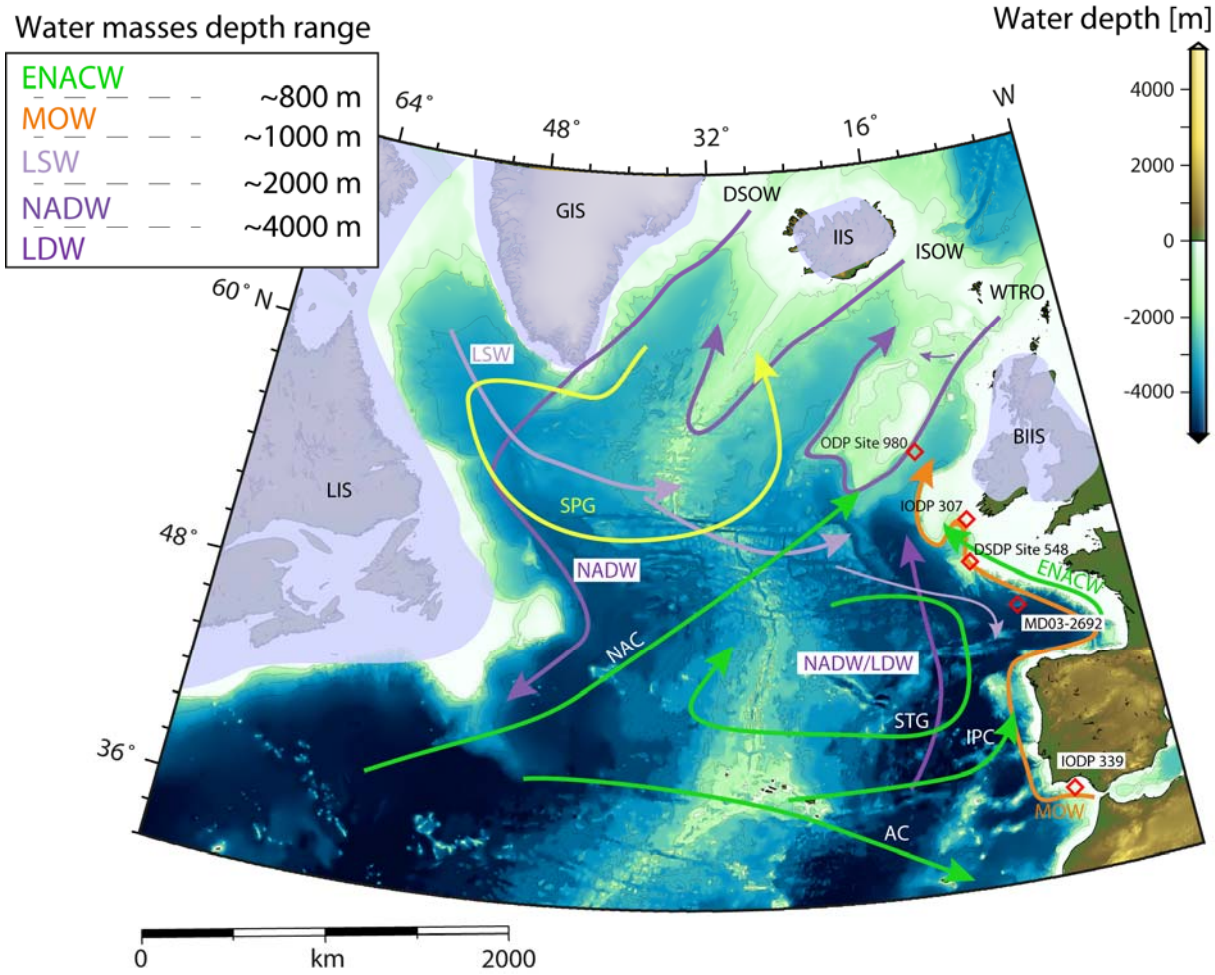

Figure 4.1 Overview map of the north Atlantic Ocean with location of DSDP Site 548 and the main modern hydrological structures (McCartney and Mauritzen, 2001; Read, 2001; Lozier and Nicole, 2008). The major ice-sheets spreading centres and their overall expansion during the last glacial maximum are indicated (Stokes and Clark, 2001; 2016). Diamonds indicate the location of sites referred to in the text: MD03-2692 (Mojtahid et al., 2005); ODP Site 980 (McManus et al., 1999); IODP Exp. 307 (Kano et al., 2007); IODP Exp. 339 (Hernández-Molina et al., 2014). **LIS**: Laurentide Ice-Sheet; **GIS**: Greenland Ice-Sheet; **IIS**: Iceland Ice-Sheet; **BIIS**: British-Irish Ice-Sheet; **NAC**: North Atlantic Current; **AC**: Azores Current; **IPC**: Iberian Poleward Current; **ENACW**: Eastern North Atlantic Central Water; **STG**: mid-depth Sub-Tropical Gyre; **SPG**: mid-depth Sub-Polar Gyre; **LSW**: Labrador Sea Water; **MOW**: Mediterranean Outflow Water; **WTRO**: Wyville-Thompson Ridge Overflow; **ISOW**: Iceland Sea Overflow Water; **DSOW**: Denmark Strait Overflow Water; **NADW**: North Atlantic Deep Water; **LDW**: Lower Deep Water.

4.2.2 Oceanographic setting

The North Atlantic Current carries warm and relatively saline sea surface water from the western sub-tropical Atlantic towards the Nordic seas via the Iceland-Scotland ridge (Fig. 4.1). This weakly stratified current forms the boundary between the relatively deep (~700 m water depth) mid-depths sub-polar and less deep (~500 m water depth) sub-tropical gyres (Read, 2001; Lozier and Nicole, 2008). The mid-depth sub-polar gyre is formed by the cyclonic recirculation of the cold (~34.9 and ~4°C) Sub-Arctic Intermediate Water (Van Aken, 2000a). The mid-depth sub-tropical gyre is formed by relatively saline and warm (~35.5 and ~11°C) North Atlantic Central Water and experiences an anticyclonic circulation that dominates the Bay of Biscay (Pingree and Le Cann, 1990). The Armorican shelf and Goban Spur are dominated by the residual poleward advection of the ENACW and the slightly cooler and saltier underlying MOW (35.6 and ~9°C; Pingree and Le Cann, 1990, 1992; Iorga and Lozier, 1999). The ENACW and MOW are centred around 500 and 800 m water depth respectively, the region being characterised by a 200 m thick surface mixed layer (Paillet et al., 1998). The ENACW is formed by the winter cooling of the Iberian poleward current, a detached northern branch of the Azores current (Fig. 4.1; Paillet and Mercier, 1997; Van Aken, 2000a). The MOW originates from the Gibraltar Strait and flows along the eastern edge of the basin until it might either recirculate within the mid-depth sub-polar gyre, either contributes to the Atlantic inflow water to the Nordic Seas (Lozier and Nicole, 2008; Bozec et al., 2011).

From 1000 to 1800 m water depth, the salinity gradually decreases to a minimum of ~34.9 (and 4°C) marking the presence of the LSW core. The LSW is formed during winter through open sea deep water convection in the Labrador Sea (Sy et al., 1997; Read, 2001). This water mass partly contributes to the formation of the North Atlantic Deep Water (NADW) that flows towards the south as a western boundary undercurrent, and partly spreads eastwards at ~1800 m water depth towards the northern Bay of Biscay (van Aken, 2000b; Read, 2001; Lozier and Nicole, 2008). Below the LSW the slightly more saline (~34.95 and ~3-2°C) NADW is found, ranging from 2200 to more than 4000 m water depth. This water mass is formed from different contributions of the dense Denmark Strait Overflow Water (DSOW) and Iceland Sea Overflow Water (ISOW), Wyville-Thompson Ridge Overflow (WTRO) and LSW (Fig. 4.1; Lee and Ellett, 1965; Kuhlbrodt et al., 2007; Legg et al., 2009; Schloesser et al., 2012). Southwest of Goban Spur, the northward-flowing NADW is formed by a recirculation of the Western North Atlantic Deep Water and LSW, potentially slightly influenced by water masses originating from the southern hemisphere (van Aken, 2000b). Below 4000 m water depth the poorly ventilated Lower Deep Water (LDW) has a salinity of 34.9 for ~2.5 °C, and is mainly formed by the Antarctic Bottom Water (AABW) originating from the Southern Ocean (van Aken, 2000b).

The present day bottom current regime at Goban Spur is dominated by bidirectional barotropic currents of semi-diurnal frequency (internal tides), characterised by peak velocities exceeding 40 cm/s, associated to rather slow (< 10 cm/s) mean along slope current (Thomsen et al., 1998; 2000; Huthnance et al., 2001; van Weering et al., 2001). The interactions between the internal tides propagating along the MOW lower interface and the overall 1.2° dipping seabed are thought to be responsible for the formation of the observed sediment waves, under a transmissive reflection conditions (Cacchione et al., 2002; Lamb, 2014; Delivet et al., 2016; Ribó et al., 2016).

4.3 Material and methods

DSDP Site 548 (48°54.95'N; 12°09.84'W; de Graciansky et al., 1985) recovered about 200 m of sediment using an advanced hydraulic piston corer, of which the top 59.9 m represent middle/upper Quaternary deposits (Caralp et al., 1985). This study focuses on the interval ranging from 0 to 51.5 m below sea floor (m bsf), of which the bottom has been correlated to Marine Isotopic Stage (MIS) 12 (Vergnaud-Grazzini and Saliège, 1985b). The cores were re-analysed using a Multi-Sensor Core Logger and an AVAATECH XRF Core Scanner. Analyses were carried out in 2009 at the IODP core repository at the University of Bremen (Germany). The Magnetic Susceptibility (MS; Fig. 4.2) was analysed at 2 cm resolution and is expressed using the international unit system (SI). XRF measurements were performed at a minimum resolution of 4 cm using a 30 seconds integration time, both at 10 kV/350 µA and 30 kV/1000 µA, over an area of 1 by 1.2 cm downcore. Results provided the relative abundance between K, Ca, Ti, Mn, Fe, Cu and Sr, of which only the XRF Fe/Ca ratio and Ti normalised ratio (Ti_{norm}) are further used. This is because both ratios are extensively documented within the Bay of Biscay and the northeast Atlantic, and because of the tight link existing between those ratios variability and climatic variations (Mojtahid et al., 2005; Toucanne et al., 2009). Results in counts per second, are presented as elemental ratios, or normalised ratio (element counts divided per total counts) following recommendations by Richter et al. (2006). In a preliminary step, the XRF Fe/Ca ratio was used to refine the planktonic oxygen isotope ($\delta^{18}O$) geochronology from Vergnaud-Grazzini and Saliège (1985b) through tuning with the SPECMAP $\delta^{18}O$ stack (Fig. 4.2; Imbrie et al., 1984).

Selected intervals, respectively covering glacial termination TV to termination TII, were sub-sampled at a 10 cm downcore resolution (Fig. 4.2). The bulk terrigenous grain-size was measured using a Malvern MasterSizer 3000 at the Department of Geology of Ghent University. Prior to the measurements, the biogenic carbonate fraction was removed using a two-fold 1 mol/l acetic acid wash. The biogenic silica and organic fractions were considered negligible. One millilitre of a 0.2% Sodium Hexametaphosphate solution was added to each sample before analysis in order to limit the

formation of aggregates before measurement (McCave and Hall, 2006). Samples were introduced into the Malvern Mastersizer using a Hydro MV module with a stirrer speed of 2500 rpm and a continuous ultrasonic bath set at 10%. The original sample quantity varied between 20 and 40 mg of dry sediment (g_{dry}) depending on the carbonate content in order to ensure a laser beam obscuration ranging from 10% to 20%. Measurements were performed using a 60 s integration time in order to ensure a good signal to noise ratio with respect to coarse grains (i.e. > 150 µm). In this study, the past bottom current intensity was assessed by means of the first grain-size mode which generally falls within or fairly close to the sortable silt range varying from 10 to 63 µm in grain-size (McCave et al., 1995). Variable input of coarse IRD material may be considered to change conditions through which the hydrodynamic sorting of the particles occurs, thus possibly affecting the sortable silt index (McCave and Hall, 2006). The region under study is markedly influenced by variable IRD inputs, which is the reason why it was chosen not to use the sortable silt index. Instead, it was preferred to provide readable and full grain-size range distribution plots.

The remaining sediment of the samples was sieved using 150 and 63 µm mesh sizes. The fraction below 63 µm was dry-weighed and archived at Ghent University, while the fraction between 63 and 150 µm was discarded. The fraction above 150 µm was dry-weighed and used for foraminifera and IRD analysis. IRD input was studied by means of coarse lithic grains counts above 250 µm (McManus et al., 1999; Auffret et al., 2002; Jullien et al., 2006; Toucanne et al., 2012). Counts were reported as number of grains per gram of dry sediment (no_{grain}/g_{dry}). The relative abundance of the polar *Neogloboquadrina pachyderma* sinistral (NPS) with respect to the sub-polar *N. incompta* (census Darling et al., 2006) was determined through counting of over 200 specimens in the fraction >150 µm. The NPS relative abundance is known as an excellent tracer of sea-surface temperatures (SST) gradient comprised between 4 to 8°C (Kipp, 1976; Kucera et al., 2005), typically associated with latitudinal shifts of the polar front (Waelbroeck et al., 1998; de Vernal et al., 2006; Eynaud et al., 2009). However, NPS relative abundance reconstructed SST are largely imprecise beyond this temperature range because of the dominance of one or the other morphospecies above 90% (Darling et al., 2006). Therefore, the NPS relative abundance is expressed as relative percentage, and primarily considered to decrease as a function of sea-surface temperatures (Kucera et al., 2005; Vázquez Riveiros et al., 2013).

The age model at DSDP Site 548 has been reviewed on the basis of the newly available data. Within the past 360 ky, the age model has been established by tuning the XRF Fe/Ca with that of site MD03-2692 (Figs. 4.1; 4.3; Table 1; Mojtahid et al., 2005), and incorporating biostratigraphic and isotopic evidence from Vergnaud-Grazzini and Saliège (1985b). Tie points were positioned within peaks and/or abrupt changes in the XRF Fe/Ca ratio signal (Fig. 4.3d; Table 4.1). The detailed

relationships between the XRF Fe/Ca and the planktonic and benthic isotope stratigraphy at site MD03-2692 is described in Mojtahid et al. (2005). Tuning was made using AnalySeries software (Paillard et al., 1996). Beyond 360 ka BP, the XRF Fe/Ca ratio was tuned using the SPECMAP $\delta^{18}O$ stack (Fig. 4.2; Table 4.1). Across glacial termination TV (~410 to 430 ka BP), the newly collected NPS relative abundances and coarse lithic grain counts were compared with the reviewed age model of Vázquez Riveiros et al. (2013) at ODP Site 980 (not shown here). Note that each ~10 m long hydraulic piston core of DSDP Site 548 was considered independently due to the absence of a composite hole at this site (de Graciansky et al., 1985). Different coverage gap ranging from 3 to 38.8 ky were found between each respective piston core (Table 4.1). The complete 4 penultimate glacial termination sequences are covered. Glacial termination TI (~18 to 15 ka BP) could not be further inspected due to possible coverage gap within this interval.

4.4 Results

The age model consists of 29 tie points ranging from 442.8 to 2 ka BP. The obtained sedimentation rates vary between ~21 to locally ~3.5 cm/ky except between 81 to 68 ka BP where sedimentation rates reach up to 43 cm/ky. The four penultimate glacial terminations, at ca. 427, 332, 245 and 125 ka BP where correlated at ~48.04, 35.4, 26.7 and 16.65 m bsf, respectively. The gap between the different cores was inferred to cover parts of the glaciations during the early stages of MIS 10, 8 and 6, and within MIS 5b and c (Fig. 4.3).

The XRF Fe/Ca ratio and XRF Ti_{norm} exhibit a marked covariance throughout the record (Fig. 4.2; Table 4.2). Intervals of relatively low XRF Fe/Ca ratio and Ti_{norm} around 45, 34, 25 and 15 cm bsf correspond to low planktonic $\delta^{18}O$ values (<1.5 ‰ V-PDB; Vergnaud-Grazzini and Saliège, 1985a) which correlates to interglacial intervals from MIS 11, MIS 9, MIS 7 and MIS 5 (Fig. 4.2). Reciprocally, higher XRF Fe/Ca ratio and Ti_{norm} values correspond to colder glacial stages of MIS 12, MIS 10, MIS 8 and MIS 6. Two intervals marked by intermediate XRF Fe/Ca values, respectively between 370 and 360 ka BP (39.5 to 38 m bsf) and between 155 and 165 ka BP (22.5 to 21.3 m bsf), correspond to relatively warm phases within MIS 10 and MIS 6 (Fig. 4.3a; Martinson et al., 1987). Within MIS 10, it is also associated with intermediate NPS relative abundance ranging from 60 to 70 % (Fig. 4.3b). Interglacial intervals are characterised by low MS values, generally averaging 10 to 15 SI, whilst an average of 20 to 25 SI is obtained during colder, glacial stages (Table 4.2). Prominent MS peaks up to 80 SI are present within MIS 12 and MIS 8, but are not observed within both MIS 10 and MIS 6 (Fig. 4.2; Table 4.2).

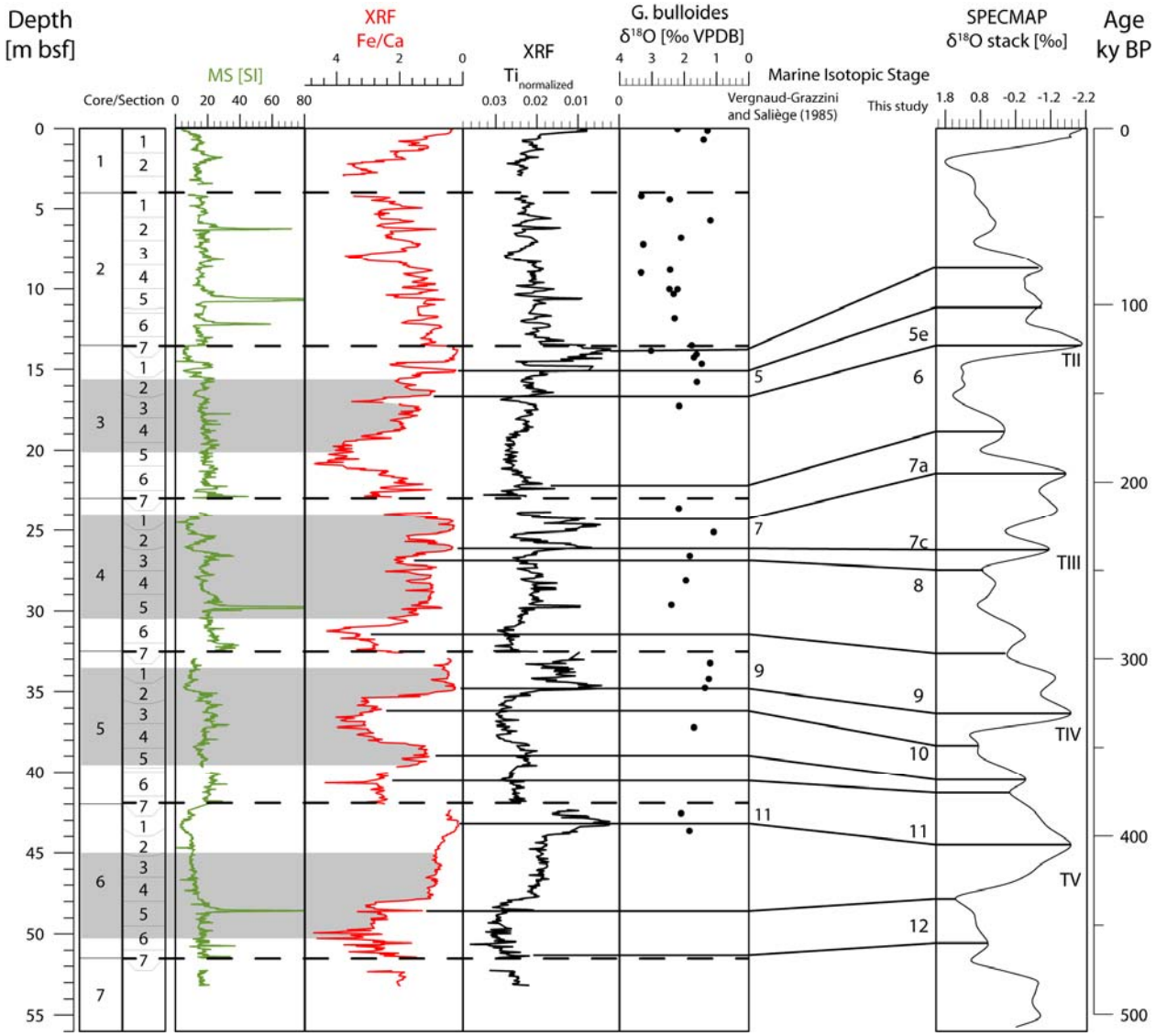

Figure 4.2 DSDP Site 548 showing its respective core and section divisions. The Magnetic Susceptibility (MS), XRF ratio Fe/Ca and Ti_{norm} are plotted together with planktonic G. bulloides $\delta^{18}O$ from (Vergnaud-Grazzini and Saliège, 1985b). Note the correlation between low planktonic $\delta^{18}O$ values and low XRF Fe/Ca ratio. The grey shaded areas indicate the subsampled intervals and the thick horizontal dashed lines represent junctions of the different hydraulic piston cores. The different tie points with the SPECMAP $\delta^{18}O$ stack (Imbrie et al., 1984; Martinson et al., 1987) used as preliminary geochronology are indicated.

Two abrupt decreases in the XRF Fe/Ca ratio (more than 1.9 in the ratio amplitude), observed at ~427 ka BP and 332 ka BP (48.04 and 35.4 m bsf), mark the glacial terminations TV and TIV (Fig. 4.3). These are correlated to abrupt decrease of the NPS relative abundance from an average of 98 and 85 % to 5.1 and 13 %, respectively across terminations TV and TIV (Table 4.2). Terminations TV and TIV are preceded by large peaks in the coarse lithic grains reaching 340 no_{grain}/g_{dry} at about 427 ka BP and 130 no_{grain}/g_{dry} at ~340 ka BP (Fig. 4.3), of which the former one is correlated to and MS peak (Fig. 4.2).

The glacial terminations TIII and TII (~ 245 ka BP and ~125 ka BP) are also associated to two abrupt decreases in the XRF Fe/Ca ratio. However, it is noted those were already preceded by a gradual rise, respectively at 260 and 145 ka BP (Fig. 4.3d), as also observed in Mojtahid et al. (2005). The presence of a XRF Fe/Ca ratio peak at about 220 ka BP (Fig. 4.3d) was correlated to the MIS 7b, corresponding to a cold MIS 7 sub-stage (Martinson et al., 1987). Variable NPS relative abundances between 25 and 40 % were obtained preceding the glacial termination TIII, from 260 to 250 ka BP. The NPS relative abundance briefly increases towards values of 75 to 80 % from about 245 to 239 ka BP. Two coarse lithic grains peaks are found at 255 ka BP and during glacial termination TIII ~240 ka BP (Fig. 4.3b). Low NPS relative abundance of 10 to 25 % is found for MIS 7c and 7a. Higher (up to 95 %) NPS relative abundances are found during MIS 7b, and a peak in coarse lithic grains of ~100 no_{grain}/g_{dry} is observed at 229 ka BP. The NPS relative abundance exhibits high values (~80 %) even though large variations are found around 141 ka BP with values briefly dropping down to 25 %. From about 138 to 121 ka BP, the NPS relative abundance gradually decreases to a minimum of ~25 % signing the onset of MIS 5e. Three moderate (below 100 no_{grain}/g_{dry}) coarse lithic grain peaks are found at 145, 125 and 120 ka BP, respectively.

The evolution of the grain-size distribution and the main grain-size mode is represented for the entire studied intervals Fig. 4.3c, while more detailed grain-size distribution profiles are given for distinct Marine Isotopic Stages (Fig. 4.4a). Overall distributions have the main grain-size mode comprised between 5 to 60 µm although two distinct distribution profiles, dominated by two distinct modes are observed (Fig. 4.4a). Glacial intervals are dominated by grain-sizes comprised between 6 and 8 µm, hereafter denominated as fine silts, which represent on average 4 % of the total relative abundance (Fig. 4.4a; Table 4.2). The same glacial intervals exhibit a marked peak between ~0.5 and 0.6 µm (~1% of the relative abundance) which represent clayey particles. Towards coarser particles, glacial intervals exhibit a slowly decreasing relative abundance of the grain-sizes from ~10 µm up to 500 µm, which indicate large distribution profiles with diversified coarse silts and sand classes and (Fig. 4.4a). It can be noted a singular exception within glacial MIS 10 interval at ~370 ka PB, which is characterised by a coarser silt mode comprised between 25 and 50 µm, and which interval was also associated with intermediate NPS relative abundance (60 to 70%).

In comparison to glacial intervals, interglacial MIS 11 exhibit a decrease in the relative abundance of the fine silt mode (down to ~3% of the total relative abundance), in favour of a coarser silt mode comprised between 20 and 30 µm (Fig. 4.3c; 4.4a; Table 4.2). A substantial reduction of the relative abundance of the clay content (down to 0.5 %) is observed, as well as of the coarse grains above 100 µm, with occasional and minor amount of coarse sand grains (>100 µm). MIS 9 and 7 exhibit a very similar grain-size distribution profile, dominated by more than 6 % by the coarse silt mode

between 30 and 45 μm. The fine silt mode represents less than 2 % of the total relative abundance and the presence of clays and sands above 100 μm represent a minor portion of the samples (Fig. 4.4a). Within MIS 5, only two samples bear a MIS 9/7-like grain-size distribution (with modes up to 50 and 60 μm) and are correlated with the NPS relative abundance minimum at ~121 ka BP.

An overall anti-correlation seems to arise between the main grain-size mode and the NPS relative abundance (Fig. 4.4b), with low NPS relative abundances corresponding to coarser silt modes. NPS relative abundances comprised above 45 % are associated to grain-size modes below 20 μm, only with exception of the 370 to 360 ka BP interval (Fig. 4.4b).

Core	Depth [m/bsf]	Age [ka BP]	Sedimentation rates [cm/ky]
1	0	2	9.92
1	0.85	10.53	14.74
1	1.8	17	24
1	3	22	22.5
1	3.45	24	22.5
***			
2	4.2	27	10.05
2	8.34	68.17	43.28
2	13.8	80.8	43.28
***			
3	13.5	104	15.91
3	17	126	10.15
3	18.18	137.63	15.81
3	19.25	144.4	18.79
3	23	164.33	18.79
***			
4	23.88	187.37	6.94
4	24.64	198.36	3.34
4	25.65	228.6	4.26
4	25.85	233.3	6.25
4	26.1	237.3	21.05
4	27.3	243	20.66
4	30.43	258.15	17.12
4	32.64	271.06	12.04
***			
5	33.37	309.88	6.77
5	34.23	322.7	10.34
5	35.44	334.39	7.01
5	36.54	350.01	17.88
5	41.9	380	17.88
***			
6	42.4	394.99	19
6	48.58	427.5	19
6	51.50	442.84	19

Table 4-1 DSDP Site 548 age model and associated interval sedimentation rates. Note the age model accounts for discontinuous junction between each hydraulic piston core.

4.5 Discussion

4.5.1 Framework and glacial termination pattern

The 51.5 m of analysed sequence are inferred to cover an age spanning from ~443 to 2 ka BP, in accordance with previously established geochronology (Vergnaud-Grazzini and Saliège, 1985b). From 440 to 100 ka BP, overall sedimentation rates are higher during glacial intervals (from 15 to 20 cm/ky) than interglacials (around or below 10 cm/ky). Those glacial versus interglacial sedimentation rates are similar in pattern and magnitude to that of the last climate cycle along Goban Spur (Auffret et al., 2002). The correlation existing between variation in the XRF Fe/Ca ratio, Ti_{norm} and light planktonic $\delta^{18}O$ values (Fig. 4.2) is fairly similar to patterns of core MD03-2692, which are shown to be mainly driven by north Atlantic climatic reorganizations over this period (Mojtahid et al., 2005). Within the northeast Atlantic, the XRF Ti_{norm} is mainly associated to the terrigenous input while the XRF Fe/Ca ratio provides a reliable terrigenous versus biogenic carbonate input proxy (Toucanne et al., 2009a; Hodell et al., 2013; Bahr et al., 2014). Thus glacial periods (MIS 12, 10, 8 and 6) are characterised by high terrigenous content and low biogenic carbonate content (high XRF Ti_{norm} and Fe/Ca ratio) relative to interglacial ones. This pattern is typical for the northeast Atlantic over the past million years and can be interpreted as increased terrigenous input associated to sedimentary system adjustments and primary productivity decrease during cold climatic events (Auffret et al., 2002; Mojtahid et al., 2005; Toucanne et al., 2009b).

Abrupt changes in the terrigenous content correlate to marked decrease in the NPS relative abundances at respectively 427, 332, 245 and 125 ka BP. Here, the NPS relative abundance reflects variations in the sea surface thermocline, associated to migration of sub-polar waters during climatic oscillations (Oppo et al., 1998; Desprat et al., 2006; Eynaud et al., 2007; 2009; Voelker et al., 2010; Vázquez Riveiros et al., 2013). The high NPS relative abundance can be thus interpreted to reflect the migration of the sub-polar front south of 48°N latitude. Abrupt decrease in NPS relative abundances are preceded by a large peak in coarse lithic grains (Fig. 4.3c). Goban Spur remained isolated from the influence of sediments drained through the Celtic and Irish margins, and thus changes in the coarse detritic sediment content reflect IRD input that are contemporaneous with major ice-sheets calving (Auffret et al., 1999; Zaragosi et al., 2001; Jullien et al., 2006; Eynaud et al., 2007; Toucanne et al., 2009b). IRD input followed by sea-surface temperature increase mark glacial terminations TV, TIV, TIII and TII, which are subsequently found synchronous to that of nearby ODP Site 980 (Oppo et al., 1998 2006; McManus et al., 1999; Vázquez Riveiros et al., 2013). Additionally, it can be noted that coarse lithic grains derived IRD peaks at ~430, 255 and 230 ka BP are also associated to marked MS peaks.

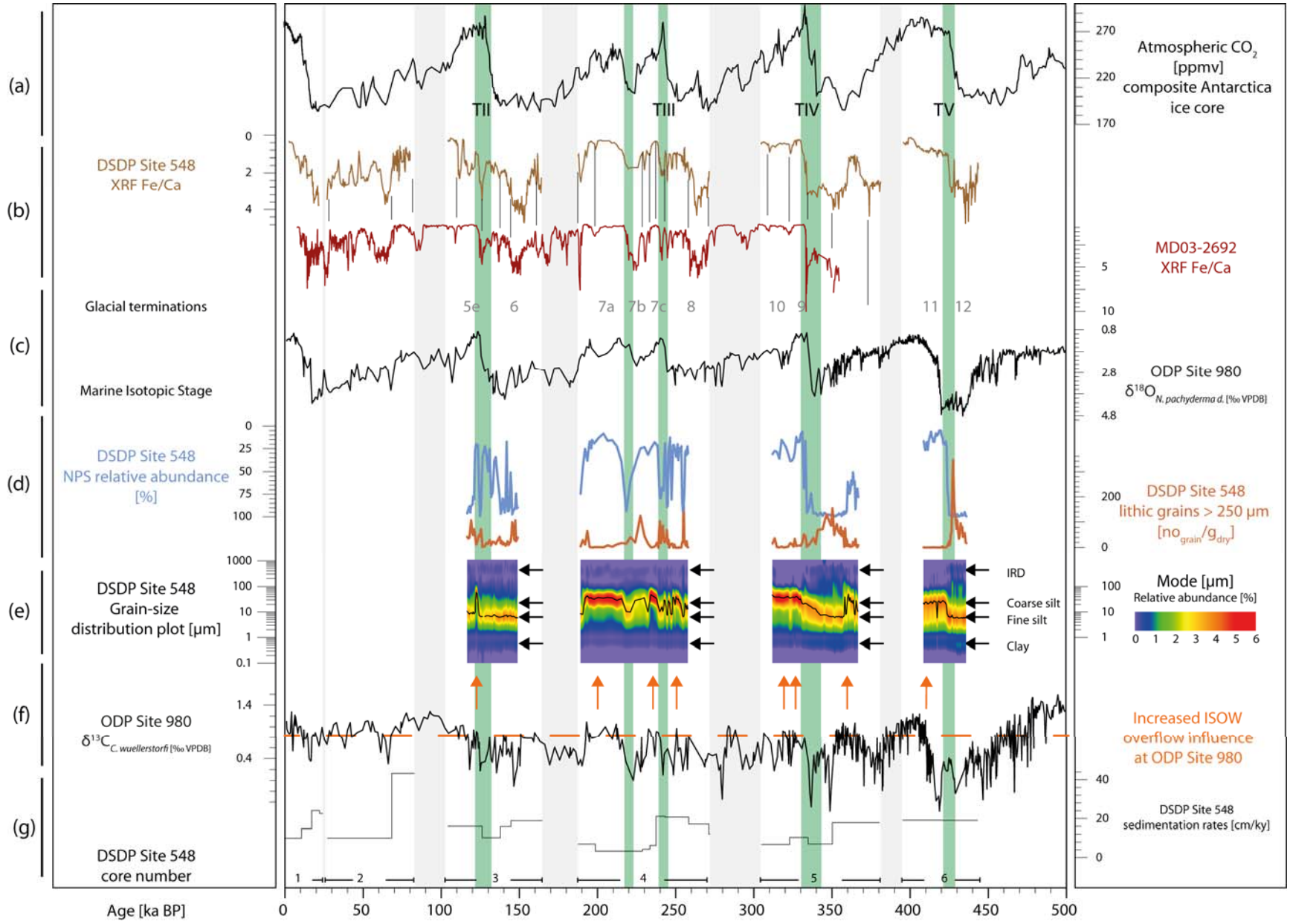
(a)
(b)
(c)
(d)
(e)
(f)
(g)
TII
TIII
TIV
TV
Glacial terminations
5e
6
7a
7b
7c
8
10
9
11
12
Marine Isotopic Stage
DSDP Site 548
XRF Fe/Ca
DSDP Site 548
NPS relative abundance
[%]
DSDP Site 548
Grain-size
distribution plot [µm]
ODP Site 980
δ13C C. wuellerstorfi [‰ VPDB]
DSDP Site 548
core number
Age [ka BP]
0
50
100
150
200
250
300
350
400
450
500
IRD
Coarse silt
Fine silt
Clay
Atmospheric CO2
[ppmv]
composite Antarctica
ice core
MD03-2692
XRF Fe/Ca
ODP Site 980
δ18O N. pachyderma d. [‰ VPDB]
DSDP Site 548
lithic grains > 250 µm
[no grain/g dry]
Mode [µm]
Relative abundance [%]
Increased ISOW
overflow influence
at ODP Site 980
DSDP Site 548
sedimentation rates [cm/ky]

Figure 4.3 DSDP Site 548 age model and palaeo-environmental data compilation over the past 500 ky. (a) EPICA Dome C and Vostok carbon dioxide concentration composite record (Petit et al., 1999; Monnin et al., 2001; Raynaud et al., 2005; Siegenthaler et al., 2005). (b) Correlation of XRF Fe/Ca signals between DSDP Site 548 and MD03-2692 (Mojtahid et al., 2005) for the past 360 ky. Tie points are indicated by the vertical black lines. Note that the age model for glacial termination TV was built using the ODP Site 980 reviewed age model from Vázquez Riveiros et al. (2013). (c) Planktonic N. pachyderma dextral $\delta^{18}O$ record from ODP Site 980 indicating sea surface conditions and respective Marine Isotopic Stages at this site (McManus et al., 1999). (d) DSDP Site 548 N. pachyderma sinistral to dextral relative abundance and coarse lithic grain counts above the 250 µm fraction. The green shaded areas correspond to studied terminations, defined as the offset between local lithic IRD peak and NPS % decrease. (e) Grain-size distribution plot and first mode. The black arrows indicate the identified grain-size classes. (f) Benthic Cibicides Wuellerstorfi $\delta^{13}C$ record from ODP Site 980. The orange arrows indicate increased $\delta^{13}C$ values, indicative for the increased influence of the Iceland-Scotland Ridge Overflow at this site (McManus et al., 1999). (g) DSDP Site 548 age model sedimentation rates. The grey shaded areas represent the interpreted missing periods between each hydraulic piston core.

The magnetic susceptibility (MS) can be used as a proxy for LIS, GIS and IIS ice sheets IRD discharge (Richter et al., 2001). On the other hand, background variations of the magnetic susceptibility (here ranging generally between 10 and 25 SI), can be related to the clay and silt content (Table 4.2). Likewise, MS variations may also be indicative for sedimentological input changes possibly associated with circulation changes (Kissel et al., 1997). Therefore MS signal is not an exclusive proxy for IRD content, and must be considered carefully when variations are associated with changes in the clay and silt content. Coarse lithic grains counts may account to IRD input sensus stricto, also representative for lower ferromagnetic grains rich sources (Richter et al., 2001; Eynaud et al., 2007). Thus, the coarse lithic grains peaks that are not associated to distinct MS peak, both within MIS 10 (~350 ka BB) and MIS 6 (~150 ka BP), may be mainly derived from a BIIS source. BIIS derived IRD layers are also documented within the northern Bay of Biscay, in particular during MIS 6 (Mojtahid et al., 2005; Eynaud et al., 2007).

Beyond changes that occurred during the penultimate glacial terminations, additional abrupt NPS relative abundance decreases, similarly preceded by coarse lithic grain peaks, are observed at approximately 255, 220 and 142 ka BP (Fig. 4.3c). These most probably represent millennial-scale, Dansgaard-Oeschger like oscillations, similar to oscillations typically documented along the Iberian margin (Martrat et al., 2007). The decrease in NPS between ~140 and 130 ka BP, thus preceding glacial termination TII, seemingly correlates with an Iberian margin interstadial warm event (Martrat et al., 2007). This warm precursor to glacial termination TII is also expressed by slightly lighter planktonic $\delta^{18}O$ values at ODP Site 980 over the same period (Fig. 4.3; Oppo et al., 2006).

Averaged interval properties	MIS 5	MIS 6	MIS 7	MIS 8	MIS 9	MIS 10	MIS 11	MIS 12	Interglacials	Glacials
Time interval [ka BP]	110 - 125	125 - 160	190 - 245	245 - 260	310 - 332	332 - 370	410 - 427	427 - 440		
MS [SI]	17	20	16	25	11	19	13	19	14	21
XRF Fe/Ca	1.55	2.69	1.1	1.35	0.51	2.48	1.2	2.88	1.09	2.35
XRF Ti_{norm}	0.02	0.024	0.018	0.021	0.013	0.026	0.021	0.029	0.018	0.025
NPS relative abundance [%]	69	69	41	38	27	86	28	98	41	84
Lithic grains > 250 µm [no_{grain}/g_{dry}]	49	29	29	16	13	46	5	100	24	48
First grain-size mode [µm]	16	6	25	21	36	15	21	6	24	12

Table 4-2 Averaged geophysical and geochemical properties for each interpreted Marine Isotopic Stage, along with NPS relative abundances, coarse lithic grain counts and first grain-size mode. Note glacial intervals consistently show higher XRF Fe/Ca and Ti normalised ratios, associated with lower first grain-size mode. Caution must be considered for averages values within intervals showing marked millennial scale modulation, in particular from MIS 8 to MIS 5.

4.5.2 Grain-size and local bottom current variability

Except coarse sands (> 100 µm) variations, which were previously interpreted as IRD inputs, the observed grain-size distributions are almost exclusively represented by shifts from fine to coarse silt modes (Figs. 4.3c; 4.4). Glacial MIS 12, 10 and 6 are characterised by the fine silt grain-size mode (below 10 µm) while interglacials are characterised by a coarser silt mode, briefly reaching up to 60 µm during MIS 5. Interglacial MIS 11 exhibits a somewhat mixed silt composition, with a main mode comprised between 20 to 30 µm, associated to a substantial fine silt relative abundance up to > 3% of the total grain-size distribution (Fig. 4.4a). In comparison, interglacials MIS 9 and 7c and 7a exhibit a better expressed coarse silt class at ~40 µm and clear decrease in the fine silt class below ~2 % of the relative abundance (Fig. 4.4a). During the cold phase of MIS 7b, the coarse silt mode is gradually less represented, and the fine silt mode gradually increases in terms of relative abundance, to dominate the sediment composition at ~220 ka BP. This pattern strongly suggests that coarsening occurred through winnowing of the fine silt fraction in favour of the coarser one, typically associated to bottom current processes (Hall and McCave, 1998; Stow and Faugères, 2008; Rebesco et al., 2014). Similar shifts in the silt mode are documented and used as a bottom current strength proxy within the northeastern Atlantic, specifically for the monitoring of the MOW flow variability (Voelker et al., 2006; Toucanne et al., 2007; Huvenne et al., 2009; Thierens et al., 2010; Hanebuth et al., 2015). Typical settling of fine (< 10 µm) silts particles dominates during periods of sluggish MOW while coarser (ranging from 20 to 60 µm) silty layers dominates periods of enhanced bottom currents (Voelker et al., 2006; Huvenne et al., 2009; Hanebuth et al., 2015). Thus the variations observed here are interpreted to primarily reflect changes in the bottom current regime (McCave and Hall, 2006).

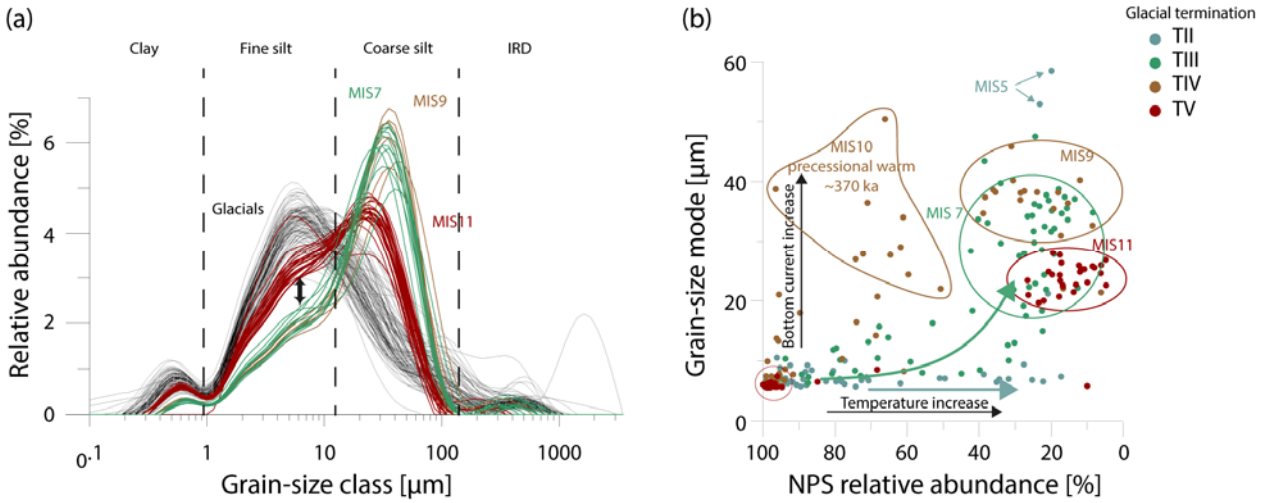

Figure 4.4 (a) Grain-size distribution for the main studied intervals with indication of the distinct grain-size classes. The arrows indicate the MIS 9 and 7a depletion in the fine silt class, relative to MIS 11. (b) Distribution plot of the main grain-size mode versus the N.pachyderma sinistral relative abundance (NPS %). Note the occurrence of two distinct modes throughout termination TV. All glacial intervals recorded a very similar main mode of ~7 µm while coarsening is observed as function of the NPS relative abundance. The arrows indicate coarsening trends, showing the NPS relative abundance increase precedes the main grain-size mode increase.

Changes in the silt mode related to MIS 11, 9 and 7c and 7a are stable and long lasting (i.e. up to tenth of thousand years) sensus Hanebuth et al. (2015). Recorded coarsening are at least equal (MIS 11) to more marked (other studied interglacials) to coarsening variations recorded within the northern Gulf of Cádiz from both Voelker et al. (2006) and Toucanne et al. (2007). Present day bottom currents in this region are associated with the MOW powerful overflow which may have regularly exceeded 40 cm/s at both sites (Hernández-Molina et al., 2011). At Goban Spur the MOW equilibrated within the ambient thermohaline circulation and mean contour current velocities barely reach 10 cm/s (Iorga and Lozier, 1999; Huthnance et al., 2001). Therefore contour current driven grain-size variation does not seem to provide a suitable driving mechanism for the coarsening trends observed. Slow thermohaline circulation also tend to rule out the possible existence of significant flow instabilities within the MOW lower interface that would be analogical to model of Hanebuth et al., 2015. Such stable, long lasting coarsening phases suggest differences with respect to the standard coarsening upward and fining upward contouritic sequence and tend to rule out intermittent processes (Toucanne et al., 2007; Mulder et al., 2013; Rebesco et al., 2014). Intermittent processes such as turbiditic flow, or possibly cascading would be expected to cause brief coarsening associated to a single or a series of events, and to regularly exhibit marked fining or coarsening upward trends (Bouma, 2000). The absence of an energetic contour current is not prone for the formation of energetic mesoscale eddies (Serra et al., 2005), and benthic storms or other oceanographic processes have never been documented in the area (Huthnance et al., 2001).

Nevertheless, the continuous nature of internal tides provides a suitable mechanism at the MOW lower interface (Gao et al., 1998). Those cause strong currents, typically ranging from 20 to 40 cm/s, interacting with the settling particles at semi-diurnal frequency (Gao et al., 1998; He et al., 2008; Hanebuth et al., 2015; Zhang et al., 2015). Internal tides are also known to dominate the present day bottom current regime, related to water mass stratification of the MOW and underlying LSW (Huthnance et al., 2001). Internal tidal driven resuspension events, associated with hydrodynamic sorting of the particles size was also directly observed at this site (Thomsen et al., 1998; 2000). The morphological expression of large scale sediment waves at Goban Spur was inferred to be dependent from the predictable reflection conditions in between the seabed and the internal tide regime (Delivet et al., 2016). Those conditions typically vary as a function of the slope gradient and the pycnal gradient related to the water mass stratification (Pomar et al., 2012; Shanmugam, 2013). During deposition of the studied interval, the local and regional bottom slope is unlikely to have changed (Delivet et al., 2016), and therefore, any change of bottom current regime can be interpreted in terms of water column stratification and local pycnal gradient change. Consequently, the settlement of fine silts during glacial periods can be interpreted to characterize more sluggish bottom currents, associated with (at least in the range of 1250 m water depths) a reduction of the pycnal gradient and water mass stratification. This strongly suggests that the formation of the large scale sediment waves described in Delivet et al. (2016) predominantly occurred during interglacial periods.

4.5.3 MOW variability along the northeast Atlantic margin

Here, interglacial periods all are characterised by a relatively high hydrodynamic regime, as indicated by the coarse silt mode. Within the northern Gulf of Cádiz, different studies evidenced those past recent interglacial periods might have been associated to relatively similar MOW circulation pattern (Rogerson et al., 2012; Bahr et al., 2015; Kaboth et al., 2016; Lofi et al., 2016). Within the Porcupine Seabight, the cold-water coral growth during interglacials of the past 500 ky has been related to the presence of the upper MOW, similar to the present MOW situation (Raddatz et al., 2014). Consequently, the coarse silt mode observed during MIS 11, 9, 7 and 5 can be interpreted to reflect the presence of MOW induced bottom currents, most probably similar to the present-day situation (Fig. 4.5a). Alternatively, the clear decrease in the grain-size silt mode during glacial periods is consistent with sluggish internal tide regime, indicative for a relatively well-mixed water column around 1250 m water depths. This suggests changes in the relative position of the MOW. Within the Porcupine Seabight, similar results suggested the deepening of the boundary layer between the MOW and ENACW during the last glacial interval (Rüggeberg et al., 2007; Van Rooij et

al., 2007b). Raddatz et al. (2014) suggested the MOW upper boundary has been located at least below the depth range of the Challenger cold-water coral mound, which is bathed by ~950 m (Li et al., 2011).

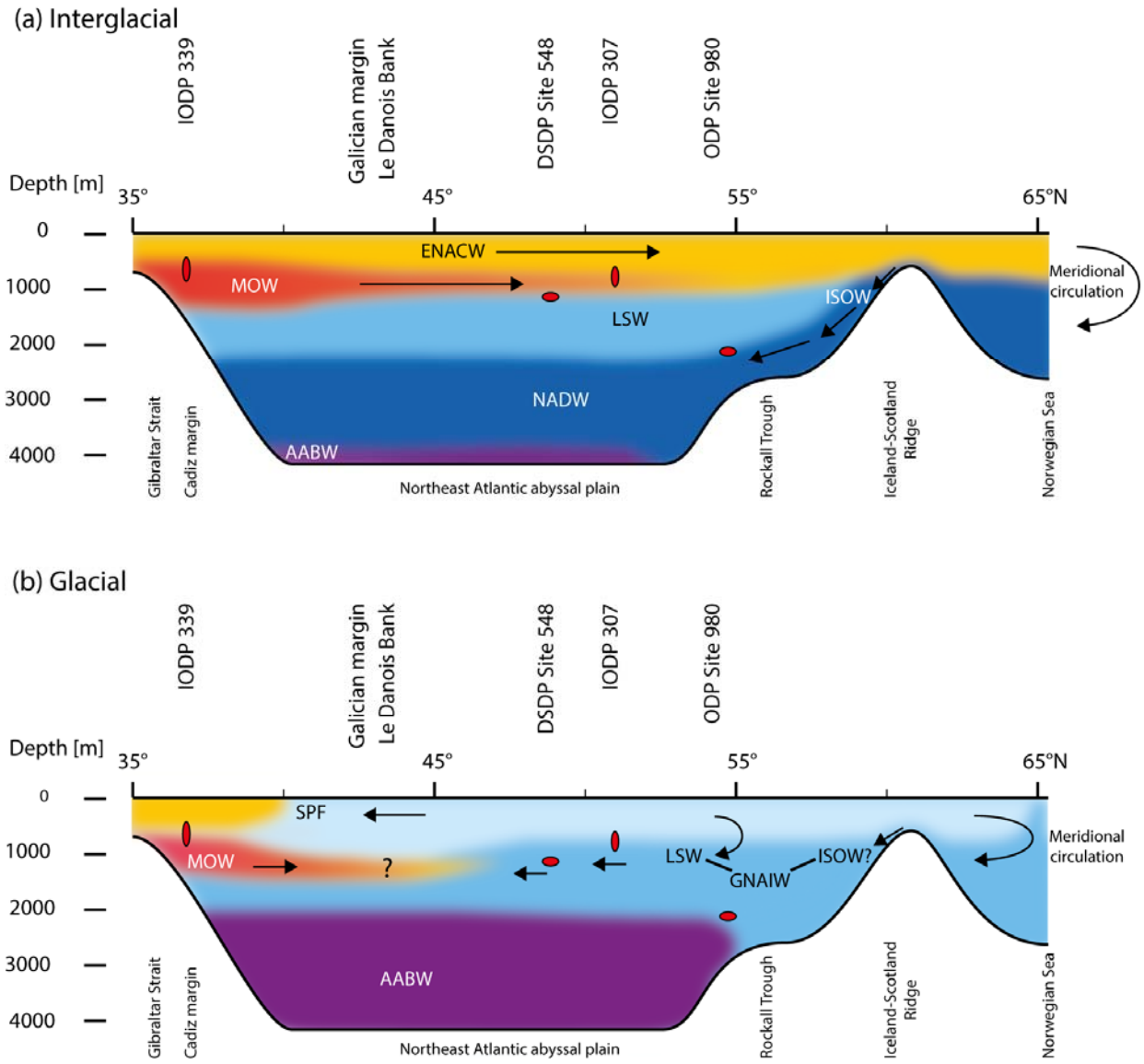

Figure 4.5 Schematic cross section of the northeast Atlantic basin. The red dots indicate the projected depth of the different drilling sites. (a) Sketch representing a modern-like circulation pattern during the studied interglacial periods. Note the shallow and enhanced northward advection of the MOW, and its lower interface affecting DSDP Site 548. (b) Sketch representing the hypothesized situation during glacial intervals, associated with a deeper MOW plume, confined south of 48°N. Note the settlement of the GNAIW, composed of water mass similar to the present day LSW and probable variable contribution of the ISOW and DSOW, and the incursion of the AABW below 2000 m water depth (McManus et al., 1999; Raymo et al., 2004; Lynch-Stieglitz et al., 2007; Bell et al., 2015; Bohm et al., 2015). The position of the sub-polar front (SPF) and sea-surface circulation along the Iberian margin is derived from (Eynaud et al., 2009; Voelker et al., 2010; Hodell et al., 2013; Maiorano et al., 2015). **ENACW**: Eastern North Atlantic Central Water; **MOW**: Mediterranean Outflow Water; **LSW**: Labrador Sea Water; **ISOW**: Iceland-Scotland Overflow Water; **NADW**: North Atlantic Deep Water; **AABW**: Antarctic Bottom Water; **GNAIW**: Glacial North Atlantic Intermediate Water.

The studied glacial periods were characterised by a global sea-level decrease which caused the shoaling of the Gibraltar sill, down to 200 m water depth (Waelbroeck et al., 2002; Rohling et al., 2014). This was associated with the cooling and the aridification of the climate over the Mediterranean Sea, leading to the formation of a denser MOW plume, settling at depths ranging from 1000 to 1400 m water depth (Rogerson et al., 2005). Despite the MOW flux was reduced by a factor of two, due to the drop of the sea-level at Gibraltar, the MOW density increase would be sufficient to form a density anomaly of at least 0.4 kg/m³ at Goban Spur latitudes (Rogerson et al., 2006; 2012). Studies carried out along the Galician margin corroborate a probable deepening of the MOW in the glacial Atlantic of about 300 to 600 m relative than today (Maestro et al., 2013; Hanebuth et al., 2015; Hernández-Molina et al., 2016a). Assuming the MOW advection roughly occurred along the same water depths from the Galician margin towards the Goban Spur, DSDP Site 548 would be influenced by a pycnal gradient similar to nowadays MOW upper boundary (Delivet et al., 2016). Such pycnal gradient would in fact be more important than the present day one, and would most probably be associated with more pronounced internal tide regime, and reflection conditions close to critical. Such conditions may be expected to lead to high bottom current intensities, which are not represented as inferred from the grain-size analysis. As a consequence, results obtained here strongly suggest that the MOW did not propagate as far north as Goban Spur during glacials of MIS 12, 10 and 6. This situation might be analogue to that of the last glacial periods, during which the MOW is thought to have remained confined south of 40°N (Schönfeld and Zahn, 2000). However, it can be noted the presence of complex and abrupt oscillations during MIS 8, which seems to be a periods of high sensitivity to Dansgaard-Oeschger like millennial scale variations within the northeast Atlantic Ocean (Fig. 4.3b, c; Martrat et al., 2007; Birner et al., 2016). A brief excursion towards coarse silt mode was also recorded around 360 ka BP. This suggests the MOW might have intermittently influenced DSDP site 548 during those last two periods.

The data clearly indicates that the rise in the grain-size mode systematically occurred after the decrease in the NPS relative abundance (Fig. 4.4b). This suggests the reintroduction of the MOW strictly postdate the incursion of sub-tropical sea-surface water at Goban Spur. During the Last Glacial Maximum, Schönfeld and Zahn (2000) suggested that the MOW low latitude confinement might have been caused and/or replaced by the introduction of the Glacial North Atlantic Intermediate Water (GNAIW). In the northeast Atlantic, GNAIW typically spread at water depths between 1500 and 2000 m water depth, while regular incursion of the AABW occurred below 2000 m (de Vernal et al., 2006; Marchitto and Broecker, 2006; Lynch-Stieglitz et al., 2007; Martrat et al., 2007; Thornalley et al., 2015). The absence of MOW at Goban Spur could be associated to changes in its flow regime and propagation mechanism, as for instance, higher MOW velocities could affect

the flow potential vorticity (Rhines and Holland, 1979; Cherubin et al., 2000). This could cause a less active MOW geostrophic branch, and increased propagation into the intermediate north Atlantic Ocean, as suggested for observed historical variations by Bozec et al. (2011). However, Bozec et al. (2011) argues that historical MOW propagation variations are driven by decadal North Atlantic Oscillation dynamics, rather than direct changes in the MOW properties. Similarly, Rogerson et al. (2012) argues that the MOW propagation and settlement is primarily driven by the circulation pattern, structure and density profile of the Atlantic, while changes in the MOW composition at the Strait of Gibraltar are by far secondary. This is partly explained by the fact the MOW encompasses a strong differentiation, in particular through North Atlantic Central Water entrainment within the northern Gulf of Cádiz, multiplying its volume by a factor 3 (Baringer and Price, 1997; 1999).

In order to investigate whether the replacement of the MOW by the GNAIW was a pervasive feature over the past 500 ky, the grain-size variation obtained at Goban Spur is compared to the benthic stable carbon isotope ($\delta^{13}C$) of ODP Site 980 (Fig. 4.3e). At that site, high benthic $\delta^{13}C$ values clearly indicate the formation of well-ventilated ISOW, most probably associated to the formation of dense, modern-like NADW, while low values indicate reduced NADW production and/or influence of the poorly ventilated AABW (McManus et al., 1999; Vázquez Riveiros et al., 2013). Here, the rise in the grain-size silt mode is observed to correlate with periods of high benthic $\delta^{13}C$ at ODP Site 980, while periods where benthic $\delta^{13}C$ are below ~0.8 ‰ are characterised by fine silts grain-size mode (Fig. 4.3d). Despite the GNAIW is formed by different contribution of the ISOW, DSOW and the Labrador open Sea convection, it seems there exists an important covariance between enhanced bottom currents at Goban Spur and the production of dense and ventilated ISOW at IODP Site 980. This suggests there might be a link, or at least a correlation, between the northward advection of the MOW at Goban Spur and the production of dense NADW. Alternatively, more sluggish bottom currents at Goban Spur, interpreted as reflecting a homogenous water column, may be explained by the presence of the GNAIW (Fig. 4.5), in accordance with scenario proposed by Schönfeld and Zahn (2000).

4.6 Conclusions

Sedimentological observations provided insight into the variability of the bottom current regime that dominated Goban Spur over some key intervals during the past 500 ky. Changes in the main grain-size mode, associated with deposition of fine (~8 to 10 μm) to coarse silts (coarser than 20 μm) indicate periods of a sluggish to enhanced bottom current regime, respectively. At this site, enhanced bottom currents are proposed to mainly reflect changes in the internal tidal regime, related to the water column stratification and the position of the MOW within the intermediate northeast Atlantic. Here, results confirm that the MOW did probably not propagate as far north of Goban Spur latitudes during glacial intervals related to MIS 12, 10 and 6. However, a more complex pattern was observed during MIS 8, possibly associated to an increased sensitivity to millennial scale variability which also affected the northward advection of the MOW. Reciprocally, interglacial periods related to MIS 11, 9, 7 and 5 showed evidences for enhanced bottom current regime, most probably indicating the presence of the MOW lower boundary, in a modern-like configuration. The results obtained here are in accordance with climatically modulated cold-water coral growth within the Porcupine Seabight, which was thus intermittently affected by processes occurring at the MOW upper boundary. The MOW re-introduction towards the Goban Spur and the Porcupine Seabight seems to have occurred only when optimal interglacial climatic conditions were restored. This may suggest that the northward advection of the MOW was conditioned by changes in the north Atlantic meridional circulation. The latitudinal variations in the northward advection of the MOW constitutes and important physical constrain on the MOW induced density anomaly within the intermediate glacial north Atlantic, that possibly have strong implications over the global climate. Therefore it seems important to better constrain those shifts, specifically at sites located along the Iberian margin, to assess the glacial MOW spatial influence.

Acknowledgments

The authors wish to express their sincere acknowledgements to Walter Hale, Alex Wülbers, and the technical staff from the IODP-BCR (Germany), for their advices, help, consideration and warm welcome. Sincere acknowledgements also to Fréderique Eynaud from the EPOC of the University of Bordeaux (France) for her correspondence and for providing the XRF dataset and age model of core MD03-2692.

References

Auffret, G.A., Bassinot, F., Dennielou, B., Ehrold, A., Grousset, F.E., Pujol, C., Zaragosi, S., 1999. IRD levels from the Celtic Margin, relation with Heinrich events, in: Friend, P., Kenyon, N.H. (Eds.), North-East Atlantic slope processes: multi-disciplinary approaches. S.O.C., Southampton, p. 15.

Auffret, G.A., Zaragosi, S., Dennielou, B., Cortijo, E., Van Rooij, D., Grousset, F.E., Pujol, C., Eynaud, F., Siegert, M., 2002. Terrigenous fluxes at the Celtic margin during the last glacial cycle. Marine Geology 188, 79-108.

Bahr, A., Jiménez-Espejo, F.J., Kolasinac, N., Grunert, P., Hernández-Molina, F.J., Röhl, U., Voelker, A.H.L., Escutia, C., Stow, D.A.V., Hodell, D., Alvarez-Zarikian, C.A., 2014. Deciphering bottom current velocity and paleoclimate signals from contourite deposits in the Gulf of Cádiz during the last 140 kyr: An inorganic geochemical approach. Geochemistry, Geophysics, Geosystems 15, 3145-3160.

Bahr, A., Kaboth, S., Jiménez-Espejo, F.J., Sierro, F.J., Voelker, A.H.L., Lourens, L., Röhl, U., Reichart, G.J., Escutia, C., Hernández-Molina, F.J., Pross, J., Friedrich, O., 2015. Persistent monsoonal forcing of Mediterranean Outflow Water dynamics during the late Pleistocene. Geology.

Baringer, M.O., Price, J.F., 1999. A review of the physical oceanography of the Mediterranean outflow. Marine Geology 155, 63-82.

Baringer, M.O.N., Price, J.F., 1997. Mixing and Spreading of the Mediterranean Outflow. Journal of Physical Oceanography 27, 1654-1677.

Bell, D.B., Jung, S.J.A., Kroon, D., 2015. The Plio-Pleistocene development of Atlantic deep-water circulation and its influence on climate trends. Quaternary Science Reviews 123, 265-282.

Bigg, G.R., Jickells, T.D., Liss, P.S., Osborn, T.J., 2003. The role of the oceans in climate. International Journal of Climatology 23, 1127-1159.

Birner, B., Hodell, D.A., Tzedakis, P.C., Skinner, L.C., 2016. Similar millennial climate variability on the Iberian margin during two early Pleistocene glacials and MIS 3. Paleoceanography 31, 203-217.

Bohm, E., Lippold, J., Gutjahr, M., Frank, M., Blaser, P., Antz, B., Fohlmeister, J., Frank, N., Andersen, M.B., Deininger, M., 2015. Strong and deep Atlantic meridional overturning circulation during the last glacial cycle. Nature 517, 73-76.

Bouma, A.H., 2000. Coarse-grained and fine-grained turbidite systems as end member models: applicability and dangers. Marine and Petroleum Geology 17, 137-143.

Bourillet, J.F., Zaragosi, S., Mulder, T., 2006. The French Atlantic margin and deep-sea submarine systems. Geo-Marine Letters 26, 311-315.

Bozec, A., Lozier, M.S., Chassignet, E.P., Halliwell, G.R., 2011. On the variability of the Mediterranean Outflow Water in the North Atlantic from 1948 to 2006. Journal of Geophysical Research-Oceans 116.

Cacchione, D.A., Pratson, L.F., Ogston, A.S., 2002. The Shaping of Continental Slopes by Internal Tides. Science 296, 724-727.

Caralp, M.H., Pujol, C., Duprat, J., Labracherie, M., 1985. Quaternaty paleoceanography of the northeastern Atlantic: microfaunal and stable isotope evidence at sites 548 and 549, in: de Graciansky, P.C., Poag, C.W., Cunningham, R., Loubere, P., Masson, D.G., Mazzullo, J.M., Montadert, L., Müller, C., Otsuka, K., Reynolds, L.A., Sigal, J., Snyder, S.W., Vaos, S.P., Waples, D. (Eds.), Initial Reports of the Deep Sea Drilling Project. U.S. Government Printing Office, Washington, pp. 817-820.

Darling, K.F., Kucera, M., Kroon, D., Wade, C.M., 2006. A resolution for the coiling direction paradox in Neogloboquadrina pachyderma. Paleoceanography 21.

Cherubin, L., Carton, X., Paillet, J., Morel, Y., Serpette, A., 2000. Instability of the Mediterranean Water undercurrents southwest of Portugal: effects of baroclinicity and of topography. Oceanologica Acta 23, 551-573.

de Graciansky, P.C., Poag, C.W., Cunningham, R., Loubere, P., Masson, D.G., Mazzullo, J.M., Montadert, L., Müller, C., Otsuka, K., Reynolds, L.A., Sigal, J., Snyder, S.W., Vaos, S.P., Waples, D., 1985. Site 548, in: de Graciansky, P.C., Poag, C.W., Cunningham, R., Loubere, P., Masson, D.G., Mazzullo, J.M., Montadert, L.,

Müller, C., Otsuka, K., Reynolds, L.A., Sigal, J., Snyder, S.W., Vaos, S.P., Waples, D. (Eds.), Initial Reports of the Deep Sea Drilling Project. U.S. Government Printing Office, Washington, pp. 33-122.

De Mol, B., Van Rensbergen, P., Pillen, S., Van Herreweghe, K., Van Rooij, D., McDonnell, A., Huvenne, V., Ivanov, M., Swennen, R., Henriet, J.-P., 2002. Large deep-water coral banks in the Porcupine Basin, southwest of Ireland. Marine Geology 188, 193-231.

de Vernal, A., Rosell-Melé, A., Kucera, M., Hillaire-Marcel, C., Eynaud, F., Weinelt, M., Dokken, T., Kageyama, M., 2006. Comparing proxies for the reconstruction of LGM sea-surface conditions in the northern North Atlantic. Quaternary Science Reviews 25, 2820-2834.

Delivet, S., Van Eetvelt, B., Monteys, X., Ribó, M., Van Rooij, D., 2016. Seismic geomorphological reconstructions of Plio-Pleistocene bottom current variability at Goban Spur. Marine Geology 378, 261-275.

Desprat, S., Sánchez Goñi, M.F., Turon, J.-L., Duprat, J., Malaizé, B., Peypouquet, J.-P., 2006. Climatic variability of Marine Isotope Stage 7: direct land–sea–ice correlation from a multiproxy analysis of a north-western Iberian margin deep-sea core. Quaternary Science Reviews 25, 1010-1026.

Dingle, R.V., Scrutton, R.A., 1979. Sedimentary succession and tectonic history of a marginal plateau (Goban Spur, Southwest of Ireland). Marine Geology 33, 45-69.

Dorschel, B., Hebbeln, D., Rüggeberg, A., Dullo, C., Freiwald, A., 2005. Growth and erosion of a cold-water coral covered carbonate mound in the Northeast Atlantic during the Late Pleistocene and Holocene. Earth and Planetary Science Letters 233, 33-44.

Dorschel, B., Hebbeln, D., Foubert, A., White, M., Wheeler, A.J., 2007. Hydrodynamics and cold-water coral facies distribution related to recent sedimentary processes at Galway Mound west of Ireland. Marine Geology 244, 184-195.

Ercilla, G., Casas, D., Estrada, F., Vázquez, J.T., Iglesias, J., García, M., Gómez, M., Acosta, J., Gallart, J., Maestro-González, A., 2008. Morphosedimentary features and recent depositional architectural model of the Cantabrian continental margin. Marine Geology 247, 61-83.

Eynaud, F., Zaragosi, S., Scourse, J.D., Mojtahid, M., Bourillet, J.F., Hall, I.R., Penaud, A., Locascio, M., Reijonen, A., 2007. Deglacial laminated facies on the NW European continental margin: The hydrographic significance of British-Irish Ice Sheet deglaciation and Fleuve Manche paleoriver discharges. Geochemistry, Geophysics, Geosystems 8.

Eynaud, F., de Abreu, L., Voelker, A., Schönfeld, J., Salgueiro, E., Turon, J.-L., Penaud, A., Toucanne, S., Naughton, F., Sánchez Goñi, M.F., Malaizé, B., Cacho, I., 2009. Position of the Polar Front along the western Iberian margin during key cold episodes of the last 45 ka. Geochemistry, Geophysics, Geosystems 10.

Foubert, A., Van Rooij, D., Blamart, D., Henriet, J.-P., 2007. X-ray imagery and physical core logging as a proxy of the content sediment cores in cold-water coral mound provinces: a case study from Porcupine Seabight, SW of Ireland. International Journal of Earth Sciences 96, 141-158.

Frank, N., Freiwald, A., Lopez-Correa, M., Wienberg, C., Eisele, M., Hebbeln, D., Van Rooij, D., Henriet, J.-P., Colin, C., Van Weering, T., de Haas, H., Buhl-Mortensen, P., Roberts, J.M., De Mol, B., Douville, E., Blamart, D., Hatte, C., 2011. Northeastern Atlantic cold-water coral reefs and climate. Geology 39, 743-746.

Gao, Z.Z., Eriksson, K.A., He, Y.B., Luo, S.S., Guo, J.H., 1998. Deep-Water Traction Current Deposits - A Study of Internal Tides, Internal Waves, Contour Currents and Their Deposits. Science Press, Beijing.

González-Pola, C., Díaz del Río, G., Ruiz-Villarreal, M., Sánchez, R.F., Mohn, C., 2012. Circulation patterns at Le Danois Bank, an elongated shelf-adjacent seamount in the Bay of Biscay. Deep Sea Research Part I: Oceanographic Research Papers 60, 7-21.

Hall, I.R., McCave, I.N., 1998. Late Glacial to Recent accumulation fluxes of sediments at the shelf edge and slope of NW Europe, 48-50°N, in: Stoker, M.S., Evans, C.D.R., Cramp, A. (Eds.), Geological Processes on Continental Margins: Sedimentation, Mass-Wasting and Stability. Geological Society, London, pp. 339-350.

Hanebuth, T.J.J., Zhang, W., Hofmann, A.L., Löwemark, L.A., Schwenk, T., 2015. Oceanic density fronts steering bottom-current induced sedimentation deduced from a 50 ka contourite-drift record and numerical modeling (off NW Spain). Quaternary Science Reviews 112, 207-225.

He, Y., Gao, Z., Luo, J., Luo, S., Liu, X., 2008. Characteristics of internal-wave and internal-tide deposits and their hydrocarbon potential. Petroleum Science 5, 37-44.

Hebbeln, D., Van Rooij, D., Wienberg, C., 2016. Good neighbours shaped by vigorous currents: Cold-water coral mounds and contourites in the North Atlantic. Marine Geology 378, 171-185.

Heinrich, H., 1988. Origin and Consequences of Cyclic Ice Rafting in the Northeast Atlantic Ocean during the Past 130,000 Years. Quaternary Research 29, 142-152.

Hernández-Molina, F.J., Serra, N., Stow, D., Llave, E., Ercilla, G., Van Rooij, D., 2011. Along-slope oceanographic processes and sedimentary products around the Iberian margin. Geo-Marine Letters, 1-27.

Hernández-Molina, F.J., Stow, D.A.V., Alvarez-Zarikian, C.A., Acton, G., Bahr, A., Balestra, B., Ducassou, E., Flood, R., Flores, J.-A., Furota, S., Grunert, P., Hodell, D., Jimenez-Espejo, F., Kim, J.K., Krissek, L., Kuroda, J., Li, B., Llave, E., Lofi, J., Lourens, L., Miller, M., Nanayama, F., Nishida, N., Richter, C., Roque, C., Pereira, H., Sanchez Goñi, M.F., Sierro, F.J., Singh, A.D., Sloss, C., Takashimizu, Y., Tzanova, A., Voelker, A., Williams, T., Xuan, C., 2014. Onset of Mediterranean outflow into the North Atlantic. Science 344, 1244-1250.

Hernández-Molina, F.J., Sierro, F.J., Llave, E., Roque, C., Stow, D.A.V., Williams, T., Lofi, J., Van der Schee, M., Arnáiz, A., Ledesma, S., Rosales, C., Rodríguez-Tovar, F.J., Pardo-Igúzquiza, E., Brackenridge, R.E., 2016b. Evolution of the gulf of Cadiz margin and southwest Portugal contourite depositional system: Tectonic, sedimentary and paleoceanographic implications from IODP expedition 339. Marine Geology 377, 7-39.

Hernández-Molina, F.J., Wåhlin, A., Bruno, M., Ercilla, G., Llave, E., Serra, N., Rosón, G., Puig, P., Rebesco, M., Van Rooij, D., Roque, D., González-Pola, C., Sánchez, F., Gómez, M., Preu, B., Schwenk, T., Hanebuth, T.J.J., Sánchez Leal, R.F., García-Lafuente, J., Brackenridge, R.E., Juan, C., Stow, D.A.V., Sánchez-González, J.M., 2016a. Oceanographic processes and morphosedimentary products along the Iberian margins: A new multidisciplinary approach. Marine Geology 378, 127-156.

Hernandez-Molina, J., Llave, E., Somoza, L., Fernandez-Puga, M.C., Maestro, A., Leon, R., Medialdea, T., Barnolas, A., Garcia, M., del Rio, V.D., Fernandez-Salas, L.M., Vazquez, J.T., Lobo, F., Dias, J.M.A., Rodero, J., Gardner, J., 2003. Looking for clues to paleoceanographic imprints: A diagnosis of the Gulf of Cadiz contourite depositional systems. Geology 31, 19-22.

Hodell, D., Crowhurst, S., Skinner, L., Tzedakis, P.C., Margari, V., Channell, J.E.T., Kamenov, G., Maclachlan, S., Rothwell, G., 2013. Response of Iberian Margin sediments to orbital and suborbital forcing over the past 420 ka. Paleoceanography 28, 185-199.

Huthnance, J.M., Coelho, H., Griffiths, C.R., Knight, P.J., Rees, A.P., Sinha, B., Vangriesheim, A., White, M., Chatwin, P.G., 2001. Physical structures, advection and mixing in the region of Goban spur. Deep-Sea Research II 48, 2979-3021.

Huvenne, V.A.I., Bailey, W.R., Shannon, P.M., Naeth, J., di Primio, R., Henriet, J.-P., Horsfield, B., de Haas, H., Wheeler, A.J., Olu-Le Roy, K., 2007. The Magellan mound province in the Porcupine Basin. International Journal of Earth Sciences 96, 85-101.

Huvenne, V.A.I., Van Rooij, D., De Mol, B., Thierens, M., O'Donnell, R., Foubert, A., 2009. Sediment dynamics and palaeo-environmental context at key stages in the Challenger cold-water coral mound formation: Clues from sediment deposits at the mound base. Deep Sea Research Part I: Oceanographic Research Papers 56, 2263-2280.

Imbrie, J., Hays, J.D., Martinson, D.G., McIntyre, A., Mix, A.C., Morley, J.J., Pisias, N.G., Prell, W.L., Shackleton, N.J., 1984. The orbital theory of Pleistocene climate: support from a revised chronology of the marine d18O record, in: Berger, A., Imbrie, J., Hays, J.D., Kukla, G., Saltzman, B. (Eds.), Milankovitch and Climate. D. Reidel Publishing Company, Hingam, pp. 269-305.

Iorga, M.C., Lozier, M.S., 1999. Signatures of the Mediterranean outflow from a North Atlantic climatology 1. Salinity and density fields. Journal of Geophysical Research-Oceans 104, 25985-26009.

Jullien, E., Grousset, F.E., Hemming, S.R., Peck, V.L., Hall, I.R., Jeantet, C., Billy, I., 2006. Contrasting conditions preceding MIS3 and MIS2 Heinrich events. Global and Planetary Change 54, 225-238.

Kaboth, S., Bahr, A., Reichart, G.-J., Jacobs, B., Lourens, L.J., 2016. New insights into upper MOW variability over the last 150kyr from IODP 339 Site U1386 in the Gulf of Cadiz. Marine Geology 377, 136-145.

Kano, A., Ferdelman, T.G., Williams, T., Henriet, J.P., Ishikawa, T., Kawagoe, N., Takashima, C., Kakizaki, Y., Abe, K., Sakai, S., Browning, E., Li, X., the IODP Expedition 307 Scientists, 2007. Age constraints on the origin and growth history of a deep-water coral mound in northeast Atlantic drilled during Integrated Ocean Drilling Program Expedition 307. Geology 35, 1051-1054.

Khélifi, N., Sarnthein, M., Andersen, N., Blanz, T., Frank, M., Garbe-Schonberg, D., Haley, B.A., Stumpf, R., Weinelt, M., 2009. A major and long-term Pliocene intensification of the Mediterranean outflow, 3.5-3.3 Ma ago. Geology 37, 811-814.

Khélifi, N., Sarnthein, M., Frank, M., Andersen, N., Garbe-Schönberg, D., 2014. Late Pliocene variations of the Mediterranean outflow. Marine Geology 357, 182-194.

Kipp, N.G., 1976. New Transfer Function for Estimating Past Sea-Surface Conditions from Sea-Bed Distribution of Planktonic Foraminiferal Assemblages in the North Atlantic. Geological Society of America Memoirs 145, 3-42.

Kissel, C., Laj, C., Lehman, B., Labeyrie, L., Bout-Roumazeilles, V., 1997. Changes in the strength of the Iceland-Scotland Overflow Water in the last 200,000 years: Evidence from magnetic anisotropy analysis of core SU90-33. Earth and Planetary Science Letters 152, 25-36.

Kuhlbrodt, T., Griesel, A., Montoya, M., Levermann, A., Hofmann, M., Rahmstorf, S., 2007. On the driving processes of the Atlantic meridional overturning circulation. Reviews of Geophysics 45.

Kucera, M., Weinelt, M., Kiefer, T., Pflaumann, U., Hayes, A., Weinelt, M., Chen, M.-T., Mix, A.C., Barrows, T.T., Cortijo, E., Duprat, J., Juggins, S., Waelbroeck, C., 2005. Reconstruction of sea-surface temperatures from assemblages of planktonic foraminifera: multi-technique approach based on geographically constrained calibration data sets and its application to glacial Atlantic and Pacific Oceans. Quaternary Science Reviews 24, 951-998.

Lamb, K.G., 2014. Internal Wave Breaking and Dissipation Mechanisms on the Continental Slope/Shelf. Annual Review of Fluid Mechanics 46, 231-254.

Lee, A., Ellett, D., 1965. On the contribution of overflow water from the Norwegian Sea to the hydrographic structure of the North Atlantic Ocean. Deep Sea Research and Oceanographic Abstracts 12, 129-142.

Legg, S., Ezer, T., Jackson, L., Briegleb, B., Danabasoglu, G., Large, W., Wu, W., Chang, Y., Özgökmen, T.M., Peters, H., Xu, X., Chassignet, E.P., Gordon, A.L., Griffies, S., Hallberg, R., Price, J., Riemenschneider, U., Yang, J., 2009. Improving Oceanic Overflow Representation in Climate Models: The Gravity Current Entrainment Climate Process Team. Bulletin of the American Meteorological Society 90, 657-670.

Li, X., Takashima, C., Kano, A., Sakai, S., Chen, Y., Xu, B., Iodp Expedition, S., 2011. Pleistocene geochemical stratigraphy of the borehole 1317E (IODP Expedition 307) in Porcupine Seabight, SW of Ireland: applications to palaeoceanography and palaeoclimate of the coral mound development. Journal of Quaternary Science 26, 178-189.

Lisiecki, L.E., Raymo, M.E., 2007. Plio-Pleistocene climate evolution: trends and transitions in glacial cycle dynamics. Quaternary Science Reviews 26, 56-69.

Lofi, J., Voelker, A.H.L., Ducassou, E., Hernández-Molina, F.J., Sierro, F.J., Bahr, A., Galvani, A., Lourens, L.J., Pardo-Igúzquiza, E., Pezard, P., Rodríguez-Tovar, F.J., Williams, T., 2016. Quaternary chronostratigraphic framework and sedimentary processes for the Gulf of Cadiz and Portuguese Contourite Depositional Systems derived from Natural Gamma Ray records. Marine Geology 377, 40-57.

Louvel, V., Dyment, J., Sibuet, J.-C., 1997. Thinning of the Goban Spur continental margin and formation of early oceanic crust: constraints from forward modelling and inversion of marine magnetic anomalies. Geophysical Journal International 128, 188-196.

Lozier, M.S., Nicole, M.S., 2008. On the Temporally Varying Northward Penetration of Mediterranean Overflow Water and Eastward Penetration of Labrador Sea Water. Journal of Physical Oceanography 38, 2097-2103.

Lynch-Stieglitz, J., Adkins, J.F., Curry, W.B., Dokken, T., Hall, I.R., Herguera, J.C., Hirschi, J.J.M., Ivanova, E.V., Kissel, C., Marchal, O., Marchitto, T.M., McCave, I.N., McManus, J.F., Mulitza, S., Ninnemann, U., Peeters, F., Yu, E.-F., Zahn, R., 2007. Atlantic Meridional Overturning Circulation During the Last Glacial Maximum. Science 316, 66-69.

Maestro, A., López-Martínez, J., Llave, E., Bohoyo, F., Acosta, J., Hernández-Molina, F.J., Muñoz, A., Jané, G., 2013. Geomorphology of the Iberian Continental Margin. Geomorphology 196, 13-35.

Maiorano, P., Marino, M., Balestra, B., Flores, J.A., Hodell, D.A., Rodrigues, T., 2015. Coccolithophore variability from the Shackleton Site (IODP Site U1385) through MIS 16-10. Global and Planetary Change 133, 35-48.

Marchitto, T.M., Broecker, W.S., 2006. Deep water mass geometry in the glacial Atlantic Ocean: A review of constraints from the paleonutrient proxy Cd/Ca. Geochemistry, Geophysics, Geosystems 7.

Martinson, D.G., Pisias, N.G., Hays, J.D., Imbrie, J., Moore, T.C., Shackleton, N.J., 1987. Age dating and the Orbital Theory of the Ice Ages: Development of a High-Resolution 0 to 300,000-Year Chronostratigraphy. Quaternary Research 27, 1-29.

Martrat, B., Grimalt, J.O., Shackleton, N.J., de Abreu, L., Hutterli, M.A., Stocker, T.F., 2007. Four Climate Cycles of Recurring Deep and Surface Water Destabilizations on the Iberian Margin. Science 317, 502-507.

Mauritzen, C., Morel, Y., Paillet, J., 2001. On the influence of Mediterranean Water on the Central Waters of the North Atlantic Ocean. Deep Sea Research Part I: Oceanographic Research Papers 48, 347-381.

McCartney, M.S., Mauritzen, C., 2001. On the origin of the warm inflow to the Nordic Seas. Progress In Oceanography 51, 125-214.

Schloesser, F., Furue, R., McCreary Jr, J.P., Timmermann, A., 2012. Dynamics of the Atlantic meridional overturning circulation. Part 1: Buoyancy-forced response. Progress In Oceanography 101, 33-62.

McCave, I.N., Manighetti, B., Robinson, S.G., 1995. Sortable silt and fine sediment size/composition slicing: Parameters for palaeocurrent speed and palaeoceanography. Paleoceanography 10, 593-610.

McCave, I.N., Hall, I.R., 2006. Size sorting in marine muds: Processes, pitfalls, and prospects for paleoflow-speed proxies, Geochemistry Geophysics Geosystems.

McManus, J.F., Oppo, D.W., Cullen, J.L., 1999. A 0.5-Million-Year Record of Millennial-Scale Climate Variability in the North Atlantic. Science 283, 971-975.

McManus, J.F., Francois, R., Gherardi, J.M., Keigwin, L.D., Brown-Leger, S., 2004. Collapse and rapid resumption of Atlantic meridional circulation linked to deglacial climate changes. Nature 428, 834-837.

Mohn, C., Rengstorf, A., White, M., Duineveld, G., Mienis, F., Soetaert, K., Grehan, A., 2014. Linking benthic hydrodynamics and cold-water coral occurrences: A high-resolution model study at three cold-water coral provinces in the NE Atlantic. Progress In Oceanography 122, 92-104.

Mojtahid, M., Eynaud, F., Zaragosi, S., Scourse, J.D., Bourillet, J.F., Garlan, T., 2005. Palaeoclimatology and palaeohydrography of the glacial stages on Celtic and Armorican margins over the last 360000 yrs. Marine Geology 224, 57-82.

Monnin, E., Indermühle, A., Dällenbach, A., Flückiger, J., Stauffer, B., Stocker, T.F., Raynaud, D., Barnola, J.-M., 2001. Atmospheric CO₂ Concentrations over the Last Glacial Termination. Science 291, 112-114.

Mulder, T., Hassan, R., Ducassou, E., Zaragosi, S., Gonthier, E., Hanquiez, V., Marchès, E., Toucanne, S., 2013. Contourites in the Gulf of Cadiz: a cautionary note on potentially ambiguous indicators of bottom current velocity. Geo-Marine Letters 33, 357-367.

Naafs, B.D.A., Hefter, J., Stein, R., 2013. Millennial-scale ice rafting events and Hudson Strait Heinrich(-like) Events during the late Pliocene and Pleistocene: a review. Quaternary Science Reviews 80, 1-28.

Naylor, D., Shannon, P.M., 1982. The Geology of Offshore Ireland and West Britain. Graham & Trotman ltd., London.

Oppo, D.W., McManus, J.F., Cullen, J.L., 1998. Abrupt Climate Events 500,000 to 340,000 Years Ago: Evidence from Subpolar North Atlantic Sediments. Science 279, 1335-1338.

Oppo, D.W., McManus, J.F., Cullen, J.L., 2006. Evolution and demise of the Last Interglacial warmth in the subpolar North Atlantic. Quaternary Science Reviews 25, 3268-3277.

Paillard, D., Labeyrie, L., Yiou, P., 1996. Macintosh Program performs time-series analysis. Eos, Transactions American Geophysical Union 77, 379-379.

Paillet, J., Mercier, H., 1997. An inverse model of the eastern North Atlantic general circulation and thermocline ventilation. Deep-Sea Research Part I-Oceanographic Research Papers 44, 1293-1328.

Paillet, J., Arhan, M., McCartney, M.S., 1998. Spreading of Labrador Sea Water in the eastern North Atlantic. Journal of Geophysical Research-Oceans 103, 10223-10239.

Petit, J.R., Jouzel, J., Raynaud, D., Barkov, N.I., Barnola, J.M., Basile, I., Bender, M., Chappellaz, J., Davis, M., Delaygue, G., Delmotte, M., Kotlyakov, V.M., Legrand, M., Lipenkov, V.Y., Lorius, C., Pepin, L., Ritz, C., Saltzman, E., Stievenard, M., 1999. Climate and atmospheric history of the past 420,000 years from the Vostok ice core, Antarctica. Nature 399, 429-436.

Pingree, R.D., Le Cann, B., 1990. Structure, strength and seasonality of the slope currents in the Bay of Biscay region. Journal of the Marine Biological Association of the United Kingdom 70, 857-885.

Pingree, R.D., Le Cann, B., 1992. Three anticyclonic Slope Water Oceanic eDDIES (SWODDIES) in the southern Bay of Biscay in 1990. Deep-Sea Research 39, 1147-1176.

Pomar, L., Morsilli, M., Hallock, P., Bádenas, B., 2012. Internal waves, an under-explored source of turbulence events in the sedimentary record. Earth-Science Reviews 111, 56-81.

Raddatz, J., Rüggeberg, A., Margreth, S., Dullo, W.-C., 2011. Paleoenvironmental reconstruction of Challenger Mound initiation in the Porcupine Seabight, NE Atlantic. Marine Geology 282, 79-90.

Raddatz, J., Rüggeberg, A., Liebetrau, V., Foubert, A., Hathorne, E.C., Fietzke, J., Eisenhauer, A., Dullo, W.-C., 2014. Environmental boundary conditions of cold-water coral mound growth over the last 3 million years in the Porcupine Seabight, Northeast Atlantic. Deep Sea Research Part II: Topical Studies in Oceanography 99, 227-236.

Raymo, M.E., Oppo, D.W., Flower, B.P., Hodell, D.A., McManus, J.F., Venz, K.A., Kleiven, K.F., McIntyre, K., 2004. Stability of North Atlantic water masses in face of pronounced climate variability during the Pleistocene. Paleoceanography 19, PA2008.

Raynaud, D., Barnola, J.-M., Souchez, R., Lorrain, R., Petit, J.-R., Duval, P., Lipenkov, V.Y., 2005. Palaeoclimatology: The record for marine isotopic stage 11. Nature 436, 39-40.

Read, J.F., 2001. CONVEX-91: water masses and circulation of the Northeast Atlantic subpolar gyre. Progress In Oceanography 48, 461-510.

Rebesco, M., Hernández-Molina, F.J., Van Rooij, D., Wåhlin, A., 2014. Contourites and associated sediments controlled by deep-water circulation processes: State-of-the-art and future considerations. Marine Geology 352, 111-154.

Ribó, M., Puig, P., Muñoz, A., Lo Iacono, C., Masqué, P., Palanques, A., Acosta, J., Guillén, J., Gómez Ballesteros, M., 2016. Morphobathymetric analysis of the large fine-grained sediment waves over the Gulf of Valencia continental slope (NW Mediterranean). Geomorphology 253, 22-37.

Rice, A.L., Thurston, M.H., New, A.L., 1990. Dense aggregations of a hexactinellid sponge, Pheromena carpenteri, in the Porcupine Seabight (northeast Atlantic Ocean), and possible causes. Progress In Oceanography 24, 179-196.

Rhines, P.B., Holland, W.R., 1979. A theoretical discussion of eddy-driven mean flows. Dynamics of Atmospheres and Oceans 3, 289-325.

Richter, T.O., Lassen, S., van Weering, T.C.E., de Haas, H., 2001. Magnetic susceptibility patterns and provenance of ice-rafted material at Feni Drift, Rockall Trough: implications for the history of the British-Irish ice sheet. Marine Geology 173, 37-54.

Richter, T.O., van der Gaast, S., Koster, B., Vaars, A., Gieles, R., de Stigter, H.C., De Haas, H., van Weering, T.C.E., 2006. The Avaatech XRF Core Scanner: technical description and applications to NE Atlantic sediments, in: Rothwell, R.G. (Ed.), New techniques in Sediment Core Analysis. Geological Society, London, pp. 39-50.

Rogerson, M., Rohling, E.J., Weaver, P.P.E., Murray, J.W., 2005. Glacial to interglacial changes in the settling depth of the Mediterranean Outflow plume. Paleoceanography 20.

Rogerson, M., Rohling, E.J., Weaver, P.P.E., 2006. Promotion of meridional overturning by Mediterranean-derived salt during the last deglaciation. Paleoceanography 21, n/a-n/a.

Rogerson, M., Rohling, E.J., Bigg, G.R., Ramirez, J., 2012. Paleoceanography of the Atlantic-Mediterranean exchange: Overview and first quantitative assessment of climatic forcing. Reviews of Geophysics 50, RG2003.

Rohling, E.J., Foster, G.L., Grant, K.M., Marino, G., Roberts, A.P., Tamisiea, M.E., Williams, F., 2014. Sea-level and deep-sea-temperature variability over the past 5.3 million years. Nature 508, 477-482.

Ruddiman, W.F., 1977. Late Quaternary deposition of ice-rafted sand in the subpolar North Atlantic (lat 40° to 65°N). Geological Society of America Bulletin 88, 1813-1827.

Rüggeberg, A., Dullo, C., Dorschel, B., Hebbeln, D., 2007. Environmental changes and growth history of a cold-water carbonate mound (Propeller Mound, Porcupine Seabight). International Journal of Earth Sciences 96, 57-72.

Sakai, S., Kano, A., Abe, K., 2009. Origin, glacial-interglacial responses, and controlling factors of a cold-water coral mound in NE Atlantic. Paleoceanography 24.

Schönfeld, J., Zahn, R., 2000. Late Glacial to Holocene history of the Mediteranean Outflow. Evidence from benthic foraminiferal assemblages and stable isotopes at the Portuguese margin. Palaeogeography, Palaeoclimatology, Palaeoecology 159, 85-111.

Serra, N., Ambar, I., Käse, R.H., 2005. Observations and numerical modelling of the Mediterranean outflow splitting and eddy generation. Deep Sea Research Part II: Topical Studies in Oceanography 52, 383-408.

Shanmugam, G., 2013. Modern internal waves and internal tides along oceanic pycnoclines: Challenges and implications for ancient deep-marine baroclinic sands. AAPG Bulletin 97, 799-843.

Siegenthaler, U., Stocker, T.F., Monnin, E., Lüthi, D., Schwander, J., Stauffer, B., Raynaud, D., Barnola, J.-M., Fischer, H., Masson-Delmotte, V., Jouzel, J., 2005. Stable Carbon Cycle–Climate Relationship During the Late Pleistocene. Science 310, 1313-1317.

Stocker, T.F., Johnsen, S.J., 2003. A minimum thermodynamic model for the bipolar seesaw. Paleoceanography 18.

Stokes, C.R., Clark, C.D., 2001. Palaeo-ice streams. Quaternary Science Reviews 20, 1437-1457.

Stokes, C.R., Margold, M., Clark, C.D., Tarasov, L., 2016. Ice stream activity scaled to ice sheet volume during Laurentide Ice Sheet deglaciation. Nature 530, 322-326.

Stow, D.A.V., Faugères, J.C., 2008. Chapter 13 Contourite Facies and the Facies Model, in: Rebesco, M., Camerlenghi, A. (Eds.), Developments in Sedimentology. Elsevier, pp. 223-256.

Sy, A., Rhein, M., Lazier, J.R.N., Koltermann, K.P., Meincke, J., Putzka, A., Bersch, M., 1997. Surprisingly rapid spreading of newly formed intermediate waters across the North Atlantic Ocean. Nature 386, 675-679.

Thierens, M., Titschack, J., Dorschel, B., Huvenne, V.A.I., Wheeler, A.J., Stuut, J.B., O'Donnell, R., 2010. The 2.6 Ma depositional sequence from the Challenger cold-water coral carbonate mound (IODP Exp. 307): Sediment contributors and hydrodynamic palaeo-environments. Marine Geology 271, 260-277.

Thierens, M., Browning, E., Pirlet, H., Loutre, M.F., Dorschel, B., Huvenne, V.A.I., Titschack, J., Colin, C., Foubert, A., Wheeler, A.J., 2013. Cold-water coral carbonate mounds as unique palaeo-archives: the Plio-Pleistocene Challenger Mound record (NE Atlantic). Quaternary Science Reviews 73, 14-30.

Thomsen, L., van Weering, T.C.E., 1998. Spatial and temporal variability of particulate matter in the benthic boundary layer at the N.W. European Continental Margin (Goban Spur). Progress In Oceanography 42, 61-76.

Thomsen, L., Gust, G., 2000. Sediment erosion thresholds and characteristics of resuspended aggregates on the western European continental margin. Deep Sea Research Part I: Oceanographic Research Papers 47, 1881-1897.

Thornalley, D.J.R., Bauch, H.A., Gebbie, G., Guo, W., Ziegler, M., Bernasconi, S.M., Barker, S., Skinner, L.C., Yu, J., 2015. A warm and poorly ventilated deep Arctic Mediterranean during the last glacial period. Science 349, 706-710.

Toucanne, S., Mulder, T., Schönfeld, J., Hanquiez, V., Gonthier, E., Duprat, J., Cremer, M., Zaragosi, S., 2007. Contourites of the Gulf of Cadiz: A high-resolution record of the paleocirculation of the Mediterranean outflow water during the last 50,000 years. Palaeogeography, Palaeoclimatology, Palaeoecology 246, 354-366.

Toucanne, S., Zaragosi, S., Bourillet, J.F., Cremer, M., Eynaud, F., Van Vliet-Lanoë, B., Penaud, A., Fontanier, C., Turon, J.L., Cortijo, E., Gibbard, P.L., 2009a. Timing of massive 'Fleuve Manche' discharges over the last 350 kyr: insights into the European ice-sheet oscillations and the European drainage network from MIS 10 to 2. Quaternary Science Reviews 28, 1238-1256.

Toucanne, S., Zaragosi, S., Bourillet, J.F., Gibbard, P.L., Eynaud, F., Giraudeau, J., Turon, J.L., Cremer, M., Cortijo, E., Martinez, P., Rossignol, L., 2009b. A 1.2 Ma record of glaciation and fluvial discharge from the West European Atlantic margin. Quaternary Science Reviews 28, 2974-2981.

Toucanne, S., Zaragosi, S., Bourillet, J.-F., Dennielou, B., Jorry, S.J., Jouet, G., Cremer, M., 2012. External controls on turbidite sedimentation on the glacially-influenced Armorican margin (Bay of Biscay, western European margin). Marine Geology 303–306, 137-153.

Van Aken, H.M., 2000a. The hydrography of the mid-latitude Northeast Atlantic Ocean II: The intermediate water masses. Deep-Sea Research I 47, 789-824.

van Aken, H.M., 2000b. The hydrography of the mid-latitude northeast Atlantic Ocean: I: The deep water masses. Deep Sea Research Part I: Oceanographic Research Papers 47, 757-788.

van Ommen, T., 2015. Palaeoclimate: Northern push for the bipolar see-saw. Nature 520, 630-631.

Van Rooij, D., De Mol, B., Huvenne, V., Ivanov, M.K., Henriet, J.-P., 2003. Seismic evidence of current-controlled sedimentation in the Belgica mound province, upper Porcupine slope, southwest of Ireland. Marine Geology 195, 31-53.

Van Rooij, D., Blamart, D., Kozachenko, M., Henriet, J.-P., 2007a. Small mounded contourite drifts associated with deep-water coral banks, Porcupine Seabight, NE Atlantic Ocean, in: Viana, A.R., Rebesco, M. (Eds.), Economic and Palaeoceanographic Importance of Contourite Deposits. Geological Society, London, pp. 225-244.

Van Rooij, D., Blamart, D., Richter, T.O., Wheeler, A.J., Kozachenko, M., Henriet, J.-P., 2007b. Quaternary sediment dynamics in the Belgica mounds province, Porcupine Seabight: Ice rafting events and contour current processes. International Journal of Earth Sciences 96, 121-140.

Van Rooij, D., Huvenne, V.A.I., Blamart, D., Henriet, J.P., Wheeler, A., de Haas, H., 2009. The Enya mounds: a lost mound-drift competition. International Journal of Earth Sciences 98, 849-863.

Van Rooij, D., Iglesias, J., Hernández-Molina, F.J., Ercilla, G., Gomez-Ballesteros, M., Casas, D., Llave, E., De Hauwere, A., Gil, S.G., Acosta, J., Henriet, J.P., 2010. The Le Danois Contourite Depositional System: interactions between the Mediterranean Outflow Water and the upper Cantabrian slope (North Iberian margin). Marine Geology 274, 1-20.

van Weering, T.C.E., Hall, I.R., de Stigter, H.C., McCave, I.N., Thomsen, L., 1998. Recent sediments, sediment accumulation and carbon burial at Goban Spur, N.W. European Continental Margin (47-50°N). Progress In Oceanography 42, 5-35.

van Weering, T.C.E., De Stigter, H.C., Balzer, W., Epping, E.H.G., Graf, G., Hall, I.R., Helder, W., Khripounoff, A., Lohse, L., McCave, I.N., Thomsen, L., Vangriesheim, A., 2001. Benthic dynamics and carbon fluxes on the NW European continental margin. Deep-Sea Research II 48, 3191-3221.

Vázquez Riveiros, N., Waelbroeck, C., Skinner, L., Duplessy, J.-C., McManus, J.F., Kandiano, E.S., Bauch, H.A., 2013. The "MIS 11 paradox" and ocean circulation: Role of millennial scale events. Earth and Planetary Science Letters 371–372, 258-268.

Vergnaud-Grazzini, C., Saliège, J.F., 1985a. Oxygen and carbon isotopic composition of benthic foraminifers at Deep Sea Drilling Project sites 548 and 549 (Hole 549A): Pleistocene climatic changes and circulation in the northeastern Atlantic, in: de Graciansky, P.C., Poag, C.W., Cunningham, R., Loubere, P., Masson, D.G., Mazzullo, J.M., Montadert, L., Müller, C., Otsuka, K., Reynolds, L.A., Sigal, J., Snyder, S.W., Vaos, S.P., Waples, D. (Eds.), Initial Reports of the Deep Sea Drilling Project. U.S. Government Printing Office, Washington, pp. 805-815.

Vergnaud-Grazzini, C., Saliège, J.F., 1985b. Pleistocene climatic changes in surface waters of the Northeastern Atlantic: Oxygen and Carbon isotopic compositions of planktonic foraminifers at Deep Sea Drilling Project sites 548 and 549, in: de Graciansky, P.C., Poag, C.W., Cunningham, R., Loubere, P., Masson, D.G., Mazzullo, J.M., Montadert, L., Müller, C., Otsuka, K., Reynolds, L.A., Sigal, J., Snyder, S.W., Vaos, S.P., Waples, D. (Eds.), Initial Reports of the Deep Sea Drilling Project. U.S. Government Printing Office, Washington, pp. 793-803.

Voelker, A.H.L., Lebreiro, S.M., Schonfeld, J., Cacho, I., Erlenkeuser, H., Abrantes, F., 2006. Mediterranean outflow strengthening during northern hemisphere coolings: A salt source for the glacial Atlantic? Earth and Planetary Science Letters 245, 39-55.

Voelker, A.H.L., Rodrigues, T., Billups, K., Oppo, D., McManus, J., Stein, R., Hefter, J., Grimalt, J.O., 2010. Variations in mid-latitude North Atlantic surface water properties during the mid-Brunhes (MIS 9–14) and their implications for the thermohaline circulation. Clim. Past 6, 531-552.

Waelbroeck, C., Labeyrie, L., Duplessy, J.C., Guiot, J., Labracherie, M., Leclaire, H., Duprat, J., 1998. Improving past sea surface temperature estimates based on planktonic fossil faunas. Paleoceanography 13, 272-283.

Waelbroeck, C., Labeyrie, L., Michel, E., Duplessy, J.C., McManus, J.F., Lambeck, K., Balbon, E., Labracherie, M., 2002. Sea-level and deep water temperature changes derived from benthic foraminifera isotopic records. Quaternary Science Reviews 21, 295-305.

Wheeler, A.J., Kenyon, N.H., Ivanov, M.K., Beyer, A., Cronin, B., McDonnell, A., Schenke, H.W., Akhmetzhanov, A.M., Satur, N., Zaragosi, S., 2003. Canyon Heads and Channel Architecture of the Gollum Channel, Porcupine Seabight, in: Mienert, J., Weaver, P.P.E. (Eds.), European margin sediment dynamics: side-scan sonar and seismic images. Springer-Verlag, Heidelberg, pp. 183-186.

White, M., Roberts, J.M., van Weering, T., 2007. Do bottom-intensified diurnal tidal currents shape the alignment of carbonate mounds in the NE Atlantic? Geo-Marine Letters 27, 391-397.

White, M., Dorschel, B., 2010. The importance of the permanent thermocline to the cold water coral carbonate mound distribution in the NE Atlantic. Earth and Planetary Science Letters 296, 395-402.

Wienberg, C., Titschack, J., 2015. Framework-Forming Scleractinian Cold-Water Corals Through Space and Time: A Late Quaternary North Atlantic Perspective, in: Rossi, S., Bramanti, L., Gori, A., Orejas Saco del Valle, C. (Eds.), Marine Animal Forests: The Ecology of Benthic Biodiversity Hotspots. Springer International Publishing, Cham, pp. 1-34.

Zaragosi, S., Eynaud, F., Pujol, C., Auffret, G.A., Turon, J.-L., Garlan, T., 2001. Initiation of the European deglaciation as recorded in the northwestern Bay of Biscay slope environments (Meriadzek Terrace and Trevelyan Escarpment): a multi-proxy approach. Earth and Planetary Science Letters 188, 493-507.

Zhang, W., Hanebuth, T.J.J., Stöber, U., 2015. Short-term sediment dynamics on a meso-scale contourite drift (off NW Iberia): Impacts of multi-scale oceanographic processes deduced from the analysis of mooring data and numerical modelling. Marine Geology.

CHAPTER 5

Bottom current variability at the Pen Duick drift during the last 50 ky

Part of the content of this chapter is intended for publication as:

Stanislas DELIVET, Thomas VANDORPE, Dominique BLAMART, Claudia WIENBERG, Frank BASSINOT, Furu MIENIS, Jan-Berend W. STUUT, David VAN ROOIJ. Bottom current variability at the Pen Duick drift during the last 50 ky (Moroccan Atlantic margin). Sedimentology.

Abstract

The analysis of a long piston core located at the foot of the Pen Duick Escarpment (35°20'N, off Morocco) revealed the chronostratigraphy, bottom current variability and evolution at the Pen Duick drift. High-resolution planktonic and benthic stable isotope measurements, along with a series of AMS^{14}C dates, evidenced that the core covers the last 50 ky, although the presence of a hiatus extending from 33 ka to 19 ka BP was identified. Grain-size and XRF measurements document the presence of enhanced bottom current conditions during cold Dansgaard-Oeschger stadials, Heinrich Event 1 and the Younger Dryas. Those intervals are also known to be associated with increased aeolian dust input over the northwest African margin, which may highlight a certain relationship between climatic changes and the local bottom current regime. The local bottom current regime is thought to be driven by increased northward advection of the Antarctic Intermediate Water into the subtropical northeast Atlantic. The presence of the hiatus implies persistent erosional and/or non-depositional conditions that could be attributed to regionally enhanced bottom currents. This hiatus, which extends from 33 to 19 ka BP, might indicate the gradual onset of the Last Glacial Maximum circulation pattern. The erosive and/or non-depositional bottom currents are further contemporary with the sustained occurrence of mound-forming cold-water corals within the Atlantic Moroccan coral province. Such enhanced bottom currents, influencing sedimentation over areas located next to forming coral mounds were also observed in many other sites along the northeast Atlantic margin. This pattern emphasizes the importance of vigorous bottom currents for the development of cold-water corals, both in terms of food particle delivery and coral framework stabilization through sediment baffling, leading to mound building.

Contributions

This manuscript was written by S. Delivet. Sediment core sub-sampling and analyses were conducted by S. Delivet, G. Isguder, C. De Jonge, M. Ranschaert and T. Vandorpe, in consultation with D. Van Rooij, D. Blamart, F. Bassinot, C. Waelbroeck, N. Vasquez-Riveiros. Interpretation and discussion of results were done by S. Delivet and draft versions of this manuscript were reviewed and commented by D. Van Rooij, C. Wienberg and T. Vandorpe.

5.1 Introduction

Contourite drifts are widespread over the world's oceans and represent sediments deposited and/or substantially reworked by the action of bottom currents (Heezen et al., 1966; Rebesco et al., 2014). They form large sediment bodies of various morphologies and various associated erosive features, ultimately forming localized deep-sea depocenters (Faugères et al., 1999; 2008; Stow et al., 2002a; Rebesco et al., 2014). The contourite paradigm has benefited from the many studies of the Contourite Drift System of the northern Gulf of Cádiz (Hernandez-Molina et al., 2003; 2016a). This Contourite Drift System was formed by the interaction between the Mediterranean Outflow Water (MOW) and the (palaeo)-topography, creating a complex Contourite Depositional System whose morphology and architecture was predominantly controlled by variations in flow pattern and strength (Gonthier et al., 1984; Nelson and Maldonaldo, 1999; Llave et al., 2006; Llave et al., 2007; Hernández-Molina et al., 2014; 2016). Over the last 50 ky, the MOW variability was found in close relationship with the high-frequency millennial-scale Dansgaard-Oeschger (D-O) oscillations and Heinrich Events (HE; Llave et al., 2006; Voelker et al., 2006; Toucanne et al., 2007; Bahr et al., 2015; Kaboth et al., 2016). Such coupling may have ultimately supported the Atlantic meridional circulation through salt supply into the intermediate north Atlantic, and could have been instrumental during the past deglaciation (Rogerson et al., 2006; 2012; Voelker et al., 2006; Bahr et al., 2015). Nowadays, numerous small-scale contourite drifts are being discovered and characterised, as for example along the Iberian margin (Hernández-Molina et al., 2011; 2016b). They are controlled by enhanced bottom currents in the vicinity of pre-existing topographic obstacles, and thus may hold critical information with respect to the variability of the local oceanic circulation pattern (Hanebuth et al., 2015; Zhang et al., 2015; Falcini et al., 2016).

In contrast to the northern Gulf of Cádiz, little is known about the contourite drifts in its southern part, along the Moroccan Atlantic margin (Fig. 5.1). Only recently, the existence of small-scale contourite drifts (*e.g.* Pen Duick drift, Renard drift) was reported from the El Arraiche mud volcano province (Figs. 5.1, 5.2; Van Rooij et al., 2011; Vandorpe et al., 2014; 2016). Those were identified as topographically controlled contourite drifts, associated with the formation of tectonic ridges and mud volcanoes (the Renard and Vernadsky Ridges, see Fig. 5.2), which locally enhance bottom currents (Vandorpe et al., 2016). Mainly found between depths ranging from 500 and 700 m water depths, the responsible bottom currents could be related to the northward flowing Antarctic Intermediate Water (AAIW) and North Atlantic Central Water (NACW; Mienis et al., 2012; Vandorpe et al., 2016). The influence of the AAIW was further corroborated during the Last Glacial Maximum (LGM) along the Moroccan Atlantic margin (Eberwein and Mackensen, 2008; Montero-Serrano et al.,

2011), and within the Atlantic Moroccan coral province surrounding the Pen Duick drift (Dubois-Dauphin et al., 2016).

The AAIW is also known to respond to D-O variations and was recognized as one major feature within the global climate-ocean interhemispheric asynchronicity model, or bipolar seesaw (Jung et al., 2010; Wainer et al., 2012; Martínez-Méndez et al., 2013; Freeman et al., 2015). Northern hemisphere D-O cooling phases, associated with reduced Atlantic meridional circulation northward heat fluxes, are coeval with warming in the tropical and subtropical Atlantic (Shackleton et al., 2000; Rahmstorf, 2002; Stocker and Johnsen, 2003; Weinelt et al., 2003; Jung et al., 2010; Henry et al., 2016). Associated changes in the deep ocean circulation pattern might influence the global atmospheric CO_2 budget through sequestration within aging deep water masses (Elliot et al., 2002; Bigg et al., 2001; 2003; McManus et al., 2004; Marchitto and Broecker, 2006; Bell et al., 2015). During D-O stadials, increased AAIW production from within the Southern Ocean is thought to be associated with the ventilation of the deep southern hemisphere water masses, potentially providing a strong feed-back to global cooling (Marchitto et al., 2007; Anderson et al., 2009; Skinner et al., 2010; Ziegler et al., 2013). Yet, the mechanisms leading to this millennial-scale climate variability are not fully understood and there is an increasing need for the characterization of the intermediate ocean water mass dynamics, as an important feature of the Atlantic meridional circulation and global ocean circulation (Lynch-Stieglitz et al., 2007; Martrat et al., 2007; Bohm et al., 2015; Freeman et al., 2015; Thornalley et al., 2015). Studies that focused on the variability of the AAIW within the western subtropical Atlantic remain somehow controversial (Huang et al., 2014; Freeman et al., 2015) while relatively few studies focused on the AAIW within the eastern sub-tropical Atlantic. Within the El Arraiche mud volcano province, studies that investigated the past variability of the AAIW mainly relied upon methods based on the Neodymium isotopes analysis from cold-water corals. Those are mainly present in the form of fossil cold-water coral mounds, consisting in a mixture of cold-water coral framework and sediment (Wienberg et al., 2015; Hebbeln et al., 2016). Although some specimen were recovered as far deep as 940 m water depth, most studied cold-water corals were retrieved from depths ranging between 500 and 700 m (Wienberg et al., 2010; Dubois-Dauphin et al., 2016). Such studies often result in robust, though discontinuous chronostratigraphic records (Montero-Serrano et al., 2011; Dubois-Dauphin et al., 2016). This is because cold-water corals do not continuously develop in one considered region, and show distinct periods of occurrence which greatly vary all along the northeast Atlantic (Wienberg et al., 2010; 2015; Frank et al., 2011). Thus, the study of the Pen Duick drift sequence could be interesting in complementing the current knowledge on the AAIW past variability.

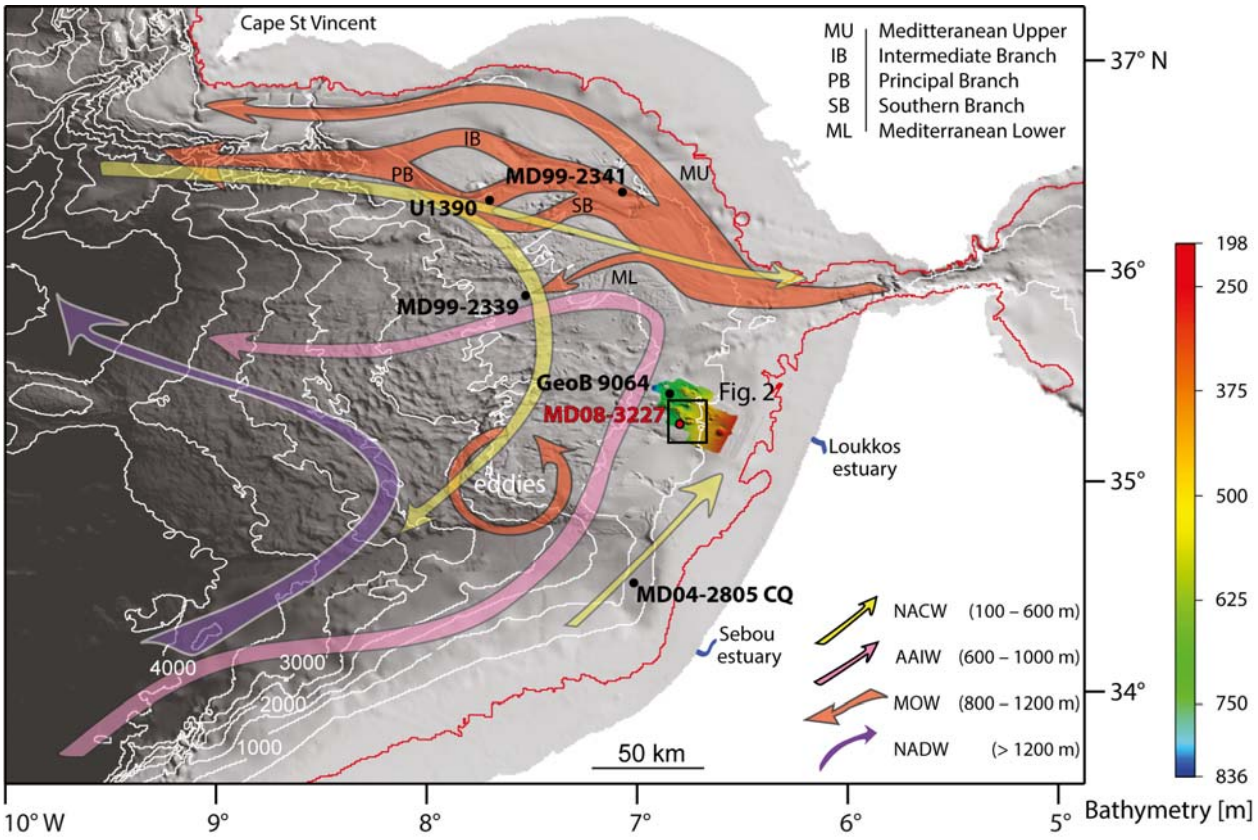

Figure 5.1 Multibeam bathymetric map of the Gulf of Cádiz (Van Rensbergen et al., 2005a; Zitellini et al., 2009) showing the location of cores MD08-3227 (this study), IODP Site U1390 (Stow et al., 2013a), MD99-2341 (Toucanne et al., 2007), MD99-2339 (Voelker et al., 2006), GeoB-9064 (Wienberg et al., 2010) and MD04-2805 CQ (Penaud et al., 2010). The red contour line indicates the present-day 120 m isobath, representing the maximum amplitude global sea-level fall during the LGM (Waelbroeck et al., 2002). The arrows indicate the present-day water masses, respective circulation pattern and main depth ranges in the study area (Carton et al., 2002; Louarn and Morin, 2011; Mienis et al., 2012; Vandorpe et al., 2016). **NACW**: North Atlantic Central Water; **AAIW**: Antarctic Intermediate Water; **MOW**: Mediterranean Outflow Water; **NADW**: North Atlantic Deep Water.

However, it is not known if such millennial-scale variability also has influenced the local bottom current regime, in analogy with the northern Gulf of Cádiz. At present, bottom currents are dominated by internal tidal processes, and the contour currents associated with the circulation of the AAIW does not exceed 10 cm/s in the vicinity of the Pen Duick drift (Mienis et al., 2012). Internal tides have driven the recent evolution and architecture of this part of the margin (Vandorpe et al., 2016). Such processes dramatically differ from those which formed the northern Gulf of Cádiz contourite drifts, typically associated with high contour current velocities (Hernández-Molina et al., 2011). There exists a knowledge gap on the sedimentary facies associated with contourite drifts formed under internal tide dominated bottom currents (Shanmugam, 2013). Moreover, little is known on the potential of such small-scaled drifts in tracing past oceanic circulation changes.

Based on a long piston core analysis, the objective of this study is to constrain the millennial-scale local sedimentation pattern and bottom current variability which has driven the formation of the Pen Duick drift. In particular, this may help to constrain how internal tidal processes are sensitive to past climate changes, and contribute to provide more core based sediment facies descriptions of their related deposits. Understanding the forcing mechanisms which have driven the formation of the Pen Duick drift, as well as their expression and variability, is necessary in order to identify whether this site has a potential to reconstruct the AAIW past variability along the eastern sub-tropical Atlantic.

5.2 Regional setting

The El Arraiche mud volcano province belongs to the Betic-Rifean domain of the Gibraltar arc, which formed due to the northwest convergence of the African and Eurasian continents (Flinch et al., 1993; 1999; Maldonaldo et al., 1999; Grevemeyer et al., 2016). It is located about 35.5°N – 35°N in the southern Gulf of Cádiz, along the Moroccan Atlantic margin, and exhibits a wide variety of seabed features (Fig. 5.2). The central part is dominated by two sub-parallel tectonic ridges, respectively the Renard and Vernadsky Ridges (Fig. 5.2). These ridges developed from a local extensional regime, in an overall compressional/transpressional setting that resulted into the progressive Plio-Pleistocene formation of the two NW-SE oriented sub-parallel anticlines (Van Rensbergen et al., 2005a; b; Medialdea et al., 2009). The seabed is punctuated by the presence of mud volcanoes, generally aligned to the tectonic ridges (*e.g.* the Gemini and the Lazarillo de Tormes mud volcanoes), which pierced the Neogene sedimentary cover and of which recent activity is still clearly visible on the seabed (Somoza et al., 2003; Van Rensbergen et al., 2005a; Vandorpe et al., 2016). In addition, numerous 10 to 20 m high cold-water coral mounds developed on top of the Renard and Vernadsky Ridges as well as on top of the 50 to 100 m high Pen Duick Escarpment (Fig. 5.2; Foubert et al., 2008; Wienberg et al., 2009; 2010; Van Rooij et al., 2011; De Mol et al., 2012). Those cold-water coral mounds are part of the larger Atlantic Morocan coral province which ranges from 200 to 1000 m water dephts. The Atlantic Morocan coral province extends over the entire El Arraiche mud volcano province and more than 40 km towards the southwest of the Pen Duick drift, mainly in the form of small scaled cold-water coral mounds directly rooted over the seabed (Foubert et al., 2008; Vandorpe et al., submitted). Today, these mounds are covered by fossil cold-water corals and coral dating revealed their growth was most pronounced during the last glacial, as living cold-water coral reefs dissappeared from the entire Gulf of Cádiz with the onset of the Holocene (Wienberg et al., 2010; Frank et al., 2011). Four distinct small scaled contourite drifts were reported in association to the above mentioned mud volcanoes and ridges (Vandorpe et al., 2016). The Pen Duick drift forms the largest and shallowest of these drifts and developed in a gentle slope gradient

that does not exceed 1° (Fig. 5.2). It is positioned at the foot of the Pen Duick Escarpment and southern flank of the Gemini mud volcano (Fig. 5.2). Seismic stratigraphy has demonstrated that it developed throughout the entire Quaternary and bears a distinct chronostratigraphic evolution compared to its northern Gulf of Cádiz counterparts (Vandorpe et al., 2014).

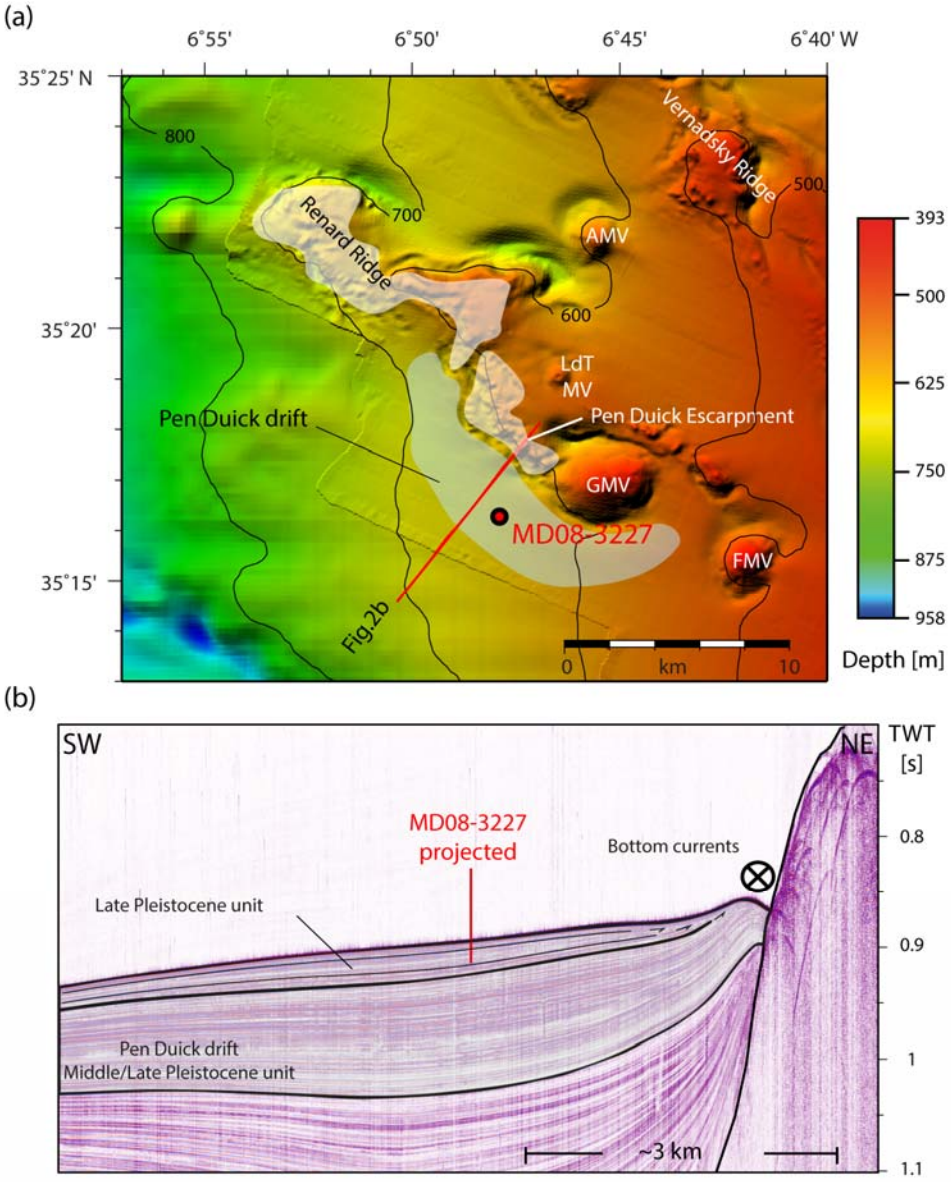

Figure 5.2 (a) High-resolution bathymetric map of the study area indicating the main seabed features in the area (Van Rensbergen et al., 2005a). The position of core MD08-3227 is indicated and was collected from the northwest trending Pen Duick drift (Vandorpe et al., 2016). On the top of the Renard Ridge and the Pen Duick Escarpment, numerous cold-water coral mounds developed, as part of the Atlantic Moroccan coral province (white shaded areas; Foubert et al., 2008; Vandorpe et al., 2016). **GMV**: Gemini mud volcano; **LdTMV**: Lazarillo de Tormes mud volcano; **FMV**: Fiuza mud volcano; **AMV**: Adamastor mud volcano. (b) High-resolution single channel sparker seismic reflection profile (*cf.* location Fig. 5.2a) and the projected position of core MD08-3227 showing the seismic stratigraphy of the Pen Duick drift (modified from Vandorpe et al., 2014). The Middle and Late Quaternary reflectors pinch out against the Pen Duick Escarpment and toplap configuration can be observed beneath the present-day smooth seabed.

The oceanography of the Moroccan Atlantic margin is dominated by the asymmetric interaction of four water masses (Fig. 5.1). Below the surface mixed layer (0 to ~100 m water depth), the North Atlantic Central Water (NACW) is found, extending from 100 to 600 m water depth. The NACW is characterised by a decreasing vertical salinity and temperature gradient from about 36.4 to 35.6 and ~18 to 12°C respectively. The AAIW is observed at water depths between 600 to 1000 m, and is characterised by low salinity (~35.6) and low (~11°C) temperatures (Llinás et al., 2002; Machín and Pelegrí, 2009). Within the El Arraiche mud volcano province, the MOW forms a saline (36.1) and warm (11.5°C) water mass that ranges between 800 and 1200 m water depth (Carracedo Segade et al., 2015). Below 1200 m water depth, the salinity and temperature decrease to minimum values below 35.5 and 8 °C, signing the presence of the North Atlantic Deep Water (NADW; Louarn and Morin, 2011).

The surface circulation pattern (surface mixed layer and NACW) is dominated by different branches originating from the Azores current, which forms the present-day Azores front (Alves and Colin de Verdière, 1999; Eberwein and Mackensen, 2006). The northern branch flows northward along the Iberian Peninsula and forms the Iberian poleward current (Pingree and Le Cann, 1990). Towards the Canary Islands, the southern branch of the Azores current forms the present-day Azores front sensus-stricto (Alves et al., 2002; Knoll et al., 2002). The central branch enters the northern Gulf of Cádiz as the eastward flowing North Atlantic Current and experiences an anticyclonic recirculation towards the south (Johnson and Stevens, 2000; Machín et al., 2006). This branch participates to the surface Atlantic inflow into the Mediterranean Sea (Jia, 2000; Millot et al., 2006). The region extending from Cape St Vincent to the Canary Islands is known as an extended sea surface temperature gradient that may represent up to 4°C (Johnson and Stevens, 2000). Below, The AAIW is formed at sub-Antarctic latitudes and flows northwards roughly centred around 800 m depths (Machín and Pelegrí, 2009). It is interrupted at the Gibraltar Strait where it is partly admixed within the MOW and experiences a cyclonic recirculation towards the central part of the Gulf of Cádiz (Fig. 5.1; Louarn and Morin, 2011). The MOW experiences a salinity decrease, from its source towards Cape St Vincent (from a maximum of about 38.4 and ~12.9°C near Gibraltar), as it admixes with the surrounding NACW and AAIW (Baringer and Price, 1997; Iorga and Lozier, 1999a). It enters the Gulf of Cádiz at very high velocities (>200 cm/s) and divides into different branches (upper, lower and principal branch) due to the influence of Coriolis forcing and the seafloor topographies (Fig. 5.1; Iorga and Lozier, 1999b; Peliz et al., 2009; Hernández-Molina et al., 2016b). Despite the fact that the MOW mainly circulates towards the north as a poleward geostrophic current, it is present within the southern Gulf of Cádiz in the form of deep mesoscale eddies (Fig. 5.1; Carton et

al., 2002; Ambar et al., 2008; Serra et al., 2010). Finally, the NADW flows towards the north as a recirculation of the western north Atlantic deep water (Louarn and Morin, 2011).

The Pen Duick drift is currently influenced by the AAIW and NACW, both flowing from south to north in the study area (Machín and Pelegrí, 2009; Mienis et al., 2012; Vandorpe et al., 2016). The local bottom current regime is characterised by a northward flow averaging 10 cm/s, associated with a strong semidiurnal internal tidal modulation with peak velocities reaching up to 30 cm/s (Mienis et al., 2012). Seasonal wind forced variations might result in a southward directed bottom current regime during the upwelling season and enhanced northeastern trade winds in summer (Peliz et al., 2005; Cropper et al., 2014). Even though seasonal upwelling is documented towards the north and south of the study area, upwelling processes are not significantly observed in the El Arraiche mud volcano province (Pelegri et al., 2005; Eberwein and Mackensen, 2006; Mienis et al., 2012).

5.3 Material and methods

All analyses presented in this study were conducted on the CALYPSO piston core MD08-3227 (35°16.28′N; 6°47.89′W), which was collected at 642 m water depth (Fig. 5.2a), during the R/V Marion Dufresne MD169-"MiCROSYSTEMS" cruise in 2008. The core consists of a 3320 cm long sediment sequence of the Pen Duick drift, mainly composed of grey to dark grey and brownish silty clays and clayey silts. The overall sediment core facies is fairly homogenous, which is typically the case within mud dominated contourite drifts (Rebesco et al., 2014). Nevertheless, the presence of a sand layer was observed ca. 551 cm bsf. The core was successively analysed over different depths ranges. The presence of a probable stratigraphic hiatus was observed, which is the reason why the geochronology could not be sufficiently resolved beyond 1800 cm bsf.

To obtain the elemental composition of the sediments, the core was analysed with the AVAATECH XRF core scanner at 1 cm resolution at the Royal NIOZ. Each measurement was performed using 30 seconds integration time, both at 10 kV/150 µA and 30 kV/500 µA, over an area of 1.2 cm by 1 cm down core. In order to avoid sediment texture and porosity effects as well as possible measurement bias (Richter et al., 2006), results are presented as elemental ratios. Alternatively, it was preferred to use the silica Si normalised ratio ($Si_{normalised} = Si_{counts}/total_{counts}$), in order to provide a signal that would represent overall variations of silica throughout the core. This can be performed in order to avoid representing relative variation between two distinct elements (Richter et al., 2006). The XRF $Si_{normalised}$ can be expected to reflect variation Si-rich minerals, which may be related to relative variations in quartz grains content (Rodrigo-Gámiz et al., 2014). Within the Moroccan Atlantic margin, relative variations in the XRF $Si_{normalised}$ ratio may typically reflect variable aeolian dust input (Eberwein et al., 2008; Penaud et al., 2010; Wienberg et al., 2010).

The core was sub-sampled at irregular intervals based on the XRF data at an average resolution of about 5 cm. The samples were sieved using a 63 µm and 150 µm mesh. Grain-size analyses were carried out on the upper 1100 cm bsf, using the sediment fraction below 63 µm. The analyses were performed using a Micromeritics Sedigraph III, providing information on the relative grain-size distribution between 2 µm to 63 µm (Fig. 5.3). Before analysis, the removal of the biogenic carbonate fraction was performed using a two-fold 1 mol/l acetic acid wash. The biogenic silica and organic fractions were considered negligible. Samples were then stirred using a rotating wheel in a 0.2% Sodium Hexametaphosphate solution for at least 24 h before measurement. In order to evaluate the relative variations within the silt population (~8 to 20 µm; Fig. 5.3), the silt mode (Fig. 5.5e) was calculated within grain-sizes ranging from 5 µm to 65 µm, thus excluding the fraction below 5 µm. The signal was smoothed using a 5-point running average (Fig. 5.5e). The dataset was acquired through four distinct measurement series, in particular with both the objective to extend the coverage and resolution of the record. Reproducibility tests were consistently performed in order to ensure comparable and homogenous results from one series to the other. For yet unknown reasons, one of those series did not provide satisfying reproducibility with respect to the 3 others. Therefore, the entire series results were discarded and the terrigenous grain-size distribution is only presented within the top 1100 cm bsf.

The fraction >150 µm was used for oxygen (planktonic $\delta^{18}O$) and carbon (planktonic $\delta^{13}C$) stable isotope measurements on mono-species samples of the planktonic foraminifer *Globigerina bulloides* at the LSCE at Gif-Sur-Yvette (France). The samples were taken at an overall minimum resolution of 10 cm within the top 1800 cm bsf (Fig. 5.3). Each analysed sample contained 15 to 30 specimens of the 250-315 µm fraction. A first series of measurements was performed in 2010 using a Delta+ Isotope Ratio Mass Spectrometry (IRMS) with MONGA-2 measurement gas. The second series was performed in 2014 using the IsoPrime AMS with KORO measurement gas. All reported values are expressed relative to the Vienna Pee Dee Belemnite standard reference (V-PDB). Several levels were measured with both methods in order to ensure consistent results. The mean external reproducibility (1σ) of carbonate standard is of 0.05 ‰ for $\delta^{18}O$ and 0.04 ‰ for $\delta^{13}C$.

Stable benthic $\delta^{18}O$ and $\delta^{13}C$ isotope compositions of the benthic foraminifer *Cibicidoides pachyderma* were measured at ~10 cm resolution. These analyses were only conducted over the top 530 cm bsf owing to the presence of a 10 cm thick (from 551 to 540 cm bsf) sharp-edged layer of poorly sorted foraminifera sands (ranging from 400 to 800 µm in grain-size) and occasional centimetre scale shell (mollusc) clasts, embedded within a muddy matrix (Fig. 5.4). The measurements were also performed at the LSCE, using the IsoPrime AMS and KORO gas. The analyses were carried out on 2 to 4 specimens selected from the 250-315 µm fraction. When *C.*

pachyderma was absent within the 250-315 µm fraction, measurements were performed using specimens of the > 315 µm fraction. The mean external reproducibility (1σ) of carbonate standard is of 0.05 ‰ for $\delta^{18}O$ and 0.04 ‰ for $\delta^{13}C$.

The above mentioned sandy sequence (551 cm bsf) was further analysed for bulk and terrigenous grain-size distribution using a Malvern Mastersizer at the Department of Geology of Ghent University. Bulk grain-size was measured at 1 cm resolution between 556 and 530 cm bsf from samples ranging from 3 to 6 mg (Fig. 5.4). Samples were primarily boiled in an Oxygen Peroxide solution in order to make sure possible organic matter traces are removed, and to assist dispersion of the particles. The terrigenous bulk grain-size was measured at 2 cm resolution over the same interval from samples ranging from 3 to 8 mg of sediment, formerly decarbonated using a two-fold 1 mol/l acid acetic wash. One millilitre of 0.2% Sodium Hexametaphosphate solution was added to each sample prior to measurement in order to limit the formation of particles aggregates (McCave and Hall, 2006). Samples were introduced into the Malvern using a Hydro MV module with a stirrer speed of 2500 rpm. Continuous ultrasonic bath was set at 10% for terrigenous bulk grain-size, and 2% for the bulk grain-size, in order to avoid breaking of the foraminiferal material. Samples were measured using a 12 second integration time.

Five AMS radiocarbon (^{14}C) dating were performed at the Poznan Radiocarbon Laboratory using samples of 2-3 mg of mono-species planktonic foraminifera *Globigerinoides ruber white* or *G. bulloides* (Table 1). The reported ^{14}C ages were calibrated (ka BP) using the OxCal 4.2 software and the IntCal13 curve for marine samples. In absence of a suitable marine reservoir calibration off the Moroccan Atlantic margin, the standard marine reservoir age correction of 0.4 ky was used (Reimer et al., 2013).

The MD08-3227 chronostratigraphy (Table 2) was established by means of the five AMS ^{14}C dates and by the correlation of the planktonic $\delta^{18}O$ record with the *G. bulloïdes* $\delta^{18}O$ record from core MD99-2339 (Voelker et al., 2006). Core MD99-2339 was collected in the central part of the Gulf of Cádiz at 1170 m water depth and spans the last ~47 ky BP (Fig. 5.1). It was here considered as a reference core because of its geographical position and its detailed age model (Voelker et al., 2006). The tuning between the two *G. bulloides* $\delta^{18}O$ records was performed using the AnalySeries software (Paillard et al., 1996).

5.4 Results

5.4.1 Age model

The age model of core MD08-3227 is based on the AMS ^{14}C control points (Table 1) and eleven additional tie points obtained from the *G. bulloides* planktonic $\delta^{18}O$ tuning (Fig. 5.5a; Table 2). The AMS ^{14}C dates revealed ages ranging from 35.5 to 0.8 ka BP, thus covering the MIS 3 to the Late Holocene (Table 1). Planktonic $\delta^{18}O$ shifts comprised between 1800 and 551 cm bsf could be correlated to D-O stadial/interstadial cycles spanning from ~50 to 32.9 ka BP, thus covering D-O cycles 12 to 7 of core MD99-2339 (Voelker et al., 2006). Within this interval, the HE4 forms the heaviest planktonic $\delta^{18}O$ values, averaging 2.2 ‰ between 1200 and 1100 cm bsf, which could be correlated to similar values, respectively between ~38.5 to 39.5 ka BP in Voelker et al. (2006). The overall interstadial planktonic $\delta^{18}O$ values gradually increase from D-O cycle 11 to 8, from ~0.4 ‰ to ~0.8 ‰, respectively (Fig. 5.5). Heavier planktonic $\delta^{18}O$ values of 1.8 and 2 ‰ are obtained for the D-O stadials 10 and 7, respectively at 1350 cm and ~650 cm bsf. Substantially lighter values of about 0.6 and 0.8 ‰ were obtained for D-O stadials 11 and 8, at about 1500 cm and 900 cm bsf respectively.

Labcode	Material	Core depth (cm)	Age (14C ± 1σ)	2σ calibrated age range (min – max yr cal BP)
Poz-75177	*G. Ruber white*	5	1280 ± 70	670 – 960
Poz-75178	*G. Ruber white*	135	7040 ± 50	7425 – 7615
Poz-68942	*G. Bulloïdes*	500	15250 ± 110	17785 – 18355
Poz-68943	*G. Bulloïdes*	525	16750 ± 150	19345 – 20120
Poz-68944	*G. Bulloïdes*	650	31700 ± 800	33865 – 37445

Table 5-1 MD08-3227 AMS ^{14}C ages. Calibration was made using the online OxCal 4.2 program and the IntCal13 marine curve (Reimer et al., 2013).

The interval comprised between 33 to 19 ka BP, which cover the late MIS3, HE3, HE2 and early LGM, is not represented in the planktonic $\delta^{18}O$ record and thus, a hiatus was inferred (Fig. 5.5a). The AMS ^{14}C dates consistently indicate that the upper 525 cm bsf of the core spans an age between 19 and 0.8 ka BP (Table 1). Heavy planktonic $\delta^{18}O$ values of ~2.2 ‰ were obtained at ~19 ka BP (529 cm bsf), which correlate with LGM planktonic $\delta^{18}O$ values of core MD99-2339 (Fig. 5.5a). Planktonic $\delta^{18}O$ values ranging from 2 to 1.6 ‰ (480 to 400 cm bsf) correlated to the HE1 between 18 and 15 ka BP. One single planktonic $\delta^{18}O$ tie-point completes the four AMS ^{14}C obtained dates from this interval. It is set on the basis of the abrupt planktonic $\delta^{18}O$ shift towards heavy values of ~1.4 ‰, marking the onset of the Younger Dryas (YD) at ~260 cm bsf, dated to ~12 ka BP in Voelker et al. (2006). The transitions from the LGM to Bölling-Allerød (B-A) and from the YD to the

early Holocene, correspond to successive shifts from heavy to light planktonic $\delta^{18}O$, from 500 cm to 350 cm bsf (2.3 to 0.2 ‰) and from 270 cm to 200 cm bsf (1.5 to -0.1 ‰), respectively (Fig. 5.3).

The benthic $\delta^{18}O$ record, available within this interval, exhibits a two-fold transition from heavy to light values, similar to the record of core MD99-2339. Those respectively correspond to HE1 where a decrease of ~0.9 ‰ occurs, and to the onset of the Holocene with corresponding decrease of ~0.5 ‰ (Fig. 5.5c). From about 10 ka BP onwards, the benthic $\delta^{18}O$ values exhibit an overall decreasing trend from 1.8 to 1.2 ‰ which can also be observed within core MD99-2339 benthic $\delta^{18}O$ record (Fig. 5.5c).

The sedimentation rates obtained with the corresponding age model range from 58 to 140 cm/ky within the 33 to 50 ka BP time interval of MIS 3, with maximum values during HE4 and D-O cycle 8. Sedimentation rates range from 40 to 19 cm/ky from the LGM to late Holocene, with a maximum rate of 40 cm/ky obtained from HE1 to the onset of the YD. The inferred hiatus was correlated between 551 and 540 cm bsf (Fig. 5.3, 5.4).

Depth [cm]	Age [ka BP]	Sedimentation rate [cm/ky]
5*	0.82	19
135*	7.52	29
259	11.72	40
500*	17.63	21
525*	18.77	21
529	18.95	7
***		
550	32.91	119
631	33.59	84
650*	33.82	84
770	35.24	140
861	35.88	86
1088	38.52	131
1202	39.38	69
1359	41.63	112
1490	42.8	58
1685	46.16	58

Table 5-2 MD08-3227 age model and associated interval sedimentation rates. The tuning was made using core MD99-2339, accounting for the presence of a hiatus at 551 cm bsf (* indicate the ^{14}C control points).

5.4.2 Stable carbon isotopic record

The planktonic $\delta^{13}C$ record is available down to 1800 cm bsf, covering the MIS 3 interval (from 50 to 33 ka BP), while the benthic $\delta^{13}C$ only is available over the top 530 cm bsf, extending from the late LGM to late Holocene. During MIS3, the overall planktonic $\delta^{13}C$ ranges from -2.34 ‰ to -0.02 ‰ with a mean value of -1 ‰ (Fig. 5.3). Overall, light planktonic $\delta^{13}C$ values correspond to heavy planktonic $\delta^{18}O$ values (Fig. 5.3). Markedly light planktonic $\delta^{13}C$ values between -0.8 and -0.6 ‰ were obtained during D-O stadials and HE4. From the late LGM to recent, the planktonic $\delta^{13}C$ varies from -2 ‰ to -0.4 ‰, and correlates well with the planktonic $\delta^{18}O$ record, with rather light planktonic $\delta^{13}C$ corresponding to intervals with heavy planktonic $\delta^{18}O$. Two marked peaks with values lighter than -0.4 ‰ are recorded respectively during HE1 and YD (450 and 250 cm bsf respectively). Those intervals are followed by heavy values reaching about -2 ‰. Those latest levels represent the heaviest values over the record and correspond to the B-A and the early Holocene (~380 and 200 cm bsf respectively). From the onset of the Holocene onwards, the planktonic $\delta^{13}C$ exhibits a slight decreasing trend reaching values up to -1.2 ‰ at the top of the core.

The benthic $\delta^{13}C$ abruptly decreases from 1 ‰ during the late LGM to a minimum of ~ 0.2 ‰ obtained during the HE1. This ~1 ‰ amplitude decrease is followed by a weak incursion with values of about 0.7 ‰ during the B-A and marks a subsequent minimum of ~0.4 ‰ during the YD. It increases from the onset of the Holocene towards values between 1 and 1.4 ‰ from 5 to 0.8 ka BP (Fig. 5.5d).

5.4.3 XRF and grain-size distribution

The XRF Fe/Ca is marked by a prominent peak between 551 and 540 cm bsf, forming a 10 cm thick decrease (Fig. 5.3). This peak marks the presence of the aforementioned coarse biogenic muddy sand layer (Fig. 5.4), characterised by coarse bulk grain-sizes ranging from ~200 to 600 µm. The terrigenous bulk analysis did not show the presence of terrigenous sands, the terrigenous fraction being primarily composed of fine silts which mode vary between 15 and 20 µm (Fig. 5.4). Interval MIS3 (i.e. from 1800 to 551 cm bsf) is characterised by cyclic XRF Fe/Ca variations of marked relative amplitude, which are observed to correlate to the respective D-O cycles (Fig. 5.3b, 4b). Those are formed by abrupt (generally representing less than 10 cm) increases of the XRF Fe/Ca ratio, followed by a gradual decrease, which occurs over 100 to 200 cm thick intervals. High XRF Fe/Ca ratios mark the stadial phase of the D-O cycles except for the transition from stadial 8 to interstadial 7 which is poorly expressed. The stadial phases of D-O cycle 12 and HE4 correspond to the largest increase in XRF Fe/Ca ratio (Fig. 5.3).

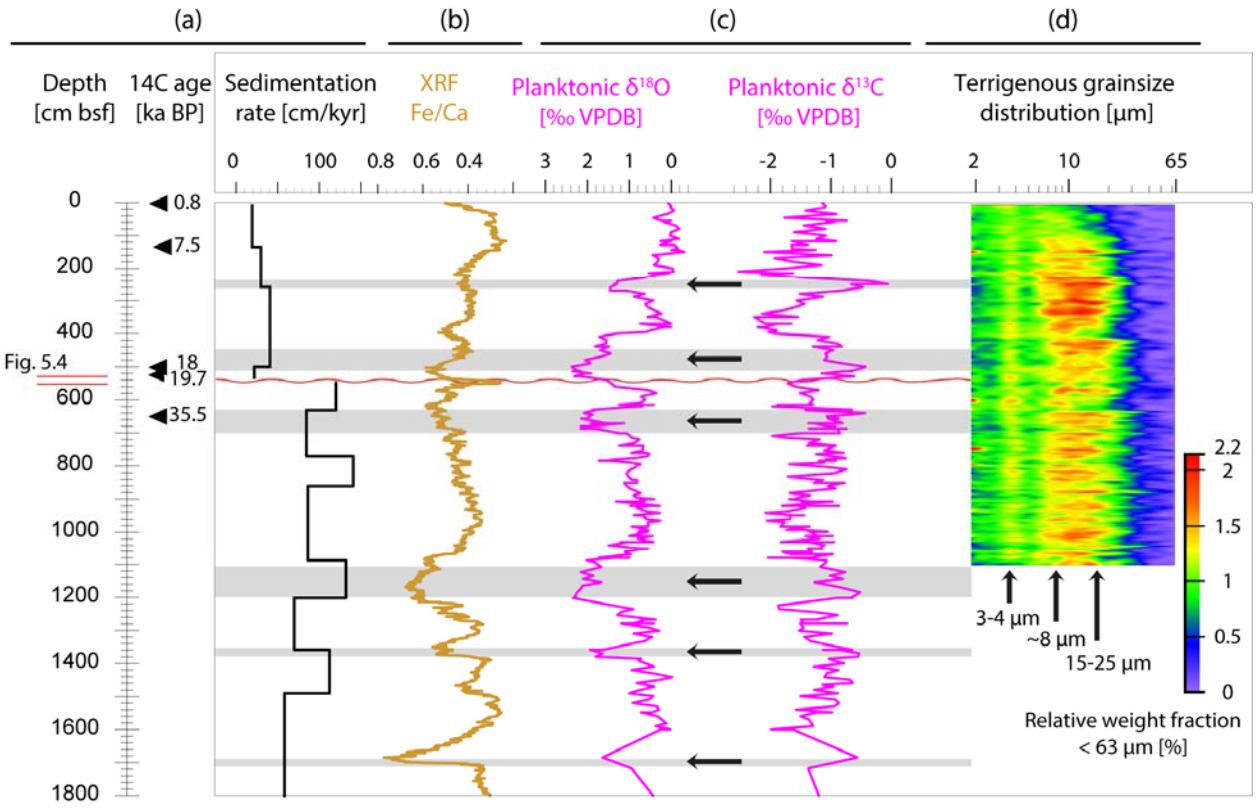

Figure 5.3 Core MD08-3227 multi-proxy record versus depth. (a) Linear depth scale with ^{14}C ages (Table 1) and interpreted sedimentation rates. (b) XRF Fe/Ca ratio. The wavy red line indicates the XRF peak observed at 551-540 cm bsf which marks a hiatus in the core. (c) Planktonic $\delta^{18}O$ and planktonic $\delta^{13}C$. The grey shaded areas show marked $\delta^{18}O$ and $\delta^{13}C$ excursions. (d) Terrigenous grain-size (<63 µm) distribution plot over the uppermost 1100 cm bsf. The black arrows indicate the distinct modes identified with their respective grain-size range.

From the late LGM onwards, the XRF Fe/Ca ratio shows a decreasing trend with two inflections at the transition from HE1 to B-A, and during the YD (~350 and 200 cm bsf respectively; Fig. 5.3b). An abrupt increase occurs during the late Holocene from about 3 ka BP (50 cm bsf). The XRF $Si_{normalised}$ curve exhibits a series of peaks throughout the record (Fig. 5.5d; green shaded areas). Those are found in association with D-O stadials, HE's and YD interval (Fig. 5.5d), even though a small amplitude peak is visible during the interstadial phase of D-O cycle 8.

The grain-size distribution plot consistently indicates the presence of two to three modes along the top 1100 cm bsf (Fig. 5.3d). A fine clay mode is present between 3 and 4 µm, an intermediate mode varying between 8 and 10 µm and a silt mode between 15 and 25 µm. The silt mode shows the relative variations existing between the two coarser silts modes (Fig. 5.5d). It displays relatively coarse values (~10 to 15 µm) during the MIS 3, with maximum values found during HE4, D-O stadial 7 and the late section of the interstadial part of D-O cycle 8. Average values are relatively low during D-O stadial 8 although it must be noted an important scatter between each measurements over this

interval (Fig. 5.5d). Similar high silt mode values (> 15 µm) are found during the late LGM and HE1, as well as during the YD. The B-A correspond to a local minimum of about 10 µm. From the onset of the Holocene, the silt mode decreases generally below 10 µm and reaches a minimum of ~7 µm during the late Holocene, roughly from 7 ka BP onwards.

5.5 Discussion

5.5.1 Stable isotopes, source and controls on sedimentation pattern

Heavy planktonic $\delta^{18}O$ values were obtained during HE4 cooling event, which correlated well with other records from the northern Gulf of Cádiz (Fig. 5.1; Voelker et al., 2006; Toucanne et al., 2007). However, the planktonic $\delta^{18}O$ record consistently shows lighter values during most of the MIS 3 when compared to those of core MD99-2339 (Fig. 5.5a; Voelker et al., 2006). Between 0.4 ‰ and 1 ‰ difference is recorded during D-O cycle 8, while offsets of ~0.8 ‰ are observed for the interstadial phases of D-O cycles 9 to 12 (Fig. 5.5a). Differences below 0.4 ‰ most probably reflect the presence of a persistent oceanographic front characterizing a sea surface temperature gradient between both sites, most probably similar to the present-day Azores Front (Rogerson et al., 2004; Penaud et al., 2011). However, the obtained values exhibits more prominent offsets, which are also marked during the period correlated to the B-A, from ~15.5 to 12.9 ka BP (Voelker et al., 2006). During the B-A, the mean difference of about 1 ‰ cannot be attributed to a local temperature, salinity gradient and/or measurement margin errors and also contrasts with values obtained from core MD04-2805 CQ to the south (Fig. 5.1; Penaud et al., 2010). This may be attributed to post depositional dissolution or early diagenetic effects which may have corrupted the isotopic signature of the selected foraminifera (Ravelo and Hillaire-Marcel, 2007). Alternatively, recurrent planktonic $\delta^{18}O$ offset may be attributed to the occurrence of bottom current reworked sediments. In contrast, the deglacial and Holocene benthic $\delta^{18}O$ relative variations are in agreement with those of core MD99-2339 (Fig. 5.5c). The benthic $\delta^{18}O$ successive decreases may primarily reflect changes in global seawater signature through the successive icesheets melting pulses of the HE1 and the end of the YD (Shackleton, 1987; Voelker et al., 2006; Rohling et al., 2014). Thus, the benthic $\delta^{18}O$ records (obtained from *C. pachyderma*) reasonably reflect bottom water properties while planktonic $\delta^{18}O$ shows regular excursions towards lighter values than expected. Here, *C. pachyderma* belongs to the epi-benthic group which species are known for their affinities with enhanced hydrodynamic environments, and stable isotope data recovered from this species are generally not noticeably affected by in-situ sediment and early diagenetic process effects (Schönfeld et al., 1997; 2000; Eberwein and Mackensen, 2006; Singh et al., 2015). However, the deviating planktonic $\delta^{18}O$ values

may have been caused by the occurrence of bottom current reworked material input. Bottom currents are known to be capable of transporting sediments over long distances which implies sediment drifts might be associated with significant reworked material input (Alonso et al., 2016; Takashimizu et al., 2016). The arrival of bottom current reworked planktonic foraminifera material, noting that bottom currents are characteristic for the site under study (Vandorpe et al., 2014), could explain the overall light planktonic $\delta^{18}O$ obtained during the D-O cycles of MIS 3 and during the onset of the B-A.

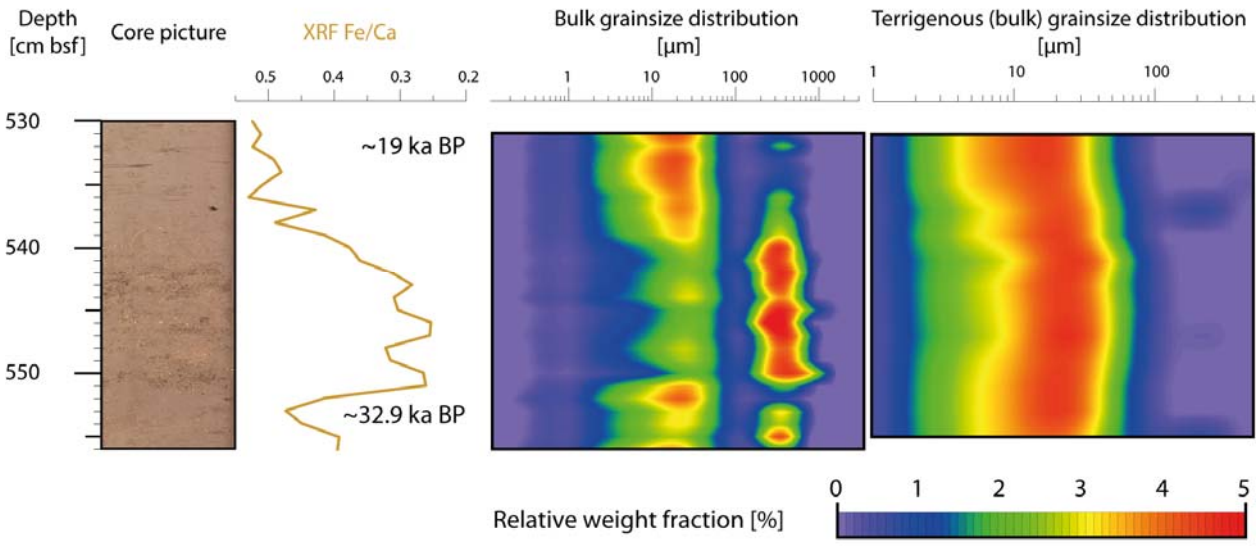

Figure 5.4 MD08-3227 bulk and terrigenous (bulk) grain-size distributions associated with the XRF Fe/Ca peak at 551-540 cm bsf (Fig. 5.3). Note the presence of biogenic coarse sands centred at 300 µm grain-size. The terrigenous fraction is represented by coarse silt fraction comprised between 10 and 30 µm. This sequence may represent 14 ky interval, and can be interpreted as a calcareous sandy contourite according to classification in Rebesco et al. (2014).

The MIS 3 interval is characterised by a pronounced cyclicity in the XRF Fe/Ca ratio (Fig. 5.5). Assuming that the calcium content mostly reflects the biogenic carbonate, this ratio primarily represents the terrigenous versus biogenic relative fraction (Weltje and Tjallingii, 2008). Here, the XRF derived terrigenous relative variations fairly resemble variations in the MD99-2339 planktonic $\delta^{18}O$ record (Fig. 5.5a). Those are characteristic for the northeast Atlantic millennial-scale D-O stadial/interstadial cycles spanning from 33 to 50 ka (Shackleton et al., 2000; Voelker et al., 2006; Martrat et al., 2007; Hodell et al., 2013). This suggests that the terrigenous versus biogenic relative fraction is primarily driven by local climatic variations, with a higher terrigenous content during D-O stadials. Similar millennial-scale variations in the terrigenous content are typically observed along the Portuguese margin (Hodell et al., 2013; 2015). The XRF Fe/Ca also experiences a marked decreasing

trend during the onset of the B-A and early Holocene, respectively at about 15 ka BP and around 10 ka BP (Voelker et al., 2006). Again, this pattern emphasizes the existing relationship between the climate regime and terrigenous versus biogenic relative fraction. Therefore, the interval between 50 and 33 ka BP is further considered continuous based on the matching cyclicity correlation of the terrigenous proxies with other records such as the planktonic $\delta^{18}O$ of site MD99-2339 (Fig. 5.5a, b).

According to the obtained age model, sedimentation rates averaged 100 cm/ky during the covered interval of MIS 3 (Fig. 5.3, Table 2). Penaud et al. (2010) also reported sedimentation rates regularly exceeding 100 cm/ky during the past 29 ka BP at site MD04-2805 CQ (Fig. 5.1). From the late LGM to late Holocene, the sedimentation rates are distinctly lower, averaging 27 cm/ky with maxima of 40 cm/ky from HE1 to YD (Table 2). A similar overall decrease from high MIS 3 and LGM sedimentation rates towards lower, Holocene, sedimentation rates were also observed from sites MD04-2805 CQ and GeoB 9064 (Penaud et al., 2010; Wienberg et al., 2010). Along the upper continental slope of the northern Gulf of Cádiz (400 to 700 m water depth), precession and eccentricity forced sea-level changes were inferred to control margin wide terrigenous supply, hence impacting sedimentation rates (Sierro et al., 1999; Lofi et al., 2015). A similar mechanism was evidenced to control the terrigenous supply along the Portuguese margin (Thomson et al., 1999; Hodell et al., 2013). Similarly, the deglacial sea-level rise may have controlled the observed decrease in the sedimentation rate with the gradual the onset of the Holocene. Here, it must be noted that overall sedimentation rates remained significantly higher than the average 15 cm/ky obtained from the nearby site GeoB 9064 (Fig. 5.1, Wienberg et al., 2010). Once more, this can be attributed to the overall bottom current controlled sedimentation. Sedimentation rates up to 100 cm/ky are comparable with those obtained from IODP Site U1390 (Fig. 5.1), located within the Doñana basin of the northern Gulf of Cádiz (Stow et al., 2013a; Hernández-Molina et al., 2014). This site was recovered from a mud dominated sheeted drift (Hernández-Molina et al., 2016a), and may represent an appropriate analogue to the Pen Duick drift. There, high sedimentation rates were attributed to the action of bottom currents which redistributed sediments mainly derived from the Guadalquivir river (Hernández-Molina et al., 2016a; Alonso et al., 2016). A similar control may explain the locally high sedimentation rates within the Pen Duick drift. Here, appropriate sediment supply originate from the river runoff of the nearby Loukkos and Sebou rivers (Fig. 5.1), whose estuaries are located 60 km to the east and 100 km to the south of the El Arraiche mud volcano province, respectively. In particular, the Sebou river is known to have constituted a major sediment supply from the Neogene to present days, and the regional oceanic circulation pattern may have redirected the Sebou river sediment plumes towards the study area (Snoussi et al., 1990; Lobo et al., 2014).

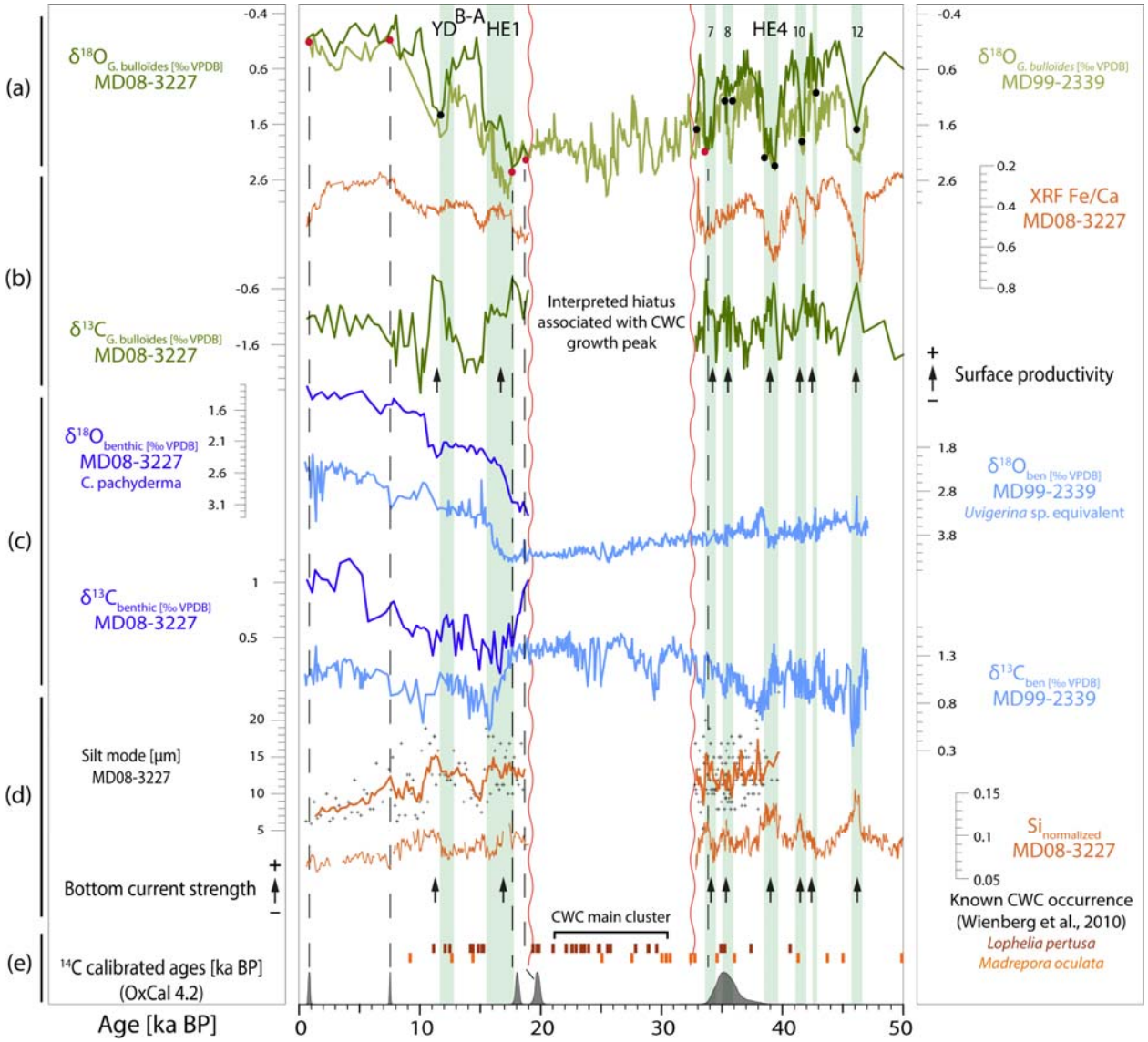

Figure 5.5 Chronostratigraphic record obtained from core MD08-3227. (a) MD08-3227 planktonic $\delta^{18}O$ record correlation with the planktonic $\delta^{18}O$ records of core MD99-2339. Red (black) dots indicate the ^{14}C ages (tie points) position. (b) MD08-3227 XRF Fe/Ca ratio and planktonic $\delta^{13}C$ data. The black arrows indicate high planktonic $\delta^{13}C$ intervals. (c) Benthic $\delta^{18}O$ and $\delta^{13}C$ records compared to those of core MD99-2339 (Voelker et al., 2006). Note the different scales due to the different species used for measurement. (d) Grain-size silt mode calculated between 5 and 65 µm grain-size range (black cross). The 5-point running average (solid line) and the XRF $Si_{normalised}$ curve are indicated. The black arrows denote peaks correlated to cold periods of the YD, HE1, HE4 and D-O stadials. (e) OxCal ^{14}C calibrated probability density functions (ka BP) for the obtained MD08-3227 radiocarbon ages. The vertical dashed lines indicate the sampled AMS ^{14}C levels (Table 1). Cold-water coral ages obtained from *Lophelia pertusa* (red) and *Madrepora oculata* (orange) collected from various cold-water coral mounds situated on top of the Renard Ridge and the Pen Duick Escarpment are indicated (Wienberg et al., 2010).

Distinct increases in the planktonic $\delta^{13}C$ record correlate to cold stadials of MIS 3 (Fig. 5.5c). Such variations are interpreted to reflect an increase in primary productivity relative to the present-day through enhanced biogenic ^{12}C export (Voelker et al., 2006; Penaud et al., 2010; 2011). The planktonic $\delta^{18}O$ values bear marked (>1 ‰) as well as weak (<0.4 ‰) incursions that are systematically correlated to increased planktonic $\delta^{13}C$ values ranging from -0.8 to -0.6 ‰. Thus, the planktonic $\delta^{13}C$ signal seems relatively robust and conspicuously increases with little planktonic $\delta^{18}O$ incursions. The D-O stadial increased primary productivity is in accordance with regional productivity patterns recorded off the Portuguese margin and Gulf of Cádiz (Eynaud et al., 2009; Incarbona et al., 2010; Penaud et al., 2011). The increased primary productivity during each respective D-O stadials may be related to the presence of persistent oceanic fronts (Penaud et al., 2011), also most probably associated to increased northwest African aridity and wind regime (Tjallingii et al., 2008). Increased windforced upwelling is typically cited as the main mechanism driving the sea surface productivity inf this region (Eberwein and Mackensen, 2008; Penaud et al., 2010; 2011; Wienberg et al., 2010). During the past 19 ky, two distinct intervals of high planktonic $\delta^{13}C$ correlated to the HE1 and the YD periods (Fig. 5.5b). Similar enhanced productivity patterns were recorded in the area, especially during HE1 which was characterised by an intense wind-driven up-welling regime triggered by enhanced northeastern trade winds (Eberwein and Mackensen, 2008; Penaud et al., 2010; 2011; Wienberg et al., 2010). The benthic $\delta^{13}C$ values are in relative agreement with MD99-2339 (Fig. 5.1) and record ^{12}C enrichment, in an inverse trend compared to the planktonic signal (Fig. 5.5c). Such signal is interpreted to indicate enhanced particulate organic matter fluxes, in accordance with enhanced sea surface primary productivity during HE1 and the YD (Eberwein and Mackensen, 2008). During the covered time of the LGM (ca. 19 to 18 ka BP), light benthic $\delta^{13}C$ characterised variable productivity and wind patterns and periodic shifts of the Azores Front position (Rogerson et al., 2004; Wienberg et al., 2010; Penaud et al., 2011).

5.5.2 Bottom current variability

Bottom currents seem to have influenced the local sedimentation pattern and to have led to high sedimentation rates and probable sustained bottom current reworked sediment inputs. Distinct peaks in the XRF $Si_{normalised}$ and in the silt mode occurred during the YD and HE1, as well as D-O stadials and HE4 (Fig. 5.5d). The XRF $Si_{normalised}$ signal might be influenced by the presence of Si-rich minerals, which in the region considered, might primarily be related to relative variations in quartz sand grains content (Rodrigo-Gámiz et al., 2014). This consistently indicates the presence intervals rich in quartz grains, associated to a coarser silt mode. Two distinct processes can be invoked to explain such variability.

Increases in the silt mode, generally up to 30-50 µm, are often interpreted as increased aeolian dust input associated to northwest African aridification periods (Holz et al., 2007; Rodrigo-Gámiz et al., 2014). Variations obtained in the silt mode at site MD08-3227 are very similar in amplitude, range and timing to those of the nearby site GeoB-9064 (Fig. 5.1), which were interpreted in terms of relative aeolian dust input variations (Wienberg et al., 2010). This interpretation is in agreement with enhanced aeolian dust input during D-O stadials off Mauritania (Tjallingii et al., 2008), and further provide a suitable driving mechanism for the wind-forced upwelling and associated productivity pattern (Penaud et al., 2010; Wienberg et al., 2010). Alternatively, similar variations may be interpreted as the result of enhanced bottom current regime typical for contourite drift sequences, through winnowing of the fine terrigenous fraction (Stow et al, 1979; 2002b; Gonthier et al., 1984; Nelson et al., 1993; McCave et al., 1995; 2006; Mulder et al., 2013; Alonso et al., 2016). Accordingly, a relative higher silt mode and Si grains content might be indicative for enhanced bottom currents at site MD08-3227 (Figs. 5.5d, 5.5).

Yet, we find no unambiguous criteria allowing their differentiation, which is partly explained by the marked covariance existing between those two proxies. Considering one or the other, both processes appear to have acted in concert, both pulling towards coarser, Si-rich sediments during the identified cold periods (Fig. 5.5). Similarly, Mulder et al. (2013) described the occurrence of complex to hybrid contourite sequences within the central part of the Gulf of Cádiz. At site GeoB-9064, Wienberg et al. (2010) considered the main coarse sediment source (i.e. >6 µm), was predominantly of aeolian dust origin. Those aeolian sourced sediments were associated to sedimentation rates up to 24 cm/ky. As mentioned earlier, sedimentation rates of ~100 cm/ky cannot be explained by a simple increase in the wind regime and aeolian dust input. Given the fact that bottom currents are known to dominate the regional sedimentation architecture (Vandorpe et al., 2014; 2016), the relatively clear and combined signal provided by the XRF $Si_{normalised}$ and silt mode may (at least partly) be attributed to stronger-than-today bottom current regime in association to cold climatic events (Fig. 5.6a, b).

XRF $Si_{normalised}$ and silt mode suggests a very strong covariance between the northwest African aridifications periods and enhanced bottom currents. The Pen Duick drift is currently influenced by the AAIW/NACW interface, and previous authors suggested a predominant influence of the AAIW, including during the LGM (Mienis et al., 2012; Vandorpe et al., 2014; 2016; Dubois-Dauphin et al., 2016). Within the sub-tropical Atlantic, D-O stadial increased AAIW production correlate with periods of reduced Atlantic meridional circulation (Marchitto et al., 2007; Anderson et al., 2009; Jung et al., 2010; Skinner et al., 2010; Henry et al., 2016). Here, enhanced advection of AAIW during D-O stadials provides a suitable mechanism to explain the bottom current variability prior to 33 ka BP.

During the last deglaciation, relatively high silt mode and XRF $Si_{normalised}$ values range from 19 to 15 ka BP and around ~12.5 ka BP, which further correlates with periods of increased AAIW influence within the western subtropical Atlantic such as recorded from Pahnke et al. (2008). Thus, the AAIW seem to have positively influenced the local bottom current regime towards more energetic conditions. During D-O stadials and HE's, the diminution of sea-surface heat and salinity fluxes towards the north Atlantic (reduced Atlantic meridional circulation) is thought to have caused the accumulation of salt within the mid-depth sub-tropical gyre (Chapman and Maslin, 1999; Pflaumann et al., 2003; Voelker et al., 2006). This suggests the existence of a more saline NACW whereas the AAIW typically characterizes regional salinity minimum. This might have led to a more prominent vertical pycnal gradient, potentially affecting the regional internal tide regime towards more energetic conditions (Cacchione et al., 2002; Pomar et al., 2012; Shanmugam, 2013). Vandorpe et al. (2015) also found geomorphological arguments suggesting that internal tides may have locally dominated the recent sediment dynamic.

5.5.3 Hiatus, processes and implications

The inferred 14 ky long hiatus seems to be contained within the 10 cm thick interval of foraminifer rich and terrigenous depleted (low XRF Fe/Ca ratio) sand layer (Fig. 5.4). Such facies may be analogue to a poorly sorted biogenic sandy contouritic sequence in the classification of Stow and Faugères (2008). The presence of this facies contrasts within the otherwise mud dominated contourite drift sequence recovered (Shanmugam, 2012; Rebesco et al., 2014). In muddy environments, the erosional threshold is generally set to bottom current velocities reaching, at least episodically, ~50 cm/s (Nichols, 2009; Stow et al., 2009; Kuijpers and Nielsen, 2015). High bottom current velocities ensure sand rich accumulation with erosion and/or non-deposition, such as typically identified for large contourite channels in the northern Gulf of Cádiz (Nelson et al., 1993; Hernández-Molina et al., 2006; Stow et al., 2013b). Here, the seismic data reveals the presence of toplap reflectors located at the foot of the Pen Duick Escarpment (Fig. 5.2b); in a configuration that resembles the expression of contourite channel sensus García et al. (2009).

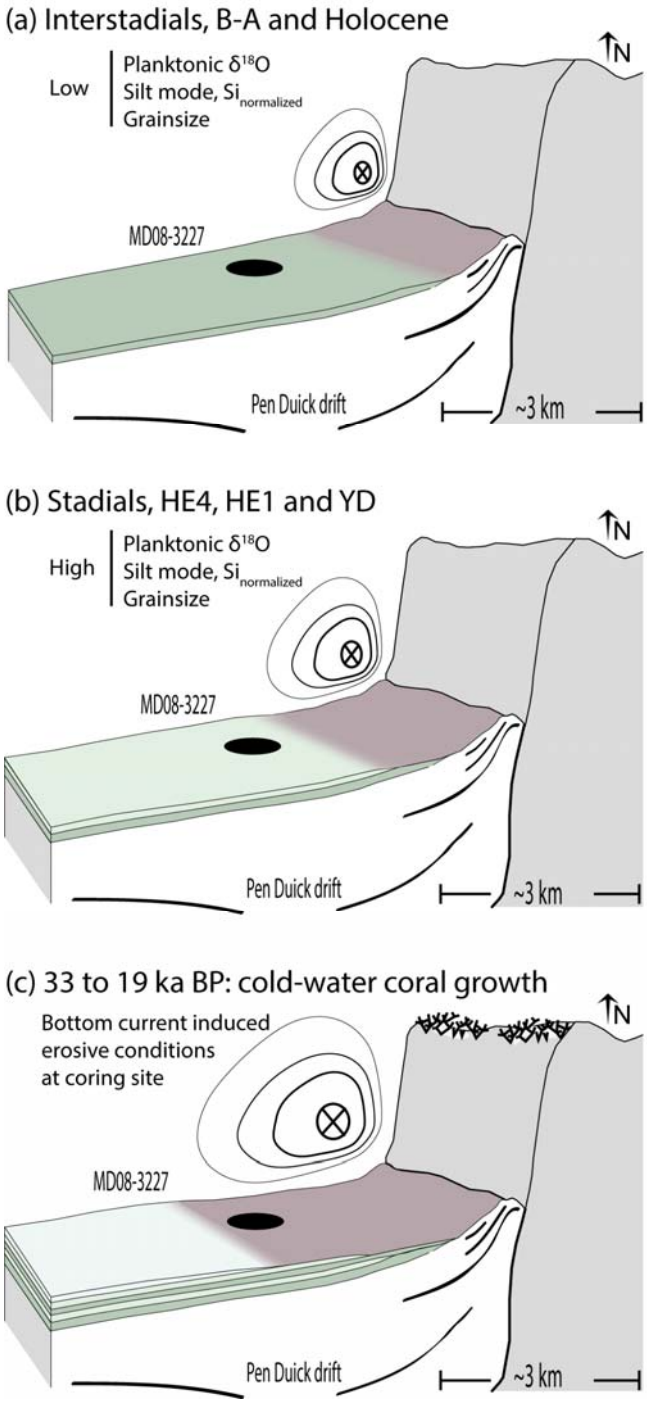

Figure 5.6 Sketch illustrating the different bottom current regimes and associated sedimentation patterns at the foot of the Pen Duick Escarpment. (a) Periods of sluggish bottom currents as recorded during MIS3 interstadials, the B-A and Holocene. The red zonation indicates probable erosive/non-depositional conditions at the foot of the escarpment, where the current lines reach their maximum intensity. (b) Enhanced bottom current conditions during D-O stadials, HE's and YD, as recorded from peaks in grain-size silt mode and XRF $Si_{normalised}$ ratio. The erosive band at the foot of the escarpment may migrate towards the south, but does not affect the coring site where high sedimentation rates remain. (c) Erosive to non-depositional bottom current conditions at coring site, associated to contemporary sustained of cold-water coral growth within the Atlantic Moroccan coral province.

However, the studied sediment core is located from about 2 to 2.5 km south from the Pen Duick drift channel where gentle seismic reflections are observed (Fig. 5.2b; Vandorpe et al., 2014). This implies that erosive and/or non-depositional bottom current conditions have dominated over a rather large area, even though its seismic and lithostratigraphic expression remained subtle. Energetic internal tides are known to from when barotropic tides interact with kilometre-scaled topographic obstacles (Garrett and Kunze, 2007; Turnewitsch et al., 2013). More pronounced internal tides generation may have induced a southward (perpendicular to the Pen Duick Escarpment) migration of the depositional centre, where the flow strength diminishes as a function of the distance from the topographic obstacle (Fig. 5.6; Turnewitsch et al., 2008; García et al., 2009; Peine et al., 2009). Likewise, the hiatus recorded at site MD08-3227 would reflect a 14 ky lasting tide-topography induced erosive and/or non-depositional conditions, indicative for regionally more energetic bottom current regime (Fig. 5.6c; Hernández-Molina et al., 2014; 2016b Rebesco et al., 2014). The late MIS 3 (roughly from 35 ka BP towards the LGM) coincides with a period of attenuation of the D-O cycles amplitude, gradually leading to the onset of the LGM (Pahnke and Zahn, 2005). The D-O cycles attenuation may have been caused by increased AAIW production, associated to sea-level decrease and reduced ocean-atmosphere heat fluxes through heat storage at intermediate (AAIW) water depths (Pahnke and Zahn, 2005; Jung et al., 2010). Accordingly, Dubois-Dauphin et al. (2016) documented increased AAIW advection, respectively at 19, ~23.5 and ~27 ka BP. The gradual onset of the LGM circulation pattern, possibly influenced by sea-level decrease which would have caused the migration of the AAIW/NACW interface, may have been responsible for the onset of erosive and/or non-depositional bottom current conditions.

The onset of bottom current induced erosive and/or non-depositional conditions coincides with a phase of pronounced cold-water coral growth within the Atlantic Moroccan coral province (Fig. 5.5; Wienberg et al., 2010; Vandorpe et al., submitted). Cold-water corals are known to form large coral thickets and exhibit a strong affinity for energetic hydrodynamic conditions (Thiem et al., 2006; Davies et al., 2008; Vertino et al., 2010). At present, *Lophelia pertusa* and *Madrepora oculata*, the dominant cold-water coral species in the Atlantic Moroccan coral province, have been reported in environments where tidally modulated current velocities reach maximum speeds of about 45 cm/s (Mienis et al., 2007; 2014; Dorschel et al., 2009). In those environments, bottom currents are generally energetic enough to induce locally erosive and/or non-depositional conditions in the surrounding area of coral mounds. Erosional threshold velocities at site MD08-3227 were previously inferred to be of at least ~50 cm/s, which is in the same range than present-day cold-water corals environment (White et al., 2005; 2007; Duineveld et al., 2007; Titschack et al., 2015; Wienberg and Titschack, 2015). In the geological record, the best known example reflecting this pattern is the

Belgica mound province (Porcupine Seabight), of which the almost entire cold-water coral growth phase occurred under erosion and/or non-depositional conditions along the adjacent areas (Kano et al., 2007; Huvenne et al., 2009; Thierens et al., 2010; Raddatz et al., 2014; Hebbeln et al., 2016).

5.6 Conclusions

This study provides a millennial-scale record from the Pen Duick drift along the Moroccan Atlantic margin showing pronounced changes in the sedimentation pattern. The action of local bottom currents have promoted the build-up of fast accumulating mud dominated sediment drift, leading to locally high sedimentation rates that reached up to 100 cm/ky. However, this fast accumulating sediment drift is seemingly associated with substantial bottom current reworked sediment inputs, which are thought to have greatly impacted on the planktonic stable isotope record. Shifts towards higher terrigenous, $Si_{normalised}$ content and coarser silt mode were observed during D-O stadials, HE4, HE1 and the YD. Those shifts could be related to the joint effect of increased aeolian dust input and enhanced bottom currents phases which seem to be both correlated over those periods. Bottom currents reached an erosional and/or non-depositional threshold, inferred from the presence of a hiatus extending from 33 to 19 ka BP. The lithological expression of this ~14 ky lasting hiatus corresponded to the accumulation of a 10 cm thick biogenic and terrigenous depleted sand layer. This may emphasize the presence of potentially long-lasting though subtle, hiatuses in otherwise fast accumulating sediment drifts, in particular associated to thin biogenic sandy contourite sequences. The possible occurrence of identification of often subtle hiatuses and bottom current reworked sediment input may become routinely considered when studying contourite drifts.

The overall bottom currents variability is thought to relate to periods of increased AAIW production and advection within the sub-tropical north Atlantic. As a consequence, the Pen Duick drift might further represent the most distal site monitoring the AAIW within the sub-tropical northeast Atlantic. Finally, we find that coral-water coral growth within the Atlantic Moroccan coral mound province mainly occurred during periods of enhanced bottom current regime, while periods of weaker bottom currents show much reduced cold-water coral occurrences. This adds-up to the numerous similar observations from the north Atlantic, emphasizing the importance of enhanced hydrodynamics for cold-water coral growth. It has been now largely evidenced that locally erosive bottom current conditions generally prevail during phases of cold-water coral growth, which in turn are known provides a unique sediment trap through baffling within the coral framework.

Acknowledgements

This study was carried out within the framework of a Ghent University BOF "Starting Grant". It was additionally part of the FWO project Contourite-3D (n° 1524713N). The authors wish to acknowledge the captains and crews of the campaigns on board of the R/V Marion Dufresne cruise MD169-MICROSYSTEMS (founded by ESF EuroDIVERSITY within the framework of project EC FP6 IP HERMES) and of the R/V Belgica cruise 2013/16-COMIC. Shiptime on board R/V Belgica was provided by BELSPO and RBINS–OD Nature.

References

Alonso, B., Ercilla, G., Casas, D., Stow, D.A.V., Rodríguez-Tovar, F.J., Dorador, J., Hernández-Molina, F.-J., 2016. Contourite vs gravity-flow deposits of the Pleistocene Faro Drift (Gulf of Cadiz): Sedimentological and mineralogical approaches. Marine Geology.

Alves, M., Gaillard, F., Sparrow, M., Knoll, M., Giraud, S., 2002. Circulation patterns and transport of the Azores Front-Current system. Deep Sea Research Part II: Topical Studies in Oceanography 49, 3983-4002.

Alves, M.L.G.R., Colin de Verdière, A., 1999. Instability Dynamics of a Subtropical Jet and Applications to the Azores Front Current System: Eddy-Driven Mean Flow. Journal of Physical Oceanography 29, 837-864.

Ambar, I., Serra, N., Neves, F., Ferreira, T., 2008. Observations of the Mediterranean Undercurrent and eddies in the Gulf of Cadiz during 2001. Journal of Marine Systems 71, 195-220.

Anderson, R.F., Ali, S., Bradtmiller, L.I., Nielsen, S.H.H., Fleisher, M.Q., Anderson, B.E., Burckle, L.H., 2009. Wind-Driven Upwelling in the Southern Ocean and the Deglacial Rise in Atmospheric CO2. Science 323, 1443-1448.

Bahr, A., Kaboth, S., Jiménez-Espejo, F.J., Sierro, F.J., Voelker, A.H.L., Lourens, L., Röhl, U., Reichart, G.J., Escutia, C., Hernández-Molina, F.J., Pross, J., Friedrich, O., 2015. Persistent monsoonal forcing of Mediterranean Outflow Water dynamics during the late Pleistocene. Geology.

Baringer, M.O.N., Price, J.F., 1997. Mixing and Spreading of the Mediterranean Outflow. Journal of Physical Oceanography 27, 1654-1677.

Bell, D.B., Jung, S.J.A., Kroon, D., 2015. The Plio-Pleistocene development of Atlantic deep-water circulation and its influence on climate trends. Quaternary Science Reviews 123, 265-282.

Bigg, G.R., Wadley, M.R., 2001. Millennial-scale variability in the oceans: an ocean modelling view. Journal of Quaternary Science 16, 309-319.

Bigg, G.R., Jickells, T.D., Liss, P.S., Osborn, T.J., 2003. The role of the oceans in climate. International Journal of Climatology 23, 1127-1159.

Bohm, E., Lippold, J., Gutjahr, M., Frank, M., Blaser, P., Antz, B., Fohlmeister, J., Frank, N., Andersen, M.B., Deininger, M., 2015. Strong and deep Atlantic meridional overturning circulation during the last glacial cycle. Nature 517, 73-76.

Cacchione, D.A., Pratson, L.F., Ogston, A.S., 2002. The Shaping of Continental Slopes by Internal Tides. Science 296, 724-727.

Carracedo Segade, L.I., Gilcoto, M., Mercier, H., Pérez, F.F., 2015. Quasi-synoptic transport, budgets and water mass transformation in the Azores–Gibraltar Strait region during summer 2009. Progress In Oceanography 130, 47-64.

Carton, X., Chérubin, L., Paillet, J., Morel, Y., Serpette, A., Le Cann, B., 2002. Meddy coupling with a deep cyclone in the Gulf of Cadiz. Journal of Marine Systems 32, 13-42.

Chapman, M.R., Maslin, M.A., 1999. Low-latitude forcing of meridional temperature and salinity gradients in the subpolar North Atlantic and the growth of glacial ice sheets. Geology 27, 875-878.

Cropper, T.E., Hanna, E., Bigg, G.R., 2014. Spatial and temporal seasonal trends in coastal upwelling off Northwest Africa, 1981–2012. Deep Sea Research Part I: Oceanographic Research Papers 86, 94-111.

Davies, A.J., Wisshak, M., Orr, J.C., Murray Roberts, J., 2008. Predicting suitable habitat for the cold-water coral Lophelia pertusa (Scleractinia). Deep Sea Research Part I: Oceanographic Research Papers 55, 1048-1062.

De Mol, L., Hilário, A., Van Rooij, D., Henriet, J.-P., 2012. 46 - Habitat Mapping of a Cold-Water Coral Mound on Pen Duick Escarpment (Gulf of Cadiz) A2 - Baker, Peter T. HarrisElaine K, Seafloor Geomorphology as Benthic Habitat. Elsevier, London, pp. 645-654.

Dorschel, B., Wheeler, A.J., Huvenne, V.A.I., de Haas, H., 2009. Cold-water coral mounds in an erosive environmental setting: TOBI side-scan sonar data and ROV video footage from the northwest Porcupine Bank, NE Atlantic. Marine Geology 264, 218-229.

Dubois-Dauphin, Q., Bonneau, L., Colin, C., Montero-Serrano, J.-C., Montagna, P., Blamart, D., Dierk, H., Van Rooij, D., Hemsing, F., Wefing, A.-M., Frank, N., 2016. South Atlantic intermediate water advances into the North-east Atlantic with reduced Atlantic meridional overturning circulation during the last glacial period. Geochemistry, Geophysics, Geosystems.

Duineveld, G.C.A., Lavaleye, M.S.S., Bergman, M.J.N., de Stigter, H., Mienis, F., 2007. Trophic structure of a cold-water coral mound community (Rockall Bank, NE Atlantic) in relation to the near-bottom particle supply and current regime. Bulletin of Marine Science 81, 449-467.

Eberwein, A., Mackensen, A., 2006. Regional primary productivity differences off Morocco (NW-Africa) recorded by modern benthic foraminifera and their stable carbon isotopic composition. Deep Sea Research Part I: Oceanographic Research Papers 53, 1379-1405.

Eberwein, A., Mackensen, A., 2008. Last Glacial Maximum paleoproductivity and water masses off NW-Africa: Evidence from benthic foraminifera and stable isotopes. Marine Micropaleontology 67, 87-103.

Elliot, M., Labeyrie, L., Duplessy, J.C., 2002. Changes in North Atlantic deep-water formation associated with the Dansgaard-Oeschger temperature oscillations (60-10 ka). Quaternary Science Reviews 21, 1153-1165.

Eynaud, F., de Abreu, L., Voelker, A., Schönfeld, J., Salgueiro, E., Turon, J.-L., Penaud, A., Toucanne, S., Naughton, F., Sánchez Goñi, M.F., Malaizé, B., Cacho, I., 2009. Position of the Polar Front along the western Iberian margin during key cold episodes of the last 45 ka. Geochemistry, Geophysics, Geosystems 10.

Falcini, F., Martorelli, E., Chiocci, F.L., Salusti, E., 2016. A general theory for the effect of local topographic unevenness on contourite deposition around marine capes: An inverse problem applied to the Italian continental margin (Cape Suvero). Marine Geology.

Faugères, J.-C., Stow, D.A.V., Imbert, P., Viana, A.R., 1999. Seismic features diagnostic of contourite drifts. Marine Geology 162, 1-38.

Faugères, J.C., Stow, D.A.V., 2008. Chapter 14 Contourite Drifts: Nature, Evolution and Controls, in: Rebesco, M., Camerlenghi, A. (Eds.), Developments in Sedimentology. Elsevier, pp. 257-288.

Flinch, J., 1993. Tectonic Evolution of the Gibraltar Arc. Rice University, Houston, Texas, p. 381.

Flinch, J.F., Vail, P.R., 1999. Plio-Pleistocene Sequence Stratigraphy and Tectonics of the Gibraltar Arc, Mesozoic and Cenozoic Sequence Stratigraphy of European Basins. SEPM Society for Sedimentary Geology, pp. 199-208.

Foubert, A., Depreiter, D., Beck, T., Maignien, L., Pannemans, B., Frank, N., Blamart, D., Henriet, J.-P., 2008. Carbonate mounds in a mud volcano province off north-west Morocco: Key to processes and controls. Marine Geology 248, 74-96.

Frank, N., Freiwald, A., Lopez-Correa, M., Wienberg, C., Eisele, M., Hebbeln, D., Van Rooij, D., Henriet, J.-P., Colin, C., Van Weering, T., de Haas, H., Buhl-Mortensen, P., Roberts, J.M., De Mol, B., Douville, E., Blamart, D., Hatte, C., 2011. Northeastern Atlantic cold-water coral reefs and climate. Geology 39, 743-746.

Freeman, E., Skinner, L.C., Tisserand, A., Dokken, T., Timmermann, A., Menviel, L., Friedrich, T., 2015. An Atlantic–Pacific ventilation seesaw across the last deglaciation. Earth and Planetary Science Letters 424, 237-244.

García, M., Hernández-Molina, F.J., Llave, E., Stow, D.A.V., León, R., Fernández-Puga, M.C., Diaz del Río, V., Somoza, L., 2009. Contourite erosive features caused by the Mediterranean Outflow Water in the Gulf of Cadiz: Quaternary tectonic and oceanographic implications. Marine Geology 257, 24-40.

Garrett, C., Kunze, E., 2007. Internal Tide Generation in the Deep Ocean. Annual Review of Fluid Mechanics 39, 57-87.

Gonthier, E., Faugères, J.-C., Stow, D.A.V., 1984. Contourite facies of the Faro Drift, Gulf of Cadiz, in: Stow, D.A.V., Piper, D.J.W. (Eds.), Fine Grained Sediments, Deep-Water Processes and Facies. Geological Society, London, pp. 275-291.

Grevemeyer, I., Matias, L., Silva, S., 2016. Mantle earthquakes beneath the South Iberia continental margin and Gulf of Cadiz – constraints from an onshore-offshore seismological network. Journal of Geodynamics.

Hanebuth, T.J.J., Zhang, W., Hofmann, A.L., Löwemark, L.A., Schwenk, T., 2015. Oceanic density fronts steering bottom-current induced sedimentation deduced from a 50 ka contourite-drift record and numerical modeling (off NW Spain). Quaternary Science Reviews 112, 207-225.

Hebbeln, D., Van Rooij, D., Wienberg, C., 2016. Good neighbours shaped by vigorous currents: Cold-water coral mounds and contourites in the North Atlantic. Marine Geology. 378, 171-185.

Heezen, B.C., Hollister, C.D., Ruddiman, W.F., 1966. Shaping of the Continental Rise by Deep Geostrophic Contour Currents. Science 152, 502-508.

Henry, L.G., McManus, J.F., Curry, W.B., Roberts, N.L., Piotrowski, A.M., Keigwin, L.D., 2016. North Atlantic ocean circulation and abrupt climate change during the last glaciation. Science 353, 470-474.

Hernández-Molina, F.J., Llave, E., Stow, D.A.V., Garcia, M., Somoza, L., Vazquez, J.T., Lobo, F.J., Maestro, A., del Rio, V.D., Leon, R., Medialdea, T., Gardner, J., 2006. The contourite depositional system of the Gulf of Cadiz: A sedimentary model related to the bottom current activity of the Mediterranean outflow water and its interaction with the continental margin. Deep-Sea Research Part Ii-Topical Studies in Oceanography 53, 1420-1463.

Hernández-Molina, F.J., Serra, N., Stow, D., Llave, E., Ercilla, G., Van Rooij, D., 2011. Along-slope oceanographic processes and sedimentary products around the Iberian margin. Geo-Marine Letters, 1-27.

Hernández-Molina, F.J., Stow, D.A.V., Alvarez-Zarikian, C.A., Acton, G., Bahr, A., Balestra, B., Ducassou, E., Flood, R., Flores, J.-A., Furota, S., Grunert, P., Hodell, D., Jimenez-Espejo, F., Kim, J.K., Krissek, L., Kuroda, J., Li, B., Llave, E., Lofi, J., Lourens, L., Miller, M., Nanayama, F., Nishida, N., Richter, C., Roque, C., Pereira, H., Sanchez Goñi, M.F., Sierro, F.J., Singh, A.D., Sloss, C., Takashimizu, Y., Tzanova, A., Voelker, A., Williams, T., Xuan, C., 2014. Onset of Mediterranean outflow into the North Atlantic. Science 344, 1244-1250.

Hernández-Molina, F.J., Sierro, F.J., Llave, E., Roque, C., Stow, D.A.V., Williams, T., Lofi, J., Van der Schee, M., Arnáiz, A., Ledesma, S., Rosales, C., Rodríguez-Tovar, F.J., Pardo-Igúzquiza, E., Brackenridge, R.E., 2016a. Evolution of the gulf of Cadiz margin and southwest Portugal contourite depositional system: Tectonic, sedimentary and paleoceanographic implications from IODP expedition 339. Marine Geology.

Hernández-Molina, F.J., Wåhlin, A., Bruno, M., Ercilla, G., Llave, E., Serra, N., Rosón, G., Puig, P., Rebesco, M., Van Rooij, D., Roque, D., González-Pola, C., Sánchez, F., Gómez, M., Preu, B., Schwenk, T., Hanebuth, T.J.J., Sánchez Leal, R.F., García-Lafuente, J., Brackenridge, R.E., Juan, C., Stow, D.A.V., Sánchez-González, J.M., 2016b. Oceanographic processes and morphosedimentary products along the Iberian margins: A new multidisciplinary approach. Marine Geology.

Hernández-Molina, F.J., Hodell, D.A., Stow, D.A.V., Alvarez-Zarikian, C., 2016. Virtual special issue on IODP Expedition 339: The Mediterranean outflow. Marine Geology 377, 1-6.

Hernandez-Molina, J., Llave, E., Somoza, L., Fernandez-Puga, M.C., Maestro, A., Leon, R., Medialdea, T., Barnolas, A., Garcia, M., del Rio, V.D., Fernandez-Salas, L.M., Vazquez, J.T., Lobo, F., Dias, J.M.A., Rodero,

J., Gardner, J., 2003. Looking for clues to paleoceanographic imprints: A diagnosis of the Gulf of Cadiz contourite depositional systems. Geology 31, 19-22.

Hodell, D., Crowhurst, S., Skinner, L., Tzedakis, P.C., Margari, V., Channell, J.E.T., Kamenov, G., Maclachlan, S., Rothwell, G., 2013. Response of Iberian Margin sediments to orbital and suborbital forcing over the past 420 ka. Paleoceanography 28, 185-199.

Hodell, D., Lourens, L., Crowhurst, S., Konijnendijk, T., Tjallingii, R., Jiménez-Espejo, F., Skinner, L., Tzedakis, P.C., Abrantes, F., Acton, G.D., Alvarez Zarikian, C.A., Bahr, A., Balestra, B., Barranco, E.L., Carrara, G., Ducassou, E., Flood, R.D., Flores, J.-A., Furota, S., Grimalt, J., Grunert, P., Hernández-Molina, J., Kim, J.K., Krissek, L.A., Kuroda, J., Li, B., Lofi, J., Margari, V., Martrat, B., Miller, M.D., Nanayama, F., Nishida, N., Richter, C., Rodrigues, T., Rodríguez-Tovar, F.J., Roque, A.C.F., Sanchez Goñi, M.F., Sierro Sánchez, F.J., Singh, A.D., Sloss, C.R., Stow, D.A.V., Takashimizu, Y., Tzanova, A., Voelker, A., Xuan, C., Williams, T., 2015. A reference time scale for Site U1385 (Shackleton Site) on the SW Iberian Margin. Global and Planetary Change 133, 49-64.

Holz, C., Stuut, J.-B.W., Henrich, R., Meggers, H., 2007. Variability in terrigenous sedimentation processes off northwest Africa and its relation to climate changes: Inferences from grain-size distributions of a Holocene marine sediment record. Sedimentary Geology 202, 499-508.

Huang, K.-F., Oppo, D.W., Curry, W.B., 2014. Decreased influence of Antarctic intermediate water in the tropical Atlantic during North Atlantic cold events. Earth and Planetary Science Letters 389, 200-208.

Huvenne, V.A.I., Van Rooij, D., De Mol, B., Thierens, M., O'Donnell, R., Foubert, A., 2009. Sediment dynamics and palaeo-environmental context at key stages in the Challenger cold-water coral mound formation: Clues from sediment deposits at the mound base. Deep Sea Research Part I: Oceanographic Research Papers 56, 2263-2280.

Incarbona, A., Martrat, B., Di Stefano, E., Grimalt, J.O., Pelosi, N., Patti, B., Tranchida, G., 2010. Primary productivity variability on the Atlantic Iberian Margin over the last 70,000 years: Evidence from coccolithophores and fossil organic compounds. Paleoceanography 25.

Iorga, M.C., Lozier, M.S., 1999a. Signatures of the Mediterranean outflow from a North Atlantic climatology 1. Salinity and density fields. Journal of Geophysical Research-Oceans 104, 25985-26009.

Iorga, M.C., Lozier, M.S., 1999b. Signatures of the Mediterranean outflow from a North Atlantic climatology 2. Diagnostic velocity fields. Journal of Geophysical Research-Oceans 104, 26011-26029.

Jia, Y., 2000. Formation of an Azores Current Due to Mediterranean Overflow in a Modeling Study of the North Atlantic. Journal of Physical Oceanography 30, 2342-2358.

Johnson, J., Stevens, I., 2000. A fine resolution model of the eastern North Atlantic between the Azores, the Canary Islands and the Gibraltar Strait. Deep Sea Research Part I: Oceanographic Research Papers 47, 875-899.

Jung, S., Kroon, D., Ganssen, G., Peeters, F., Ganeshram, R., 2010. Southern Hemisphere intermediate water formation and the bi-polar seesaw, PAGES News, pp. 36-38.

Kaboth, S., Bahr, A., Reichart, G.-J., Jacobs, B., Lourens, L.J., 2016. New insights into upper MOW variability over the last 150kyr from IODP 339 Site U1386 in the Gulf of Cadiz. Marine Geology 377, 136-145.

Kano, A., Ferdelman, T.G., Williams, T., Henriet, J.P., Ishikawa, T., Kawagoe, N., Takashima, C., Kakizaki, Y., Abe, K., Sakai, S., Browning, E., Li, X., the IODP Expedition 307 Scientists, 2007. Age constraints on the origin and growth history of a deep-water coral mound in northeast Atlantic drilled during Integrated Ocean Drilling Program Expedition 307. Geology 35, 1051-1054.

Knoll, M., Hernández-Guerra, A., Lenz, B., López Laatzen, F., Machín, F., Müller, T.J., Siedler, G., 2002. The Eastern Boundary Current system between the Canary Islands and the African Coast. Deep Sea Research Part II: Topical Studies in Oceanography 49, 3427-3440.

Kuijpers, A., Nielsen, T., 2015. Near-bottom current speed maxima in North Atlantic contourite environments inferred from current-induced bedforms and other seabed evidence. Marine Geology.

Llave, E., Schönfeld, J., Hernandez-Molina, F.J., Mulder, T., Somoza, L., Diaz-del Rio, V., Sanchez-Almazo, I., 2006. High-resolution stratigraphy of the Mediterranean outflow contourite system in the Gulf of Cadiz during the late Pleistocene: The impact of Heinrich events. Marine Geology 277, 241-262.

Llave, E., Hernandez-Molina, F.J., Somoza, L., Stow, D.A.V., Diaz del Rio, G., 2007. Quaternary evolution of the contourite depositional system in the Gulf of Cadiz, in: Viana, A.R., Rebesco, M. (Eds.), Economic and Palaeoceanographic Significance of Contourite Deposits. Geological Society, London, pp. 49-79.

Llinás, O., Rueda, M.J., Pérez Marrero, J., Pérez-Martell, E., Santana, R., Villagarcía, M.G., Cianca, A., Godoy, J., Maroto, L., 2002. Variability of the Antarctic intermediate waters in the Northern Canary Box. Deep Sea Research Part II: Topical Studies in Oceanography 49, 3441-3453.

Lobo, F.J., Le Roy, P., Mendes, I., Sahabi, M., 2014. Chapter 9 The Gulf of Cádiz continental shelves. Geological Society, London, Memoirs 41, 109-130.

Lofi, J., Voelker, A.H.L., Ducassou, E., Hernández-Molina, F.J., Sierro, F.J., Bahr, A., Galvani, A., Lourens, L.J., Pardo-Igúzquiza, E., Pezard, P., Rodríguez-Tovar, F.J., Williams, T., 2015. Quaternary chronostratigraphic framework and sedimentary processes for the Gulf of Cadiz and Portuguese Contourite Depositional Systems derived from Natural Gamma Ray records. Marine Geology.

Louarn, E., Morin, P., 2011. Antarctic Intermediate Water influence on Mediterranean Sea Water outflow. Deep Sea Research Part I: Oceanographic Research Papers 58, 932-942.

Lynch-Stieglitz, J., Adkins, J.F., Curry, W.B., Dokken, T., Hall, I.R., Herguera, J.C., Hirschi, J.J.M., Ivanova, E.V., Kissel, C., Marchal, O., Marchitto, T.M., McCave, I.N., McManus, J.F., Mulitza, S., Ninnemann, U., Peeters, F., Yu, E.-F., Zahn, R., 2007. Atlantic Meridional Overturning Circulation During the Last Glacial Maximum. Science 316, 66-69.

Machín, F., Pelegrí, J.L., Marrero-Díaz, A., Laiz, I., Ratsimandresy, A.W., 2006. Near-surface circulation in the southern Gulf of Cádiz. Deep Sea Research Part II: Topical Studies in Oceanography 53, 1161-1181.

Machín, F., Pelegrí, J.L., 2009. Northward Penetration of Antarctic Intermediate Water off Northwest Africa. Journal of Physical Oceanography 39, 512-535.

Maldonaldo, A., Somoza, L., Pallarés, L., 1999. The Betic orogen and the Iberain-African boundary in the Gulf of Cadiz: geological evolution (central North Atlantic). Marine Geology 155, 9-43.

Marchitto, T.M., Broecker, W.S., 2006. Deep water mass geometry in the glacial Atlantic Ocean: A review of constraints from the paleonutrient proxy Cd/Ca. Geochemistry, Geophysics, Geosystems 7.

Marchitto, T.M., Lehman, S.J., Ortiz, J.D., Flückiger, J., van Geen, A., 2007. Marine Radiocarbon Evidence for the Mechanism of Deglacial Atmospheric CO2 Rise. Science 316, 1456-1459.

Martínez-Méndez, G., Hebbeln, D., Mohtadi, M., Lamy, F., De Pol-Holz, R., Reyes-Macaya, D., Freudenthal, T., 2013. Changes in the advection of Antarctic Intermediate Water to the northern Chilean coast during the last 970 kyr. Paleoceanography 28, 607-618.

Martrat, B., Grimalt, J.O., Shackleton, N.J., de Abreu, L., Hutterli, M.A., Stocker, T.F., 2007. Four Climate Cycles of Recurring Deep and Surface Water Destabilizations on the Iberian Margin. Science 317, 502-507.

McCave, I.N., Manighetti, B., Robinson, S.G., 1995. Sortable silt and fine sediment size/composition slicing: Parameters for palaeocurrent speed and palaeoceanography. Paleoceanography 10, 593-610.

McCave, I.N., Hall, I.R., 2006. Size sorting in marine muds: Processes, pitfalls, and prospects for paleoflow-speed proxies, Geochemistry Geophysics Geosystems.

McManus, J.F., Francois, R., Gherardi, J.M., Keigwin, L.D., Brown-Leger, S., 2004. Collapse and rapid resumption of Atlantic meridional circulation linked to deglacial climate changes. Nature 428, 834-837.

Medialdea, T., Somoza, L., Pinheiro, L.M., Fernández-Puga, M.C., Vázquez, J.T., León, R., Ivanov, M.K., Magalhaes, V., Díaz-del-Río, V., Vegas, R., 2009. Tectonics and mud volcano development in the Gulf of Cádiz. Marine Geology 261, 48-63.

Mienis, F., de Stigter, H., White, M., Duineveld, G.C.A., de Haas, H., van Weering, T., 2007. Hydrodynamic controls on cold-water coral growth and carbonate-mound development at the SW and SE Rockall Trough Margin, NE Atlantic Ocean. Deep-Sea Research I 54, 1655-1674.

Mienis, F., De Stigter, H.C., De Haas, H., Van der Land, C., Van Weering, T.C.E., 2012. Hydrodynamic conditions in a cold-water coral mound area on the Renard Ridge, southern Gulf of Cadiz. Journal of Marine Systems 96–97, 61-71.

Mienis, F., Duineveld, G.C.A., Davies, A.J., Lavaleye, M.M.S., Ross, S.W., Seim, H., Bane, J., van Haren, H., Bergman, M.J.N., de Haas, H., Brooke, S., van Weering, T.C.E., 2014. Cold-water coral growth under extreme environmental conditions, the Cape Lookout area, NW Atlantic. Biogeosciences 11, 2543-2560.

Millot, C., Candela, J., Fuda, J.-L., Tber, Y., 2006. Large warming and salinification of the Mediterranean outflow due to changes in its composition. Deep Sea Research Part I: Oceanographic Research Papers 53, 656-666.

Montero-Serrano, J.-C., Frank, N., Colin, C., Wienberg, C., Eisele, M., 2011. The climate influence on the mid-depth Northeast Atlantic gyres viewed by cold-water corals. Geophysical Research Letters 38.

Mulder, T., Hassan, R., Ducassou, E., Zaragosi, S., Gonthier, E., Hanquiez, V., Marchès, E., Toucanne, S., 2013. Contourites in the Gulf of Cadiz: a cautionary note on potentially ambiguous indicators of bottom current velocity. Geo-Marine Letters 33, 357-367.

Nelson, C.H., Baraza, J., Maldonaldo, A., 1993. Mediterranean undercurrent sandy contourites, Gulf of Cadiz, Spain. Sedimentary Geology 82, 103-131.

Nelson, C.H., Maldonaldo, A., 1999. The Cadiz margin study off Spain: an introduction. Marine Geology 155, 3-8.

Nichols, G.A., 2009. Sedimentology and Stratigraphy, second ed. Wiley-Blackwell, Chichester (419 pp.).

Pahnke, K., Zahn, R., 2005. Southern Hemisphere Water Mass Conversion Linked with North Atlantic Climate Variability. Science 307, 1741-1746.

Pahnke, K., Goldstein, S.L., Hemming, S.R., 2008. Abrupt changes in Antarctic Intermediate Water circulation over the past 25,000[thinsp]years. Nature Geosci 1, 870-874.

Paillard, D., Labeyrie, L., Yiou, P., 1996. Macintosh Program performs time-series analysis. Eos, Transactions American Geophysical Union 77, 379-379.

Palomino, D., López-González, N., Vázquez, J.-T., Fernández-Salas, L.-M., Rueda, J.-L., Sánchez-Leal, R., Díaz-del-Río, V., 2016. Multidisciplinary study of mud volcanoes and diapirs and their relationship to seepages and bottom currents in the Gulf of Cádiz continental slope (northeastern sector). Marine Geology 378, 196-212.

Pelegri, J.L., Aristegui, J., Cana, L., Gonzalez-Davila, M., Hernandez-Guerra, A., Hernandez-Leon, S., Marrero-Diaz, A., Montero, M.F., Sangra, P., Santana-Casiano, M., 2005. Coupling between the open ocean and the coastal upwelling region off northwest Africa: water recirculation and offshore pumping of organic matter. Journal of Marine Systems 54, 3-37.

Peliz, A., Marchesiello, P., Santos, A.M.P., Dubert, J., Teles-Machado, A., Marta-Almeida, M., Le Cann, B., 2009. Surface circulation in the Gulf of Cadiz: 2. Inflow-outflow coupling and the Gulf of Cadiz slope current. Journal of Geophysical Research: Oceans 114.

Peliz, Á., Dubert, J., Santos, A.M.P., Oliveira, P.B., Le Cann, B., 2005. Winter upper ocean circulation in the Western Iberian Basin—Fronts, Eddies and Poleward Flows: an overview. Deep Sea Research Part I: Oceanographic Research Papers 52, 621-646.

Penaud, A., Eynaud, F., Turon, J.L., Blamart, D., Rossignol, L., Marret, F., Lopez-Martinez, C., Grimalt, J.O., Malaizé, B., Charlier, K., 2010. Contrasting paleoceanographic conditions off Morocco during Heinrich events (1 and 2) and the Last Glacial Maximum. Quaternary Science Reviews 29, 1923-1939.

Penaud, A., Eynaud, F., Voelker, A., Kageyama, M., Marret, F., Turon, J.L., Blamart, D., Mulder, T., Rossignol, L., 2011. Assessment of sea surface temperature changes in the Gulf of Cadiz during the last 30 ka: implications for glacial changes in the regional hydrography. Biogeosciences 8, 2295-2316.

Peine, F., Turnewitsch, R., Mohn, C., Reichelt, T., Springer, B., Kaufmann, M., 2009. The importance of tides for sediment dynamics in the deep sea—Evidence from the particulate-matter tracer 234Th in deep-sea environments with different tidal forcing. Deep Sea Research Part I: Oceanographic Research Papers 56, 1182-1202.

Pflaumann, U., Sarnthein, M., Chapman, M., d'Abreu, L., Funnell, B., Huels, M., Kiefer, T., Maslin, M., Schulz, H., Swallow, J., van Kreveld, S., Vautravers, M., Vogelsang, E., Weinelt, M., 2003. Glacial North Atlantic: Sea-surface conditions reconstructed by GLAMAP 2000. Paleoceanography 18.

Pingree, R.D., Le Cann, B., 1990. Structure, strength and seasonality of the slope currents in the Bay of Biscay region. Journal of the Marine Biological Association of the United Kingdom 70, 857-885.

Pomar, L., Morsilli, M., Hallock, P., Bádenas, B., 2012. Internal waves, an under-explored source of turbulence events in the sedimentary record. Earth-Science Reviews 111, 56-81.

Raddatz, J., Rüggeberg, A., Liebetrau, V., Foubert, A., Hathorne, E.C., Fietzke, J., Eisenhauer, A., Dullo, W.-C., 2014. Environmental boundary conditions of cold-water coral mound growth over the last 3 million years in the Porcupine Seabight, Northeast Atlantic. Deep Sea Research Part II: Topical Studies in Oceanography 99, 227-236.

Rahmstorf, S., 2002. Ocean circulation and climate during the past 120,000 years. Nature 419, 207-214.

Ravelo, A.C., Hillaire-Marcel, C., 2007. Chapter Eighteen The Use of Oxygen and Carbon Isotopes of Foraminifera in Paleoceanography, in: Claude, H.M., Anne De, V. (Eds.), Developments in Marine Geology. Elsevier, pp. 735-764.

Rebesco, M., Hernández-Molina, F.J., Van Rooij, D., Wåhlin, A., 2014. Contourites and associated sediments controlled by deep-water circulation processes: State-of-the-art and future considerations. Marine Geology 352, 111-154.

Reimer, P.J., Bard, E., Bayliss, A., Beck, J.W., Blackwell, P.G., Bronk Ramsey, C., Buck, C.E., Cheng, H., Edwards, R.L., Friedrich, M., Grootes, P.M., Guilderson, T.P., Haflidason, H., Hajdas, I., Hatté, C., Heaton, T.J., Hoffmann, D.L., Hogg, A.G., Hughen, K.A., Kaiser, K.F., Kromer, B., Manning, S.W., Niu, M., Reimer, R.W., Richards, D.A., Scott, E.M., Southon, J.R., Staff, R.A., Turney, C.S.M., van der Plicht, J., 2013. IntCal13 and Marine13 Radiocarbon Age Calibration Curves 0–50,000 Years cal BP.

Richter, T.O., van der Gaast, S., Koster, B., Vaars, A., Gieles, R., de Stigter, H.C., De Haas, H., van Weering, T.C.E., 2006. The Avaatech XRF Core Scanner: technical description and applications to NE Atlantic sediments, in: Rothwell, R.G. (Ed.), New techniques in Sediment Core Analysis. Geological Society, London, pp. 39-50.

Rodrigo-Gámiz, M., Martínez-Ruiz, F., Rodríguez-Tovar, F.J., Jiménez-Espejo, F.J., Pardo-Igúzquiza, E., 2014. Millennial- to centennial-scale climate periodicities and forcing mechanisms in the westernmost Mediterranean for the past 20,000 yr. Quaternary Research 81, 78-93.

Rogerson, M., Rohling, E.J., Weaver, P.P.E., Murray, J.W., 2004. The Azores Front since the Last Glacial Maximum. Earth and Planetary Science Letters 222, 779-789.

Rogerson, M., Rohling, E.J., Weaver, P.P.E., 2006. Promotion of meridional overturning by Mediterranean-derived salt during the last deglaciation. Paleoceanography 21.

Rogerson, M., Rohling, E.J., Bigg, G.R., Ramirez, J., 2012. Paleoceanography of the Atlantic-Mediterranean exchange: Overview and first quantitative assessment of climatic forcing. Reviews of Geophysics 50, RG2003.

Rohling, E.J., Foster, G.L., Grant, K.M., Marino, G., Roberts, A.P., Tamisiea, M.E., Williams, F., 2014. Sea-level and deep-sea-temperature variability over the past 5.3 million years. Nature 508, 477-482.

Schönfeld, J., 1997. The impact of the Mediterranean Outflow Water (MOW) on the benthic foraminiferal assemblages and surface sediments at te southern Portuguese continental margin. Marine Micropaleontology 29, 211-236.

Schönfeld, J., Zahn, R., 2000. Late Glacial to Holocene history of the Mediteranean Outflow. Evidence from benthic foraminiferal assemblages and stable isotopes at the Portuguese margin. Palaeogeography, Palaeoclimatology, Palaeoecology 159, 85-111.

Serra, N., Ambar, I., Boutov, D., 2010. Surface expression of Mediterranean Water dipoles and their contribution to the shelf/slope – open ocean exchange. Ocean Sci. 6, 191-209.

Shackleton, N.J., 1987. Oxygen Isotopes, Ice Volume and Sea-Level. Quaternary Science Reviews 6, 183-190.

Shackleton, N.J., Hall, M.A., Vincent, E., 2000. Phase relationships between millennial-scale events 64,000-24,000 years ago. Paleoceanography 15, 565-569.

Shanmugam, G., 2012. Handbook of Petroleum Exploration and Production, 9. Elsevier.

Shanmugam, G., 2013. Modern internal waves and internal tides along oceanic pycnoclines: Challenges and implications for ancient deep-marine baroclinic sands. AAPG Bulletin 97, 799-843.

Sierro, F.J., Flores, J.A., Baraza, J., 1999. Late glacial to recent paleoenvironmental changes in the Gulf of Cadiz anf formation of sandy contourite layers. Marine Geology 155, 157-172.

Singh, A.D., Rai, A.K., Tiwari, M., Naidu, P.D., Verma, K., Chaturvedi, M., Niyogi, A., Pandey, D., 2015. Fluctuations of Mediterranean Outflow Water circulation in the Gulf of Cadiz during MIS 5 to 7: Evidence from benthic foraminiferal assemblage and stable isotope records. Global and Planetary Change 133, 125-140.

Skinner, L.C., Fallon, S., Waelbroeck, C., Michel, E., Barker, S., 2010. Ventilation of the Deep Southern Ocean and Deglacial CO2 Rise. Science 328, 1147-1151.

Snoussi, M., Jouanneau, J.M., Latouche, C., 1990. Flux de matières issues de bassins versants de zones semi-arides (Bassins du Sebou et du Souss, Maroc). Importance dans le bilan global des apports d'origine continentale parvenant à l'Océan Mondial. Journal of African Earth Sciences (and the Middle East) 11, 43-54.

Somoza, L., Diaz-del Rio, V., Leon, R., Ivanov, M.K., Fernandez-Puga, M.C., Gardner, J., Hernandez-Molina, F.J., Pinheiro, L., Rodero, J., Lobato, A., Maestro, A., Vazquez, J.T., Medialdea, T., Fernandez-Salas, L.M., 2003. Seabed morphology and hydrocarbon seepage in the Gulf of Cadiz mud volcano area: Acoustic imagery, multibeam and ultra-high resolution seismic data. Marine Geology 195, 153-176.

Stocker, T.F., Johnsen, S.J., 2003. A minimum thermodynamic model for the bipolar seesaw. Paleoceanography 18.

Stow, D.A.V., Lovell, J.B.P., 1979. Contourites: Their Recognition in Modern and Ancient Sediments. Earth-Science Reviews 14, 251-291.

Stow, D.A.V., Faugères, J.-C., Howe, J.A., Pudsey, C.J., Viana, A.R., 2002a. Bottom currents, contourites and deep-sea sediment drifts: current state-of-the-art, in: Stow, D.A.V., Pudsey, C.J., Howe, J.A., Faugères, J.-C., Viana, A.R. (Eds.), Deep-Water Contourite Systems: Modern Drifts and Ancient Series, Seismic and Sedimentary Characteristics. Geological Society, London, pp. 7-20.

Stow, D.A.V., Pudsey, C.J., Howe, J.A., Faugères, J.-C., Viana, A.R., 2002b. Deep-Water Contourite Systems: Modern Drifts and Ancient Series, Seismic and Sedimentary characteristics. Geological Society, London.

Stow, D.A.V., Faugères, J.C., 2008. Chapter 13 Contourite Facies and the Facies Model, in: Rebesco, M., Camerlenghi, A. (Eds.), Developments in Sedimentology. Elsevier, pp. 223-256.

Stow, D.A.V., Hernandez-Molina, F.J., Llave, E., Sayago-Gil, M., del Rio, V.D., Branson, A., 2009. Bedform-velocity matrix: The estimation of bottom current velocity from bedform observations. Geology 37, 327-330.

Stow, D.A.V., Hernández-Molina, F.J., Alvarez Zarikian, C.A., Scientists, t.E., 2013a. Proceedings IODP, 339. Integrated Ocean Drilling Program Management International, Tokyo.

Stow, D.A.V., Hernández-Molina, F.J., Llave, E., Bruno, M., García, M., Díaz del Rio, V., Somoza, L., Brackenridge, R.E., 2013b. The Cadiz Contourite Channel: Sandy contourites, bedforms and dynamic current interaction. Marine Geology 343, 99-114.

Takashimizu, Y., Kawamura, R., Rodríguez-Tovar, F.J., Dorador, J., Ducassou, E., Hernández-Molina, F.J., Stow, D.A.V., Alvarez-Zarikian, C.A., 2016. Reworked tsunami deposits by bottom currents: Circumstantial evidences from Late Pleistocene to Early Holocene in the Gulf of Cádiz. Marine Geology 377, 95-109.

Thiem, Ø., Ravagnan, E., Fosså, J.H., Berntsen, J., 2006. Food supply mechanisms for cold-water corals along a continental shelf edge. Journal of Marine Systems 60, 207-219.

Thierens, M., Titschack, J., Dorschel, B., Huvenne, V.A.I., Wheeler, A.J., Stuut, J.B., O'Donnell, R., 2010. The 2.6 Ma depositional sequence from the Challenger cold-water coral carbonate mound (IODP Exp. 307): Sediment contributors and hydrodynamic palaeo-environments. Marine Geology 271, 260-277.

Thomson, J., Nixon, S., Summerhayes, C.P., Schönfeld, J., Zahn, R., Grootes, P., 1999. Implications for sedimentation changes on the Iberian margin over the last two glacial/interglacial transitions from (230Thexcess)0 systematics. Earth and Planetary Science Letters 165, 255-270.

Thornalley, D.J.R., Bauch, H.A., Gebbie, G., Guo, W., Ziegler, M., Bernasconi, S.M., Barker, S., Skinner, L.C., Yu, J., 2015. A warm and poorly ventilated deep Arctic Mediterranean during the last glacial period. Science 349, 706-710.

Titschack, J., Baum, D., De Pol-Holz, R., López Correa, M., Forster, N., Flögel, S., Hebbeln, D., Freiwald, A., 2015. Aggradation and carbonate accumulation of Holocene Norwegian cold-water coral reefs. Sedimentology 62, 1873-1898.

Tjallingii, R., Claussen, M., Stuut, J.B.W., Fohlmeister, J., Jahn, A., Bickert, T., Lamy, F., Rohl, U., 2008. Coherent high- and low-latitude control of the northwest African hydrological balance. Nature Geoscience 1, 670-675.

Toucanne, S., Mulder, T., Schönfeld, J., Hanquiez, V., Gonthier, E., Duprat, J., Cremer, M., Zaragosi, S., 2007. Contourites of the Gulf of Cadiz: A high-resolution record of the paleocirculation of the Mediterranean outflow water during the last 50,000 years. Palaeogeography, Palaeoclimatology, Palaeoecology 246, 354-366.

Turnewitsch, R., Reyss, J.-L., Nycander, J., Waniek, J.J., Lampitt, R.S., 2008. Internal tides and sediment dynamics in the deep sea—Evidence from radioactive 234Th/238U disequilibria. Deep Sea Research Part I: Oceanographic Research Papers 55, 1727-1747.

Turnewitsch, R., Falahat, S., Nycander, J., Dale, A., Scott, R.B., Furnival, D., 2013. Deep-sea fluid and sediment dynamics—Influence of hill- to seamount-scale seafloor topography. Earth-Science Reviews 127, 203-241.

Van Rensbergen, P., Depreiter, D., Pannemans, B., Henriet, J.-P., 2005a. Seafloor expression of sediment extrusion and intrusion at the El Arraiche mud volcano field, Gulf of Cadiz. Journal of Geophysical Research 110, F02010.

Van Rensbergen, P., Depreiter, D., Pannemans, B., Moerkerke, G., Van Rooij, D., Marsset, B., Akhmanov, G., Blinova, V., Ivanov, M.K., Rachidi, M., Magalhaes, V., Pinheiro, L., Henriet, J.-P., 2005b. The El Arraiche mud volcano field at the Moroccan Atlantic slope, Gulf of Cadiz. Marine Geology 219, 1-17.

Van Rooij, D., Blamart, D., De Mol, L., Mienis, F., Pirlet, H., Wehrmann, L.M., Barbieri, R., Maignien, L., Templer, S.P., de Haas, H., Hebbeln, D., Frank, N., Larmagnat, S., Stadnitskaia, A., Stivaletta, N., van Weering, T., Zhang, Y., Hamoumi, N., Cnudde, V., Duyck, P., Henriet, J.P., 2011. Cold-water coral mounds on the Pen Duick Escarpment, Gulf of Cadiz: The MiCROSYSTEMS project approach. Marine Geology 282, 102-117.

Vandorpe, T., Van Rooij, D., de Haas, H., 2014. Stratigraphy and paleoceanography of a topography-controlled contourite drift in the Pen Duick area, southern Gulf of Cádiz. Marine Geology 349, 136-151.

Vandorpe, T., Martins, I., Vitorino, J., Hebbeln, D., García, M., Van Rooij, D., 2016. Bottom currents and their influence on the sedimentation pattern in the El Arraiche mud volcano province, southern Gulf of Cadiz. Marine Geology 378, 114-126.

Vandorpe, T., Wienberg, C., Hebbeln, D., Van den Berghe, M., Gaide, S., Wintersteller, P., Van Rooij, D., submitted. Initiation and aggradation of buried cold-water corals mounds in the Atlantic Moroccan Coral Province, southern Gulf of Cádiz. Palaeogeaography, Palaeoclimatology, palaeoecology.

Vertino, A., Savini, A., Rosso, A., Di Geronimo, I., Mastrototaro, F., Sanfilippo, R., Gay, G., Etiope, G., 2010. Benthic habitat characterization and distribution from two representative sites of the deep-water SML Coral Province (Mediterranean). Deep Sea Research Part II: Topical Studies in Oceanography 57, 380-396.

Voelker, A.H.L., Lebreiro, S.M., Schonfeld, J., Cacho, I., Erlenkeuser, H., Abrantes, F., 2006. Mediterranean outflow strengthening during northern hemisphere coolings: A salt source for the glacial Atlantic? Earth and Planetary Science Letters 245, 39-55.

Waelbroeck, C., Labeyrie, L., Michel, E., Duplessy, J.C., McManus, J.F., Lambeck, K., Balbon, E., Labracherie, M., 2002. Sea-level and deep water temperature changes derived from benthic foraminifera isotopic records. Quaternary Science Reviews 21, 295-305.

Wainer, I., Goes, M., Murphy, L.N., Brady, E., 2012. Changes in the intermediate water mass formation rates in the global ocean for the Last Glacial Maximum, mid-Holocene and pre-industrial climates. Paleoceanography 27.

Weinelt, M., Vogelsang, E., Kucera, M., Pflaumann, U., Sarnthein, M., Voelker, A., Erlenkeuser, H., Malmgren, B.A., 2003. Variability of North Atlantic heat transfer during MIS 2. Paleoceanography 18.

Weltje, G.J., Tjallingii, R., 2008. Calibration of XRF core scanners for quantitative geochemical logging of sediment cores: Theory and application. Earth and Planetary Science Letters 274, 423-438.

White, M., Mohn, C., de Stigter, H., Mottram, G., 2005. Deep-water coral development as a function of hydrodynamics and surface productivity around the submarine banks of the Rockall Trough, NE Atlantic, in: Freiwald, A., Roberts, J.M. (Eds.), Cold-Water Corals and Ecosystems. Springer Berlin Heidelberg, pp. 503-514.

White, M., Roberts, J.M., van Weering, T., 2007. Do bottom-intensified diurnal tidal currents shape the alignment of carbonate mounds in the NE Atlantic? Geo-Marine Letters 27, 391-397.

Wienberg, C., Hebbeln, D., Fink, H.G., Mienis, F., Dorschel, B., Vertino, A., Correa, M.L., Freiwald, A., 2009. Scleractinian cold-water corals in the Gulf of Cádiz--First clues about their spatial and temporal distribution. Deep Sea Research Part I: Oceanographic Research Papers 56, 1873-1893.

Wienberg, C., Frank, N., Mertens, K.N., Stuut, J.-B., Marchant, M., Fietzke, J., Mienis, F., Hebbeln, D., 2010. Glacial cold-water coral growth in the Gulf of Cádiz: Implications of increased palaeo-productivity. Earth and Planetary Science Letters 298, 405-416.

Wienberg, C., Titschack, J., 2015. Framework-Forming Scleractinian Cold-Water Corals Through Space and Time: A Late Quaternary North Atlantic Perspective, in: Rossi, S., Bramanti, L., Gori, A., Orejas Saco del Valle, C. (Eds.), Marine Animal Forests: The Ecology of Benthic Biodiversity Hotspots. Springer International Publishing, Cham, pp. 1-34.

Zhang, W., Hanebuth, T.J.J., Stöber, U., 2015. Short-term sediment dynamics on a meso-scale contourite drift (off NW Iberia): Impacts of multi-scale oceanographic processes deduced from the analysis of mooring data and numerical modelling. Marine Geology.

Ziegler, M., Diz, P., Hall, I.R., Zahn, R., 2013. Millennial-scale changes in atmospheric CO2 levels linked to the Southern Ocean carbon isotope gradient and dust flux. Nature Geosci 6, 457-461.

CHAPTER 6

Early-middle Pleistocene Mediterranean Outflow Water controlled sedimentation along the Moroccan Atlantic Margin

The material and dataset presented in this chapter is being further studied and complemented within the framework of a Master thesis at the Department of Geology of Ghent University. The additional data and revised form of this manuscript will be considered for publication in Marine Geology.

Abstract

Based on the sedimentological analysis of a long piston core recovered from the Atlantic Moroccan margin (35°12'N, 968 m water depth), this study investigates the sedimentary environment variability at water depths currently influenced by the regular incursion of Mediterranean mesoscale eddies. Sediment spectrophotometry lightness, XRF Fe/Ca ratio, as well as coccolith assemblages indicate that the sediment core is characterised by overall low sedimentation rates, and covers the middle/upper Quaternary from about 1650 ka BP to recent. The sediment physical and geochemical properties indicate the presence of an obliquity and precessional climatic modulation, which is particularly well expressed from ~1650 to 1200 ka BP. This climate modulation is being gradually altered during the Early-Middle Pleistocene Transition, from about 1200 to 500 ka BP. Within this interval, variations in the terrigenous clay and silt grain-size distribution (ranging from ~4 to 30 μm) are largely associated with the variable occurrence of discontinuous silt lenses and foraminifera rich sandy pockets, rust coloured and moderately bioturbated horizons. Those intervals were inferred to be associated with decreased sedimentation rates (generally <1cm/ky), and are interpreted to correspond to silty and sandy calcareous contouritic sequences. The evolution of the sedimentary facies indicate the presence of gradually more energetic bottom currents as glaciations gradually became more pronounced during the Early-Middle Pleistocene Transition. From about 460 ka BP, an abrupt facies change, associated with the emplacement of coarse sand layer, most probably reflects the occurrence of a seismically triggered mass wasting event. Such event could represent a local analogue to the Late Quaternary Discontinuity, which was widely documented along the northern Gulf of Cádiz Contourite Depositional System. Subsequently, no climatic signal could be recognized within the upper 450 cm bsf sequence, which nevertheless could be inferred to an age younger than ~460 ka BP. This could reflect the onset of more energetic bottom currents, caused by changes in the circulation pattern, or alternatively by changes in the local slope gradient associated to a margin wide tectonic adjustment. Gradually more pronounced sea-level decreases during glacial intervals are thought to have influenced the MOW flow towards higher velocities, causing increased formation rate of Mediterranean mesoscale eddies. More prominent incursion of Mediterranean eddies is thought to have influenced the local pycnal gradient, causing enhanced tide-topography interactions and internal wave processes.

Contributions

This manuscript was written by S. Delivet. Analyses were conducted by S. Delivet and L. Beaufort in consultation with D. Van Rooij, D. Blamart and F. Bassinot and facilitated by F. Mienis, J-B. Stuut. Interpretation and discussion of results were done by S. Delivet, D. Van Rooij and F. Bassinot.

6.1 Introduction

Dominated by the exchanges between the Atlantic Ocean and the Mediterranean Sea, the circulation pattern of the Gulf of Cádiz is among the most complex worldwide (Peliz et al., 2007). The overflow of deep Mediterranean water from the Strait of Gibraltar, so-called Mediterranean Outflow Water (MOW), forms a prominent salinity anomaly into the intermediate north Atlantic (Iorga and Lozier, 1999). Nowadays, a substantial portion of the MOW evolves as a poleward geostrophic undercurrent which can be traced as far as 55°N, and that is transferred to key sites of production of North Atlantic Deep Water (Reid, 1979; New et al., 2001; Bigg et al., 2003; Lozier and Nicole, 2008; Bozec et al., 2011; Rogerson et al., 2012). Another important portion is known to detach from the geostrophic limb through the formation of MOW derived mesoscale eddies (Mediterranean eddies), and to propagate southwestward into the open Atlantic Ocean (Ambar et al., 2008; Serra et al., 2002; 2005; 2010). This eddy-driven flow (Rhines and Holland, 1979; Dewar and Meng, 1995) is responsible for the presence of an ~1200 m water depth MOW salinity anomaly which can be traced as far as 10°N and ~20°W (Mazé et al., 1997; Iorga and Lozier, 1999; Alves et al., 2011). Therefore, the distribution of the MOW within the north Atlantic Ocean also depends on the formation rate of Mediterranean eddies, their pathway and subsequent dissipation (Richardson et al., 2000; Bozec et al., 2011; Barbosa Aguiar et al., 2013).

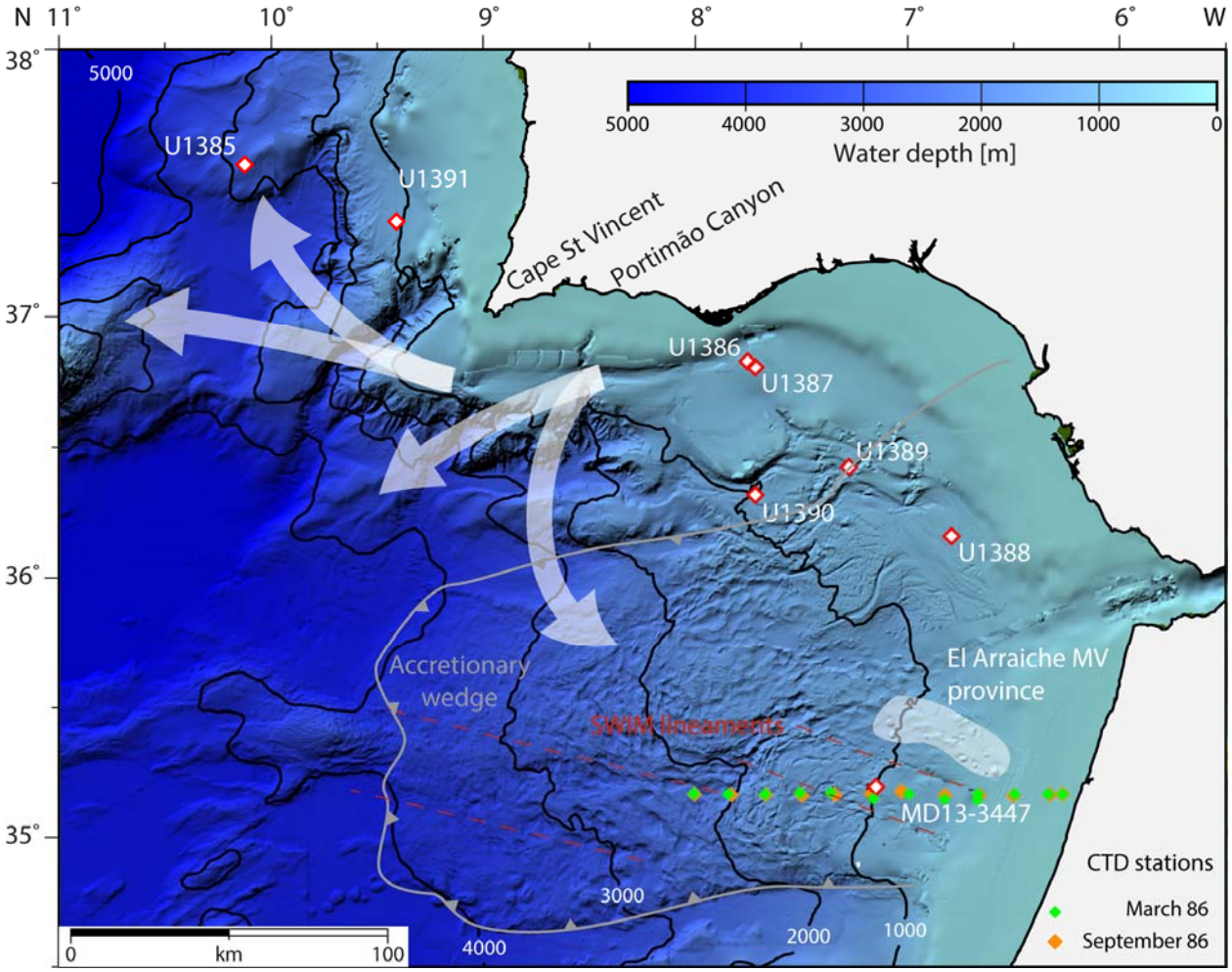

Figure 6.1 Bathymetric map showing the position of core MD13-3447 with respect to the El Arraiche mud volcano province. The limits of the Gibraltar Arc accretionary wedge and the SWIM lineaments are indicated after (Zitellini et al., 2009). IODP Exp 339 sites are indicated by red diamonds (Hernández-Molina et al., 2016b). The white arrows indicate the present-days main areas of generation of MOW-derived mesoscale eddies and their respective pathways (Serra et al., 2005). The orange (green) diamonds indicate the location of the CTD stations from September (March) 1986, respectively (World Ocean Database, 2013).

Up to now, many studies have focused on the MOW variability along its northward geostrophic pathway. It is known to be associated with enhanced bottom currents which governed the formation of a Plio-Pleistocene Contourite Depositional Complex along the northwest European margin (Van Rooij et al., 2007; 2010; Khélifi et al., 2014; Hernández-Molina et al., 2011; 2016a, b; Delivet et al., 2016). Within the Porcupine Seabight, the MOW has established favourable hydrodynamic conditions for the development of benthic cold-water corals (CWC) ecosystems and the rapid accumulation coral mounds (Rice et al., 1990; White and Dorschel, 2010; Mohn et al., 2014; Raddatz et al., 2014; Wienberg and Titschack, 2015; Hebbeln et al., 2016). In contrast, only few studies have focused on the MOW variability along its (eddy-driven) southern pathway. Furthermore, the few studies referring to the past variability of the MOW south of the Strait of Gibraltar largely remained limited to the last

climate cycle (Zahn and Sarnthein, 1987; Eberwein and Mackensen, 2008; Montero-Serrano et al., 2011). Such contrast may be partly attributed to the absence of clearly identified MOW-induced sediment drift along the northwest African margin. Few multi-disciplinary studies have been able to describe the impact of propagating mesoscale eddies on the bottom current regime, and ultimately the sedimentation pattern (Turnewitsch et al., 2004; Hanebuth et al., 2015; Zhang et al., 2015). Nevertheless, the influence of the Mediterranean eddies along the northwest African margin, as well as their impact on the sedimentation most probably constitutes the largest knowledge gap regarding the palaeo-oceanography of the MOW (Rogerson et al., 2012).

Recently, large fields of small-scaled and partly buried CWC mounds were discovered within the proximal area south of the Strait of Gibraltar (roughly at 35.5°N), within depths ranging between ~500 and 1100 m (Foubert et al., 2008; Van Rooij et al., 2014; Vandorpe et al., 2015; submitted). These CWC mounds developed along well defined stratigraphic levels suggesting an important environmental control (Vandorpe et al., submitted). CWC mounds composition typically consists of a mixture of CWC framework embedded in a sediment matrix (Rüggeberg et al., 2007; Titschack et al., 2009; Thierens et al., 2013). Their development is known to strongly depend on the hydrodynamic regime, which plays a role in terms of nutrient availability for the living CWC, as well as sediment supply for the stabilization of the coral framework (Wienberg and Titschack, 2015; Hebbeln et al., 2016). The fields of small-scaled CWC mounds are located roughly west/southwest of the El Arraiche mud volcano province (Fig. 6.1), currently influenced by the regular incursion of Mediterranean eddies at depths ranging from 800 to 1200 m (Mienis et al., 2012; Vandorpe et al., 2015). The question thus arises about the role the MOW may have played in the development of the CWC mounds of this area, by analogy with the CWC mounds of the Porcupine Seabight (Van Rooij et al., 2011). The Mediterranean eddies are known to be associated with azimuthal velocities up to 20 cm/s within the central part of the Gulf of Cádiz (Ambar et al., 2008; Serra et al., 2010). Such velocities may induce contouritic processes (Stow et al., 2009; Rebesco et al., 2014; Kuijpers and Nielsen, 2015; Hernández-Molina et al., 2016a), and may have positively influenced the regional bottom current regime for the growth of CWC and coral mound accretion (Mienis et al., 2007; Mienis et al., 2009; Wienberg and Titschack, 2015; Hebbeln et al., 2016). Additionally, the Mediterranean eddies are responsible for the presence of a variable, though persistent, MOW salinity anomaly ranging from 800 to 1200 m water depth (Fig. 6.2; Carton et al., 2002; Serra et al., 2005; 2010; Mienis et al., 2012; Vandorpe et al., 2015). Such salinity anomaly influences the local vertical pycnal gradient, which may in turn result in enhanced internal tide regime and associated tide-topographic interactions (Cacchione et al., 2002; Pomar et al., 2012; Shanmugam, 2013). Internal tides already have been cited to locally drive the sedimentation pattern and architecture in the El Arraiche mud

volcano province, although the bottom current variability below 800 m water depth remains relatively unconstrained (Mienis et al., 2012; Vandorpe et al., 2015). Yet, only few indications of bottom currents associated to the buried CWC mounds were found (Vandorpe et al., submitted).

The aim of this study is to investigate the past variability of the bottom current regime at a site currently influenced by the Mediterranean eddies within the Moroccan Atlantic margin. As such, this study constitutes the first sedimentological assessment of Mediterranean eddies induced bottom currents within the southern Gulf of Cádiz, and may provide valuable information on the past depositional environment variability in which the local CWC mounds developed. In a second step, the obtained record is compared to results from IODP Exp. 339, in order to establish if there exist a connection between the northern Gulf of Cádiz Contourite Depositional System and the bottom current evolution within its southern counterpart.

6.2 Regional setting

6.2.1 Geological setting

The present day geomorphological structure of the northern Gulf of Cádiz greatly relates to the regional tectonic forces, the Neogene mud-volcano and fluid venting activity, and to the onset of the MOW since the re-opening of the Strait of Gibraltar at 5.33 Ma (Hernández-Molina et al., 2016c; Palomino et al., 2016). The studied area is located about 15 km southwest of the El Arraiche mud volcano province (Fig. 6.1), of which the Plio-Pleistocene evolution has responded to a similar interactions between tectonic, fluids venting activity and variable hydrodynamic regime (Van Rensbergen et al., 2005; Van Rooij et al., 2011; Vandorpe et al., 2015). The tectonic regime is associated to the convergence between the African and Eurasian plates, and has been active from the Mesozoic to present, resulting in the formation of the present day Gibraltar Arc and accretionary wedge (Fig. 6.1; Flinch, 1993; Flinch and Vail, 1999; Medialdea et al., 2009). The studied sediment core was recovered from 968 m water depth, on the gently north-westward dipping (~1.5°) flank of a slightly elevated ridge (Fig. 6.1). This ridge is formed within a narrow seismogenic corridor, associated with the presence of a linear strike-slip fault zone referred to as the SWIM lineaments (Fig. 6.1; Zitellini et al., 2009; Grevemeyer et al., 2016).

The core was recovered in a hemipelagic environment influenced by a sub-humid climate regime (Snoussi et al., 1990; Penaud et al., 2010). Aeolian and riverine input locally induced high to very high sedimentation rates, ranging from 25 to 100 cm/ky (Penaud et al., 2010; Wienberg et al., 2010). Topographically driven sediment drifts were largely recognized at depths ranging from 800 to 300 m whereas little geomorphological evidences of bottom current activity could be evidenced

below this range (Vandorpe et al., 2015; submitted). Within the El Arraiche mud volcano province, the development of contourite drifts is thought to have begun with the onset of the Quaternary at ~2.7 Ma, under the influence of the Antarctic Intermediate Water (AAIW; Vandorpe et al., 2014).

6.2.2 Oceanographic setting

The regional water mass stratification and circulation patterns are dominated by the exchange between the Atlantic Ocean and Mediterranean Sea (Jia, 2000; Johnson and Stevens, 2000; Rogerson et al., 2012; Peliz et al., 2013; Carracedo Segade et al., 2015). The local vertical water mass stratification is composed of a ~100 m thick seasonal surface mixed layer, followed by a thermocline marking the relatively warm and low salinity (35.6 and ~12°C) North Atlantic Central Water (NACW, Fig. 6.2). The presence of a salinity and temperature minimum (35.5 and ~11°C) centred at 700 m water depths signs the Antarctic Intermediate Water (AAIW; Machín and Pelegrí, 2009; Louarn and Morin, 2011). The MOW is marked by a salinity maximum (36.2 to 36.3 and ~11°C) and is observed to seasonally vary between water depths ranging from 800 to 1200 m (Fig. 6.2). Below the MOW lower boundary, generally between ~1300 and 1500 m water depth, the cold and low salinity (~34.95 and ~4-2°C) North Atlantic Deep Water is found (Criado-Aldeanueva et al., 2006).

Nowadays, the local water column is strongly dependent on the dynamics associated to the Mediterranean eddies (Barbosa Aguiar et al., 2013). Influenced by the Coriolis force, the MOW circulates against the northern Gulf of Cádiz slope and undergoes a strong differentiation which mainly occurs through the entrainment of NACW (Baringer and Price, 1999). Both processes, together with sea bottom frictional effect, are thought to be responsible for splitting the MOW into different branches, which have reached their density equilibrium in the region of the Portimão Canyon (Borenäs et al., 2002; Rogerson et al., 2012; Barbosa Aguiar et al., 2015). This region is also observed to be associated with the generation of the Mediterranean eddies, typically bearing a strong MOW signature (Serra and Ambar, 2002; Ambar et al., 2008). Those Mediterranean eddies form up to 800 m thick vortices ranging from 25 to 100 km diameter (Serra et al., 2010). They detach from the slope and the main flow filaments to propagate towards the south within the intermediate open ocean, generally between 800 and 1200 m water depth (Carton et al., 2002; Serra et al., 2005). Alternatively, Cape St Vincent constitutes another important centre of generation of Mediterranean eddies that propagate towards the west, northwest and partly along the Iberian margin (Serra et al., 2005; Ambar et al., 2008; Barbosa Aguiar et al., 2013). The generation rate of Mediterranean eddies was estimated to ~15 eddies/yr with an average duration of 1.7 yr

(Richardson et al., 2000; Barbosa Aguiar et al., 2013). The Mediterranean eddies are observed to rapidly dissipate when interacting with a sloping seabed or seamount, and subsequently form a MOW-like salinity anomaly (Fig. 6.2; Richardson et al., 2000). Nevertheless, few Mediterranean eddies were observed to only change their course without fully dissipating when interacting with the Atlantic Moroccan margin (Ambar et al., 2008; Barbosa Aguiar et al., 2013).

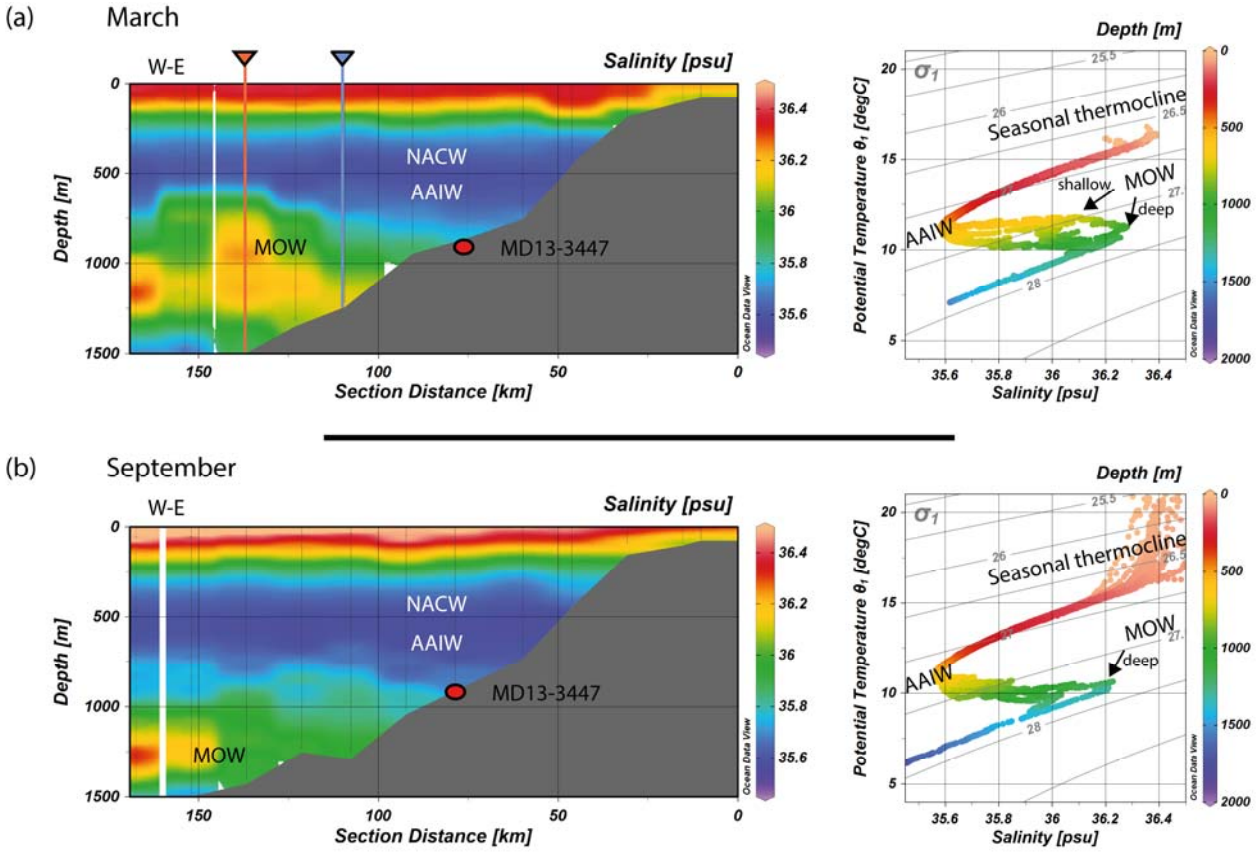

Figure 6.2 Salinity profiles showing the water mass stratification during (a) march and (b) September 1986. The location of the CTD stations is indicated Fig. 6.1 (World Ocean Database 2013). Temperature versus salinity diagrams showing the density and properties of the respective water masses are indicated. The bathymetry is inferred from the bottom of the CTD casts. Note the presence of a prominent salinity anomaly ranging between ~800 and 1200 m water depth during March, reflecting the incursion of deep and shallow (black arrows) Mediterranean mesoscale eddies (Mediterranean dipoles; Serra et al., 2010). During September, the MOW anomaly is centred around 1200 m water depth. The projected depth of core MD13-3447 is indicated. The red (blue) triangle indicates the location of the profiles used to compute the natural internal tide angle of energy propagation. **NACW**: North Atlantic Central Water; **AAIW**: Antarctic Intermediate Water; **MOW**: Mediterranean Outflow Water.

Both sub-surface float observations and numerical modelling indicate southward propagating deep anticyclonic Mediterranean eddies (generally centred around 1200 m water depths), often coupled with shallower cyclonic Mediterranean eddies (~800 m water depths), also referred to as Mediterranean water dipoles (Serra et al., 2002; 2005). Although their formation mechanism is still

under debate, those dipoles are thought to be formed from baroclinic flow instabilities of the main MOW flow branches, and possibly from the influence of seabed irregularities when passing the Portimão Canyon and Cape St Vincent (Cherubin et al., 2000; Serra et al., 2002; 2005). The Mediterranean eddies and Mediterranean dipoles have slow lateral transport, generally below 5 cm/s (Richardson et al., 2000; Serra et al., 2010). Nevertheless, direct observations evidenced deep anticyclonic Mediterranean eddies are associated with azimuthal velocities ranging from ~12 to 25 cm/s within the central part of the Gulf of Cádiz whereas velocities in the shallower cyclone structure are generally slower than 20 cm/s (Carton et al., 2002; Serra et al., 2002; 2005; Alves et al., 2011). Given their size, a single eddy event may influence bottom currents along horizontal segments of few tens of kilometres and vertical depth range of few hundreds of metres (Fig. 6.2).

6.3 Material and methods

6.3.1 Sediment analyses

This study is based upon the analysis of the CALYPSO piston core MD13-3447 (35°11.64'N; 7°8.88'W; 968 m water depth) which was collected during the R/V Marion Dufresne MD194 EuroFLEETS Gateways cruise in 2013. The core recovered a 2413 cm long sediment sequence mainly consisting of tenth to few tenth of centimetres thick bi-gradational (coarsening and fining upward), brown to light grey foraminifera rich clayey sandy silts and clayey silts to silty clay (Fig. 6.3). It contains an overall variable very moderate to moderate bioturbation and mottled silt facies, as well as frequent rust coloured horizons and centimetre scaled dark grey foraminifer rich irregulars sandy pockets (Fig. 6.5).

The core was analysed using a Multi-Sensor Core Logger (MSCL) at the department of Geology at Ghent University. The magnetic susceptibility and colour spectrophotometry lightness L* and red over green ratio a* were measured at 2 mm downcore resolution. Results are expressed in the international system of units (SI). MSCL line scan images were obtained using a camera aperture of 5.60 and an exposure time of 20 ms, providing images of 200 (191) pixels/cm of vertical (horizontal) resolution.

The semi-quantitative elemental composition was analysed using an AVAATECH XRF core scanner at the Royal NIOZ. Measurements were performed at 1 cm resolution over a slit area of 1.2 for 1 cm downcore. All samples were measured both at 10 kV/500 µA and 30 kV/500 µA, using a 10 s integration time. Results are presented as elemental ratios, or normalised ratio (element counts divided per total counts) following recommendations in (Richter et al., 2006).

The bulk terrigenous grain-size was analysed using a Malvern MasterSizer 3000 at the Department of Geology at Ghent University. A variable amount of sediment ranging from 20 to 60 mg was decarbonated applying a two-fold ~40 ml of 1 mol/l acetic acid wash. The weight of the sample was formerly adapted in order to ensure a 10 to 20 % laser obscuration range and measurements were performed using a 12 s integration time. The biogenic silica and organic fractions were considered negligible. One millilitre of 0.2% Sodium Hexametaphosphate solution was added to each sample prior to measurement in order to limit the formation of aggregates (McCave and Hall, 2006). Samples were introduced into the Malvern using a Hydro MV module with a stirrer speed of 2500 rpm and a continuous ultrasonic bath set at 10%.

6.3.2 Age model

The MD13-3447 age model was established by the tuning of the lightness L* signal with that of IODP Site U1385 (Hodell et al., 2015) and integrates chronostratigraphic evidences from coccolith assemblage analyses. Within the North Atlantic, various distinct coccolith species typically succeeded during the Quaternary, exhibiting marked temporal and spatial changes of relative abundances, as well as first, last and common occurrences (Raffi, 2002). Therefore, coccoliths assemblages have a very important biostratigraphic and biochronologic potential over the period of time under investigation. In this study, this approach was selected in order to provide some biostratigraphic age references, to assist and provide the necessary framework to perform the lightness L* tuning. Moreover, coccolith biostratigraphy covers time periods much beyond the coverage of ^{14}C and Uranium dating techniques, respectively around 45 and 500 ka BP (Bronk Ramsey, 2008). The coccolith analyses (Fig. 6.3d) were performed at the Laboratoire des Sciences du Climat et de l'Environnement at Gif-sur-Yvette (France). The tuning was performed using the AnalySeries software (Paillard et al., 1996), and tie points were placed using characteristic peaks and/or abrupt amplitude changes (Fig. 6.4; Table 6.1). Beyond the time range of IODP Site U1385, roughly at 1400 ka BP, the tuning was performed using the globally distributed LR04-benthic δ18O stack (Lisiecki and Raymo, 2005) and the MD13-3447 XRF Fe/Ca ratio (Fig. 6.4b; Table 6.1).

6.3.3 Critical seabed slope calculation

The structure and variability of the water column at site MD13-3447 was studied through seasonally selected CTD salinity profiles (Fig. 6.2; World Ocean Database, 2013). The potential temperature was computed using a standard reference pressure of 1 bar, and plots were made using Ocean Data View software (Schlitzer, 2012). Additionally, two different salinity profiles presenting distinct MOW anomalies were selected to investigate the possible influence of the water column

profile on the internal tide regime. The first profile was selected for displaying a pronounced MOW salinity anomaly ranging from 800 to 1200 m water, while the second showed a less marked anomaly at 1200 m water depth (Fig. 6.2). Both profiles were analysed to estimate the angle of energy propagation of semidiurnal internal tides and subsequently obtain the critical seabed slope angle (Cacchione et al., 2002). The critical seabed slope angle γ (°) with respect to the semi-diurnal internal tide frequency is computed using equation from Southard and Cacchione (1972):

$$c = \arctan\left(\sqrt{\left(\frac{\sigma^2 - f^2}{N^2 - \sigma^2}\right)}\right)$$

Where c (°) is the angle of internal tidal energy propagation within the water column relative to the horizontal. The Coriolis parameter f at 35°N was equal to 8.37 E-05 rad/s and obtained from the Ocean Data View software (Schlitzer, 2012). Sigma represents the internal tide frequency M2, $\sigma = 0.14 \times 10^{-3}\, rad/s$ (van Haren et al., 2002). The Brunt–Väisälä frequency N (cycl/s) was computed from the CTD profiles using the Ocean Data view software. Outliers due to noise in the record (Schlitzer, 2012) were deleted, whereas the noise was reduced applying an 11 point average filtering.

6.4 Results

6.4.1 Coccolith assemblages

The coccoliths analysis shows distinct assemblages throughout the core. The base of the core (2410 cm bsf) was characterised by abundant *Pseudoemiliana lacunosa* and traces of *Cyctococcolithina macintyrei*. Between 1110 to 1000 cm bsf, the assemblages consisted in *small Gephyrocapsa*, *P. lacunosa* and *P. lacunosa elliptic*, with the additional presence of *G. oceanica* at 1110 cm bsf. The presence of Eocene species was noted at 1040 cm and 1065 cm, representing reworked material. Similar species were observed between 740 and 670 cm bsf, though *P. lacunosa* was relatively more abundant. The co-occurrence of *P. lacunosa* and *G. caribbeanica* characterised levels at 620 and 645 cm bsf (Fig. 6.3). The presence of *Reticulofenestra asanoi* was noted for samples comprised between 1110 and 670 cm bsf, with exception at 1000 cm bsf. Samples above 305 cm bsf were characterised by the absence of *P. lacunosa.* Levels between 305 and 200 cm bsf showed different relative abundances of *G. caribbeanica*, *G. ericsonii* and *Emiliana huxlei* (Fig. 6.3d). *E. huxlei* was abundant at 5 cm bsf.

6.4.2 Age model and sedimentation rates

The obtained age model correlates the core interval between 2413 and 455 cm bsf to an age spanning from 1650 (*C. macintyrei*) to 467 ka BP, with *P. lacunosa* and *G. caribbeanica* co-occurrence roughly correlated at 590 ka BP (Fig. 6.4; Table 6.1). No correlation could be established on the basis of the lightness L* signal within the interval ranging from 455 to 0 cm bsf. This interval was thus discarded although it must span within the past 450 ka BP. An almost peak to peak correlation with the lightness signal of IODP Site U1385 allowed the definition of 40 tuning points between ~1390 to 467 ka BP. Six additional tie points were obtained from the XRF Fe/Ca and LR04-benthic δ18O stack tuning, between 1653 and 1414 ka BP (Table 6.1). Overall constant sedimentation rates averaging 1.9 cm/ky were obtained within the 1600 to 1100 ka BP interval. Similar ~2 cm/ky sedimentation rates were obtained within the more recent 1100 to 460 ka BP interval, although different intervals of very low sedimentation rates (below 1 cm/ky) are present (Fig. 6.4). Those low sedimentation rates are observed between MIS 24 and 22, as well as during glacial stages of MIS 16 and 14. Moreover, a large interval comprising MIS 20 to 18 (from ~820 to 730 ka BP), was correlated to levels ranging from 888 to 867 cm bsf, resulting in sedimentation rates below 0.5 cm/ky over this period. The obtained sedimentation rates briefly reached 5.5 and 6.7 cm/ky, respectively at ~1100 and 725 ka BP, roughly between MIS 33 and 32 and at the transition from MIS18 to 17.

6.4.3 Sediment facies

The overall sediment core lithology is dominated by brown to light grey clayey sandy silts to clayey silty sands (Fig. 6.3). The sand fraction is mainly represented by variations in the foraminifera content as only few prominent terrigenous fine sand peaks are found at ~695, 455 and 35 cm bsf (Figs. 6.3a). Interbedded clayey silts to clayey silty sand variations are organized into tens to few tens of centimetres thick sequences (Fig. 6.3). Contacts are predominantly bi-gradational, associated to coarsening and fining upward, with noticeable exception of sandy horizons at 455 and 35 cm bsf. Variable very moderate to moderate bioturbation and mottled silt facies, as well as frequent rust coloured horizons are observed throughout (Fig. 6.3). The latter facies tend to be more marked within coarse silty sand intervals. Additionally, numerous centimetre scaled dark grey foraminifer rich irregular sandy pockets facies can be observed (Figs. 6.3; 6.5; 6.6). This facies seem first to appear during MIS 45 (~1950 cm bsf) and is being gradually more frequent from 1100 cm bsf (~1000 ka BP) onwards (Fig. 6.3). More frequent abrupt and irregular (sharp) contacts were observed within the interval comprised between ~1400 and 1300 ka BP (Fig. 6.3; 6.5). Similar more frequent sharp contacts were also evidenced within distinct intervals throughout to core (Fig. 6.3b; grey shaded areas).

	L* tuning	XRF Fe/Ca tuning	
	IODP Site U1385	LR-04_stack	
Depth [cm bsf]	Age [ka BP]	Age [ka BP]	Sedimentation rate [cm/ky]
455	467		1.85
522.8	503.69		1.85
597	543.9		0.04
598	569.5		1.70
637.5	592.7		0.73
655.8	617.9		1.74
669.9	626		2.25
687	633.6		0.60
709.1	670.7		1.94
749.4	691.5		1.73
752	693		2.23
795.5	712.5		1.93
810	720		6.71
867	728.5		0.51
878.2	750.45		0.25
888	790		0.56
904.16	818.7		2.64
930	828.5		1.81
960.8	845.5		2.86
1005.2	861		2.57
1065.5	884.5		0.55
1082.8	916.2		0.74
1100	939.4		0.40
1102	944.4		1.99
1129	958		1.36
1161.6	982		0.87
1175.5	997.9		1.11
1194.4	1014.9		2.79
1231	1028		0.87
1248.4	1048.1		1.31
1273	1066.88		2.90
1354.6	1095		5.57
1466	1115		1.19
1523.6	1163.6		2.28
1582	1189.2		2.00
1670	1233.2		2.00
1761.2	1278.77		2.19
1831.5	1310.94		0.77
1858.5	1345.85		1.26
1912.5	1388.74		2.06
1986		1414.5	0.18
2067		1452	1.78
2156		1502	1.78
2220		1538	1.37
2273.1		1576.8	1.83
2413		1653.4	

Table 6-1 MD13-3447 interpreted age model. It is based on both lightness signal with that of IODP Site U1385, and XRF Fe/Ca correlated with the LR-04 benthic stack from Lisiecki and Raymo (2005).

Figures 6.5 and 6.6 describe the sedimentary facies of some key intervals that were associated with ~1 cm or lower sedimentation rates. Those present noticeable occurrences of grey to dark grey

irregular foraminifer rich sandy pockets (Fig. 6.5). Prior to ca. 1200 ka BP, those are centimetre-scaled and seem randomly associated within the variable facies and physical sediment properties. Abrupt lithological contacts are more frequently observed from 1650 to ~460 ka BP, in particular associated with cold, glacial periods (Fig. 6.6). Observations show that the interval correlated from 810 to 740 ka BP, exhibit increased occurrences of foraminifer rich sandy pockets. During MIS 16 and 14, those gradually increase in size and reach up few centimetres sized pockets, which are embedded in brownish grey mottled sandy silts to silty sands. The pocket limits are abrupt and their overall shapes are very irregular (Figs. 6.6b, c, d). Overall texture and grain-size changes remained gradational within MIS 16, which however was characterised by the occurrence of coarse terrigenous grain-size distribution (Figs.6.3; 6.6c). Glacial stage of MIS 14 is characterised by a large occurrence of dark grey foraminifer rich sands, and the presence of two abrupt contact of coarsening upward sediments (Fig. 6.6d).

At 455 cm bsf, a 15 cm thick layer of dark grey to light brown foraminifer rich coarse sands is interbedded within light grey to brownish sandy silts (Fig. 6.6e). This layer is associated to a large peak in the magnetic susceptibility signal and coarse terrigenous particles up to 100 µm in grain-size (Fig. 6.3). Several sharp contacts are observed and fining upward silty sands to sandy silts sequence is present from 441 to ~435 cm bsf. Finally, a relatively coarse sand layer (up to 100 µm in terrigenous grain-size) was found at 35 cm bsf. It consists of a sharp based and fining upward ~10 cm thick grey to light grey sand to silty sand layer embedded within grey, slightly bioturbated, sandy silts bearing rust coloured levels (Fig. 6.6f). Only little evidence of dark grey foraminifer rich sand pockets can be noted below and above the sequence which contrasts with the previous facies.

6.4.4 Physical and geochemical data

The overall sediment physical properties show consistent patterns between glacial versus interglacial conditions. Overall interglacials are marked by large intervals of well-defined minimum XRF Fe/Ca ratio, magnetic susceptibility (<25 SI) and maximum in the lightness L* with values generally above 50 (Fig. 6.3). Alternatively, glacials are characterised by relatively higher XRF Fe/Ca ratio (from 0.2 to 0.4), and marked by a small amplitude (of the order of ~0.1 amplitude) and higher frequency variability. These high frequency XRF Fe/Ca ratio variations corresponds by few tenths of centimetres periodic low amplitudes oscillations. Such oscillations are typically present within the coarse clayey silty sand lithologies (Fig. 6.3). Those are also clearly visible within the lightness L* signal and magnetic susceptibility record, varying between 25 and 50 SI. The red over green ratio a* parameter shows a more complex pattern throughout the record. Rust coloured iron rich horizon are systematically marked by high red over green ratio a* values (Fig. 6.3). However this it must be

noted that peaks in the red over green ratio a* are not exclusively associated with this facies, and more generally signs bright brownish to reddish intervals.

From 1650 to 1200 ka BP, glacial intervals bear the highest (>0.3 in amplitude) XRF Fe/Ca ratio throughout, with exception of MIS 44 and 42 which are marked by complex variations, of overall low XRF Fe/Ca ratio. Interglacials correspond to higher lightness L* and lower magnetic susceptibility values (generally below 25 SI), although the relative amplitude of those variations may be different within each proxies.

From about 1200 to 460 ka BP, glacial periods appear to be less prominent in the XRF Fe/Ca ratio which tends to oscillate between 0.04 and 0.2 ratio values, thus significantly lower than older glacial stages (Figs6.3 & 6.4). This patterns appear relatively similar than that previously observed for MIS 44 and 42, between 1400 and 1300 ka BP (Fig. 6.4b). Those intervals, comprising MIS 20, 18, 16 and 14 are also associated to sedimentation rates below 1 cm/ky.

The transition from MIS 13 and 12 (ca. 460 ka BP; 455 cm bsf) corresponds to the most prominent feature within the core, marked by a large peak in magnetic susceptibility record, up to 120 SI, that is associated with very low lightness signal. Within the section of the core that could not be correlated (above 455 cm bsf), it is observed a very low XRF Fe/Ca ratio (below 0.1) between 400 and 200 cm bsf, also marked by a large peak in the lightness L* signal.

6.4.5 Grain-size distribution

The grain-size distribution of the terrigenous fraction is dominated by clayey silt particles with a mean grain-size of ~7 µm (Fig. 6.3a). The grain-size distribution mainly varies from 2 to ~50 µm grain-sizes with only few exceptions represented by peaks up to 100 µm, respectively at ~700 cm bsf (within MIS 16), 455 to 445 cm bsf (~460 ka BP) and 30 cm bsf. Particle grain-sizes outside the 2 to 50 µm range represent less than 2% of the total relative fraction (Fig. 6.3a).

Between 1650 and 460 ka BP, two distinct trends can be observed. Prior to 1200 ka BP, interglacials are characterised by distinctly coarser terrigenous grain-sizes (varying from 10 to 20 µm) than glacials (Fig. 6.3a). From MIS 37 (at about 1250 ka BP and ~1650 cm bsf), interglacial intervals are characterised by gradually lower terrigenous grain-size distribution, with characteristic minimum values comprised between 4 to 8 µm during MIS 17 and 13 (Fig. 6.3a). A more complex variability is observed during glacial intervals, characterised by high frequency variations ranging from approximately 6 to 15 µm in grain-size. Such variations are particularly prominent within intervals of variable XRF Fe/Ca ratio (Fig. 6.3). Nevertheless, no clear relationship between XRF Fe/Ca ratio, magnetic susceptibility, lightness L* and the grain-size distribution pattern could be evidenced so far (Fig. 6.5).

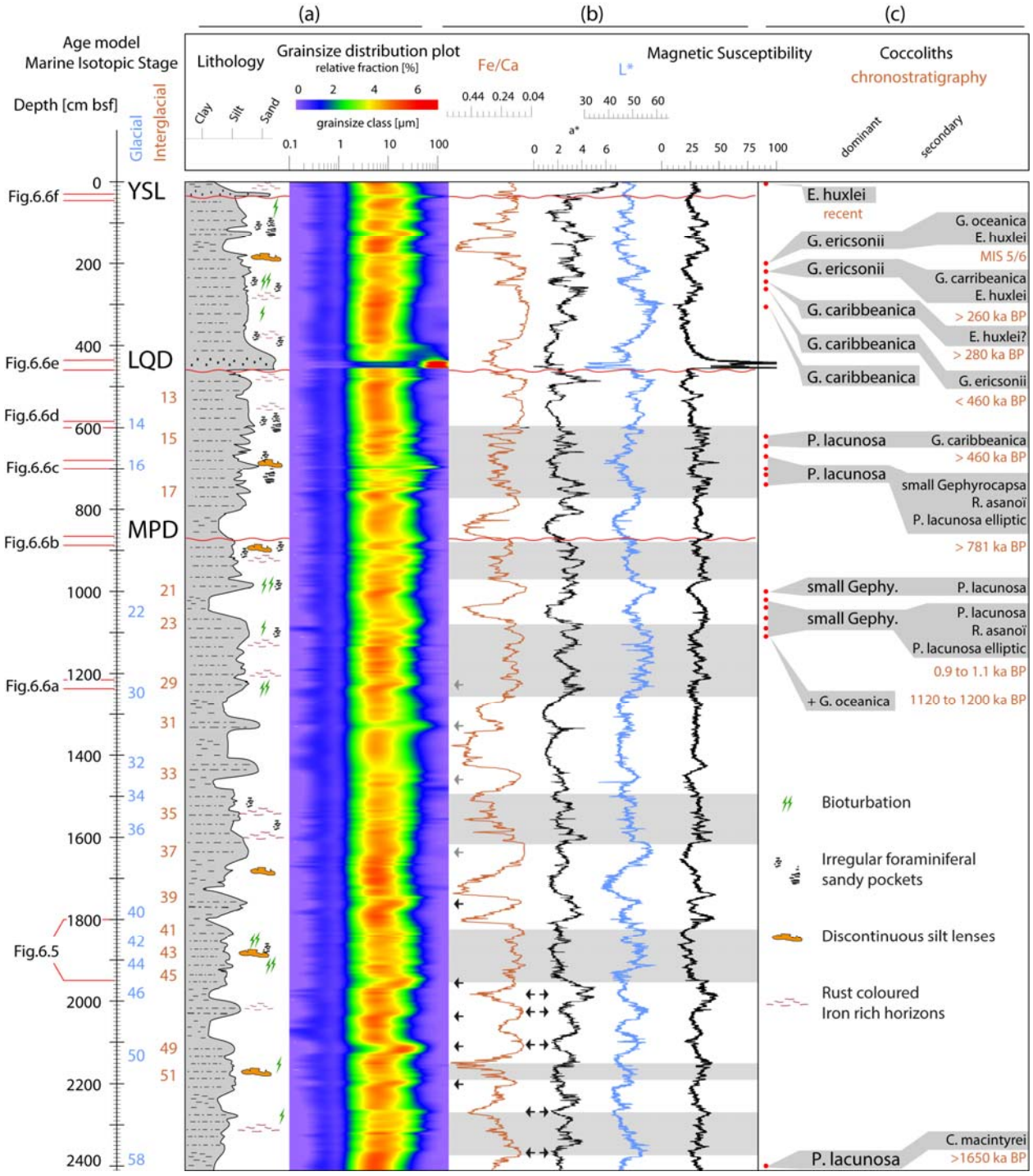

Figure 6.3 MD13-3447 multi-proxy record versus depth. (a) Lithological log and grain-size distribution plot of the terrigenous fraction comprised between 0.1 to 150 µm. (b) XRF Fe/Ca ratio, red over green ratio a*, lightness L* and Magnetic Susceptibility (MS) record. The double arrows indicate some clear intervals where maximum and minimum XRF Fe/Ca ratio values correspond to minimums the red over green ratio a* values. Simple arrows indicate interglacials that are associated with relatively coarse grain-size distribution. The grey shaded areas correspond to intervals with higher frequency variability. (c) Coccolith observations with dominant, secondary species and interpreted chronostratigraphic range. The age model Marine Isotopic Stages are indicated as well as interpreted major erosional events and the respective depth of Figs.6.5 and 6.6 (red lines). **MPD**: Middle Pleistocene Discontinuity; **LQD**: Late Quaternary Discontinuity; **YSL**: Younger Sand Layer.

6.4.6 Seabed and internal tide reflection conditions

The calculation of the internal tidal critical slope angle shows that reflection conditions depend upon the salinity profile over the water column (Fig. 6.7). In particular, distinct critical slope angle values are obtained at the transition zone between the AAIW and MOW, from ~500 to 600 m water depth. Obtained values for the critical slope angle range from ~5° to 2°, and reach a maximum between 150 and 200 m water depth, within the permanent thermocline (Figs.6.2 & 6.7). Nowadays, internal tidal reflection conditions are transmissive in the vicinity of Site MD13-3447, with a γ/c ratio varying between ~0.75 and 0.5 between 900 and 1100 m water depth. Within this depth range, differences due to changes in the MOW salinity anomaly impact on the ratio value. The changes in the depth range of the MOW salinity anomaly are shown to be more important between water depths from 600 and 900 m, where a difference of 0.2 in the ratio amplitude is found. From about 1100 m water depth onwards, the critical slope angle range from 1.5 to 2° (Fig. 6.7) when a deep MOW salinity anomaly is coupled with a shallow one as observed in Fig. 6.2a.

6.5 Discussion

6.5.1 General chronostratigraphic framework

The age model ranges from ~1650 to 460 ka BP (2413 to 455 cm bsf), in accordance with the coccolithophore assemblages, overall representative of the past 1500 ka BP (Pujos, 1988). The bottom of the core (at 2410 cm bsf) is correlated to an age of ~1650 ka BP (MIS 58). This is in accordance with the occurrence of *C. macintyrei* within the north Atlantic, which last common appearance is set around 1600 ka BP (Raffi, 2002). The levels associated with the co-occurrence of *G. caribbeanica* and *P. lacunosa* (645 and 620 cm bsf) were here correlated to the MIS 15, roughly between 600 and 580 ka BP. This is in accordance with the known association of G. caribbeanica and *P. lacunosa* at IODP Site U1385, which mainly occurs between 600 and 420 ka BP (Balestra et al., 2015). Within the northeast Atlantic *R. asanoï* mainly cluster within a time range between 1110 and 850 ka BP (Raffi, 2002; Raffi et al., 2006; Balestra et al., 2015). At Site MD13-3447, R. asanoï was observed both from 1110 to 1020 cm bsf and around 740 and 670 cm bsf. The lower interval was correlated between 950 and 870 ka BP, in accordance with *R. asanoï* common appearance range reported at IODP Site U1385 (Balestra et al., 2015). The upper interval (740 to 670 cm bsf) was correlated to younger ages, ranging between MIS 17 and 15, and thus the presence of *R. asanoï* is thought to relate to reworked material input.

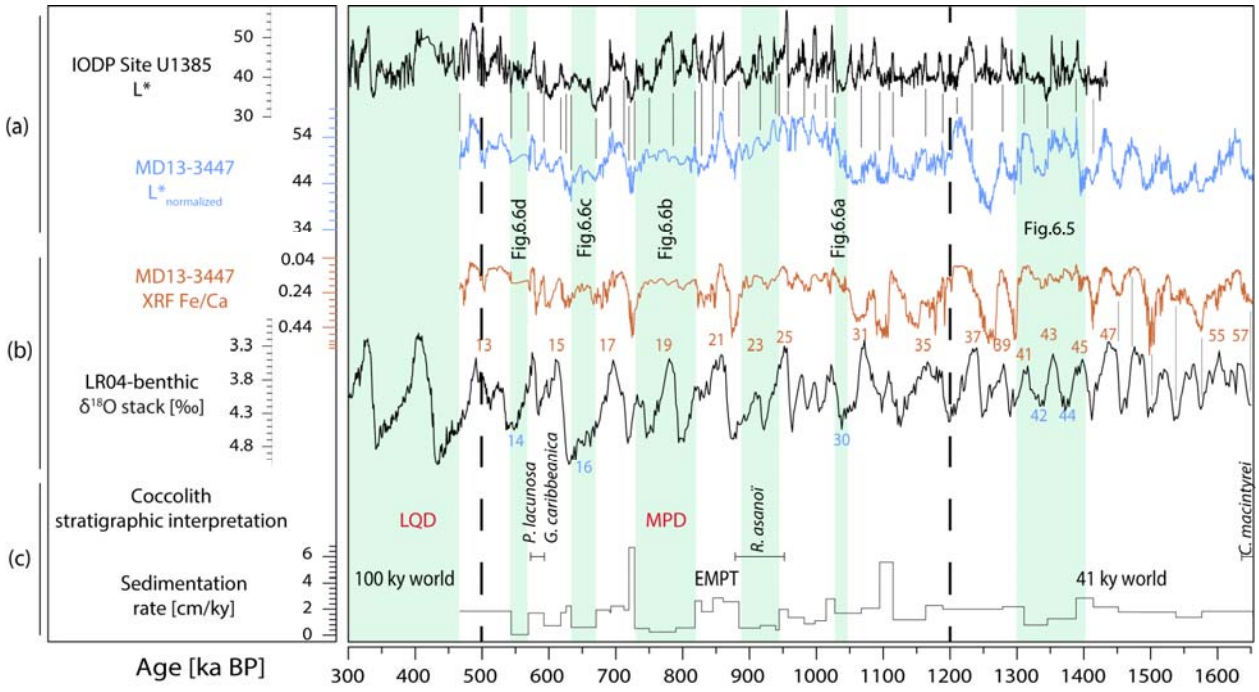

Figure 6.4 Interpreted age model for the interval comprised between 2410 and 455 cm bsf. (a) Correlation between the IODP Site U1385 (Hodell et al., 2015) and MD13-3447 lightness signals. The black lines indicate the position of the tie-points. (b) Comparison between the XRF Fe/Ca ratio and the LR04-benthic δ18O stack (Lisiecki and Raymo, 2005). The black lines indicate a few additional tie points beyond the range of IODP Site U1385. The numbers indicate the respective Marine Isotopic Stage (Lisiecki and Raymo, 2005). (c) Age model sedimentation rates with main coccolith biochronological constrains. The respective position of the Early-Middle Pleistocene Transition is indicated (Head and Gibbard, 2005). The shaded areas indicate intervals with relatively low sedimentation rates (Fig. 6.5; 6.6). **MPD**: Middle Pleistocene Discontinuity; **LQD**: Late Quaternary Discontinuity.

From 1350 to 460 ka BP, comparison of the local lightness L* signal with that of IODP Site U1385 allowed an almost peak to peak correlation (Fig. 6.4). However it should be noted that correlation within intervals where obtained sedimentation rates are below 1 cm/ky is subject to large imprecision (Fig. 6.4, shaded areas). Such similar trends suggest the existence of a common driving mechanism for the sediment colour (Giosan et al., 2002a). At IODP site U1385, the sediment colour and lightness are known to exhibit very strong orbital signal, in particular at the precession frequency (Hodell et al., 2013; 2015). Comparison between the XRF Fe/Ca ratio with the LR04-benthic δ18O supports the existence a strong link between sediments properties and climatic conditions at orbital frequencies (Fig. 6.4b). The XRF Fe/Ca ratio has often been used as a terrigenous versus biogenic proxy within the northeast Atlantic (Toucanne et al., 2009a; 2009b; Bahr et al., 2014). Here, overall interglacials are characterised by clayey silty sands, low terrigenous content and relatively high biogenic carbonate (low XRF Fe/Ca ratio) compared to glacials. Along the Iberian margin, increases in the XRF Fe/Ca ratio at orbital frequencies mainly represent the dilution of biogenic carbonate through enhanced terrigenous input forced by sea-level variations (Thomson et al., 1999; Hodell et al., 2013; Maiorano et al., 2015). In contrast, millennial-scale variations in the XRF Fe/Ca ratio may

represent decreases in the primary productivity (Martrat et al., 2007; Incarbona et al., 2010; Hodell et al., 2013). Here, large amplitude XRF Fe/Ca ratio changes correlate to large amplitude climatic variations such as recorded in Lisiecki and Raymo (2005), indicating a strong orbital control (Fig. 6.4). Following this logic, variations of smaller amplitude and higher frequency in the XRF Fe/Ca ratio could represent sub-orbital fluctuations, associated to millennial-scale climate variability in primary productivity. Along the Iberian margin, millennial-scale climate variations, similar to Dansgaard-Oeschger oscillations during MIS 3, are known to be a persistent feature during the past 1500 ky (Martrat et al., 2007; Hodell et al., 2015; Tzedakis et al., 2015; Birner et al., 2016). However, the sedimentation rates obtained here do not exceed a few centimetres per thousand of year, and thus the millennial-scale variability might not be fully captured.

The considered period covers part of the obliquity dominated glacial interglacial alternations (41 ky world) and most of the Early Middle Pleistocene Transition (EMPT; ~1200 to 500 ka BP) sensus Head and Gibbard (2005). The EMPT is a lengthy phase of gradual climate reorganization after which the modern climate regime established (Raymo et al., 2004). It consists in a global cooling trend, associated to increased contrast between maximum glacial and interglacial conditions, as well as a gradual glacial/interglacial frequency shift from ~41 ky to ~100 ky periodicity (Raymo et al., 2004; Clark et al., 2006; Trauth et al., 2007; 2009; Bell et al., 2015; Maslin and Brierley, 2015). Marked increases in the XRF Fe/Ca ratio characterize most glacial intervals within the 41 ky world, with noticeable exception of MIS 42 and 44 (Fig. 6.5). This suggests the local sedimentation have responded in a similar pattern than the western Iberian margin during the 41 ky world (Hodell et al., 2015). During the EMPT, the high XRF Fe/Ca ratio signature of the glacial intervals is much less marked whereas this interval is associated with gradually more intense glaciations, increased in ice-sheet volume and sea-level variations (Rohling et al., 2014; Tzedakis et al., 2015). Instead, those intervals are marked by gradually more prominent and variable sandy facies and foraminifera sand pockets, associated with discontinuous silt lenses and variable bioturbation (Fig. 6.3).

The 100 ky world climate regime is generally considered to be fully established at ~650 or ~500 ka BP (Head and Gibbard, 2005; Naafs et al., 2013). Thus this period is mostly represented by the interval which could not be tuned and which is represented by the top 455 cm of the sediment core. The absence of *P. lacunosa* above 455 cm bsf (467 ka BP) corroborates that this sediment interval is younger than ~460 ka BP (Pujos, 1988). Towards the top of the core (5cm bsf), E. huxlei is abundant, suggesting a last climatic cycle age (Pujos, 1988; Raffi et al., 2006). This suggests that relationships between the XRF Fe/Ca ratio, climate and sea-level variations, which were relatively well expressed during the 41 ky world, have gradually been altered (or changed) during the EMPT.

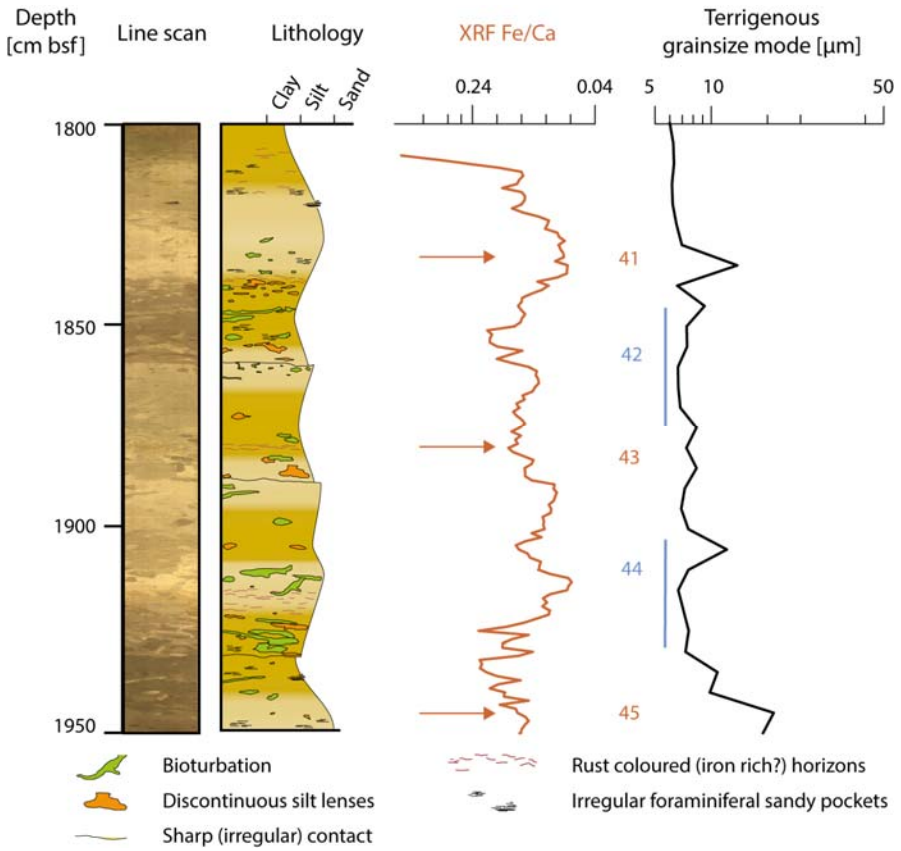

Figure 6.5 Sedimentological log of a typical interval characterised by variable terrigenous silt grain-size distributions (Figs.6.3; 6.4). Interbedded brown to light brown and light grey foraminifer rich silty sands to sandy silts are organised into fining and coarsening upward sequences. The numbers indicate the interpreted age model Marine Isotopic Stages. Note the overall presence of bioturbation, silt lenses and foraminifera sand pockets associated with few sharp contacts. The glacial versus interglacial XRF Fe/Ca modulation tends to disappear (arrows).

6.5.2 Facies association

Prior to MIS 36 (~1200 ka BP), interglacials are marked by distinctly coarser terrigenous silts than glacial periods (Fig. 6.3). This contrast is observed to be reduced from MIS 37 (characterised by grain-size distribution around 10 µm), and gradually disappear throughout of the EMPT (Fig. 6.3a, grey arrows). From MIS 21 to 13, interglacials are characterised by minimum terrigenous grain-size distribution overall below 10 µm. In comparison, the terrigenous grain-size distribution within glacial intervals is associated to complex and high frequency variations, typically between values from 6 to ~10 µm in the grain-size mode (Figs.6.5). However, the terrigenous grain-size distribution could not comprehensively be linked to overall textural, lightness L* and XRF Fe/Ca ratio changes (Fig. 6.3; 6.5). This might be attributed to the presence of moderate bioturbation and mottled facies which is associated with the presence of discontinuous silt lenses and highly variable terrigenous content (Fig. 6.5). Here, the terrigenous grain-size distribution varies from silty clays to clayey silts, typically represented by changes from 4 to ~17 µm (Alonso et al., 2016). Textural variations are mainly

associated with coarser biogenic (foraminifer) sand (Fig. 6.3). Textural changes are largely bi-gradational, varying from mottled sandy silts to silty sands facies. Such facies is very similar to the contourites facies from the northern Gulf of Cádiz (Faugères et al., 1984; Gonthier et al., 1984; Stow et al., 2002; 2008; Rebesco et al., 2014). The few sharp contacts observed (e.g. Fig. 6.5) suggest the presence of hiatuses of short duration (Rebesco et al., 2014). Those are common within contouritic sequences which are formed by energetic bottom currents (Shanmugam, 2013; Rebesco et al., 2014). Gradational transitions are often associated with rust coloured horizons, which may indicate well oxygenated conditions, often interpreted as an indicator for energetic bottom currents (Shanmugam, 2008; Rebesco et al., 2014). Pronounced variations in the red over green ratio a* (red/green ratio) may be considered as a proxy for bottom water ventilation and red-ox conditions (Giosan et al., 2002b; Hodell et al., 2013). This is because iron oxides typically experience colour changes from green to red depending on its oxidation state (Giosan et al., 2002b; Croudace et al., 2015). Likewise, higher values in the red over green ratio a* may be indicative for oxidant conditions, possibly marking well ventilated bottom water (Hodell et al., 2013). Here, well ventilated bottom water may possibly be associated with more pronounced bottom currents. However, the oxidation state of the sediment also depends on the sedimentation rates, and must be considered with caution here (Giosan et al., 2002b; Hodell et al., 2013). Very variable terrigenous grain-size distribution, associated to mottled facies and occasional sharp contacts may be considered as suitable macroscopic indications of the influence of energetic bottom currents (Martín–Chivelet et al., 2008; Alonso et al., 2016). However, no clear identification of contourite sequence from the climatically driven changes could be made in this study. This might partly be attributed to the low sedimentation rates and to the overprinted climatic signal.

From about 950 ka BP onwards, glacial intervals are associated to a substantial decrease in the sedimentation rates (below 1 cm/ky). The most marked decrease in sedimentation rates during the EMPT ranges from ~810 to 740 ka BP, and thus includes the MIS 19 interglacial (Fig. 6.6b). This interval is shown to be associated with a marked increase in the relative presence of dark grey sandy pockets (Fig. 6.6b). These pockets are irregularly distributed below and within a ~10 cm thick coarsening and fining upward grey sandy silt to silty sand layer sequence. The dark grey sand pockets facies is subsequently more represented during MIS 16 and MIS 14, where their size may reach few centimetres both in the lateral and vertical dimensions. This facies, characterised by very irregular shapes (Figs.6.6c, d), seem fairly analogous to irregular sands pockets in mottled silts facies described in (Gonthier et al., 1984). This facies has been further incorporated into the subdivision C3 of the standard contourite facies model, and thus may be interpreted as an indicator of energetic bottom currents (Stow and Faugères, 2008; Rebesco et al., 2014).

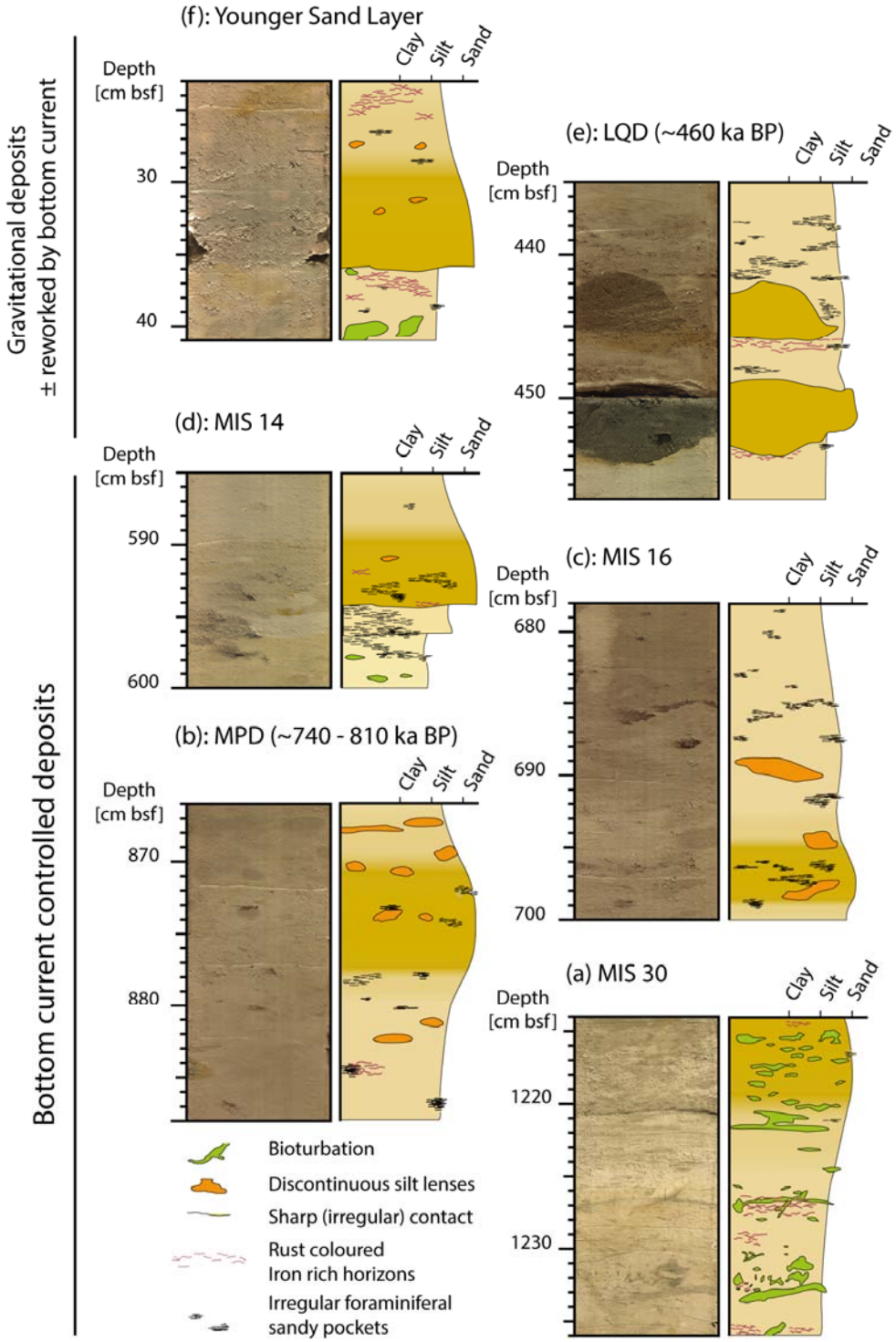

Figure 6.6 Sedimentological log of some key intervals, interpreted to be associated with stratigraphic gaps of variable duration (Figs.6.3; 6.4). (a) Moderately bioturbated transition between Marine Isotopic Stage (MIS) 30 and 29. (b) Middle Pleistocene Discontinuity with frequent occurrence of irregular foraminifera sand pockets and mottled facies. (c) MIS 16 interval characterised by variable proportion of sands and irregular foraminifera rich sands pockets. (d) MIS14 interval characterised by abrupt contacts of overall coarsening upward sediments. (e) Lower Quaternary Discontinuity with massive foraminifer rich, dark grey sands, bearing very irregular and abrupt lower and upper contacts. (f) Sharp based terrigenous rich and fining upward sand layer, denominated as "Younger Sand Layer".

Glacial intervals of the EMPT are characterised by relatively low XRF Fe/Ca ratio when compared to the signature that glacials have prior to ~1200 ka BP (Fig. 6.4). An inverse trend is visible within the lightness L* signal (Fig. 6.7). This can be explained by the fact lightness and relative terrigenous versus biogenic content are intimately linked along the Iberian margin (Hodell et al., 2013; 2015), and more generally within marine sediments (Giosan et al, 2002a; b). However, the existing precessional and obliquity signal is still relatively well-expressed within the lightness L* signal, which has allowed correlation with IODP site U1385. In contrast, the diagnostic of glacial intervals using comparison between the XRF Fe/Ca and the globally distributed LR04-Benthic stack is no longer possible over the EMPT (Fig. 6.4; 6.7). Here, the relative increase in biogenic fraction (low XRF Fe/Ca ratio) may have been caused by the action of bottom currents, which might have caused winnowing of the terrigenous fraction, as supported from sediment facies indications (Fig. 6.6; 6.7). A similar process was proposed to explain variation in biogenic versus terrigenous content within contourite drift sequences of the northern Gulf of Cádiz (Lofi et al., 2015). Moreover, MIS 14 is characterised by two sharp contacts showing textural coarsening upward (Fig. 6.6d). This could be regarded of a basecut-out contourite sequence (incomplete coarsening upward sequence), which may be characteristic for highly energetic bottom current (Alonso et al., 2016). Overall sediment facies observations prior to ~500 ka BP show consistent indications of gradually increased bottom current controlled sedimentation, possibly associated with gradually less energetic bottom current regime conditions during interglacials.

At 455 cm bsf (~460 ka BP), a pronounced facies change occurs, characterised by the emplacement of coarse sands (up to 100 µm in the terrigenous grain-size), bearing an abrupt lower contact (Fig. 6.6e). The large contrast in the grain-size distribution is also marked by a prominent magnetic susceptibility peak, which most probably indicates a change sediment source (Alonso et al., 2016). This facies seem fairly similar to turbiditic sequences described in the Faro Drift palaeo-moat domain (Alonso et al., 2016). This strongly suggests the emplacement of a fine grained (Tc/Td in Bouma subdivisions) turbiditic sequence (Bouma, 1964; Stow and Shanmugam, 1980; Shanmugam, 1997; Bouma, 2000). Likewise, the overlying lenticular dark grey massive sand layer at 445 cm bsf may be interpreted as a convolute layer belonging to a single turbiditic event (Stow and Shanmugam, 1980). Nevertheless, it can be noted that the sequence is overlain by a fining upward dark grey sandy facies (Fig. 6.6e) very similar to that observed within previous glacial intervals. This could indicate post depositional bottom current reworking and thus the contemporaneous existence of energetic bottom currents. Given the emplacement of the sediment core, such event most probably originates from the destabilisation of sediments deposited in an upstream area. It might be associated to a seismically triggered mass wasting event. Those typically have long recurrence time

and such trigger mechanism is the most likely within low slope gradient and non-glaciated margins (Evans et al., 2005; Leynaud et al., 2009). Finally, the younger sand layer at 35 cm bsf (Fig. 6.6f) bears a sharp basal contact associated with large amplitude terrigenous grain-size distribution contrast, relatively similar to the previous sequence. This also suggests a possible turbiditic origin, even though the clear colour and facies contrast suggests a different sediment source (Fig. 6.6b; a). This layer could be analogous to the Younger Sand Layer recorded within the northern Gulf of Cádiz contourite drift system, and which forms a widespread and fast accumulating coarsening and fining upward sequence during the last deglacial (Takashimizu et al., 2016). Similarly to layer observed here, the northern Gulf of Cádiz Younger Sand Layer shows distinct terrigenous content and thus was proposed to possibly indicate a tsunami related origin, associated with subsequent bottom current reworking (Takashimizu et al., 2016). Here, further radiocarbon dating would be necessary in order to relate those layers into a single trigger mechanism.

6.5.3 Sedimentary environment evolution

Two distinct superimposed processes were identified to have driven the sedimentation pattern of the past 1650 ky BP. Changes in the sediment lightness L* and XRF Fe/Ca ratio seem primarily driven by climatic and sea-level variations at orbital and sub-orbital frequencies. The second impacted on the terrigenous grain-size distribution and the relative biogenic versus terrigenous fraction (Fig. 6.7). This superimposed process could be attributed to the action of vigorous bottom currents on the basis of sedimentological facies indications.

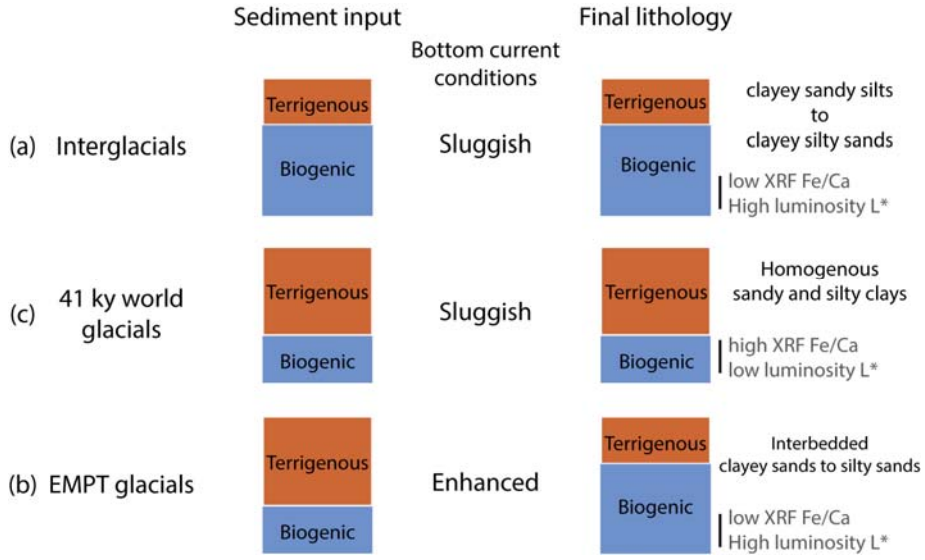

Figure 6.7 Diagram illustrating the process through which the climatic modulation of the physical parameters is being deteriorated by the action of enhanced bottom currents. (a) Interglacial conditions are characterised by larger biogenic inputs and have a low XRF Fe/Ca ratio and high lightness L*. (b) Glacial conditions Prior to EMPT (41 ky world) are characterised by higher terrigenous input leading to low XRF Fe/Ca and Lightness. (c) Glacial situation during the EMPT have presumably a similar sediment input than (b). The winnowing of the fine terrigenous fraction is thought to occur under enhanced bottom current conditions, leading to high XRF Fe/Ca ratio and relatively high lightness L*.

The overall sedimentation rates are significantly lower than those obtained from other coring sites located within this portion of the Moroccan margin, which often reached up to 30 cm/ky (Penaud et al., 2010; Wienberg et al., 2010). Here, the reason might relate to the hydrographic setting, as the studied core was recovered from the upper limb of an elevated ridge. Such elevated promontories typically receive less sedimentation, especially when influenced by the action of strong bottom currents (Turnewitsch et al., 2004). Likewise, the action of bottom currents might also be responsible for the reduction of the sedimentation rates during glacial intervals over the EMPT, in accordance with more pronounced bottom current indications. Substantial decreases in the sedimentation rates mark enhanced bottom current during cold phases of MIS 23, 16 and 14 (Fig. 6.4). Those coincide with marked sea-level changes which are known to exert an important hydraulic control at the Strait of Gibraltar, and thus on the Mediterranean-Atlantic exchange (Rohling et al., 2014). Sea-level forced changes of hydraulic conditions are responsible for the settlement of a denser and deeper MOW plume within the intermediate North Atlantic (Rogerson et al., 2005; 2006; 2010; Voelker et al., 2006). This typically caused higher flow velocities within depth range between 800 and 1500 m most probably in a similar pattern than observed for the past climate cycle (Rogerson et al., 2006; 2012). Higher flow velocities might have influenced the MOW potential vorticity, and thus Mediterranean eddies formation rate (Rhines and Holland, 1979; Serra and

Ambar, 2002; Barbosa Aguiar et al., 2013). The Mediterranean eddies, which have azimuthal velocities up to 20 cm/s, could possibly be responsible for the enhanced bottom current conditions at the studied site (Stow et al., 2009). Several Mediterranean eddies generated yearly may potentially influence the bottom current regime over the entire Atlantic Moroccan margin. Independently from the influence of the Mediterranean eddies themselves, their propagation and subsequent dissipation induce the presence of an important salinity anomaly having a MOW signature (Fig. 6.2). This salinity anomaly influences the water column stratification and associated vertical pycnal gradient (Fig. 6.2). Marked pycnal gradients have an important potential for the development of enhanced semi-diurnal internal tides and internal waves processes (Shanmugam et al., 2012). Here, only internal tidal processes are considered because it is by far the dominant frequency of internal wave processes in the region (Mienis et al., 2012). Internal tidal refection conditions were assessed at present through the computation of the γ/c ratio, which is further observed to locally reach values up to 0.75, due to the influence of the MOW (Fig. 6.8). Here this value is fairly close to near-critical reflection conditions (McPhee-Shaw, 2006). Similar reflection conditions were involved in the formation of large scale sediment waves, showing the ability of internal wave processes to mobilise sediments (Ribó et al., 2016). A more pronounced MOW anomaly in the study area could lead to the establishment of near-critical reflection conditions, typically marked by ratios $0.8 < \gamma/c < 1.3$ (Fig. 6.8; McPhee-Shaw, 2006). Under such conditions, energetic internal tide and seabed interactions are predicted by numerical models (Pomar et al., 2012; Shanmugam, 2013; Lamb, 2014). All arguments presented here converge to strengthen the hypothesis that sea-level forced changes in the MOW flow regime provides a suitable driving mechanism for glacially enhanced local bottom current regime.

Within the northern Gulf of Cádiz, two distinct regional discontinuities occurred at ~900 to 600 ka BP and around 500 ka BP, and are referred to as the Middle Pleistocene Discontinuity (MPD) and the Late Quaternary Discontinuity (LQD), respectively (Lofi et al., 2015). Here, the prolonged decrease in sedimentation recorded between ~810 and 740 ka BP is roughly contemporary to the MPD. The MPD is represented by ~400 to 100 ky long hiatuses at IODP Sites U1390 and U1391, respectively (Fig. 6.1; Lofi et al., 2015) and may be related to changes in the MOW regime, although it is known to be roughly contemporary with a northeast Atlantic tectonic event (Stein et al., 1986; Hernández-Molina et al., 2016c; Lofi et al., 2015). Both IODP Sites U1390 and U1391 were recovered within a similar depth range than the present Site MD13-3447 (Fig. 6.1). Here, both a regional tectonic adjustment and/or a MOW regime change might as well explain the local corresponding hiatus.

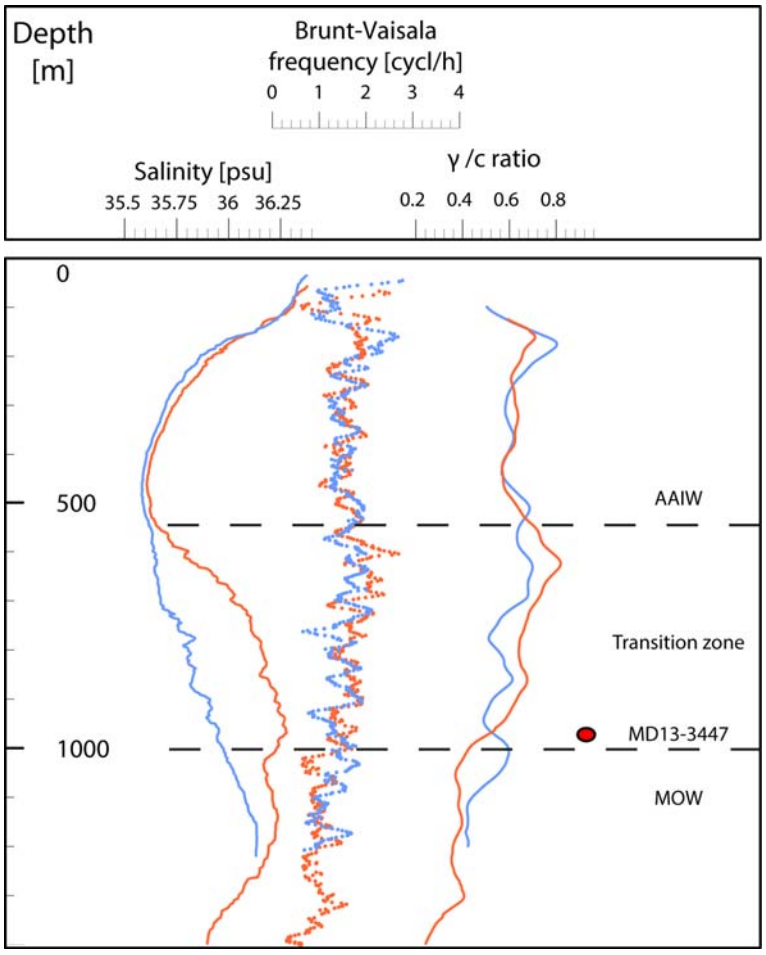

Figure 6.8 Critical slope angle computed with respect to semi-diurnal internal tide propagation within a Antarctic Intermediate Water dominated profile (blue), and a Mediterranean Outflow Water dominated profile (orange; Fig. 6.2). The red dot indicates the projected depth of core MD13-3447. Critical reflection conditions are reached when the seabed and internal tide propagation angle ratio (γ/c) is equal or close to 1. Here transmissive reflection conditions are present, although it can be note the important variability of the (γ/c) ratio within the transition zone between the saline MOW signature and the less saline AAIW.

The subsequent LQD was also mainly recorded from hiatuses at sites U1390 and U1391, and corresponded to a condensed interval at Site U1385 (Hernández-Molina et al., 2016c; Hodell et al., 2015; Lofi et al., 2015). Within the El Arraiche mud volcano province, a substantial mud extrusion event was tentatively correlated to MIS 9 (Vandorpe et al., 2014), which thus was also roughly contemporary with the LQD. Here, the LQD seem roughly synchronous to the base of the turbiditic layer at ~460 ka BP, which would thus correspond to seismically triggered mass wasting event and/or a major mud volcano reactivation event (Figs.6.4, 6.6e). However, it is unclear if the LQD was related with a regional tectonic adjustment within the northern Gulf of Cádiz (Hernández-Molina et al., 2016c). This periods (~500 ka BP) further corresponds to the growth of CWC and small scale CWC mounds accretion between ~800 and 1000 m water depths west of the El Arraiche mud volcano province (Vandorpe et al., submitted). Within the entire Moroccan coral mound province, the

CWC are known to mainly thrive during glacial periods (Wienberg et al., 2010; Vandorpe et al., submitted). Prior to 500 ka BP, glacial bottom currents were shown to be gradually more energetic, and to alter the climatic signal within the sediment record. The current study document abrupt facies change with the onset of turbiditic event possibly associated with energetic bottom currents. Thus, the LQD seem to correspond to a margin wide event, most probably associated with regional tectonic readjustment, mud volcano activity, and change in the overall bottom current regime at ~900 m water depths.

6.6 Conclusions

The studied sediment core reveals a complex and variable sedimentation history from ~1600 ka BP to present. The main changes in sediment facies and physical sediment properties seem to have occurred during the EMPT, which marks the gradual onset of the modern climate regime. Prior to ~1200 ka BP, the local sedimentation seems to be driven by climatic changes at orbital frequencies, in a similar pattern than the Iberian margin. Gradually more vigorous bottom currents seem to have developed during glacial periods of the EMPT. Those bottom currents may be responsible for the deterioration for the climatic signal within the physical sediment properties, noticeably impacting on the terrigenous content and the sedimentation rates. With the onset of the modern climate regime (roughly at 500 ka BP), the climatically driven variation in sediment colour lightness L* and XRF Fe/Ca ratio could not be further recognized. This might have been caused by different factors possibly involving regional tectonic adjustment, a local reactivation of mud volcanoes and/or changes in the bottom current regime.

Here, changes in the local bottom current regime are thought to be driven by changes in the MOW flow conditions and circulation pattern. Sea-level forced hydraulic conditions changes at the Strait of Gibraltar may have influenced the MOW flow potential vorticity, which could have in turn increased the formation rate of Mediterranean eddies. Increased incursion of Mediterranean eddies may have directly influenced the bottom current regime, or indirectly by influencing the local internal tide regime. Likewise enhanced MOW bottom currents could have contributed to the establishment of regionally favourable conditions for the growth of CWC within depths comprised between 800 and 1000 m water depths. This would confirm a certain analogy with CWC of the Porcupine Seabight. Despite the absence of large-scale contourite drifts comparable to those of the northern Gulf of Cádiz, the MOW seems to have greatly impacted on the local sedimentation pattern. The area has thus an important potential characterizing the past variability of Mediterranean eddies related flow, which constitute a substantial mechanism driving the spreading of the MOW within the North Atlantic Ocean. Additionally, results presented here draw the attention on erosive process that may be acting

at orbital and sub-orbital time-scales, and which diagnostic is generally unsuccessful from seismic geomorphological studies. Local vertical variations in the water column stratification and associated internal tides/waves processes seem to provide the best mechanism driving leading to the occurrence of erosive and/or non-depositional conditions. This emphasizes on the importance of tide-topographic interactions in the development and expression of generally subtle contouritic processes.

Acknowledgements

This study was carried out within the framework of a Ghent University BOF "Starting Grant". The authors wish to acknowledge the captains and crews of the campaign on board of the R/V Marion Dufresne cruise MD194-Gateways (2013), which was founded by EC FP7 'Research Infrastructures' EuroFLEETS project.

References

Alonso, B., Ercilla, G., Casas, D., Stow, D.a.V., Rodriguez-Tovar, F.J., Dorador, J., Hernandez-Molina, F.J., 2016. Contourite vs gravity-flow deposits of the Pleistocene Faro Drift (Gulf of Cadiz): Sedimentological and mineralogical approaches. Marine Geology 377, 77-94.

Alves, J.M.R., Carton, X., Ambar, I., 2011. Hydrological Structure, Circulation and Water Mass Transport in the Gulf of Cadiz. International Journal of Geosciences 2, 432-456.

Ambar, I., Serra, N., Neves, F., Ferreira, T., 2008. Observations of the Mediterranean Undercurrent and eddies in the Gulf of Cadiz during 2001. Journal of Marine Systems 71, 195-220.

Bahr, A., Jiménez-Espejo, F.J., Kolasinac, N., Grunert, P., Hernández-Molina, F.J., Röhl, U., Voelker, A.H.L., Escutia, C., Stow, D.A.V., Hodell, D., Alvarez-Zarikian, C.A., 2014. Deciphering bottom current velocity and paleoclimate signals from contourite deposits in the Gulf of Cádiz during the last 140 kyr: An inorganic geochemical approach. Geochemistry, Geophysics, Geosystems 15, 3145-3160.

Balestra, B., Flores, J.A., Hodell, D.A., Hernández-Molina, F.J., Stow, D.A.V., 2015. Pleistocene calcareous nannofossil biochronology at IODP Site U1385 (Expedition 339). Global and Planetary Change 135, 57-65.

Barbosa Aguiar, A.C., Peliz, Á., Carton, X., 2013. A census of Meddies in a long-term high-resolution simulation. Progress In Oceanography 116, 80-94.

Barbosa Aguiar, A.C., Peliz, A., Neves, F., Bashmachnikov, I., Carton, X., 2015. Mediterranean outflow transports and entrainment estimates from observations and high-resolution modelling. Progress In Oceanography 131, 33-45.

Baringer, M.O., Price, J.F., 1999. A review of the physical oceanography of the Mediterranean outflow. Marine Geology 155, 63-82.

Bell, D.B., Jung, S.J.A., Kroon, D., 2015. The Plio-Pleistocene development of Atlantic deep-water circulation and its influence on climate trends. Quaternary Science Reviews 123, 265-282.

Bigg, G.R., Jickells, T.D., Liss, P.S., Osborn, T.J., 2003. The role of the oceans in climate. International Journal of Climatology 23, 1127-1159.

Birner, B., Hodell, D.A., Tzedakis, P.C., Skinner, L.C., 2016. Similar millennial climate variability on the Iberian margin during two early Pleistocene glacials and MIS 3. Paleoceanography 31, 203-217.

Borenäs, K.M., Wåhlin, A.K., Ambar, I., Serra, N., 2002. The Mediterranean outflow splitting—a comparison between theoretical models and CANIGO data. Deep Sea Research Part II: Topical Studies in Oceanography 49, 4195-4205.

Bouma, A., 1964. Turbidites, in: Bouma, A.H., Brouwer, A. (Eds.), Developments in Sedimentology. Elsevier, pp. 247-256.

Bouma, A.H., 2000. Coarse-grained and fine-grained turbidite systems as end member models: applicability and dangers. Marine and Petroleum Geology 17, 137-143.

Bozec, A., Lozier, M.S., Chassignet, E.P., Halliwell, G.R., 2011. On the variability of the Mediterranean Outflow Water in the North Atlantic from 1948 to 2006. Journal of Geophysical Research: Oceans 116.

Bronk Ramsey, C., 2008. Radiocarbon dating: revolution in understanding. Archaeometry 50, 249-275.

Cacchione, D.A., Pratson, L.F., Ogston, A.S., 2002. The Shaping of Continental Slopes by Internal Tides. Science 296, 724-727.

Carracedo Segade, L.I., Gilcoto, M., Mercier, H., Pérez, F.F., 2015. Quasi-synoptic transport, budgets and water mass transformation in the Azores–Gibraltar Strait region during summer 2009. Progress In Oceanography 130, 47-64.

Carton, X., Chérubin, L., Paillet, J., Morel, Y., Serpette, A., Le Cann, B., 2002. Meddy coupling with a deep cyclone in the Gulf of Cadiz. Journal of Marine Systems 32, 13-42.

Cherubin, L., Carton, X., Paillet, J., Morel, Y., Serpette, A., 2000. Instability of the Mediterranean Water undercurrents southwest of Portugal: effects of baroclinicity and of topography. Oceanologica Acta 23, 551-573.

Clark, P.U., Archer, D., Pollard, D., Blum, J.D., Rial, J.A., Brovkin, V., Mix, A.C., Pisias, N.G., Roy, M., 2006. The middle Pleistocene transition: characteristics, mechanisms, and implications for long-term changes in atmospheric pCO2. Quaternary Science Reviews 25, 3150-3184.

Criado-Aldeanueva, F., García-Lafuente, J., Vargas, J.M., Del Río, J., Vázquez, A., Reul, A., Sánchez, A., 2006. Distribution and circulation of water masses in the Gulf of Cadiz from in situ observations. Deep Sea Research Part II: Topical Studies in Oceanography 53, 1144-1160.

Croudace, I.W., Rothwell, G., (eds.), 2015. Micro-XRF Studies of Sediment Cores: Applications of a non-destructive tool for the environmental sciences. Springer Netherlands.

Delivet, S., Van Eetvelt, B., Monteys, X., Ribó, M., Van Rooij, D., 2016. Seismic geomorphological reconstructions of Plio-Pleistocene bottom current variability at Goban Spur. Marine Geology 378, 261-275.

Dewar, W.K., Meng, H., 1995. The Propagation of Submesoscale Coherent Vortices. Journal of Physical Oceanography 25, 1745-1770.

Eberwein, A., Mackensen, A., 2008. Last Glacial Maximum paleoproductivity and water masses off NW-Africa: Evidence from benthic foraminifera and stable isotopes. Marine Micropaleontology 67, 87-103.

Evans, D., Harrison, Z., Shannon, P.M., Laberg, J.S., Nielsen, T., Ayers, S., Holmes, R.W., Hoult, R., Lindberg, B., Haflidason, H., Long, D., Kuijpers, A., Andersen, E.S., Bryn, P., 2005. Palaeoslides and other mass failures of Pliocene to Pleistocene age along the Atlantic continental margin of NW Europe. Marine and Petroleum Geology 22, 1131-1148.

Faugères, J.-C., Gonthier, E., Stow, D.A.V., 1984. Contourite drift molded by deep Mediterranean outflow. Geology 12, 296-300.

Flinch, J., 1993. Tectonic Evolution of the Gibraltar Arc. Rice University, Houston, Texas, p. 381.

Flinch, J.F., Vail, P.R., 1999. Plio-Pleistocene Sequence Stratigraphy and Tectonics of the Gibraltar Arc, Mesozoic and Cenozoic Sequence Stratigraphy of European Basins. SEPM Society for Sedimentary Geology, pp. 199-208.

Foubert, A., Depreiter, D., Beck, T., Maignien, L., Pannemans, B., Frank, N., Blamart, D., Henriet, J.-P., 2008. Carbonate mounds in a mud volcano province off north-west Morocco: Key to processes and controls. Marine Geology 248, 74-96.

Giosan, L., Flood, R.D., Aller, C.A., 2002a. Paleoceanographic significance of sediment color on western North Atlantic drifts: I. Origin of color. Marine Geology 189, 25-41.

Giosan, L., Flood, R.D., Grützner, J., Mudie, P., 2002b. Paleoceanographic significance of sediment color on western North Atlantic Drifts: II. Late Pliocene-Pleistocene sedimentation. Marine Geology 189, 43-61.

Gonthier, E., Faugères, J.-C., Stow, D.A.V., 1984. Contourite facies of the Faro Drift, Gulf of Cadiz, in: Stow, D.A.V., Piper, D.J.W. (Eds.), Fine Grained Sediments, Deep-Water Processes and Facies. Geological Society, London, pp. 275-291.

Grevemeyer, I., Matias, L., Silva, S., 2016. Mantle earthquakes beneath the South Iberia continental margin and Gulf of Cadiz - constraints from an onshore-offshore seismological network. Journal of Geodynamics 99, 39-50.

Hanebuth, T.J.J., Zhang, W., Hofmann, A.L., Löwemark, L.A., Schwenk, T., 2015. Oceanic density fronts steering bottom-current induced sedimentation deduced from a 50 ka contourite-drift record and numerical modeling (off NW Spain). Quaternary Science Reviews 112, 207-225.

Head, M.J., Gibbard, P.L., 2005. Early-Middle Pleistocene transitions: an overview and recommendation for the defining boundary, in: Head, M.J., Gibbard, P.L. (Eds.), Early-Middle Pleistocene Transitions: The Land-Ocean Evidence. Geological Society, London, pp. 1-18.

Hebbeln, D., Van Rooij, D., Wienberg, C., 2016. Good neighbours shaped by vigorous currents: Cold-water coral mounds and contourites in the North Atlantic. Marine Geology 378, 171-185.

Hernández-Molina, F.J., Wåhlin, A., Bruno, M., Ercilla, G., Llave, E., Serra, N., Rosón, G., Puig, P., Rebesco, M., Van Rooij, D., Roque, D., González-Pola, C., Sánchez, F., Gómez, M., Preu, B., Schwenk, T., Hanebuth, T.J.J., Sánchez Leal, R.F., García-Lafuente, J., Brackenridge, R.E., Juan, C., Stow, D.a.V., Sánchez-González, J.M., 2016a. Oceanographic processes and morphosedimentary products along the Iberian margins: A new multidisciplinary approach. Marine Geology 378, 127-156.

Hernández-Molina, F.J., Hodell, D.A., Stow, D.a.V., Alvarez-Zarikian, C., 2016b. Virtual special issue on IODP Expedition 339: The Mediterranean outflow. Marine Geology 377, 1-6.

Hernández-Molina, F.J., Sierro, F.J., Llave, E., Roque, C., Stow, D.a.V., Williams, T., Lofi, J., Van Der Schee, M., Arnáiz, A., Ledesma, S., Rosales, C., Rodríguez-Tovar, F.J., Pardo-Igúzquiza, E., Brackenridge, R.E., 2016c. Evolution of the gulf of Cadiz margin and southwest Portugal contourite depositional system: Tectonic, sedimentary and paleoceanographic implications from IODP expedition 339. Marine Geology 377, 7-39.

Hernández-Molina, F.J., Serra, N., Stow, D., Llave, E., Ercilla, G., Van Rooij, D., 2011. Along-slope oceanographic processes and sedimentary products around the Iberian margin. Geo-Marine Letters, 1-27.

Hernandez-Molina, J., Llave, E., Somoza, L., Fernandez-Puga, M.C., Maestro, A., Leon, R., Medialdea, T., Barnolas, A., Garcia, M., del Rio, V.D., Fernandez-Salas, L.M., Vazquez, J.T., Lobo, F., Dias, J.M.A., Rodero, J., Gardner, J., 2003. Looking for clues to paleoceanographic imprints: A diagnosis of the Gulf of Cadiz contourite depositional systems. Geology 31, 19-22.

Hodell, D., Crowhurst, S., Skinner, L., Tzedakis, P.C., Margari, V., Channell, J.E.T., Kamenov, G., Maclachlan, S., Rothwell, G., 2013. Response of Iberian Margin sediments to orbital and suborbital forcing over the past 420 ka. Paleoceanography 28, 185-199.

Hodell, D., Lourens, L., Crowhurst, S., Konijnendijk, T., Tjallingii, R., Jiménez-Espejo, F., Skinner, L., Tzedakis, P.C., Abrantes, F., Acton, G.D., Alvarez Zarikian, C.A., Bahr, A., Balestra, B., Barranco, E.L., Carrara, G., Ducassou, E., Flood, R.D., Flores, J.-A., Furota, S., Grimalt, J., Grunert, P., Hernández-Molina, J., Kim, J.K., Krissek, L.A., Kuroda, J., Li, B., Lofi, J., Margari, V., Martrat, B., Miller, M.D., Nanayama, F., Nishida, N., Richter, C., Rodrigues, T., Rodríguez-Tovar, F.J., Roque, A.C.F., Sanchez Goñi, M.F., Sierro Sánchez, F.J., Singh, A.D., Sloss, C.R., Stow, D.A.V., Takashimizu, Y., Tzanova, A., Voelker, A., Xuan, C., Williams, T., 2015. A reference time scale for Site U1385 (Shackleton Site) on the SW Iberian Margin. Global and Planetary Change 133, 49-64.

Incarbona, A., Martrat, B., Di Stefano, E., Grimalt, J.O., Pelosi, N., Patti, B., Tranchida, G., 2010. Primary productivity variability on the Atlantic Iberian Margin over the last 70,000 years: Evidence from coccolithophores and fossil organic compounds. Paleoceanography 25.

Iorga, M.C., Lozier, M.S., 1999. Signatures of the Mediterranean outflow from a North Atlantic climatology 1. Salinity and density fields. Journal of Geophysical Research-Oceans 104, 25985-26009.

Jia, Y., 2000. Formation of an Azores Current Due to Mediterranean Overflow in a Modeling Study of the North Atlantic. Journal of Physical Oceanography 30, 2342-2358.

Johnson, J., Stevens, I., 2000. A fine resolution model of the eastern North Atlantic between the Azores, the Canary Islands and the Gibraltar Strait. Deep Sea Research Part I: Oceanographic Research Papers 47, 875-899.

Khélifi, N., Sarnthein, M., Frank, M., Andersen, N., Garbe-Schönberg, D., 2014. Late Pliocene variations of the Mediterranean outflow. Marine Geology 357, 182-194.

Kuijpers, A., Nielsen, T., 2015. Near-bottom current speed maxima in North Atlantic contourite environments inferred from current-induced bedforms and other seabed evidence. Marine Geology.

Leynaud, D., Mienert, J., Vanneste, M., 2009. Submarine mass movements on glaciated and non-glaciated European continental margins: A review of triggering mechanisms and preconditions to failure. Marine and Petroleum Geology 26, 618-632.

Lamb, K.G., 2014. Internal Wave Breaking and Dissipation Mechanisms on the Continental Slope/Shelf. Annual Review of Fluid Mechanics 46, 231-254.

Lofi, J., Voelker, A.H.L., Ducassou, E., Hernández-Molina, F.J., Sierro, F.J., Bahr, A., Galvani, A., Lourens, L.J., Pardo-Igúzquiza, E., Pezard, P., Rodríguez-Tovar, F.J., Williams, T., 2016. Quaternary chronostratigraphic framework and sedimentary processes for the Gulf of Cadiz and Portuguese Contourite Depositional Systems derived from Natural Gamma Ray records. Marine Geology 377, 40-57.

Louarn, E., Morin, P., 2011. Antarctic Intermediate Water influence on Mediterranean Sea Water outflow. Deep Sea Research Part I: Oceanographic Research Papers 58, 932-942.

Lisiecki, L.E., Raymo, M.E., 2005. A Pliocene-Pleistocene stack of 57 globally distributed benthic delta O-18 records (vol 20, art no PA1003, 2005). Paleoceanography 20.

Lozier, M.S., Nicole, M.S., 2008. On the Temporally Varying Northward Penetration of Mediterranean Overflow Water and Eastward Penetration of Labrador Sea Water. Journal of Physical Oceanography 38, 2097-2103.

Machín, F., Pelegrí, J.L., 2009. Northward Penetration of Antarctic Intermediate Water off Northwest Africa. Journal of Physical Oceanography 39, 512-535.

Maiorano, P., Marino, M., Balestra, B., Flores, J.A., Hodell, D.A., Rodrigues, T., 2015. Coccolithophore variability from the Shackleton Site (IODP Site U1385) through MIS 16-10. Global and Planetary Change 133, 35-48.

Martín–Chivelet, J., Fregenal–Martínez, M.A., Chacón, B., 2008. Chapter 10 Traction Structures in Contourites, in: Rebesco, M., Camerlenghi, A. (Eds.), Developments in Sedimentology. Elsevier, pp. 157-182.

Martrat, B., Grimalt, J.O., Shackleton, N.J., de Abreu, L., Hutterli, M.A., Stocker, T.F., 2007. Four Climate Cycles of Recurring Deep and Surface Water Destabilizations on the Iberian Margin. Science 317, 502-507.

Maslin, M.A., Brierley, C.M., 2015. The role of orbital forcing in the Early Middle Pleistocene Transition. Quaternary International 389, 47-55.

Mazé, J.P., Arhan, M., Mercier, H., 1997. Volume budget of the eastern boundary layer off the Iberian Peninsula. Deep Sea Research Part I: Oceanographic Research Papers 44, 1543-1574.

Mccave, I.N., Hall, I.R., 2006. Size sorting in marine muds: Processes, pitfalls, and prospects for paleoflow-speed proxies. Geochemistry, Geophysics, Geosystems 7.

McPhee-Shaw, E., 2006. Boundary–interior exchange: Reviewing the idea that internal-wave mixing enhances lateral dispersal near continental margins. Deep Sea Research Part II: Topical Studies in Oceanography 53, 42-59.

Medialdea, T., Somoza, L., Pinheiro, L.M., Fernández-Puga, M.C., Vázquez, J.T., León, R., Ivanov, M.K., Magalhaes, V., Díaz-del-Río, V., Vegas, R., 2009. Tectonics and mud volcano development in the Gulf of Cádiz. Marine Geology 261, 48-63.

Mienis, F., De Stigter, H., White, M., Duineveld, G.C.A., De Haas, H., Van Weering, T., 2007. Hydrodynamic controls on cold-water coral growth and carbonate-mound development at the SW and SE Rockall Trough Margin, NE Atlantic Ocean. Deep-Sea Research I 54, 1655-1674.

Mienis, F., De Stigter, H.C., De Haas, H., Van Weering, T.C.E., 2009. Near-bed particle deposition and resuspension in a cold-water coral mound area at the Southwest Rockall Trough margin, NE Atlantic. Deep Sea Research Part I: Oceanographic Research Papers 56, 1026-1038.

Mienis, F., De Stigter, H.C., De Haas, H., Van der Land, C., Van Weering, T.C.E., 2012. Hydrodynamic conditions in a cold-water coral mound area on the Renard Ridge, southern Gulf of Cadiz. Journal of Marine Systems 96–97, 61-71.

Mohn, C., Rengstorf, A., White, M., Duineveld, G., Mienis, F., Soetaert, K., Grehan, A., 2014. Linking benthic hydrodynamics and cold-water coral occurrences: A high-resolution model study at three cold-water coral provinces in the NE Atlantic. Progress In Oceanography 122, 92-104.

Montero-Serrano, J.-C., Frank, N., Colin, C., Wienberg, C., Eisele, M., 2011. The climate influence on the mid-depth Northeast Atlantic gyres viewed by cold-water corals. Geophysical Research Letters 38.

Naafs, B.D.A., Hefter, J., Stein, R., 2013. Millennial-scale ice rafting events and Hudson Strait Heinrich(-like) Events during the late Pliocene and Pleistocene: a review. Quaternary Science Reviews 80, 1-28.

New, A.L., Barnard, S., Herrmann, P., Molines, J.-M., 2001. On the origin and pathway of the saline inflow to the Nordic Seas: insights from models. Progress In Oceanography 48, 255-287.

Paillard, D., Labeyrie, L., Yiou, P., 1996. Macintosh Program performs time-series analysis. Eos, Transactions American Geophysical Union 77, 379-379.

Palomino, D., López-González, N., Vázquez, J.-T., Fernández-Salas, L.-M., Rueda, J.-L., Sánchez-Leal, R., Díaz-del-Río, V., 2016. Multidisciplinary study of mud volcanoes and diapirs and their relationship to seepages and bottom currents in the Gulf of Cádiz continental slope (northeastern sector). Marine Geology 378, 196-212.

Peliz, A., Dubert, J., Marchesiello, P., Teles-Machado, A., 2007. Surface circulation in the Gulf of Cadiz: Model and mean flow structure. Journal of Geophysical Research: Oceans 112, n/a-n/a.

Peliz, A., Boutov, D., Cardoso, R.M., Delgado, J., Soares, P.M.M., 2013. The Gulf of Cadiz–Alboran Sea sub-basin: Model setup, exchange and seasonal variability. Ocean Modelling 61, 49-67.

Penaud, A., Eynaud, F., Turon, J.L., Blamart, D., Rossignol, L., Marret, F., Lopez-Martinez, C., Grimalt, J.O., Malaizé, B., Charlier, K., 2010. Contrasting paleoceanographic conditions off Morocco during Heinrich events (1 and 2) and the Last Glacial Maximum. Quaternary Science Reviews 29, 1923-1939.

Pomar, L., Morsilli, M., Hallock, P., Bádenas, B., 2012. Internal waves, an under-explored source of turbulence events in the sedimentary record. Earth-Science Reviews 111, 56-81.

Pujos, A., 1988. Spatio-temporal distribution of some quaternary coccoliths. Oceanologica Acta 11, 65 - 77.

Raddatz, J., Rüggeberg, A., Liebetrau, V., Foubert, A., Hathorne, E.C., Fietzke, J., Eisenhauer, A., Dullo, W.-C., 2014. Environmental boundary conditions of cold-water coral mound growth over the last 3 million years in the Porcupine Seabight, Northeast Atlantic. Deep Sea Research Part II: Topical Studies in Oceanography 99, 227-236.

Raffi, I., 2002. Revision of the early-middle pleistocene calcareous nannofossil biochronology (1.75–0.85 Ma). Marine Micropaleontology 45, 25-55.

Raffi, I., Backman, J., Fornaciari, E., Pälike, H., Rio, D., Lourens, L., Hilgen, F., 2006. A review of calcareous nannofossil astrobiochronology encompassing the past 25 million years. Quaternary Science Reviews 25, 3113-3137.

Raymo, M.E., Oppo, D.W., Flower, B.P., Hodell, D.A., McManus, J.F., Venz, K.A., Kleiven, K.F., McIntyre, K., 2004. Stability of North Atlantic water masses in face of pronounced climate variability during the Pleistocene. Paleoceanography 19, PA2008.

Rebesco, M., Hernández-Molina, F.J., Van Rooij, D., Wåhlin, A., 2014. Contourites and associated sediments controlled by deep-water circulation processes: State-of-the-art and future considerations. Marine Geology 352, 111-154.

Reid, J., 1979. On the contribution of the Mediterranean Sea outflow to the Norwegian-Greenland Sea. Deep Sea Research Part A. Oceanographic Research Papers 26, 1199.

Rhines, P.B., Holland, W.R., 1979. A theoretical discussion of eddy-driven mean flows. Dynamics of Atmospheres and Oceans 3, 289-325.

Ribó, M., Puig, P., Muñoz, A., Lo Iacono, C., Masqué, P., Palanques, A., Acosta, J., Guillén, J., Gómez Ballesteros, M., 2016. Morphobathymetric analysis of the large fine-grained sediment waves over the Gulf of Valencia continental slope (NW Mediterranean). Geomorphology 253, 22-37.

Rice, A.L., Thurston, M.H., New, A.L., 1990. Dense aggregations of a hexactinellid sponge, *Pheromena carpenteri*, in the Porcupine Seabight (northeast Atlantic Ocean), and possible causes. Progress In Oceanography 24, 179-196.

Richardson, P.L., Bower, A.S., Zenk, W., 2000. A census of Meddies tracked by floats. Progress In Oceanography 45, 209-250.

Richter, T.O., van der Gaast, S., Koster, B., Vaars, A., Gieles, R., de Stigter, H.C., De Haas, H., van Weering, T.C.E., 2006. The Avaatech XRF Core Scanner: technical description and applications to NE Atlantic sediments, in: Rothwell, R.G. (Ed.), New techniques in Sediment Core Analysis. Geological Society, London, pp. 39-50.

Rogerson, M., Rohling, E.J., Weaver, P.P.E., Murray, J.W., 2005. Glacial to interglacial changes in the settling depth of the Mediterranean Outflow plume. Paleoceanography 20.

Rogerson, M., Rohling, E.J., Weaver, P.P.E., 2006. Promotion of meridional overturning by Mediterranean-derived salt during the last deglaciation. Paleoceanography 21.

Rogerson, M., Colmenero-Hidalgo, E., Levine, R.C., Rohling, E.J., Voelker, A.H.L., Bigg, G.R., Schönfeld, J., Cacho, I., Sierro, F.J., Löwemark, L., Reguera, M.I., de Abreu, L., Garrick, K., 2010. Enhanced Mediterranean-Atlantic exchange during Atlantic freshening phases. Geochemistry Geophysics Geosystems 11, Q08013.

Rogerson, M., Rohling, E.J., Bigg, G.R., Ramirez, J., 2012. Paleoceanography of the Atlantic-Mediterranean exchange: Overview and first quantitative assessment of climatic forcing. Reviews of Geophysics 50, RG2003.

Rohling, E.J., Foster, G.L., Grant, K.M., Marino, G., Roberts, A.P., Tamisiea, M.E., Williams, F., 2014. Sea-level and deep-sea-temperature variability over the past 5.3 million years. Nature 508, 477-482.

Rüggeberg, A., Dullo, C., Dorschel, B., Hebbeln, D., 2007. Environmental changes and growth history of a cold-water carbonate mound (Propeller Mound, Porcupine Seabight). International Journal of Earth Sciences 96, 57-72.

Schlitzer, R., 2012. Ocean Data View, http://odv.awi.de.

Serra, N., Ambar, I., 2002. Eddy generation in the Mediterranean undercurrent. Deep Sea Research Part II: Topical Studies in Oceanography 49, 4225-4243.

Serra, N., Ambar, I., Käse, R.H., 2005. Observations and numerical modelling of the Mediterranean outflow splitting and eddy generation. Deep Sea Research Part II: Topical Studies in Oceanography 52, 383-408.

Serra, N., Ambar, I., Boutov, D., 2010. Surface expression of Mediterranean Water dipoles and their contribution to the shelf/slope – open ocean exchange. Ocean Sci. 6, 191-209.

Shanmugam, G., 1997. The Bouma Sequence and the turbidite mind set. Earth-Science Reviews 42, 201-229.

Shanmugam, G., 2008. Chapter 5 Deep-water Bottom Currents and their Deposits, in: Rebesco, M., Camerlenghi, A. (Eds.), Developments in Sedimentology. Elsevier, pp. 59-81.

Shanmugam, G., 2013. Modern internal waves and internal tides along oceanic pycnoclines: Challenges and implications for ancient deep-marine baroclinic sands. AAPG Bulletin 97, 799-843.

Snoussi, M., Jouanneau, J.M., Latouche, C., 1990. Flux de matières issues de bassins versants de zones semi-arides (Bassins du Sebou et du Souss, Maroc). Importance dans le bilan global des apports d'origine continentale parvenant à l'Océan Mondial. Journal of African Earth Sciences (and the Middle East) 11, 43-54.

Southard, J.B., Cacchione, D.A., 1972. Experiments on Bottom Sediment Movement by Breaking InternalWaves. In: Swift, D.J., Duane, D.B., Pilkey, O.H. (Eds.), Shelf Sediment Transport: Process and Pattern. Hutchinson & Ross, Stroudsburg, Pa., Dowden, pp. 83–97.

Stein, R., Sarnthein, M., Suendermann, J., 1986. Late Neogene submarine erosion events along the north-east Atlantic continental margin, in: Summerhayes, C.P., Shackleton, N.J. (Eds.), North Atlantic Palaeoceanography. Geological Society, London, pp. 103-118.

Stow, D.A.V., Shanmugam, G., 1980. Sequence of structures in fine-grained turbidites: Comparison of recent deep-sea and ancient flysch sediments. Sedimentary Geology 25, 23-42.

Stow, D.A.V., Faugères, J.-C., Howe, J.A., Pudsey, C.J., Viana, A.R., 2002. Bottom currents, contourites and deep-sea sediment drifts: current state-of-the-art, in: Stow, D.A.V., Pudsey, C.J., Howe, J.A., Faugères, J.-C., Viana, A.R. (Eds.), Deep-Water Contourite Systems: Modern Drifts and Ancient Series, Seismic and Sedimentary Characteristics. Geological Society, London, pp. 7-20.

Stow, D.A.V., Faugères, J.C., 2008. Chapter 13 Contourite Facies and the Facies Model, in: Rebesco, M., Camerlenghi, A. (Eds.), Developments in Sedimentology. Elsevier, pp. 223-256.

Stow, D.A.V., Hernandez-Molina, F.J., Llave, E., Sayago-Gil, M., del Rio, V.D., Branson, A., 2009. Bedform-velocity matrix: The estimation of bottom current velocity from bedform observations. Geology 37, 327-330.

Takashimizu, Y., Kawamura, R., Rodríguez-Tovar, F.J., Dorador, J., Ducassou, E., Hernández-Molina, F.J., Stow, D.A.V., Alvarez-Zarikian, C.A., 2016. Reworked tsunami deposits by bottom currents: Circumstantial evidences from Late Pleistocene to Early Holocene in the Gulf of Cádiz. Marine Geology 377, 95-109.

Thierens, M., Browning, E., Pirlet, H., Loutre, M.F., Dorschel, B., Huvenne, V.a.I., Titschack, J., Colin, C., Foubert, A., Wheeler, A.J., 2013. Cold-water coral carbonate mounds as unique palaeo-archives: the Plio-Pleistocene Challenger Mound record (NE Atlantic). Quaternary Science Reviews 73, 14-30.

Thomson, J., Nixon, S., Summerhayes, C.P., Schönfeld, J., Zahn, R., Grootes, P., 1999. Implications for sedimentation changes on the Iberian margin over the last two glacial/interglacial transitions from (230Thexcess)0 systematics. Earth and Planetary Science Letters 165, 255-270.

Titschack, J., Thierens, M., Dorschel, B., Schulbert, C., Freiwald, A., Kano, A., Takashima, C., Kawagoe, N., Li, X., 2009. Carbonate budget of a cold-water coral mound (Challenger Mound, IODP Exp. 307). Marine Geology 259, 36-46.

Toucanne, S., Zaragosi, S., Bourillet, J.F., Cremer, M., Eynaud, F., Van Vliet-Lanoë, B., Penaud, A., Fontanier, C., Turon, J.L., Cortijo, E., Gibbard, P.L., 2009a. Timing of massive 'Fleuve Manche' discharges over the last 350 kyr: insights into the European ice-sheet oscillations and the European drainage network from MIS 10 to 2. Quaternary Science Reviews 28, 1238-1256.

Toucanne, S., Zaragosi, S., Bourillet, J.F., Gibbard, P.L., Eynaud, F., Giraudeau, J., Turon, J.L., Cremer, M., Cortijo, E., Martinez, P., Rossignol, L., 2009b. A 1.2 Ma record of glaciation and fluvial discharge from the West European Atlantic margin. Quaternary Science Reviews 28, 2974-2981.

Trauth, M.H., Maslin, M.A., Deino, A.L., Strecker, M.R., Bergner, A.G.N., Dühnforth, M., 2007. High- and low-latitude forcing of Plio-Pleistocene East African climate and human evolution. Journal of Human Evolution 53, 475-486.

Trauth, M.H., Larrasoaña, J.C., Mudelsee, M., 2009. Trends, rhythms and events in Plio-Pleistocene African climate. Quaternary Science Reviews 28, 399-411.

Turnewitsch, R., Reyss, J.-L., Chapman, D.C., Thomson, J., Lampitt, R.S., 2004. Evidence for a sedimentary fingerprint of an asymmetric flow field surrounding a short seamount. Earth and Planetary Science Letters 222, 1023-1036.

Tzedakis, P.C., Margari, V., Hodell, D.A., 2015. Coupled ocean–land millennial-scale changes 1.26 million years ago, recorded at Site U1385 off Portugal. Global and Planetary Change 135, 83-88.

van Haren, H., Maas, L., van Aken, H., 2002. On the nature of internal wave spectra near a continental slope. Geophysical Research Letters 29, 57-51-57-53.

Van Rensbergen, P., Depreiter, D., Pannemans, B., Moerkerke, G., Van Rooij, D., Marsset, B., Akhmanov, G., Blinova, V., Ivanov, M., Rachidi, M., Magalhaes, V., Pinheiro, L., Cunha, M., Henriet, J.-P., 2005. The El Arraiche mud volcano field at the Moroccan Atlantic slope, Gulf of Cadiz. Marine Geology 219, 1-17.

Van Rooij, D., Blamart, D., Kozachenko, M., Henriet, J.-P., 2007. Small mounded contourite drifts associated with deep-water coral banks, Porcupine Seabight, NE Atlantic Ocean, in: Viana, A.R., Rebesco, M. (Eds.), Economic and Palaeoceanographic Importance of Contourite Deposits. Geological Society, London, pp. 225-244.

Van Rooij, D., Iglesias, J., Hernández-Molina, F.J., Ercilla, G., Gomez-Ballesteros, M., Casas, D., Llave, E., De Hauwere, A., Gil, S.G., Acosta, J., Henriet, J.P., 2010. The Le Danois Contourite Depositional System: interactions between the Mediterranean Outflow Water and the upper Cantabrian slope (North Iberian margin). Marine Geology 274, 1-20.

Van Rooij, D., Blamart, D., De Mol, L., Mienis, F., Pirlet, H., Wehrmann, L.M., Barbieri, R., Maignien, L., Templer, S.P., de Haas, H., Hebbeln, D., Frank, N., Larmagnat, S., Stadnitskaia, A., Stivaletta, N., van Weering, T., Zhang, Y., Hamoumi, N., Cnudde, V., Duyck, P., Henriet, J.P., 2011. Cold-water COLD-WATER CORAL mounds on the Pen Duick Escarpment, Gulf of Cadiz: The MiCROSYSTEMS project approach. Marine Geology 282, 102-117.

Van Rooij, D., Vandorpe, T., Delivet, S., Hebbeln, D., Wienberg, C., Martins, I.M., Belgica COMIC; MD194 Gateway; MSM36 MoccoMebo Shipboard Scientific parties, 2014. Buried cold-water coral mound provinces and contourite drifts along the Eastern Atlantic margin: controls, interactions and connectivity. in: Van Rooij, D. et al. (Ed.) (2014). Book of Abstracts. 2nd Deep-Water Circulation Congress: The Contourite Log-book. Ghent, Belgium, 10-12 September 2014. VLIZ Special Publication 69, 49-50.

Vandorpe, T., Van Rooij, D., de Haas, H., 2014. Stratigraphy and paleoceanography of a topography-controlled contourite drift in the Pen Duick area, southern Gulf of Cádiz. Marine Geology 349, 136-151.

Vandorpe, T., Martins, I., Vitorino, J., Hebbeln, D., García, M., Van Rooij, D., 2016. Bottom currents and their influence on the sedimentation pattern in the El Arraiche mud volcano province, southern Gulf of Cadiz. Marine Geology 378, 114-126.

Voelker, A.H.L., Lebreiro, S.M., Schonfeld, J., Cacho, I., Erlenkeuser, H., Abrantes, F., 2006. Mediterranean outflow strengthening during northern hemisphere coolings: A salt source for the glacial Atlantic? Earth and Planetary Science Letters 245, 39-55.

Vandorpe, T., Wienberg, C., Hebbeln, D., Van den Berghe, M., Gaide, S., Wintersteller, P., Van Rooij, D., submitted. Initiation and aggradation of buried cold-water corals mounds in the Atlantic Moroccan Coral Province, southern Gulf of Cádiz. Palaeogeography, Palaeoclimatology, Palaeoecology.

White, M., Dorschel, B., 2010. The importance of the permanent thermocline to the cold water coral carbonate mound distribution in the NE Atlantic. Earth and Planetary Science Letters 296, 395-402.

Wienberg, C., Frank, N., Mertens, K.N., Stuut, J.-B., Marchant, M., Fietzke, J., Mienis, F., Hebbeln, D., 2010. Glacial cold-water coral growth in the Gulf of Cádiz: Implications of increased palaeo-productivity. Earth and Planetary Science Letters 298, 405-416.

Wienberg, C., Titschack, J., 2015. Framework-Forming Scleractinian Cold-Water Corals Through Space and Time: A Late Quaternary North Atlantic Perspective, in: Rossi, S., Bramanti, L., Gori, A., Orejas Saco del Valle, C. (Eds.), Marine Animal Forests: The Ecology of Benthic Biodiversity Hotspots. Springer International Publishing, Cham, pp. 1-34.

World Ocean Database, 2013. https://www.nodc.noaa.gov/OC5/WOD13/data13geo.html.

Zahn, R., Sarnthein, M., 1987. Benthic isotope evidence for changes of the Mediterranean Outflow during the Late Quaternary. Paleoceanography 2, 543-559.

Zhang, W., Hanebuth, T.J.J., Stöber, U., 2015. Short-term sediment dynamics on a meso-scale contourite drift (off NW Iberia): Impacts of multi-scale oceanographic processes deduced from the analysis of mooring data and numerical modelling. Marine Geology.

Zitellini, N., Gracia, E., Matias, L., Terrinha, P., Abreu, M.A., DeAlteriis, G., Henriet, J.P., Danobeitia, J.J., Masson, D.G., Mulder, T., Ramella, R., Somoza, L., Diez, S., 2009. The quest for the Africa-Eurasia plate boundary west of the Strait of Gibraltar. Earth and Planetary Science Letters 280, 13-50.

CHAPTER 7

Discussion, conclusions and outlook

Research on contourites carries the explicit objective to trace, characterize and discriminate the sedimentological expression of the variety of the existing oceanographic processes in the past ocean, to which internal tides and internal waves belong (Faugères and Stow, 2008; Hernández-Molina et al., 2011; Rebesco et al., 2014; Van Rooij et al., 2016). Their discrimination remains challenging because of the association of processes of different space and time scales and variability, characterised by drastically different potential energies (Hanebuth et al., 2015; Zhang et al., 2015; Chen et al., 2016; Ercilla et al., 2016; Hernández-Molina et al., 2016a). This PhD dissertation investigated the expression of internal tidal dominated bottom currents from both geomorphological and sedimentological criteria within 3 distinct geographic locations. Common characteristics shared between those sites were (i) low slope gradients, varying from ~1 to 1.5° (ii) moderate mean contour current, generally below 10 cm/s (Huthnance et al., 2001; Mienis et al., 2012) (iii) energetic intermittent bidirectional internal tidal bottom currents, typically reaching peak velocities up to 30 cm/s (Thomsen and van Weering, 1998; Mienis et al., 2012) (iv) widespread regional occurrence of past or present cold-water coral thriving ecosystems (Dorschel et al., 2005; Van Rooij et al., 2007; Foubert et al., 2008). Nonetheless, each site revealed very different sedimentary facies successions which were explained in terms of sediment source contributions (hemipelagic, ice-rafted, aeolian and bottom current reworked sediments), primarily driven by variations in climate, bottom current (contouritic) processes, and in a lesser extent density driven (turbiditic) processes. The following discussion first provides a review on deep-marine tidal bottom current controlling factors, as an important step in order to understand the range of application and limits of this study. Then, the progress made understanding the impact, expression and controls that tide-topography interactions may exert on the sedimentary record are reviewed.

7.1 Characteristics and diagnostic criteria of internal tidal deposits

7.1.1 Deep-marine tidal bottom currents

Barotropic tides are depth independent while baroclinic motions result from the density distribution of the fluid, using the potential energy available in stratified water columns (Shanmugam, 2013). Marked pycnal gradients are not a necessary feature for the generation and propagation of internal waves/tides since the hydrostatic pressure gradient well supports those features (Garrett and Munk, 1979; Shanmugam, 2013). Nevertheless, in addition to (depth independent) tide-topography interactions, energetic internal tides and/or waves processes occur associated with the permanent pycnocline (generally around ~200 m water depth) and the secondary density stratifications observed within water column (Shanmugam, 2013; Lamb, 2014). The permanent pycnocline is being the most marked density gradient in the ocean which explains the particular response of this interface with respect to internal wave processes (Apel, 2000, 2002; Klymak et al., 2011; Sánchez-Garrido et al., 2011). Processes along this interface received much attention as they are often visible from sea surface using radars and carry considerable potential energy (Apel, 2002).

The present study strictly applied to secondary pycnal gradients, at water depths mainly remote from the influence of sea surface processes and processes occurring along the permanent pycnocline. Noteworthy there exist a variety of breaking wave mechanisms, either reflecting over the seabed and/or being generated at near critical slopes, which result from a full combination of fluid motions that should ideally be considered distinctly (Lamb et al., 2014). The bottom current regime along both the Irish and Atlantic Moroccan margins can be denominated as "deep-marine tidal bottom currents" sensus Shanmugam (2013), in which the different contribution of barotropic and (internal) baroclinic processes are unknown (White and Dorschel, 2010; Mienis et al., 2012; Mulder et al., 2012). This is because the respective contribution of barotropic versus baroclinic motions, being generated locally and/or remotely, is mainly not discriminated from time-series acquired along discrete geographic locations (Gao et al., 1998). The comprehensive discrimination and predictability of these respective contributions is an important future challenge, to which the development of high-resolution modelling may constitute the most promising approach (Lamb, 2014; Zhang et al., 2015).

Nevertheless, it is possible to qualitatively assess the influence of more or less marked pycnal gradient by calculating tide-topography reflection conditions, as the local density gradient is formulated within the equations of Southard and Cacchione (1972). Sub-critical reflection conditions may occur at any depth and for any pycnal gradient profile (Garrett and Kunze, 2007). Therefore tide-topographic interactions and their effect on sediment redistribution are in fact significant at

potentially all depth ranges (Turnewitsch et al., 2008; Turnewitsch et al., 2013). Assuming the slope gradient of a considered region didn't significantly change over a certain period of time, the sedimentological impact of tide-topography interactions may primarily vary as function of the reflection conditions, which are in turn driven by variations in the local pycnal gradient. Likewise, varying bottom current regime may be, in some cases, indicative for variation in the local pycnal gradient and water column stratification.

7.1.2 Geomorphological characteristics

Geomorphological studies provide the most coherent criteria for the diagnostic of contourites, which however is limited to large time-scales, rarely providing information on millennial time-scales (Hernández-Molina et al., 2016a). However, robust link between the seabed physiography, the circulation of bottom water masses and the morphology of the formed contourite drifts can be established (Faugères et al., 1999; Rebesco et al., 2014; Van Rooij et al., 2016). Wynn and Stow (2002) attached a similar importance of geomorphological studies for the diagnostic of deep sea sediment waves, as well as for the identification of their formation process. Chapter 3 (this dissertation) provides arguments to which extent the field of large-scale sediment waves at Goban Spur, as well as its geomorphological evolution, can be compared and integrated within the MOW Contourite Depositional Complex (Fig. 7.1). Mounded separated drifts (among others) formed both within the northern Gulf of Cádiz and the Le Danois Contourite Depositional Systems (Van Rooij et al., 2010; Hernández-Molina et al., 2016c). They have a marked elongation up to few tens of kilometres despite the irregular and complex physiography of both margins. Such characteristic is typically indicative for the existence of consistent and energetic contour currents interacting with the slope (Faugères et al., 1993; Faugères et al., 1999; Stow et al., 2002; Hernández-Molina et al., 2008; Rebesco and Camerlenghi, 2008). This feature does no longer exist along the Irish margin, where the drifts continuity is mainly controlled by (palaeo)-topographic irregularities (Van Rooij et al., 2003; Van Rooij et al., 2007). Kilometres-scaled drift are more frequent and tend to be isolated to each other rather than forming a continuous and single elongated drift structure (Fig. 7.1; Van Rooij et al., 2007). One may consider this observation as indicative for a change in the main oceanographic process that has driven their formation (Fig. 7.1).

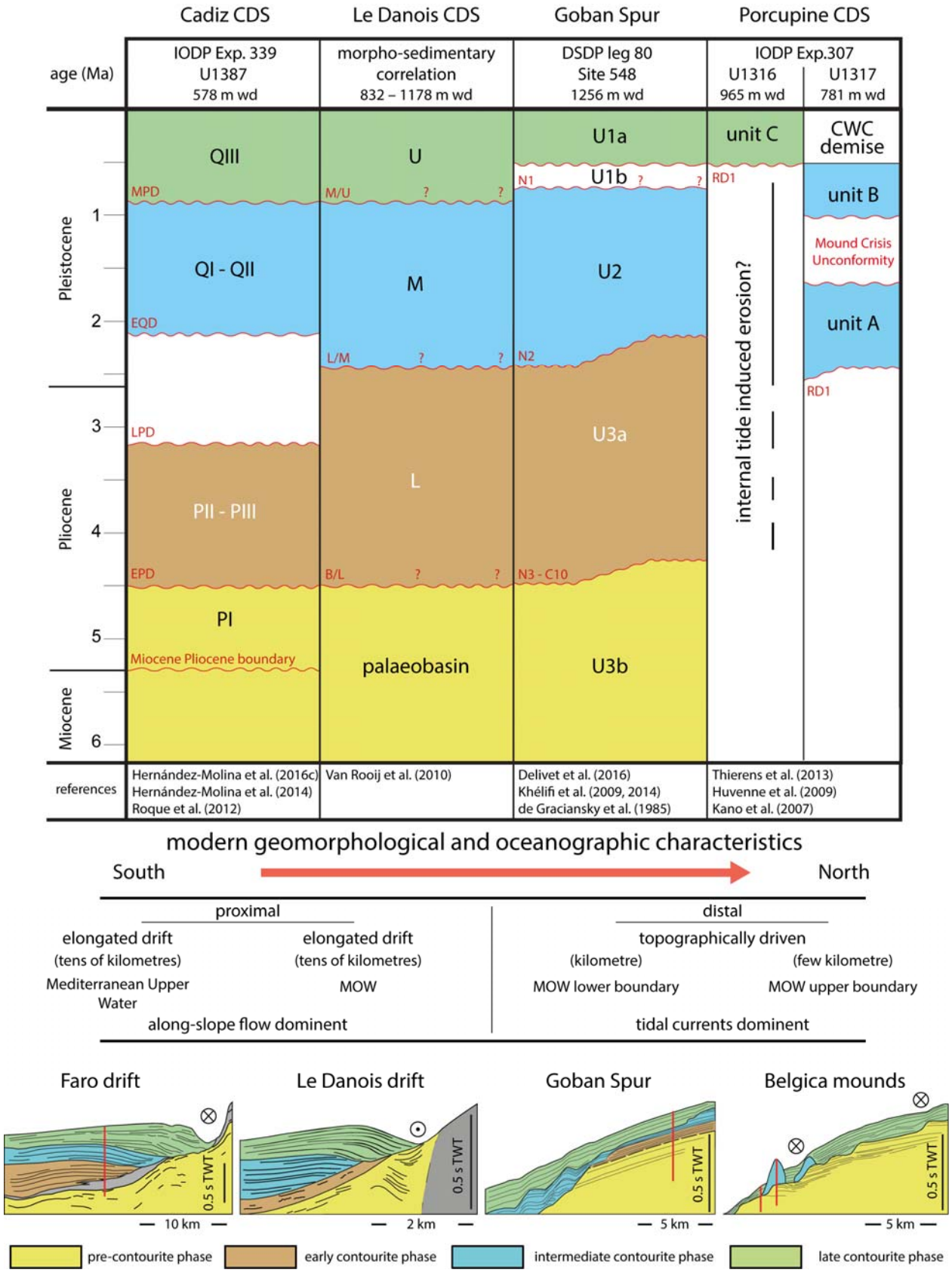
Cadiz CDS
Le Danois CDS
Goban Spur
Porcupine CDS
age (Ma)
IODP Exp. 339
U1387
578 m wd
morpho-sedimentary
correlation
832 – 1178 m wd
DSDP leg 80
Site 548
1256 m wd
IODP Exp.307
U1316
965 m wd
U1317
781 m wd
Pleistocene
Pliocene
Miocene
1
2
3
4
5
6
QIII
QI - QII
PII - PIII
PI
U
M
L
palaeobasin
U1a
U1b
U2
U3a
U3b
unit C
internal tide induced erosion?
CWC
demise
unit B
Mound Crisis
Unconformity
unit A
MPD
EQD
LPD
EPD
Miocene Pliocene boundary
M/U
L/M
B/L
N1
N2
N3 - C10
RD1
RD1
references
Hernández-Molina et al. (2016c)
Hernández-Molina et al. (2014)
Roque et al. (2012)
Van Rooij et al. (2010)
Delivet et al. (2016)
Khélifi et al. (2009, 2014)
de Graciansky et al. (1985)
Thierens et al. (2013)
Huvenne et al. (2009)
Kano et al. (2007)
modern geomorphological and oceanographic characteristics
South
North
proximal
distal
elongated drift
(tens of kilometres)
Mediterranean Upper
Water
elongated drift
(tens of kilometres)
MOW
topographically driven
(kilometre)
MOW lower boundary
(few kilometre)
MOW upper boundary
along-slope flow dominent
tidal currents dominent
Faro drift
Le Danois drift
Goban Spur
Belgica mounds
0.5 s TWT
10 km
2 km
5 km
5 km
pre-contourite phase
early contourite phase
intermediate contourite phase
late contourite phase

Figure 7.1 Plio-Pleistocene evolution of some major sites of the Mediterranean Outflow Water Contourite Drift Complex. Depositional units, hiatuses and main phases of drift development are compared with interpreted seismic geomorphological reconstructions. Note the contrast between (proximal) elongated drifts formed in along-slope dominated bottom current regime and (distal) kilometre-scale and topographically controlled drifts formed in deep-marine tidal bottom currents dominated environments. The growth of cold-water coral mounds within the Porcupine Seabight occurred under erosive and/or non-depositional conditions at site U1316, which may be attributed to enhanced tide-topographic interactions.

The geomorphological study conducted on Goban Spur constitutes one of the few examples of bedforms (large-scale sediment waves) which could be primarily attributed to internal tidal processes (He et al., 2008; Ribó et al., 2016). The orientation and evolution of those bedforms could not be attributed to any observed or reasonable contour current pattern, past or present. More interestingly, the (palaeo-)slope gradient morphology and morphological evolution of the sediment waves can be comprehensively related to internal tide/wave reflection conditions, in a similar pattern than Ribó et al. (2016). Such bedforms are largely absent from the Porcupine Seabight and Moroccan Atlantic margin. Similarly to the Porcupine Seabight, the Moroccan Atlantic margin contourite drifts are generally a few kilometres long, topographically driven, and tend to form isolated structures, rather than being connected to each other (Vandorpe et al., 2014; 2016; submitted). This is because moat/channel and drift structures tend to be much less developed when the topographic obstacles against which they develop have slopes below 11° (Vandorpe et al., 2016). Internal tidal current modulation was largely recognized, and tidal processes were actually proposed as primary mechanism within the Moroccan Atlantic margin, mainly on the basis of their marked asymmetry around mud volcanoes (Vandorpe et al., 2016). Such differentiation was not possible from within the Porcupine Seabight, which might also have been influenced by downslope (turbiditic) processes, leading to overall complex margin architecture (Van Rooij et al., 2003; 2007; 2009). Internal tides interacting with a rough topography locally prevent sedimentation and induce enhanced suspended particulate matter (McPhee-Shaw, 2006; Turnewitsch et al., 2008; 2013; Peine et al., 2009). In such conditions, suspended particles are easily redistributed by slow, though persistent, contour currents associated to the northward flowing the MOW and ENACW (White, 2003). Likewise, the small-scale moats and drifts features rather represent mixed processes, in which internal tides constitute an important process nearby rough topographic obstacles and consistent contour currents in redistributing sediments (Van Rooij et al., 2007).

Another increasingly identified internal tidal product end-member relates to their potential in inducing long term erosive and/or non-depositional conditions (Cacchione et al., 2002). This concerns in particular the formation of contouritic terraces, which are more and more recognized as

originating from enhanced internal tide/wave processes at water masses boundaries (Maestro et al., 2013; Preu et al., 2013; Ercilla et al., 2016; Hernández-Molina et al., 2016a; Juan et al., 2016). The ability of deep-marine tidal bottom currents to induce erosion depend on preconditioning factors such as the slope gradient and the (palaeo-) seabed morphology, and the local variation in the pycnal gradient (Garrett and Kunze, 2007; Shanmugam, 2013a; Lamb, 2014). Along Goban Spur, the regionally smooth slope did not lead to erosive conditions with respect to tide-topography interactions, and enhanced internal tide regime was inferred from ~4.5 to 4.2 Ma. However, several authors have insisted on the existence of regionally critical to sub-critical tide-topography interactions within the Porcupine Seabight (Rice et al., 1990; White et al., 2005; 2010; Dorschel et al., 2007; Mohn et al., 2014). Within the Porcupine Seabight, the youngest sequences recovered prior the regional discontinuity RD1 are ca. 8.9 Ma (Kano et al., 2007), which predate the onset of enhanced tide-topography interactions at Goban Spur (Fig. 7.1). Various evidences of enhanced bottom currents associated to the Porcupine RD1 erosion, in particular at the base of the cold-water coral mounds have been reported (Huvenne et al., 2009; Raddatz et al., 2011). Laterally to the cold-water coral mounds, sedimentation lagged from ~ 1.24 to 0.42 Ma depending on the location (Kano et al., 2007). Cold-water corals are known to develop under energetic internal tidal bottom currents along this part of the margin (Mohn et al., 2014; Raddatz et al., 2014; Hebbeln et al., 2016). Despite the RD1 discontinuity is regionally complex, and probably the result of several incision phases (Van Rooij et al., 2009), one may infer that the stratigraphic gap, at least comprised between the cold-water coral mound initiation (ca. 3 Ma), and the drift development (ca. 1.24 to 0.42 Ma), is mainly caused by bottom current processes (Huvenne et al., 2009). Tide-topography interactions provide a suitable mechanism for explaining, at least part of, the lengthy RD1. Such process might possibly have been active from ~4.2 Ma onwards, as deduced from Goban Spur (Fig. 7.1). From about 0.5 Ma onwards, the climatically modulated MOW may have only intermittently induced enhanced internal tidal processes, also provide a suitable mechanism for the recent complex sediment drift history, in which numerous of millennial-scaled hiatuses are found (Dorschel et al., 2005; Ovrebo et al., 2006; Rüggeberg et al., 2007; Van Rooij et al., 2009). However, geomorphological studies largely fail in the diagnostic of such millennial-scale hiatuses, and sediment core analysis is required. Nevertheless, it can be established a certain analogy between the complex and discontinuous sequences recovered from the Moroccan Atlantic margin and those of the Porcupine Seabight. This highlights that internal tides might constitute one major erosional process along both margins, both on millennial and larger time-scales, in accordance with Cacchione et al. (2002).

7.1.3 Sediment facies

Still today, core-based diagnostic of contourites, and foremost the diagnostic of different contouritic processes remains most challenging (Van Rooij et al., 2016). This includes studies conducted along the northern Gulf of Cádiz, where yet the standard contourite facies model was first proposed (Gonthier et al., 1984; Mulder et al., 2013; Alonso et al., 2016; Hernández-Molina et al., 2016b; Lofi et al., 2016; Nishida, 2016; Takashimizu et al., 2016). Nevertheless, cores recovered from previously identified sediment drifts provide critical information on their sediment facies and facies variations, possibly indicative for palaeoceanographic variations at sub-millennial to millennial time-scales (Gonthier et al., 1984; Voelker et al., 2006; Toucanne et al., 2007; Alonso et al., 2016). Since diagnostic criteria mostly remain ambiguous, geomorphological studies conducted over a certain site prior coring are of paramount importance when working on modern series. The first internal wave deposits (also referred to as internalites) have been introduced by pioneering works of Gao and Eriksson (1991). There has since been a strong effort in order to propose lithological, sedimentary facies models and diagnostic criteria for internal wave deposits (Fig. 7.2; Gao et al., 1998; Shanmugam, 2003; He et al., 2008; Mulder et al., 2012; Pomar et al., 2012). Internal wave deposit can form at any depth, even though they are more frequently observed at depths associated with the permanent pycnocline, where internal tides and waves are generally more energetic (Pomar et al., 2012; Shanmugam, 2013a). So far, clear diagnostic observations have only been possible from outcrops, and strongly rely on the identification of bidirectional sedimentary traction structures, such as bidirectional cross bedding, flaser bedding, wavy and lenticular bedding, as well as alternating bedload conditions (Fig. 7.2; Gao and Eriksson, 1991; Shanmugam, 2003; Bádenas et al., 2012). Lateral facies variations and traction structures mostly are not observed from sediment core data, which might explain a certain delay in their recognition in the present day marine sediments. Hydrodynamic sorting associated with deep-marine tidal bottom currents have been proven to occur at present, as for example on the Goban Spur (Thomsen et al., 1998; 2000; van Weering et al., 1998), and the western Iberian margin (Quaresma et al., 2007). Even though particle grain-size distribution remains one major feature within contouritic sequences, it might still remain ambiguous with respect to the variety of existing contouritic processes, which overall resulted in very similar sedimentary facies (He et al., 2008; Shanmugam, 2013a; Rebesco et al., 2014).

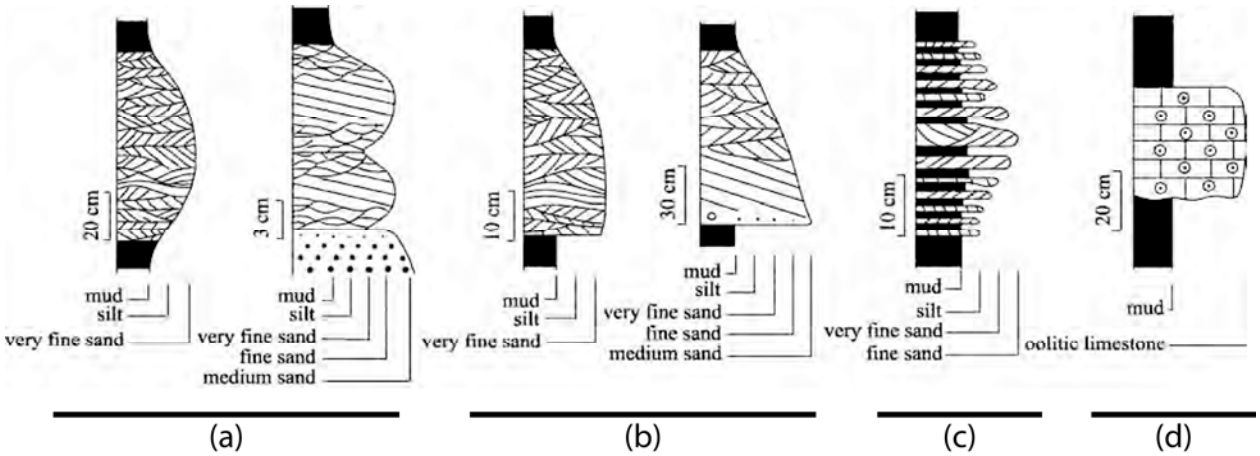

Figure 7.2 Examples of existing internal tide and wave driven deposits (modified from He et al. (2008); original figure in Gao et al., 1998). (a) Coarsening and fining upward sequences of cross laminated sandstone interbedded with dark shales deposited in submarine canyons. (b) Fining upward sequences of cross bedded and cross laminated sandstones from unchannelized continental slope environment. (c) Thickening and thinning upward rhythmic successions of bidirectional cross bedded sandstone and mudstone deposited in deep water environment. (d) Mudstone and foraminiferal, oolitic or sandy oolitic limestone with flaser, wavy and lenticular bedding showing alternating bedload suspension deposition in deep water environment.

Interestingly, the sequence recovered from the Pen Duick drift (MD08-3227; Table 7.1) was characterised by an important vertical scatter, with large terrigenous silt distribution changes from adjacent samples. This variability was expressed below the millennial time-scale and overprinted the larger, Dansgaard-Oeschger like, millennial scale variations which still could be evidenced from larger trends. Mud drifts are known to form thick and homogeneous accumulations, generally devoid of traction and sedimentary structures (Rebesco et al., 2014), and such structures could not be observed in this study (Table 7.1). However, the vertical terrigenous silt scatter may be interpreted to originate from alternating bedload, with highly variable traction/suspension/deposition conditions. Such conditions might be inherent to tide-topography interactions models (Southard and Cacchione, 1972; Gao et al., 1998). On the other hand, homogenous and persistent changes in terrigenous grain-size might also be considered to reflect the continuous nature of internal tides, sweeping the seabed a semi-diurnal frequency (Gao et al., 1998). This would be analogue to results obtained from DSDP Site 548 where vertically homogeneous coarsening towards silty contourites was lasting from few millennia up to ~20 ky (Table 7.1). Here, the main argument that can be found to explain this facies contrast must involve the differences in sedimentation rates. The sedimentation obtained from the Pen Duick drift (~100 cm/ky) may have been large enough to capture the alternating bedload conditions whereas this would have not been the case for sedimentation rates at Goban Spur (~20 cm/ky).

		DSDP 548; Irish margin	MD08-3227; Atlantic Moroccan margin	MD13-3447; Atlantic Moroccan margin
latitude; longitude – depth		48.916°N; 12.164°W - 1256 m water depths	35.271°N; 6.798°W - 642 m water depth	35.194°N; 7.148°W - 968 m water depth
local slope gradient		1.5°	1°	1.5°
		sedimentation		
		hemipelagic; Ice Rafter Debris	contourite drift; hemipelagic; aeolian; (turbiditic?)	hemipelagic; aeolian; turbiditic
Lithology		clayey silts with variable amount of biogenic content interbedded with occasional IRD-rich coarse sand layers	silty clays and clayey silts with variable amount of aeolian dust and biogenic content	biogenic-rich silty clays and clayey silts, interbedded with coarse biogenic rich silty sands and few terrigenous-rich fine sands layers
sedimentation rates		varying from 20 to 40 cm/ky	varying from ~20 to ~100 cm/ky	generally below 4 cm/ky
investigated period		500 to 100 ka PB	50 ka BP to recent	1500 ka BP to recent
time-scale		sub-millennial to millennial	millennial	sub-millennial
		present day bottom current regime		
water mass		interface MOW/LSW	AAIW/NACW	MOW
bottom current regime	mean along-slope	≤ 5 cm/s northward; reduced or reversed in spring	7.6 to 8.8 cm/s northward	unknown
	internal tidal	~ 20 cm/s; up to 37 cm/s in winter	30 cm/s	unknown
	Other	unknown	unknown	mesoscale eddies (up to ~25 cm/s of azimuthal velocity)
regime denomination		Deep Marine Tidal Bottom Currents	Deep Marine Tidal Bottom Currents	Deep Marine Tidal Bottom Currents? Eddy driven currents?
Tide-topography reflection conditions		transmissive to near-critical ($0.6 < \gamma/c < 0.8$)	transmissive ($0.45 < j/c < 0.5$)	transmissive ($0.5 < j/c < 0.6$)
		proxy for past bottom current variations		
methodology		terrigenous silt grain-size composition	terrigenous silt grain-size composition	terrigenous silt gain-size composition and sediment facies observations
data range (type)		terrigenous fraction between 0.01 to 1000 µm (Malvern)	terrigenous fraction below 63 µm (Sedigraph)	terrigenous fraction between 0.01 to 1000 µm (Malvern)
first mode amplitude of variations		below 10 µm to generally 30 - 40 µm; locally up to 55 µm	below 10 µm to generally 15 - 20 µm	below 10 µm to 30 µm
variability		homogenous over several millennia	highly variable below millennial time-scale	sub-millennial scale variations
Other diagnostic criteria	facies and traction features	not recognized	not recognized	irregular sand pockets (see therein); variable bioturbation; discontinuous silt lenses; sharp and irregular contacts; rust coloured horizons
	erosive structures	not recognized	Sharp based biogenic rich silty sand layer	sharp and irregular contacts; presence of sandy horizons
	turbiditic	not recognized	possible	sharp based terrigenous rich and fining upward sand layers
		interpretation for past bottom current variations		
magnitude of bottom currents		similar to present days during interglacials; reduced during Marine isotopic stages 12, 10, 8 and 6	more energetic than present days during Dansgaard-Oeschger stadials, Heinrich events; erosive during the LGM	gradually more energetic during glacials of the EMPT; dominantly erosive from ca. 500 ka BP to recent
implications		reduced pycnal gradient affecting internal tidal motions	increased along slope motions and/or internal tidal motions	increased bottom currents and/or internal tidal motions
proposed driving mechanism		replacement of the MOW by the GNAIW	increased advection of AAIW and/or increased pycnal gradient at the AAIW/NACW interface	probable margin-wide tectonic adjustments; increased influence of mesoscale eddy formation rate during sea-level low stands
key controlling factors		climate; water column stratification	climate; water column stratification; sea-level	tectonic; climate; sea-level

Table 7-1 Summary of the main characteristics and sedimentological observations for the investigated sediment cores. Present day and inferred past bottom current regime variations are provided along with the methodologies and interpreted key controlling factors. Note that the covered period of time and resolution of the record varies from site to site.

Ultimately, site MD13-3447 (Atlantic Moroccan margin; 968 m water depth) was characterised by very low sedimentation rates, and the increasing appearance of an irregular, coarse foraminifer rich sandy pockets facies. Those were interpreted as traction structures associated to bottom currents (contouritic sub-division C3), and would represent traction lag deposits and enhanced clay and silt particle transport (Martín–Chivelet et al., 2008; Stow et al., 2009; Shanmugam, 2013a). However, those last facies models were designed and established for sediments redistributed from energetic unidirectional flow (Stow et al., 2002; 2008; McCave and Hall, 2006; Faugères and Stow, 2008). Unidirectional flow induce marked lateral transport of particles, and thus, an important lateral continuity, formation of elongated structures and widespread lithological changes and discontinuities (Fig. 7.3a; Stow et al., 2002; Faugères and Stow, 2008; Rebesco and Camerlenghi, 2008; Rebesco et al., 2014; Alonso et al., 2016; Takashimizu et al., 2016). Here, the lateral continuity of the sand pockets varies within few centimetres, and shapes are laterally poorly defined (Figs. 7.2b, c). This may suggest that the lateral transport may not have been as important as suggested from existing models (Shanmugam, 2008, 2013a). Tidal motions are restored by gravitational forces, which induce compensated bidirectional flow, and thus small mean lateral transport of the particles (Thomsen and van Weering, 1998; Hanebuth et al., 2015; Zhang et al., 2015). A variable internal tidal regime could induce cycles of particle traction/suspension of overall small lateral particle transport, which could explain the formation of the irregular sand pocket facies (Fig. 7.3d). Along the western Iberian mid-shelf, Quaresma et al. (2007) accordingly observed that internal tidal bottom currents, typically ranging from 10 to 20 cm/s, where able to separate sand particles (>100 μm grain-size) from the fine clay and silt fractions which remained in suspension. Alternatively, repeated incursions of alternatively cyclonic and anticyclonic Mediterranean mesoscale eddies, intermittently interacting with the seabed may also induce variable cycles of particle traction/suspension of overall small mean lateral transport. However, little is known about mesoscale eddies and seabed interactions, and their significance for the bottom current regime in this area. Some Mediterranean mesoscale eddies were observed to interact with the Atlantic Moroccan margin and to change their course without fully dissipating (Ambar et al., 2008; Barbosa Aguiar et al., 2013). There exists yet no long term monitoring for the influence of those structures on the regional bottom current regime. Nevertheless, the variable incursion of Mediterranean mesoscale eddies is known to influence on the local pycnal gradient, which in turn may cause variable deep-marine tidal bottom current conditions.

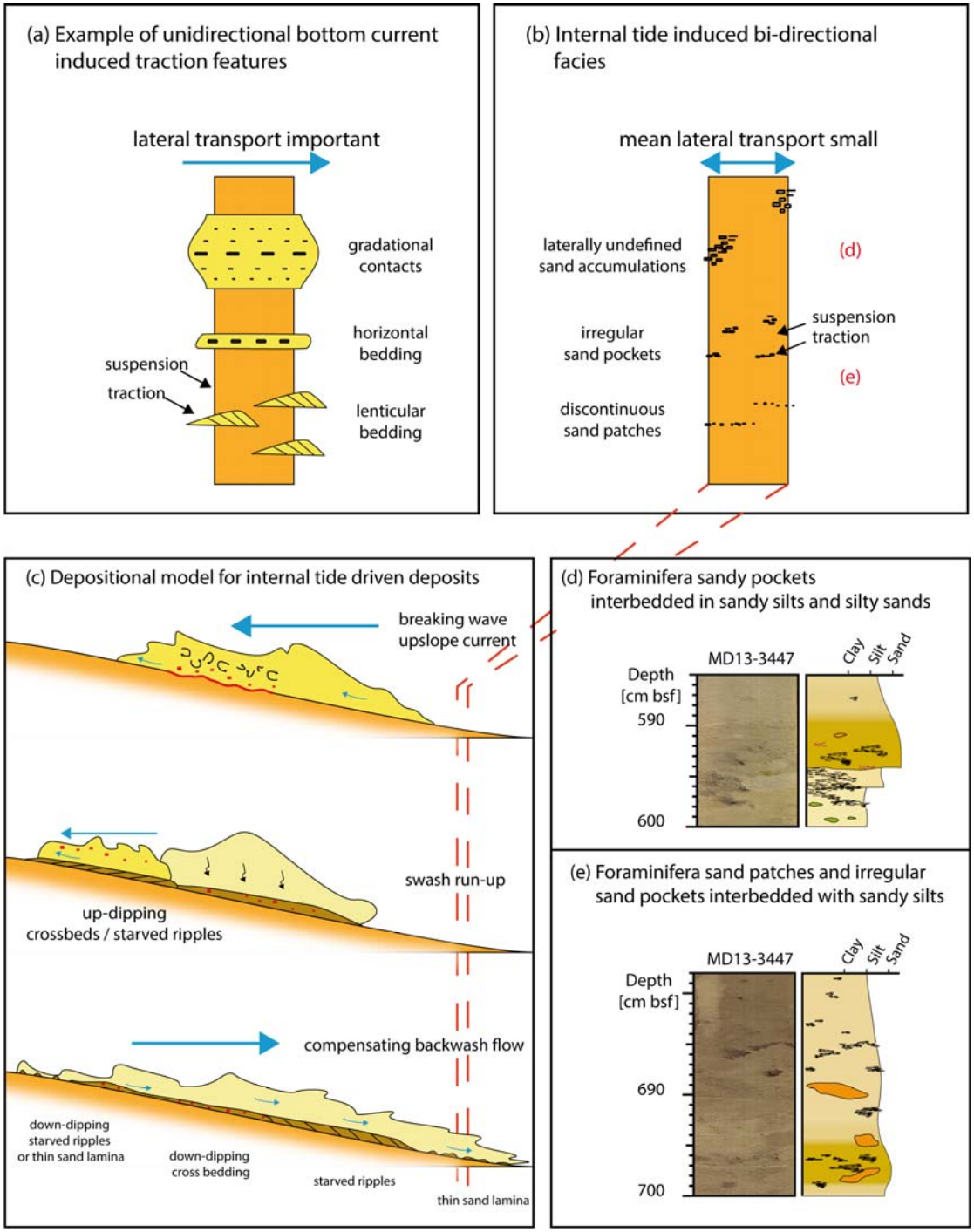

Figure 7.3 Examples of sedimentary traction features formed under different bottom current regime. (a) Few examples of bottom current traction structures, varying from lenticular to continuous bedding, formed from consistent (unidirectional) lateral transport (simplified after Shanmugam, 2008, 2013). (b) Proposed model for internal tidal bi-directional traction features. The small mean lateral transport result in the formation coarse and discontinuous patches over the seafloor. Laterally undefined vertical accumulations may correspond to the vertical development of those patches under variable internal tidal regime. (c) Internal tide driven depositional model proposed from (Bádenas et al., 2012). Internal tide breaking and interaction with sloping seabed was derived from (Southard and Cacchione, 1972). (d) and (e) Foraminifera rich irregular sand pockets, proposed to correspond to internal tide traction structure, analogue to model in (b).

Here we propose a depositional model based on bidirectional transport of particles presumably driven by deep-marine tidal bottom currents. Repeated traction/suspension/deposition of coarse sands and foraminifera material group in the form of small patches of lag deposits over the sea floor (Fig. 7.3b). The agglutination of coarse particles may be driven by roughness changes and formation of rough spots of coarse material on the seabed. The internal tide regime being characterised by intermittent bottom currents, in the current case most probably modulated by the incursion of MOW meddies, episodes of more sluggish internal tides allow the deposition of suspended particles. Several cycles of traction versus suspension deposition may allow the vertical development of the sand pockets. Such facies model may in fact be relatively analogue to depositional model proposed from Bádenas et al. (2012), in particular with the formation of starved ripples and thin sand lamina (Fig. 7.3c). However, the presented facies most probably represents accumulations formed over several hundreds of years, to potentially few thousand years, as the inferred sedimentation rates did not exceed 2 cm/ky. Thus this facies cannot be seen as swash run-up and/or compensating backwash flow deposits, but should rather be seen as their long term impact. Such facies most probably represent abrasive surfaces and associated lag deposits, potentially containing hiatuses of short duration (below 1 ky) caused by erosional and/or non-depositional conditions. The diagnostic criteria for internal tidal deposits largely remain ambiguous and require more case studies, in order to provide enough analogues for the models (Shanmugam, 2013b). Such facies model could be integrated to other bidirectional internal wave facies models such as proposed in Bádenas et al. (2012). By no means may the presented facies and discussion be considered to stand as a demonstration. However, few research lines could be identified and might deserve attention for future studies.

7.2 Summary of conclusions

DSDP Site 548 on Goban Spur provides an overall more complete Plio-Pleistocene sedimentary record when compared to sites recovered during IODP Exp. 307, within the Porcupine Seabight to the north. The seismic geomorphological analysis evidenced the presence of a few erosional events which were attributed to slope failure. The presence of an energetic depositional environment was evidenced from the presence of a large scale sediment wave field. The correlation between the newly obtained seismic stratigraphy with the geophysical well logging data permitted to constrain the time-dependent sediment dynamics, and to better understand the DSDP Site 548 record, in particular regarding the nature of its stratigraphic unit boundaries. The architecture of the deposits were both the result of changes in the local slope gradient induced from slope failure events, and long term changes in the MOW regime, impacting on the tide-topographic interactions. The initial introduction of the MOW is thought to have occurred roughly between 4.5 and 4.2 Ma. This was suggested from the presence of a smooth discontinuity (Goban Spur local discontinuity N3), which may sign the onset of energetic bottom currents, possibly associated with the initial introduction of the MOW. The influence of the MOW during the late Pliocene was subsequently corroborated from 3.63 Ma onwards (Khélifi et al., 2014). The vertical succession evolved from sub-parallel, high amplitude, reflectors in low slope gradient (ca. 4.5 to 2.5 Ma), to relatively large amplitude and migrating large-scale sediment waves in an overall higher slope gradient (ca. 2.2 to 0.5 Ma). Aggradational sediment waves of smaller amplitude were observed in intermediate slope gradient (from ~0.5 Ma to recent). This vertical architecture evolution is thought to be very analogous to the spatial evolution of an internal wave induced large scale sediment wave field in the Gulf of Valencia (Ribó et al., 2016). These architectural changes emphasize the importance of the slope gradient in tide-topographic interactions, which is also one main parameter in the equation Southard and Cacchione (1972). The onset of energetic bottom currents at Goban Spur occurred over a period which is largely absent from the Porcupine Seabight due to the presence of the regional unconformity RD1. Such results have implications for the onset of enhanced internal tidal processes along the eastern slope of the Porcupine Seabight, which were thus, established prior the initial development of large cold-water coral provinces at ca. 3 to 2.7 Ma, at least for the current state of knowledge (Raddatz et al., 2014). The Goban Spur is thus identified to have an important potential in establishing initial introduction of the MOW within the northeast Atlantic during the early Pliocene. Moreover, it has further a great potential in studying the sedimentological expression and characteristic of deep sea sediment waves dynamics associated to internal tidal processes and deep- marine tidal bottom currents.

DSDP Site 548 sediment core analysis provided some bottom current regime insights over the past 500 ka BP, during which the MOW is known to experience a marked climatic modulation. The

precise timing of the four penultimate deglacial periods could be identified using XRF Fe/Ca correlation with a site located along the northern Bay of Biscay. This correlation was further constrained from *Neogloboquadrina pachyderma* sinistral relative abundances, which provides an appropriate proxy for sub-tropical versus sub-polar sea surface temperatures in the area. The bottom current regime variations were studied by means of the terrigenous grain-size distribution. Fine clay and silt particles depletion consistently occurred during warm sea-surface temperature conditions and strictly post-dated glacials and deglacials. At this site, such variations could be related here to reflect the winnowing of fine sediment particles under enhanced tide-topographic interactions. Such hydrodynamic sorting associated with deep-marine tidal bottom currents has been directly observed to act at Goban Spur during the present-day, providing a suitable modern analogue (Thomsen et al., 1998; 2000). Considering that the local slope gradient is unlikely to have significantly changed over the studied period, as suggested from the geomorphological analysis, those variations could be directly related to changes in the internal tide angle of propagation, which constituted the only unconstrained parameter influencing tide-topographic interactions. Such changes are thought to be driven by the variable incursion of MOW at this site, which today constitutes a prominent water mass in the vertical stratification. Enhanced tide-topographic interactions, associated to the northward incursion of MOW were thus inferred to occur during interglacials of Marine Isotopic Stages 11, 9, 7 and 5. Comparison between the DSDP Site 548 bottom current record and the benthic oxygen isotope record from the nearby IODP Site 680 evidenced the existence of a certain coupling between periods of production of dense (modern-like) NADW and the MOW northward propagation towards the Irish margin. This pattern is analogue to scenario proposed by Schönfeld and Zahn (2000) during the Last Glacial Maximum. The present results have implications in terms of environment variability, specifically associated to bottom currents and erosional processes within the Porcupine Seabight.

The two studies carried out along the Atlantic Moroccan margin differ in terms of depth and time range, as well as water mass influence. A long piston core study revealed the sedimentary record of the Pen Duick drift 35°16.3'N, 642 m water depth. Planktonic and benthic stable isotope measurements, along with a series of AMS ^{14}C dates, revealed a complex chronostratigraphic evolution extending down to 50 ka BP. High sedimentation rates (~100 cm/ky during Marine Isotopic Stage 3 and ~30 cm/ky during the last deglacial) were most probably associated with the large occurrence of bottom current reworked sediment inputs, which are thought to have dramatically impacted on the overall planktonic stable isotope record. Grain-size analyses evidenced highly variable terrigenous silt distribution within the ~6 to 30 µm range, further correlated to XRF major terrigenous elements relative variations. Those were interpreted to reflect enhanced bottom current conditions, in particular during cold Dansgaard-Oeschger stadials, Heinrich Event 1 and the Younger

Dryas. The local bottom current regime is thought to be driven by increased northward advection of the Antarctic Intermediate Water into the subtropical northeast Atlantic, which characterizes a regional salinity minimum. The presence of a hiatus extending from 33 ka to 19 ka BP was also inferred. This hiatus was identified to be associated with a 10 cm thick calcareous (biogenic) sandy contourite sequence (Rebesco et al., 2014), interpreted to sign a lengthy period of bottom current induced erosional and/or non-depositional conditions. At this site, such bottom current induced erosional and/or non-depositional conditions are most probably induced from enhanced internal tidal processes, established during the gradual onset of the Last Glacial Maximum circulation pattern. Such enhanced internal tide bottom current regime is most probably associated with decreasing sea-level, causing the migration of the boundary between the NACW and AAIW, which characterize a strong pycnal gradient in the region. Interestingly, erosive and/or non-depositional bottom currents are further contemporary with the sustained and regional occurrence of mound-forming cold-water corals within the Atlantic Moroccan coral province (Wienberg et al., 2010). This pattern emphasizes the importance of vigorous bottom currents for cold-water corals, both in terms of food particle delivery and coral framework stabilization through sediment baffling, leading to mound building.

Subsequently, the study of an ultimate long piston core revealed the sediment dynamics at depths influenced by the regular incursion of mesoscale Mediterranean eddies. Sediment spectrophotometry luminosity correlation with IODP Site U1385, XRF Fe/Ca ratio, as well as coccolith assemblage analyses indicated the sediment core roughly covered the past 1650 ka BP. Variations in the terrigenous clay and silt grain-size distribution (ranging from ~4 to 30 µm), together with variable occurrence of discontinuous silt lenses and foraminifera rich sandy pockets, rust coloured and moderately bioturbated horizons dominated a large part of the sediment sequence. Those were interpreted as converging arguments indicating the influence of energetic bottom currents at this site. Overall low sedimentation rates, mainly varying around 2 cm/ky and often below 1 cm/ky may both be related to a sediment starved environment (located on top of a promontory), and may indicate that transport largely dominated over sedimentation at this site. Three distinct phases could be identified and were mainly contemporaneous with large climatic changes. The marked climate modulation, existing within the sediment geophysical and geochemical properties, prior to ~1650 to 1200 ka BP, was gradually altered during the Early-Middle Pleistocene Transition (roughly between 1200 and 500 ka BP). From ~1200 ka BP onwards, coarse intervals are associated with low XRF Fe/Ca ratio, and substantial decrease in the sedimentation rates (below 1 cm/ky). Such variations were interpreted to indicate the presence of enhanced bottom currents, which may have caused the winnowing of the fine terrigenous clay and silt fraction, leading to important textural changes. Based upon the facies evolution, it is inferred gradually more energetic bottom currents as glaciations

became more prominent. From about 460 ka BP, an abrupt facies change, punctually marked by terrigenous grain-sizes up to 100 µm, most probably reflects the occurrence of a seismically triggered mass wasting even. Such even could represent a local analogue to the Late Quaternary Discontinuity, widely described along the northern Gulf of Cádiz Contourite Depositional System (Hernández-Molina et al., 2016c; Lofi et al., 2016). Subsequently, no climatic signal could be recognized within the upper 450 cm bsf sequence, which nevertheless could be inferred to an age younger than 460 ka BP. This could reflect the onset of more energetic bottom currents, caused by changes in the circulation pattern and/or changes of the local slope gradient, possibly associated to a margin wide tectonic adjustment. Sea-level forced MOW flow conditions is thought to be the driving mechanism for the variable bottom current regime at this site. This may have caused enhanced formation of Mediterranean mesoscale eddies and more prominent local pycnal gradient and associated tide-topography interactions.

7.3 Outlook

This work has been carried out during a phase in which the contourite paradigm is experiencing a large diversification (Rebesco et al., 2014; Hernández-Molina et al., 2016b; Van Rooij et al., 2016). The interest arises as the circulation of intermediate water masses, for a long time largely understudied and unconstrained, appears to be as important as the surface to deep water convection (Freeman et al., 2015; van Ommen, 2015). This requires the investigation of sites located along the slopes and shelf breaks, fundamentally influenced by the action of a variety of bottom currents. In opposition to the inherent simplicity and predictable nature of turbiditic currents concepts, it seems the yet relatively numerous concepts defined within contourite paradigm, only form the prelude to its ultimate ambitions and requirements.

The need for holistic and multidisciplinary approach: bottom current processes are various in nature and thus characterised by the association of processes of different space and time variability, characterised by drastically different potential energies and flow velocities (Rebesco et al., 2014). Aiming to provide robust diagnostic criteria and concepts that drive the fossilisation of such oceanographic processes thus requires a fine understanding of oceanographic and sedimentary processes, as well as of the distinct processes occurring at their interface (Hernández-Molina et al., 2016a; Van Rooij et al., 2016). The recent multiplication of multidisciplinary studies integrating hydrodynamic measurements, geomorphological, sedimentological as well as 3-D numerical modelling have provided unprecedented insights on the driving mechanisms and relative contribution of those different processes (Turnewitsch et al., 2004; Hernández-Molina et al., 2011; Preu et al.,

2013; Mohn et al., 2014; Hanebuth et al., 2015; Zhang et al., 2015; Falcini et al., 2016; Ribó et al., 2016). Any of the research chapters presented here largely benefited from previous physical oceanographic studies conducted on those specific sites. In the future, each of them can potentially be integrated within more holistic study, integrating for example numerical modelling. Such approach implies close collaboration of distinct scientific fields, which today appears to be promising in many issues inherent to the contourite paradigm, and also more specifically to internal waves/tides and topographic interactions (Lamb et al., 2014).

Sediment composition and terrigenous silt proxy saturation: three distinct sediment cores were studied and showed significant differences in the sedimentary facies, and distinct variability within the terrigenous clay and silt grain-size distribution, as well as biogenic content and texture. Important local sediment supply controls are superimposed on controls bottom currents may exert themselves (Van Rooij et al., 2016). In this thesis, the use of terrigenous silt proxy in order to infer more or less energetic bottom current conditions has proven overall useful. Nevertheless, it was much less convincing when the biogenic sand fraction was large, as for example along the Atlantic Moroccan margin. This was in particular true when bottom currents induced erosion and/or non-depositional conditions at both sites MD08-3227 and MD13-3447. Within those intervals, the coarse biogenic (mainly foraminiferal sands) material was embedded in a matrix having a fine terrigenous silts distribution. More attention thus needs to be given on the overall sediment composition and texture. In the future, this composition should be considered in order to weight the significance of terrigenous silt proxies.

Magnitude of internal tidal induced bottom currents: tide-topographic interactions and internal tidal processes are relatively heterogeneous processes within the world wide ocean (Simmons et al., 2004). Those were shown to be important both along Goban Spur and the Atlantic Moroccan margin prior this thesis. In contrast, barotropic tide and propagating (baroclinic) internal tides within the water column may also compensate in certain settings, as for example shown along the northwest Iberian margin (Hanebuth et al., 2015; Zhang et al., 2015). There, the bidirectional (tidal) bottom current motions would rarely exceed 15 cm/s. This emphasizes more work can be done on the predictability and ability of internal tidal processes to induce energetic (>15 cm/s) bottom currents over the seabed. If the calculation of internal tidal reflection conditions with respect to a certain sloping seabed provided interesting predictable arguments, this calculation is not based on the actual bottom current motions on the seabed at a particular site. This strongly discourages an internal tidal interpretation in the absence of direct seabed bottom current velocity measurements. Internal waves

and tides generation, propagation and dissipation, as well as their role in ocean mixing have been the focus of many studies (Gao et al., 1998; Nycander, 2005; McPhee-Shaw, 2006; Garrett and Kunze, 2007). Nevertheless the effects those motions may have in terms of sediment transport and influence on the sediment archive seem to have been overlooked, and more work can be done (Lamb, 2014). In particular, internal tides are thought more energetic along strong pycnal gradients. In certain location, the amplitude of tidal motion may reach a hundred of meter, such as for example along the Atlantic Moroccan margin (Mienis et al., 2012). There seems to be no comprehensive link between internal tidal amplitude and induced bottom current motion velocities and transport magnitude, at least not yet as a tool available for sedimentological studies.

Variability of the MOW along its northern pathway: both oceanographic and palaeo-oceanographic studies have pointed out the presence of the MOW along the Irish margin may constitute one major ingredient for the development of past and present cold-water corals and coral mounds. Nowadays, the distribution of living cold-water corals seems to align along the permanent thermocline, which is greatly influenced by the presence of the MOW in the region (White and Dorschel, 2010; Mohn et al., 2014). During periods of enhanced cold-water coral accretion (ca. 3 to 2.1 Ma and 1 to 0.5 Ma), the build-up of a stable stratified water column, characterised by the presence of the MOW, is also thought to have played an important role (Li et al., 2011; Raddatz et al., 2014). Nevertheless this role is not trivial as variations in primary productivity are overall found correlated over the same periods, which may similarly positively or negatively influence environmental conditions for the growth of cold-water corals. Overall decrease in primary productivity was proposed as most probable mechanism to explain the cold-water coral decay during the mound crisis unconformity respectively between ~1.7 to 1 Ma (Fig. 7.1; Raddatz et al., 2014). In analogy to the past 500 ka BP, DSDP Site 548 has an important potential in studying the past behaviour of the MOW and local oceanographic conditions prior, during and beyond this mound crisis unconformity. Beyond additional constrains on the past behaviour of the MOW, this may dramatically improve and complete the knowledge of past oceanographic changes during periods of thriving and decaying cold-water coral ecosystems. The drilling of a new hole at this site would be beneficial in order to obtain a continuous composite core section. This could be performed along with the drilling of Le Danois Bank in the southern Bay of Biscay (Van Rooij et al., 2010), which Contourite Depositional System remains unexplored. The Le Danois Bank is located at an intermediate site between the Galician and Irish margin and thus might help constraining the recent MOW variability within the southern Bay of Biscay. It might also represent an intermediate Contourite Depositional System within the continuum existing between the contour currents versus internal tidal formed sediment drifts.

Spatial characterization of the Pen Duick Escarpment and erosive mechanism: chapter 5 characterised the presence of a hiatus which was proposed to be caused by regionally more energetic bottom current conditions. The regional bottom current regime is thought to be influenced by the presence of the Pen Duick Escarpment which constitutes a topographic obstacle that controlled the corresponding drift formation (Vandorpe et al., 2014). Per definition, the concept of a topographically driven sediment drift implies that deposition might still have occurred at distance of the topographic obstacle increase (Fig. 5.5). Nevertheless, some studies have evidenced only little lateral facies variations within small-scale drift sequences (Hanebuth et al., 2015) and thus, this hypothesis needs to be further tested. This could be done by recovering a sediment core transect along the Pen Duick drift as a function of the distance from the escarpment, in order to characterize the spatial extend of the hiatus obtained.

Overall, the Moroccan Atlantic and Irish margins are characterised by climatically modulated and bottom current controlled sedimentation, with alternations of periods of sluggish, energetic to erosion and/or non-depositional conditions. Those changes are site specific and widely asynchronous, which illustrates on how changes in the local water column stratification profile widely controlled sedimentation. A better understanding of mechanisms driving tide-topography interactions, specifically the characterization of erosional and/or non-depositional thresholds, constitute an important future challenge which might lead to important breakthrough within the contourite paradigm. This study has provided distinct contourite sediment facies descriptions and identified most probable driving mechanisms, overall converging towards internal tidal processes, which contrast with most established models. Thus those might be considered a possible analogues for future core based studies.

References

Alonso, B., Ercilla, G., Casas, D., Stow, D.A.V., Rodriguez-Tovar, F.J., Dorador, J., Hernandez-Molina, F.J., 2016. Contourite vs gravity-flow deposits of the Pleistocene Faro Drift (Gulf of Cadiz): Sedimentological and mineralogical approaches. Marine Geology 377, 77-94.

Ambar, I., Serra, N., Neves, F., Ferreira, T., 2008. Observations of the Mediterranean Undercurrent and eddies in the Gulf of Cadiz during 2001. Journal of Marine Systems 71, 195-220.

Apel, J.R., 2000. Solitons near Gibraltar: views from the European remote sensing satellites. Report GOA 1.

Apel, J.R., 2002. Oceanic internal waves and solitons. An atlas of oceanic internal solitary waves, 1-40.

Bádenas, B., Pomar, L., Aurell, M., Morsilli, M., 2012. A facies model for internalites (internal wave deposits) on a gently sloping carbonate ramp (Upper Jurassic, Ricla, NE Spain). Sedimentary Geology 271–272, 44-57.

Barbosa Aguiar, A.C., Peliz, Á., Carton, X., 2013. A census of Meddies in a long-term high-resolution simulation. Progress In Oceanography 116, 80-94.

Cacchione, D.A., Pratson, L.F., Ogston, A.S., 2002. The Shaping of Continental Slopes by Internal Tides. Science 296, 724-727.

Chen, H., Xie, X., Zhang, W., Shu, Y., Wang, D., Vandorpe, T., Van Rooij, D., 2016. Deep-water sedimentary systems and their relationship with bottom currents at the intersection of Xisha Trough and Northwest Sub-Basin, South China Sea. Marine Geology 378, 101-113.

Dorschel, B., Hebbeln, D., Rüggeberg, A., Dullo, C., Freiwald, A., 2005. Growth and erosion of a cold-water coral covered carbonate mound in the Northeast Atlantic during the Late Pleistocene and Holocene. Earth and Planetary Science Letters 233, 33-44.

Dorschel, B., Hebbeln, D., Foubert, A., White, M., Wheeler, A.J., 2007. Hydrodynamics and cold-water coral facies distribution related to recent sedimentary processes at Galway Mound west of Ireland. Marine Geology 244, 184-195.

Ercilla, G., Juan, C., Hernández-Molina, F.J., Bruno, M., Estrada, F., Alonso, B., Casas, D., Farran, M.l., Llave, E., García, M., Vázquez, J.T., D'Acremont, E., Gorini, C., Palomino, D., Valencia, J., El Moumni, B., Ammar, A., 2016. Significance of bottom currents in deep-sea morphodynamics: An example from the Alboran Sea. Marine Geology 378, 157-170.

Falcini, F., Martorelli, E., Chiocci, F.L., Salusti, E., 2016. A general theory for the effect of local topographic unevenness on contourite deposition around marine capes: An inverse problem applied to the Italian continental margin (Cape Suvero). Marine Geology.

Faugères, J.-C., Mézerais, M.L., Stow, D.A.V., 1993. Contourite drift types and their distribution in the North and South Atlantic Ocean basins. Sedimentary Geology 82, 189-203.

Faugères, J.-C., Stow, D.A.V., Imbert, P., Viana, A.R., 1999. Seismic features diagnostic of contourite drifts. Marine Geology 162, 1-38.

Faugères, J.C., Stow, D.A.V., 2008. Chapter 14 Contourite Drifts: Nature, Evolution and Controls, in: Rebesco, M., Camerlenghi, A. (Eds.), Developments in Sedimentology. Elsevier, pp. 257-288.

Foubert, A., Depreiter, D., Beck, T., Maignien, L., Pannemans, B., Frank, N., Blamart, D., Henriet, J.-P., 2008. Carbonate mounds in a mud volcano province off north-west Morocco: Key to processes and controls. Marine Geology 248, 74-96.

Freeman, E., Skinner, L.C., Tisserand, A., Dokken, T., Timmermann, A., Menviel, L., Friedrich, T., 2015. An Atlantic–Pacific ventilation seesaw across the last deglaciation. Earth and Planetary Science Letters 424, 237-244.

Gao, Z.Z., Eriksson, K.A., 1991. Internal-tide deposits in an Ordovician submarine channel: Previously unrecognized facies? Geology 19, 734-737.

Gao, Z.Z., Eriksson, K.A., Youbin, H., Shunshe, L., Jianhua, G., 1998. Deep-Water Traction Current Deposits - a Study of Internal Tides, Internal Waves, Contour Currents and Their Deposits. Science Press, Beijing.

Garrett, C., Munk, W., 1979. Internal Waves in the Ocean. Annual Review of Fluid Mechanics 11, 339-369.

Garrett, C., Kunze, E., 2007. Internal Tide Generation in the Deep Ocean. Annual Review of Fluid Mechanics 39, 57-87.

Gonthier, E., Faugères, J.-C., Stow, D.A.V., 1984. Contourite facies of the Faro Drift, Gulf of Cadiz, in: Stow, D.A.V., Piper, D.J.W. (Eds.), Fine Grained Sediments, Deep-Water Processes and Facies. Geological Society, London, pp. 275-291.

Hanebuth, T.J.J., Zhang, W., Hofmann, A.L., Löwemark, L.A., Schwenk, T., 2015. Oceanic density fronts steering bottom-current induced sedimentation deduced from a 50 ka contourite-drift record and numerical modeling (off NW Spain). Quaternary Science Reviews 112, 207-225.

He, Y., Gao, Z., Luo, J., Luo, S., Liu, X., 2008. Characteristics of internal-wave and internal-tide deposits and their hydrocarbon potential. Petroleum Science 5, 37-44.

Hebbeln, D., Van Rooij, D., Wienberg, C., 2016. Good neighbours shaped by vigorous currents: Cold-water coral mounds and contourites in the North Atlantic. Marine Geology 378, 171-185.

Hernández-Molina, F.J., Maldonado, A., Stow, D.A.V., 2008. Sediment drift of Abyssal plains and oceanic basins, in: Rebesco, M., Camerlenghi, A. (Eds.), Contourites. Elsevier.

Khélifi, N., Sarnthein, M., Frank, M., Andersen, N., Garbe-Schönberg, D., 2014. Late Pliocene variations of the Mediterranean outflow. Marine Geology 357, 182-194.

Hernández-Molina, F.J., Serra, N., Stow, D., Llave, E., Ercilla, G., Van Rooij, D., 2011. Along-slope oceanographic processes and sedimentary products around the Iberian margin. Geo-Marine Letters, 1-27.

Hernández-Molina, F.J., Hodell, D.A., Stow, D.A.V., Alvarez-Zarikian, C., 2016b. Virtual special issue on IODP Expedition 339: The Mediterranean outflow. Marine Geology 377, 1-6.

Hernández-Molina, F.J., Sierro, F.J., Llave, E., Roque, C., Stow, D.A.V., Williams, T., Lofi, J., Van der Schee, M., Arnáiz, A., Ledesma, S., Rosales, C., Rodríguez-Tovar, F.J., Pardo-Igúzquiza, E., Brackenridge, R.E., 2016c. Evolution of the gulf of Cadiz margin and southwest Portugal contourite depositional system: Tectonic, sedimentary and paleoceanographic implications from IODP expedition 339. Marine Geology 377, 7-39.

Hernández-Molina, F.J., Wåhlin, A., Bruno, M., Ercilla, G., Llave, E., Serra, N., Rosón, G., Puig, P., Rebesco, M., Van Rooij, D., Roque, D., González-Pola, C., Sánchez, F., Gómez, M., Preu, B., Schwenk, T., Hanebuth, T.J.J., Sánchez Leal, R.F., García-Lafuente, J., Brackenridge, R.E., Juan, C., Stow, D.A.V., Sánchez-González, J.M., 2016a. Oceanographic processes and morphosedimentary products along the Iberian margins: A new multidisciplinary approach. Marine Geology 378, 127-156.

Huthnance, J.M., Coelho, H., Griffiths, C.R., Knight, P.J., Rees, A.P., Sinha, B., Vangriesheim, A., White, M., Chatwin, P.G., 2001. Physical structures, advection and mixing in the region of Goban spur. Deep-Sea Research II 48, 2979-3021.

Huvenne, V.A.I., Van Rooij, D., De Mol, B., Thierens, M., O'Donnell, R., Foubert, A., 2009. Sediment dynamics and palaeo-environmental context at key stages in the Challenger cold-water coral mound formation: Clues from sediment deposits at the mound base. Deep Sea Research Part I: Oceanographic Research Papers 56, 2263-2280.

Juan, C., Ercilla, G., Javier Hernández-Molina, F., Estrada, F., Alonso, B., Casas, D., García, M., Farran, M.l., Llave, E., Palomino, D., Vázquez, J.-T., Medialdea, T., Gorini, C., D'Acremont, E., El Moumni, B., Ammar, A., 2016. Seismic evidence of current-controlled sedimentation in the Alboran Sea during the Pliocene and Quaternary: Palaeoceanographic implications. Marine Geology.

Kano, A., Ferdelman, T.G., Williams, T., Henriet, J.P., Ishikawa, T., Kawagoe, N., Takashima, C., Kakizaki, Y., Abe, K., Sakai, S., Browning, E., Li, X., the IODP Expedition 307 Scientists, 2007. Age constraints on the origin and growth history of a deep-water coral mound in northeast Atlantic drilled during Integrated Ocean Drilling Program Expedition 307. Geology 35, 1051-1054.

Khélifi, N., Sarnthein, M., Frank, M., Andersen, N., Garbe-Schönberg, D., 2014. Late Pliocene variations of the Mediterranean outflow. Marine Geology 357, 182-194.

Klymak, J.M., Alford, M.H., Pinkel, R., Lien, R.-C., Yang, Y.J., Tang, T.-Y., 2011. The Breaking and Scattering of the Internal Tide on a Continental Slope. Journal of Physical Oceanography 41, 926-945.

Lamb, K.G., 2014. Internal Wave Breaking and Dissipation Mechanisms on the Continental Slope/Shelf. Annual Review of Fluid Mechanics 46, 231-254.

Li, X., Takashima, C., Kano, A., Sakai, S., Chen, Y., Xu, B., Iodp Expedition, S., 2011. Pleistocene geochemical stratigraphy of the borehole 1317E (IODP Expedition 307) in Porcupine Seabight, SW of Ireland: applications to palaeoceanography and palaeoclimate of the coral mound development. Journal of Quaternary Science 26, 178-189.

Lofi, J., Voelker, A.H.L., Ducassou, E., Hernández-Molina, F.J., Sierro, F.J., Bahr, A., Galvani, A., Lourens, L.J., Pardo-Igúzquiza, E., Pezard, P., Rodríguez-Tovar, F.J., Williams, T., 2016. Quaternary chronostratigraphic framework and sedimentary processes for the Gulf of Cadiz and Portuguese Contourite Depositional Systems derived from Natural Gamma Ray records. Marine Geology 377, 40-57.

Maestro, A., López-Martínez, J., Llave, E., Bohoyo, F., Acosta, J., Hernández-Molina, F.J., Muñoz, A., Jané, G., 2013. Geomorphology of the Iberian Continental Margin. Geomorphology 196, 13-35.

Martín–Chivelet, J., Fregenal–Martínez, M.A., Chacón, B., 2008. Chapter 10 Traction Structures in Contourites, in: Rebesco, M., Camerlenghi, A. (Eds.), Developments in Sedimentology. Elsevier, pp. 157-182.

McCave, I.N., Hall, I.R., 2006. Size sorting in marine muds: Processes, pitfalls, and prospects for paleoflow-speed proxies. Geochemistry, Geophysics, Geosystems 7.

McPhee-Shaw, E., 2006. Boundary–interior exchange: Reviewing the idea that internal-wave mixing enhances lateral dispersal near continental margins. Deep Sea Research Part II: Topical Studies in Oceanography 53, 42-59.

Mienis, F., De Stigter, H.C., De Haas, H., Van der Land, C., Van Weering, T.C.E., 2012. Hydrodynamic conditions in a cold-water coral mound area on the Renard Ridge, southern Gulf of Cadiz. Journal of Marine Systems 96–97, 61-71.

Mohn, C., Rengstorf, A., White, M., Duineveld, G., Mienis, F., Soetaert, K., Grehan, A., 2014. Linking benthic hydrodynamics and cold-water coral occurrences: A high-resolution model study at three cold-water coral provinces in the NE Atlantic. Progress In Oceanography 122, 92-104.

Mulder, T., Zaragosi, S., Garlan, T., Mavel, J., Cremer, M., Sottolichio, A., Sénéchal, N., Schmidt, S., 2012. Present deep-submarine canyons activity in the Bay of Biscay (NE Atlantic). Marine Geology 295–298, 113-127.Mulder, T., Hassan, R., Ducassou, E., Zaragosi, S., Gonthier, E., Hanquiez, V., Marchès, E., Toucanne, S., 2013. Contourites in the Gulf of Cadiz: a cautionary note on potentially ambiguous indicators of bottom current velocity. Geo-Marine Letters 33, 357-367.

Nishida, N., 2016. Microstructure of muddy contourites from the Gulf of Cádiz. Marine Geology 377, 110-117.

Nycander, J., 2005. Generation of internal waves in the deep ocean by tides. Journal of Geophysical Research: Oceans 110, C10028.

Ovrebo, L.K., Haughton, P.D.W., Shannon, P.M., 2006. A record of fluctuating bottom currents on the slopes west of the Porcupine Bank, offshore Ireland - implications for Late Quaternary climate forcing. Marine Geology 225, 279-309.

Peine, F., Turnewitsch, R., Mohn, C., Reichelt, T., Springer, B., Kaufmann, M., 2009. The importance of tides for sediment dynamics in the deep sea—Evidence from the particulate-matter tracer 234Th in deep-sea environments with different tidal forcing. Deep Sea Research Part I: Oceanographic Research Papers 56, 1182-1202.

Pomar, L., Morsilli, M., Hallock, P., Bádenas, B., 2012. Internal waves, an under-explored source of turbulence events in the sedimentary record. Earth-Science Reviews 111, 56-81.

Preu, B., Hernández-Molina, F.J., Violante, R., Piola, A.R., Paterlini, C.M., Schwenk, T., Voigt, I., Krastel, S., Spiess, V., 2013. Morphosedimentary and hydrographic features of the northern Argentine margin: The

interplay between erosive, depositional and gravitational processes and its conceptual implications. Deep Sea Research Part I: Oceanographic Research Papers 75, 157-174.

Quaresma, L.S., Vitorino, J., Oliveira, A., da Silva, J., 2007. Evidence of sediment resuspension by nonlinear internal waves on the western Portuguese mid-shelf. Marine Geology 246, 123-143.

Raddatz, J., Rüggeberg, A., Margreth, S., Dullo, W.-C., 2011. Paleoenvironmental reconstruction of Challenger Mound initiation in the Porcupine Seabight, NE Atlantic. Marine Geology 282, 79-90.

Raddatz, J., Rüggeberg, A., Liebetrau, V., Foubert, A., Hathorne, E.C., Fietzke, J., Eisenhauer, A., Dullo, W.-C., 2014. Environmental boundary conditions of cold-water coral mound growth over the last 3 million years in the Porcupine Seabight, Northeast Atlantic. Deep Sea Research Part II: Topical Studies in Oceanography 99, 227-236.

Rebesco, M., Camerlenghi, A., 2008. Contourites, Developments in Sedimentology. Elsevier.

Rebesco, M., Hernández-Molina, F.J., Van Rooij, D., Wåhlin, A., 2014. Contourites and associated sediments controlled by deep-water circulation processes: State-of-the-art and future considerations. Marine Geology 352, 111-154.

Ribó, M., Puig, P., Muñoz, A., Lo Iacono, C., Masqué, P., Palanques, A., Acosta, J., Guillén, J., Gómez Ballesteros, M., 2016. Morphobathymetric analysis of the large fine-grained sediment waves over the Gulf of Valencia continental slope (NW Mediterranean). Geomorphology 253, 22-37.

Rice, A.L., Thurston, M.H., New, A.L., 1990. Dense aggregations of a hexactinellid sponge, *Pheromena carpenteri*, in the Porcupine Seabight (northeast Atlantic Ocean), and possible causes. Progress In Oceanography 24, 179-196.

Rüggeberg, A., Dullo, C., Dorschel, B., Hebbeln, D., 2007. Environmental changes and growth history of a cold-water carbonate mound (Propeller Mound, Porcupine Seabight). International Journal of Earth Sciences 96, 57-72.

Sánchez-Garrido, J.C., Sannino, G., Liberti, L., García Lafuente, J., Pratt, L., 2011. Numerical modeling of three-dimensional stratified tidal flow over Camarinal Sill, Strait of Gibraltar. Journal of Geophysical Research: Oceans 116.

Schönfeld, J., Zahn, R., 2000. Late Glacial to Holocene history of the Mediteranean Outflow. Evidence from benthic foraminiferal assemblages and stable isotopes at the Portuguese margin. Palaeogeography, Palaeoclimatology, Palaeoecology 159, 85-111.

Shanmugam, G., 2003. Deep-marine tidal bottom currents and their reworked sands in modern and ancient submarine canyons. Marine and Petroleum Geology 20, 471-491.

Shanmugam, G., 2008. Chapter 5 Deep-water Bottom Currents and their Deposits, in: Rebesco, M., Camerlenghi, A. (Eds.), Developments in Sedimentology. Elsevier, pp. 59-81.

Shanmugam, G., 2013a. Modern internal waves and internal tides along oceanic pycnoclines: Challenges and implications for ancient deep-marine baroclinic sands. AAPG Bulletin 97, 799-843.

Shanmugam, G., 2013b. Comment on “Internal waves, an under-explored source of turbulence events in the sedimentary record” by L. Pomar, M. Morsilli, P. Hallock, and B. Bádenas [Earth-Science Reviews, 111 (2012), 56–81]. Earth-Science Reviews 116, 195-205.

Simmons, H.L., Hallberg, R.W., Arbic, B.K., 2004. Internal wave generation in a global baroclinic tide model. Deep Sea Research Part II: Topical Studies in Oceanography 51, 3043-3068.

Southard, J.B., Cacchione, D.A., 1972. Experiments on Bottom Sediment Movement by Breaking InternalWaves. In: Swift, D.J., Duane, D.B., Pilkey, O.H. (Eds.), Shelf Sediment Transport: Process and Pattern. Hutchinson & Ross, Stroudsburg, Pa., Dowden, pp. 83–97.

Stow, D.A.V., Faugères, J.-C., Howe, J.A., Pudsey, C.J., Viana, A.R., 2002. Bottom currents, contourites and deep-sea sediment drifts: current state-of-the-art. Geological Society, London, Memoirs 22, 7-20.

Stow, D.A.V., Faugères, J.C., 2008. Chapter 13 Contourite Facies and the Facies Model, in: Rebesco, M., Camerlenghi, A. (Eds.), Developments in Sedimentology. Elsevier, pp. 223-256.

Stow, D.A.V., Hernandez-Molina, F.J., Llave, E., Sayago-Gil, M., del Rio, V.D., Branson, A., 2009. Bedform-velocity matrix: The estimation of bottom current velocity from bedform observations. Geology 37, 327-330.

Takashimizu, Y., Kawamura, R., Rodríguez-Tovar, F.J., Dorador, J., Ducassou, E., Hernández-Molina, F.J., Stow, D.A.V., Alvarez-Zarikian, C.A., 2016. Reworked tsunami deposits by bottom currents: Circumstantial evidences from Late Pleistocene to Early Holocene in the Gulf of Cádiz. Marine Geology 377, 95-109.

Thomsen, L., van Weering, T.C.E., 1998. Spatial and temporal variability of particulate matter in the benthic boundary layer at the N.W. European Continental Margin (Goban Spur). Progress In Oceanography 42, 61-76.

Thomsen, L., Gust, G., 2000. Sediment erosion thresholds and characteristics of resuspended aggregates on the western European continental margin. Deep Sea Research Part I: Oceanographic Research Papers 47, 1881-1897.

Toucanne, S., Mulder, T., Schönfeld, J., Hanquiez, V., Gonthier, E., Duprat, J., Cremer, M., Zaragosi, S., 2007. Contourites of the Gulf of Cadiz: A high-resolution record of the paleocirculation of the Mediterranean outflow water during the last 50,000 years. Palaeogeography, Palaeoclimatology, Palaeoecology 246, 354-366.

Turnewitsch, R., Reyss, J.-L., Chapman, D.C., Thomson, J., Lampitt, R.S., 2004. Evidence for a sedimentary fingerprint of an asymmetric flow field surrounding a short seamount. Earth and Planetary Science Letters 222, 1023-1036.

Turnewitsch, R., Reyss, J.-L., Nycander, J., Waniek, J.J., Lampitt, R.S., 2008. Internal tides and sediment dynamics in the deep sea—Evidence from radioactive 234Th/238U disequilibria. Deep Sea Research Part I: Oceanographic Research Papers 55, 1727-1747.

Turnewitsch, R., Falahat, S., Nycander, J., Dale, A., Scott, R.B., Furnival, D., 2013. Deep-sea fluid and sediment dynamics—Influence of hill- to seamount-scale seafloor topography. Earth-Science Reviews 127, 203-241.

van Ommen, T., 2015. Palaeoclimate: Northern push for the bipolar see-saw. Nature 520, 630-631.

Van Rooij, D., De Mol, B., Huvenne, V., Ivanov, M.K., Henriet, J.-P., 2003. Seismic evidence of current-controlled sedimentation in the Belgica mound province, upper Porcupine slope, southwest of Ireland. Marine Geology 195, 31-53.

Van Rooij, D., Blamart, D., Kozachenko, M., Henriet, J.-P., 2007. Small mounded contourite drifts associated with deep-water coral banks, Porcupine Seabight, NE Atlantic Ocean, in: Viana, A.R., Rebesco, M. (Eds.), Economic and Palaeoceanographic Importance of Contourite Deposits. Geological Society, London, pp. 225-244.

Van Rooij, D., Huvenne, V.A.I., Blamart, D., Henriet, J.P., Wheeler, A., de Haas, H., 2009. The Enya mounds: a lost mound-drift competition. International Journal of Earth Sciences 98, 849-863.

Van Rooij, D., Iglesias, J., Hernández-Molina, F.J., Ercilla, G., Gomez-Ballesteros, M., Casas, D., Llave, E., De Hauwere, A., Gil, S.G., Acosta, J., Henriet, J.P., 2010. The Le Danois Contourite Depositional System: interactions between the Mediterranean Outflow Water and the upper Cantabrian slope (North Iberian margin). Marine Geology 274, 1-20.

Van Rooij, D., Campbell, C., Rueggeberg, A., Wahlin, A., 2016. The contourite log-book: significance for palaeoceanography, ecosystems and slope instability. Marine Geology 378, 1-4.

van Weering, T.C.E., Hall, I.R., de Stigter, H.C., McCave, I.N., Thomsen, L., 1998. Recent sediments, sediment accumulation and carbon burial at Goban Spur, N.W. European Continental Margin (47-50°N). Progress In Oceanography 42, 5-35.

Vandorpe, T., Van Rooij, D., de Haas, H., 2014. Stratigraphy and paleoceanography of a topography-controlled contourite drift in the Pen Duick area, southern Gulf of Cádiz. Marine Geology 349, 136-151.

Vandorpe, T., Martins, I., Vitorino, J., Hebbeln, D., García, M., Van Rooij, D., 2016. Bottom currents and their influence on the sedimentation pattern in the El Arraiche mud volcano province, southern Gulf of Cadiz. Marine Geology 378, 114-126.

Vandorpe, T., Wienberg, C., Hebbeln, D., Van den Berghe, M., Gaide, S., Wintersteller, P., Van Rooij, D., submitted. Initiation and aggradation of buried cold-water corals mounds in the Atlantic Moroccan Coral Province, southern Gulf of Cádiz. Palaeogeography, Palaeoclimatology, Palaeoecology.

Vandorpe, T, 2016, Contourite drifts and cold-water coral mounds in the Atlantic Moroccan Coral Province: origin, evolution and driving forces. Ph.D. Thesis, Ghent University, Belgium.

Voelker, A.H.L., Lebreiro, S.M., Schonfeld, J., Cacho, I., Erlenkeuser, H., Abrantes, F., 2006. Mediterranean outflow strengthening during northern hemisphere coolings: A salt source for the glacial Atlantic? Earth and Planetary Science Letters 245, 39-55.

White, M., 2003. Comparison of near seabed currents at two locations in the Porcupine Sea Bight - implications for benthic fauna. Journal of the Marine Biological Association of the United Kingdom 83, 683-686.

White, M., Mohn, C., de Stigter, H., Mottram, G., 2005. Deep-water coral development as a function of hydrodynamics and surface productivity around the submarine banks of the Rockall Trough, NE Atlantic, in: Freiwald, A., Roberts, J.M. (Eds.), Cold-Water Corals and Ecosystems. Springer Berlin Heidelberg, pp. 503-514.

White, M., Dorschel, B., 2010. The importance of the permanent thermocline to the cold water coral carbonate mound distribution in the NE Atlantic. Earth and Planetary Science Letters 296, 395-402.

Wienberg, C., Frank, N., Mertens, K.N., Stuut, J.-B., Marchant, M., Fietzke, J., Mienis, F., Hebbeln, D., 2010. Glacial cold-water coral growth in the Gulf of Cádiz: Implications of increased palaeo-productivity. Earth and Planetary Science Letters 298, 405-416.

Zhang, W., Hanebuth, T.J.J., Stöber, U., 2015. Short-term sediment dynamics on a meso-scale contourite drift (off NW Iberia): Impacts of multi-scale oceanographic processes deduced from the analysis of mooring data and numerical modelling. Marine Geology.

GHENT
UNIVERSITY